Angiotensin II Type 1 Receptor (AT_1R) Changes in Animal Model of Chronic Kidney Disease: Evaluation and Pharmacotherapy

By

Basma Ismail

Thesis submitted to the
Faculty of Graduate and Posdoctoral Studies
in partial fulfillment of the requirements
for a doctoral degree in Cellular and Molecular Medicine.

Department of Cellular and Molecular Medicine

Faculty of Medicine

University of Ottawa

ABSTRACT

Cardiovascular complications represent the leading cause of death in chronic kidney disease (CKD) patients. Significant renal mass reduction induced by 5/6 subtotal nephrectomy (Nx) animal model leads to a chain of events that culminates in hypertension and CKD. The renin angiotensin (Ang) system (RAS) is known to be dysregulated, specifically Ang type 1 receptor (AT_1R) plays a major role in development and progression of the disease. However, conflicting results have been reported on intrarenal AT_1R levels, and the impact of antihypertensive drugs on RAS signaling is divergent. We hypothesize that PET imaging will be able to quantify kidney AT_1R expression reliably in healthy and disease states. The broad objectives of this research project were: (i) to develop a positron emission tomography (PET) probe capable of detecting changes in the AT_1R binding in the kidney; (ii) to elucidate the nature/temporal role of renal AT_1R in Nx rat model of CKD; and (iii) to explore the predictive value of non-invasive PET imaging of AT_1R to guide the use of antihypertensive therapy in preventing the progression of the disease. The novel selective AT_1R PET radioligand [^{18}F]FPyKYNE-losartan was successfully used with PET in detecting renal AT_1Rs at early and late stages of the CKD. The PET results correlated well with *in vitro* [^{125}I]-[Sar^1, Ile^8]Ang II autoradiography. Over the time-course of the study (10-20 weeks), the Nx rats exhibited renal impairment, proteinuria and sustained hypertension. Echocardiography indicated the development of cardiac hypertrophy most likely secondary to the hyperdynamic circulation. These abnormalities were associated with increasing plasma and kidney levels of Ang II, and compensatory downregulation of renal AT_1Rs. ACEI enalapril attenuated renal impairment, hypertension and prevented

progression of cardiac hypertrophy in Nx rats. This was successfully accomplished through reduction of systemic and kidney Ang II, and consequent normalization of renal AT_1R as measured by PET (and autoradiography). The non-dihydropyridine CCB diltiazem also reduced blood pressure but did not normalize renal AT_1R expression. Diltiazem induced elevation in Ang II levels in plasma, kidney and heart, associated with exacerbation of renal and cardiac dysfunction, and no change in AT_1R renal expression. This outcome adds value to the use of [^{18}F]FPyKYNE-losartan PET for determination of receptor abnormalities with progression of the disease and monitoring of therapy.

ACKNOWLEDGMENTS

I would like to sincerely thank my supervisor Dr. Jean DaSilva for his mentoring, guidance, and continuous faith in my abilities to pursue and accomplish my PhD. To my co-supervisor Dr. Rob Beanlands, I am grateful for your knowledge that has helped in the interpretation of findings and for your encouragement throughout the years of my research project. I would like to extend my thanks to my TAC members Dr. Kevin Burns, Dr. Patrick Burgon and Dr. Richard Hebert for all their experienced feedbacks on my research. I would also like to acknowledge the University of Ottawa and the Ottawa Heart Institute for the funding support.

I have had the privilege of working with so many wonderful people. To Drs. Stephanie Thorn and James Thackeray, I will always be grateful for your technical and academic expertise, and the constant support you provided me that greatly contributed to this work. To Marika Kolajova and Dr. Tayebeh Hadizad, thanks for your friendship and all the endless coffee breaks that made it a pleasure to come to the lab every day.

The experiments in this thesis could not have been completed without the contributions of the ACVS staff, the radiochemistry lab and the imaging physics group including Keegan Flowers, Dr. Etienne Croteau, Myra Kordos, Christine Archur and Julia Lockwood; and the many members of the PET Biotesting lab over the years. I would like to especially thank Dr. Rob deKemp, for providing his expert assistance with the imaging results.

Finally, I dedicate this thesis to my family: I would never have gotten this far without them. To my loving husband Mohamed, for supporting me unconditionally; my parents and sisters, who have never stopped encouraging me; and my precious kids, Ahmed and Anas who mean the world to me.

TABLE OF CONTENTS

LIST OF TABLES

LIST OF FIGURES

LIST OF ABBREVIATIONS

%ID/g	percent of the injected dose per gram of tissue
AA	arachidonic acid
AC	adenyl cyclase
ACE	angiotensin converting enzyme
ACEI	ACE inhibitor
Ang	Angiotensin
ARBS	AT1R blockers
AT1R	Ang type 1 receptor
AT2R	Ang type 2 receptor
AT4R	Ang type 4 receptor
Bmax	Maximal binding density
Bq	Becquerel
C-11	carbon-11
CCB	calcium channel blocker
Ci	Curie
CKD	chronic kidney disease
CPM	Counts per minute
Cr	creatinine
$CuSO_4$	copper(II) sulfate
DAG	diacyl glycerol
DV	distribution volume
EDV	end diastolic volume
EGFR	epidermal growth factor receptor
eGFR	estimated glomerular filtration rate
EOB	end of beam
ESRD	end-stage renal disease
F-18	fluorine-18
FOV	field of view
GAPDH	Glyceraldehyde 3-phosphate dehydrogenase
GPCR	G-protein coupled receptor

GRKs	GPCR kinases
HF	heart failure
HFpEF	heart failure with preserved EF
HPLC	high-performance liquid chromatography
HRMS	high-resolution mass spectrometry
I/R	ischemia/reperfusion
IC50	Half maximal inhibitory concentration
ICP	inductively coupled plasma
IDV	integrated density volume
IP3	inositol-1,4,5-triphosphate
KBR	kidney-to-blood ratio
Kd	Dissociation constant
KF	potassium fluoride
LA	left atrium
LDL	low-density lipoprotein
LOX_1R	oxidized low-density lipoprotein receptor
LV	left ventricle
LVEF	LV ejection fraction
MAP	mitogen-activated protein
MBF	myocardial blood flow
MI	myocardial infarction
N-13	nitrogen-13
NF-κB	nuclear factor-kappaB
NMR	Nuclear magnetic resonance
Nx	5/6 nephrectomy
NxD	Nx + diltiazem
NxE	Nx + enalapril
O-15	oxygen- 15
PA	phosphatidic acid
PAI	plasminogen activator inhibitor
PET	positron emission tomography

PKC	protein kinase C
PLA2	phopholipase A2
PLC	phospholoipase C
PLD	phospholipase D
PPARγ	Peroxisome proliferator-activated receptor gamma
QC	quality qontrol
RAS	renin angiotensin system
RBF	Renal blood flow
RMS	Root Mean Squared
ROI	Regions of interest
Rt	retention time
SAR	structure-activity relationship
SBP	systolic blood pressure
SPECT	single photon emission tomography
SUV	standardized/specific uptake value
SV	stroke volume
TAC	time-activity curve
TFA	Trifluoroacetic acid
TGF	transforming growth factor
TLC	thin layer chromatography
TM	transmembrane
VOI	volumes of interest
VSMC	vascular smooth muscle cells

CHAPTER 1: INTRODUCTION

1.0. INTRODUCTION

1.1. Renin Angiotensin System (RAS)

The renin angiotensin (Ang) system (RAS) is a crucial neuro-humoral pathway involved in the homeostasis of the cardiovascular system. RAS is known to play a key role in regulation of sodium and body fluids, blood pressure, and autonomic activity. Accordingly RAS dysregulation contributes to cardiac, vascular and renal diseases via a variety of mechanisms. Recently, it was discovered that the RAS hormonal cascade is more complex than initially identified with multiple tissue-specific enzymes, effector molecules, and receptors that have pleomorphic effects independent of the circulating RAS. Studying the alterations in this vital multi-complex system is important given the beneficial effects of RAS blockers in reducing morbidity and mortality associated with hypertension, atherosclerosis, heart failure, stroke, renal failure and diabetes (Yusuf et al. 2000, Igarashi et al. 2001, Henriksen et al. 2004).

1.1.1. RAS Cascade

Classically, RAS is considered an endocrine system whose main active hormone is the Ang II. The substrate of the system, angiotensinogen, an α-glycoprotein, is released from the liver (Depierre et al. 1978, Hall 2003, Menard et al. 2010) and is cleaved in the circulation by the highly specific protease, renin which is secreted from the juxtaglomerular apparatus of the kidney (Sealey et al. 1977, Hackenthal et al. 1990, Persson et al. 2004) to form the decapeptide Ang I. Ang I is subsequently converted to the octapeptide Ang II by Ang converting enzyme (ACE), a membrane-bound metalloproteinase, predominantly expressed on the surface of endothelial cells in the pulmonary circulation (Soubrier et al. 1993, Corvol et al. 1995, Costerousse et al. 1998,

Hall 2003). Alternative pathway of Ang II formation has been identified in the heart where the majority of Ang I is cleaved by the serine protease, chymase (Wolny et al. 1997). Ang II can be degraded to Ang III or Ang (1-7) by angiotensinases and ACE2, respectively. ACE2 is a carboxypeptidase that also facilitates the conversion of Ang I to Ang (1-9). Ang (1-7) is a metabolite that antagonizes the vasoconstrictory effect of Ang II (Crackower et al. 2002) (Figure 1.1).

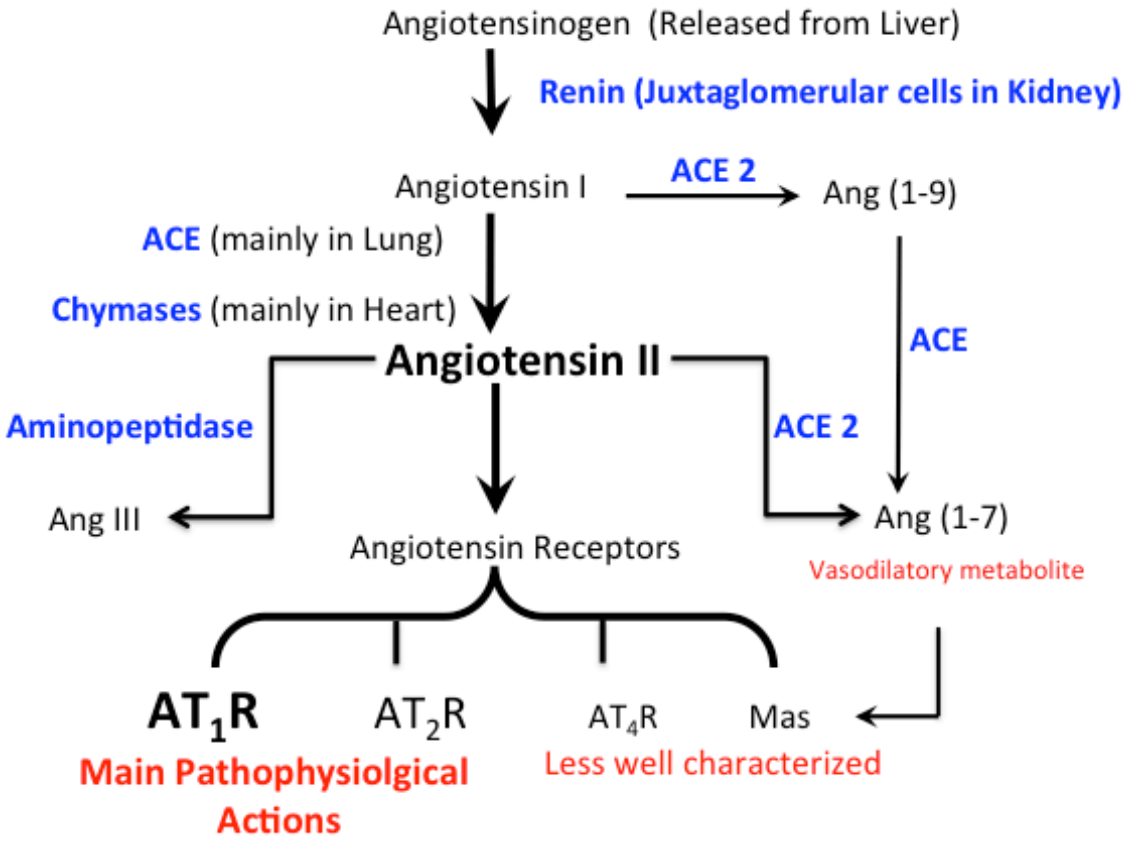

Figure 1.1: A Simple schematic representation of the main components of the renin angiotensin system (RAS). Angiotensinogen is released from the liver and is cleaved into Ang I by renin released from kidney. Ang I is activated into Ang II by Ang converting enzyme (ACE) found predominantly in lung. Main biological actions of Ang II are accomplished by AT_1R and AT_2R.

1.1.2. Angiotensin II

Ang II is the active regulatory effector peptide responsible for much of the RAS action via Ang II type 1 and type 2 receptors (AT_1Rs, AT_2Rs). As the primary effector molecule of the RAS system, Ang II has emerged as a critical hormone that directly constricts vascular smooth muscle cells, enhances myocardial contractility, stimulates aldosterone production and increases sodium reabsorption, stimulates release of catecholamines, increases sympathetic nervous system activity, and stimulates thirst and salt appetite (Bayorh et al. 2002, Ferrario et al. 2004, Paul et al. 2006, Kobori et al. 2007). Chronic effects of Ang II include promoting cell growth and migration, extracellular matrix deposition, vascular proliferation and tissue remodeling. Ang II serves as a focal point in integrating all of these complex processes to help maintain blood pressure and regulate blood flow to vital organs such as the heart and kidney (Mehta and Griendling 2007).

Structure-activity relationship (SAR) studies have shown that the Tyr^4, His^6, Phe^8 amino acid residues and the C-terminus of the Ang II peptide are critical to its biological activity. Additionally, the Val^3, Ile^5 and Pro^7 amino acid residues are proposed to be responsible for the conformational structure and folding of the peptide and thus are likely responsible for the proper orientation of the Ang II pharmacophore. Ang II has high affinity for AT_1R by maintaining multiple points of contact with the receptor. Interactions between the Tyr^4 residue in Ang II and Asn^{111} in transmembrane (TM) domain 3 of AT_1R and Phe^8 of Ang II and His^{256} of TM6 of the receptor are required to fully convert the receptor to its activated form (Noda et al. 1995, Noda et al. 1996). Furthermore, it is suggested that replacing the amino acid Asp^1 with Sar^1 actually enhances the agonistic activity and reduces degradation. This exchange, in combination with the replacement of

Phe[8] (which is known to be important for the biological activity of Ang II) with Ile[8], form the basis for the synthetic Sar[1],Ile[8]-Ang II peptide chemical structure. This peptide in turn forms the basis for the radioligand, [^{125}I]Sar[1],Ile[8]-Ang II, that is widely used to study Ang receptors (Tzakos et al. 2004).

1.1.3. Angiotensin II and the AT_1R in Disease

It is assumed that elevated Ang II levels may only become detrimental when the balance of the RAS is perturbed (due to genetic, environmental, and lifestyle factors such as elevated blood pressure (Danser 2010, Xu et al. 2010). Accumulated evidence from animal experiments suggests that over-stimulation of AT_1R by Ang II is implicated in the pathophysiology of various cardiovascular diseases, (Griendling et al. 1996, Pitt et al. 2000) such as hypertension, atherosclerosis, HF, fibrosis, thrombosis, coronary ischemia, LV and vascular hypertrophy, and inflammation (Ibrahim 2006, Higuchi et al. 2007). In humans, cardiac Ang II formation measured from aorta to coronary sinus, increased with the severity of HF (Serneri et al. 2001). Elevated levels of Ang II and subsequent over-stimulation of the AT_1R may also contribute to the pathophysiology of impaired glucose tolerance and hyperglycemia, glomerulosclerosis (Dzau and Re 1994) and renal failure (Kim and Iwao 2000).

However the interaction between Ang II and AT_1R in the kidney appear to be more complicated. Both AT_1R mRNA and specific Ang II binding were increased in cultured proximal tubes in response to infusion of Ang II indicating that Ang II positively regulates its own receptors in the proximal tubules (Cheng et al. 1995). This is unlike the condition in the renal glomerulus and vasculature, where AT_1R density is increased when Ang II levels are low and is reduced when Ang II is high (Gunther et al. 1980, Skorecki

et al. 1983). To summarize, the density of AT_1R in the kidney cortex may represent the averaging of the deferential expression of the receptors in the vasculature/glomeruli and proximal tubules.

1.1.4. Angiotensin II Receptors

Ang II binds to at least 3 different receptors, AT_1R, AT_2R and AT_4R (Berk 2003, Paul et al. 2006, Kobori et al. 2007). In addition, Ang II also binds to Mas receptors, but receptor action is less well characterized. While AT_1R is dominant in adult tissues, AT_2R is the main Ang II receptor in fetus. Some studies have shown that AT_2R may be expressed in response to disease (Masaki et al. 1998, Akishita et al. 2000, Akishita et al. 2000), while others have documented that AT_2R has the opposite downstream effects to AT_1R by promoting apoptosis, inhibiting growth, lowering blood pressure and reducing inflammation (Nakajima et al. 1995, Masaki et al. 1998).

Although less is known of the AT_4R, it is reported to be a vasodilatory peptide in most vascular beds. AT_4R is also detected in organs such as the heart, kidney and adrenal glands with well-characterized roles. In 2001, AT_4R was purified and identified as an insulin-regulated aminopeptidase (IRAP) (Albiston et al. 2001). There is a close association between the distribution of IRAP and GLUT4 within the insulin-responsive tissues suggesting that AT_4 ligands may play a role in modulating glucose uptake into cells (Albiston et al. 2001). Ang IV and AT_4R are involved in learning and memory in rodents. These effects are postulated to be mediated through binding to IRAP and prolonging the half-life of various neuropeptides in brain regions that are involved in cognitive processing (Chai et al. 2004). It was also found to improve memory in animal models of amnesia, and has potential for treatment of Alzheimer's disease (Lew et al.

2003). The physiological roles played by Ang IV and AT_4R in blood pressure and renal regulation remain uncertain, given that Ang IV can also activate AT_1Rs (reviewed in (Zhuo et al. 2013)).

Furthermore, new insights have been provided on the smaller peptide, Ang (1–7). It was reported to play beneficial cardiovascular, blood pressure, and renal hemodynamic effects (reviewed in (Dilauro and Burns 2009). Thirteen years ago, Mas was shown to be the functional receptor for Ang (1-7) in kidneys and other tissues (Santos et al. 2003). Subsequent studies primarily from Ferrario's group confirmed that Ang (1–7) has significant vasodepressor and antihypertensive actions in hypertensive animals or humans, which may counteract the actions of Ang II either directly or indirectly by stimulation of prostaglandins and nitric oxide (Ferrario 2006, Ferrario and Varagic 2010). However, other studies revealed that Ang-(1–7) may also activate AT_1R and AT_2R to induce similar effects as Ang II although the exact interaction is not clearly defined yet (reviewed in (Dilauro and Burns 2009) and (Zhuo et al. 2013)). Thus it is clear that controversies remain with respect to the specific roles of Ang (1-7) and Mas receptor. The most physiologically important and researched of these receptors is the AT_1R, which is the focus of my thesis project.

1.2. Angiotensin II Type 1 Receptor (AT_1R)

Most of the known physiological effects of Ang II are mediated by AT_1Rs, which are widely distributed in all organs, including liver, adrenals, brain, lung, kidney, heart, and vasculature (Table 1.1) (Mehta and Griendling 2007). Composed of 359 amino acids, the AT_1R (40 kDa) belongs to the seven-transmembrane superfamily of G protein-coupled receptors (GPCRs) (Timmermans et al. 1993, Paul et al. 2006). In rodents, two isoforms

have been identified that share 95% amino acid sequence identity (Iwai and Inagami 1992, Sandberg et al. 1992) but there are marked differences in the non-coding regions, suggesting possible variations in the mechanism of receptor transcriptional regulation. The $AT_{1A}R$ gene is localized on chromosome 17 q12 and the $AT_{1B}R$ on chromosome 2 q24 (Griendling et al. 1996). Pharmacologically and functionally, the two receptor subtypes are indistinguishable in regards to their ligand binding and signal transduction and activation properties (Gasc et al. 1994). However the two receptor subtypes, $AT_{1A}R$ and $AT_{1B}R$, are expressed in different proportions in different tissues. $AT_{1A}R$ mRNA is most prominent in cardiovascular tissues: kidney, heart, liver, adrenal gland, brain, lung, fat and gonads; whereas $AT_{1B}R$ expression is more dominant in endocrinal tissues such as the adrenal gland, pituitary gland, brain and testis in the adult mouse (Burson et al. 1994). In the rat kidney, 73% of AT_1Rs are $AT_{1A}R$ (Llorens-Cortes et al. 1994). *In vivo* experiments show that the $AT_{1A}R$ isoform may be more important than $AT_{1B}R$ in regulation of blood pressure, since mice with a disrupted AT_{1A} gene had lower blood pressure than controls and lost the normal pressor response to exogenous Ang II (Ito et al. 1995). By contrast large animals such as pig and dogs encode only one gene for the AT_1R similar to humans (Buxton and Brunton 1983, Iwai and Inagami 1992, Wagenaar et al. 2002). Hence they present a preferable transition and successful link translating basic imaging techniques and data analysis to applications in humans.

Table 1.1: Relative distribution of AT_1R in rat, rabbit and monkeys according to Chang and colleagues. Data is adapted from binding assays performed using [^{125}I]Sar1,Ile8- Ang II (Chang and Lotti 1991).

Species	Tissue	Counts (CPM /mg tissue)	Ratio
Rat	Adrenal cortex	23466	1460
	Kidney cortex	6284	391
	Aorta	122	7.61
	Brain	317	19.8
	Heart	16	1
Rabbit	Adrenal cortex	46582	1454
	Kidney cortex	1501	46.9
	Aorta	124	3.87
	Brain	114	3.54
	Heart	32	1
Monkey	Adrenal cortex	3848	316
	Kidney cortex	449	36.8
	Aorta	146	12
	Brain	63	5.19
	Heart	12	1

1.2.1. AT_1R Signaling

Traditionally, Ang II signaling pathway has been divided into two classifications: G protein and non-G protein related signaling. Evidence shows that upon activation by an agonist, AT_1R couples to $G_{\alpha q}$ and $G_{\alpha i}$ complexes (Ushio-Fukai et al. 1998), which inhibit adenylyl cyclase (AC) with subsequent decreased availability of cAMP; and activate effectors including phospholipase C (PLC), phospholipase A_2 (PLA_2), and phospholipase D (PLD), and ion channels, such as L-type and T-type voltage-sensitive calcium channels. Downstream second messengers such as inositol-1,4,5-triphosphate (IP_3), diacylglycerol (DAG), phosphatidic acid (PA) and arachidonic acid (AA) contribute to the vasoconstrictive properties of Ang II (Griendling et al. 1987, de Gasparo et al. 2000, Wagenaar et al. 2002, Kaschina and Unger 2003).

In addition to activating the G protein-dependent mechanisms, Ang II signals via several other intracellular pathways, including receptor tyrosine kinases and non-receptor tyrosine kinases, NADH/NADPH oxidases, and the nuclear factor-kappaB (NF-κB) pathway. Other G protein-independent signaling pathways include mitogen-activated protein (MAP) kinase, FAK and JAK/STAT that lead to phosphorylation of other kinases and transcription factors in the nucleus to promote cell proliferation and differentiation (Mehta and Griendling 2007) (Figure 1.2).

Acutely, increased levels of Ang II lead to enhanced AT_1R activation while, chronic exposure to Ang II downregulates its own receptors (Griendling et al. 1987, Lassegue et al. 1995, Touyz et al. 1999). The temporal pattern of signaling pathway activation is the most likely determinants of a particular functional response. For example, activation of the G protein-dependent pathway and generation of IP_3 occurs in seconds, while MAP

kinase and JAK/STAT activation occurs in minutes to hours (Schmitz et al. 1998, Marrero et al. 2004).

In addition to its roles in cardiovascular and renal disease, activation of the AT_1R promotes tumor progression and metastasis through its growth-promoting and proangiogenic activities and may also participate in the development of metabolic diseases (Hunyady and Catt 2006). It has been shown to transactivate other receptors like activation of epidermal growth factor receptor (EGFR) leading to synthesis of transforming growth factor β (TGF β) and fibronectin (Eguchi et al. 1998, Fukai et al. 1999). Ang II is also implicated in the upregulation of oxidized low-density lipoprotein receptor, LOX_1R, which may suggest a role for AT_1R in the progression of atherosclerosis (Li et al. 1999). Therefore, AT_1R activation of several signaling pathways makes it an intriguing target for therapy.

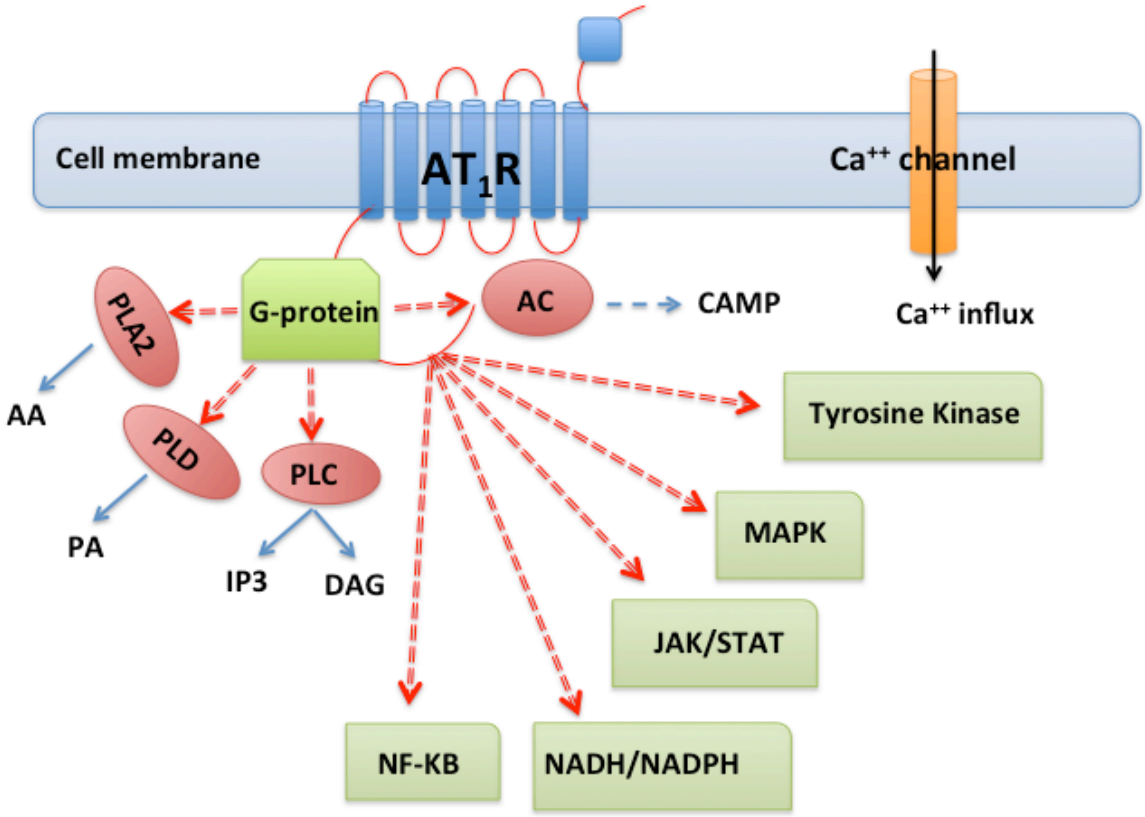

Figure 1.2: AT_1R signaling pathway. Ang II binding to AT_1R activates several signal transduction systems, including Gαq activation of the downstream effectors (PLC, PLA2 and PLD) generating intracellular second messengers (IP3, DAG, AA and PA) leading to sustained PKC activation, and sustained muscle contraction; Gαi inhibition of adenylyl cyclase (AC); opening of calcium channels contributing to the vasoconstriction. In addition, Ang II activates tyrosine kinases and mediates other growth stimulatory pathways, such as MAP kinases which are implicated in VSMC differentiation, proliferation, migration, and fibrosis. JAK/STAT activation is involved in promoting cellular survival, migration, adhesion, and apoptosis, nuclear-factor Kappa B (NF-κB) implicated in hypertension and inflammatory diseases. ANG II is also a potent mediator of oxidative stress NADH/NAPDH oxidative pathways.

1.2.2. AT_1R Regulation

Investigations of receptor expression in rodent vascular and renal cells focused on $AT_{1A}Rs$, as these are the predominant isoform in these cells (Burson et al. 1994). The rat $AT_{1A}R$ gene contains regulatory elements in the 5' flanking sequence that both positively and negatively regulate expression (Murasawa et al. 1993).

AT_1R signaling is regulated by similar mechanisms to other GPCRs. Short term regulation of receptor response is accomplished once Ang II binds to AT_1R and the receptor is phosphorylated (Oppermann et al. 1996, Balmforth et al. 1997, Van Kats et al. 1997) through protein kinase C (PKC) and GPCR kinases (GRKs) 2 and 5, resulting in desensitization (Oppermann et al. 1996). β-arrestin proteins (1 or 2) bind to the phosphorylated AT_1R, disrupting coupling to G proteins and attenuating further signaling through these pathways (Thomas et al. 1995, Ouali et al. 1997, Hunyady and Catt 2006). The phosphorylated receptor is now a target for endocytosis via clathrin-coated pits (Ouali et al. 1997, Ferguson 2001). Furthermore, *in vivo* evidence has emerged suggesting that G protein–independent signaling possibly transmitted via β-arrestins, can independently contribute to the development of cardiac hypertrophy and failure. β-arrestins, by acting as signaling scaffolds, initiate secondary waves of signal transduction independently of G proteins, at the same time as they uncouple GPCR. They may transmit G protein–independent signals that regulate VSMC migration and cardiomyocyte hypertrophy (reviewed in (Seachrist and Ferguson 2003, Drake et al. 2006). Notably, GPCR-bound β-arrestins activate the Src family tyrosine kinases, the ERK1/2, JNK3 and MAP kinase cascades; many of which are critical components of growth pathway activation. The E3 ubiquitin ligase, the cyclic AMP phosphodiesterase,

diacylglycerol kinase, the inhibitor of NF-κB and the Ser/Thr protein phosphatase are also among unique catalytic activity proteins that are recruited to β-arrestins. Additionally β-arrestins provide sub-cellular localization to the signaling cascade they induce, as compared to G protein signaling which diffuses throughout the cell all the way down to the cell nucleus (Luttrell and Gesty-Palmer 2010). The significance of this compartmentalization is that it affects the signaling events produced subsequently (reviewed in (Lymperopoulos and Negussie 2013).

The C-terminus has been shown to be essential for proper AT_1R internalization as receptors mutated to be lacking the C-terminus impairs Ang II induced endocytosis (Mukherjee et al. 1982, Thomas et al. 1995, Hunyady et al. 1996). The vesicles in which GPCRs endocytosis occur, are enriched with GPCR specific phosphatases (Ferguson 2001). If the cell requires AT_1R to be returned to the plasma membrane, GPCR phosphatases would act on the receptor, dephosphorylating it, and the receptor is recycled. Rab4 and Rab11, small GTPases, have been shown to be involved in the recycling of AT_1R (Seachrist and Ferguson 2003, Esseltine and Ferguson 2013). GPCR recycling may take minutes while internalization occurs within seconds.

Longer-term regulation of AT_1R expression occurs largely through transcriptional and post-transcriptional mechanisms (Guo and Inagami 1994, Nickenig and Bohm 1997, Sanders et al. 2005). Chronic stimulation of the AT_1R by its agonist, Ang II, decreases the receptor mRNA and protein expression (Gunther et al. 1980, Lassegue et al. 1995). The mechanism for this downregulation has been established to be decreased transcription (Lassegue et al. 1995) and/or decreased transcript stability (Nickenig 2002). This downregulation of AT_1R expression observed with Ang II stimulation is particularly

important in disease states characterized by an activated RAS.

1.2.3. AT_1R and Other Effectors

Estrogen (Nickenig et al. 2000) and EGF (Guo and Inagami 1994, Nickenig and Murphy 1994) have been demonstrated to downregulate AT_1R expression through a decreased rate of transcription (Nickenig and Murphy 1994) and post-translationally through decreased localization to the cell surface (Ullian et al. 2004).

Upregulation of AT_1R by other factors such as low-density lipoproteins, LDL (Nickenig and Bohm 1997) and insulin (Takayanagi et al. 1992) has also been illustrated. LDL treatment of rat vascular smooth muscle cells (VSMCs) increased AT_1R transcript and protein levels (Nickenig et al. 2000) by increasing transcript stability (Nickenig and Bohm 1997). The upregulation of AT_1R gene expression by insulin, like that of LDL, is accomplished by influencing the half-life of the mRNA transcript (Nickenig et al. 1998). The stabilization of the mRNA by insulin is proposed to involve MAP kinase proteins. Although post-transcriptional modulation of expression is the predominant mechanism in these cases, changes in protein expression are ultimately affected (Nickenig et al. 1998). Defective regulation of GPCRs occurs in numerous human diseases. On this account, changes in AT_1R protein expression can be investigated non-invasively *in vivo* using imaging modalities.

1.3. Tissue RAS

The RAS has been acknowledged as an endocrine, paracrine, autocrine, and intracrine system (Re 2003, Re and Cook 2006, Suzaki et al. 2006). Whereas the systemic RAS is seen as a regulator of blood volume, electrolyte balance and blood pressure, the local RAS is thought to be involved in growth (Gibbons et al. 1992, Itoh et al. 1993),

proliferation, protein synthesis, regional hemodynamic regulation, and organ function (Paul et al. 1993, de Gasparo et al. 2000). Various studies have demonstrated the presence of local RAS in the brain, heart, adrenal glands, and vasculature as well as in the kidney (Kunapuli and Kumar 1987, Allen et al. 1990, Dostal and Baker 1993, Allen et al. 2000). The main significance of tissue RAS is that it can be regulated independently of the circulatory RAS but still can interact with the latter.

1.3.1. Myocardial AT_1R Distribution

The predominant physiological role of the cardiac RAS is the maintenance of an appropriate cellular balance between inducing or inhibiting cell growth and proliferation as well as mediating adaptive responses to myocardial stress (Paul et al. 2006). Ang II mediates myocyte hypertrophy due to activation of the AT_1R as an adaptive response to increased myocardial stress. While hypertrophy of cardiomyocytes acts initially as a compensatory mechanism to preserve cardiac function, it becomes a major risk factor for congestive heart failure and sudden cardiac death and overall mortality (Mehta and Griendling 2007). Chronically, activation of the cardiac RAS may not only lead to cardiac hypertrophy and diastolic dysfunction but also to progressive systolic dysfunction, cardiac enlargement, and heart failure (Hunyady and Catt 2006). Both the AT_1 and the AT_2 receptors are expressed mostly localized on cardiomyocytes (Rogers et al. 1986, Booz and Baker 1996, Bader et al. 2001). Normal fibroblasts express AT_1R only but can recruit the AT_2R under certain pathological conditions (Senbonmatsu et al. 2000). Rat cardiac fibroblasts mainly express AT_1R, ranging from 65% to 100% (Villarreal et al. 1993, Matsubara et al. 1994) with maximum binding capacity of 31.4 ± 11.4 x 103 sites/cell (Crabos et al. 1994). In the human heart, the greatest density of AT_1R (>70%)

occurs in association with the conduction system and basal ganglia (Tsutsumi et al. 1998, Wharton et al. 1998), consistent with inotropic and chronotropic effects.

1.3.2. Renal AT_1R Distribution

Kidney cortex exhibits 40 fold higher expression than myocardium, as assessed by *in vitro* binding assay in monkeys (Chang and Lotti 1991). AT_1R are distributed in a 4:3 ratio between the medulla and the cortex (Tan et al. 2004, Huang et al. 2009), where AT_1R constitute >90% of total Ang II binding in the cortex. AT_1Rs are widely distributed on luminal membranes throughout the nephron segments, including proximal tubule, thick ascending limb of Loop of Henle, macula densa, distal tubule, and collecting ducts (Harrison-Bernard et al. 2002). In rats, the $AT_{1A}R$ is predominant in all nephron segments excepting the glomeruli, where the $AT_{1A}R$ and $AT_{1B}R$ roughly equivalent (Kakinuma et al. 1993, de Gasparo et al. 2000). Quantitative autoradiography in rats demonstrated AT_1R density in the kidney as: 1,186±73 in the medulla and 872±35 fmol/mg in the cortex (Huang et al. 2009). Presence of a distinct intra-renal RAS provides a complexity in interpreting the role of this system, thus local AT_1R is considered critical receptors in cardiovascular and renal pathophysiology. It is important to note that in rat heart, the AT_1R density is very low and is approximately 400 fold lower than in the kidneys (Chang and Lotti 1991), which makes the AT_1Rs in heart easily saturated and can be largely affected by the injected dose and specific activity (lower specific activity = higher mass) of tracer used for positron emission tomography (PET) imaging.

Although almost every organ in the body has elements of RAS, the kidney is unique in having every component of the RAS with compartmentalization between the tubular and interstitial networks as well as their intracellular accumulation. Renin is released

primarily from the juxtaglomerular cells on the afferent arterioles of the kidney. Intrarenal Angiotensinogen is synthesized in the epithelial cells of the proximal tubule. In the human kidney, ACE is localized primarily on the brush border membrane of the proximal tubule, whereas in rats, ACE is expressed mainly on the endothelial cells of the renal microvasculature (Kobori et al. 2007).

1.4. Role of AT_1R in Cardiovascular Diseases

The locally generated, rather than the circulating Ang II, initiate many of the deleterious actions attributed to AT_1R activation (Hunyady and Catt 2006). Accumulated evidence from animal experiments suggests that over-stimulation of AT_1R by Ang II is implicated in the pathophysiology of various cardiovascular diseases, (Griendling et al. 1996, Pitt et al. 2000, Cohn and Tognoni 2001) such as hypertension, atherosclerosis, heart failure (HF), fibrosis, thrombosis, coronary ischemia, left ventricle (LV) hypertrophy, and inflammation (Dzau and Re 1994, Ibrahim 2006, Higuchi et al. 2007, Dimitrijevic et al. 2009). The effects of the RAS as it pertains to the cardiovascular system are mediated by direct action on the vasculature, AT_1R in kidney (Crowley et al. 2005, Crowley et al. 2006) and brain (Veerasingham and Raizada 2003).

In addition, AT_1R also mediates overproduction of reactive oxygen species that amplifies AT_1R signaling in cardiovascular cells, leukocytes, and monocytes inducing potent growth-promoting, proinflammatory, and profibrotic actions (Hunyady and Catt 2006). A complex cellular and molecular mechanisms produces the dynamic sequence of events that alter the tissue structure and function, thereby molecular imaging and quantification of AT_1R during its involvement in these processes may improve the therapeutic interventions in the future.

1.4.1. AT_1R in Myocardial Infarction and Heart Failure

Changes in local RAS activity play an important role in the pathology of ventricular hypertrophy, myocardial infarction (MI), cardiac remodeling and HF. Expression of myocardial RAS components including angiotensinogen, ACE, Ang II and AT_1R are increased in the heart after MI (Takano et al. 2003). Increased AT_1 mRNA and/or upregulation of AT_1Rs have been observed in the heart and vessel walls in post-MI animal models, and after mechanical injury, stretch or turbulence, or LV pressure overload (Zhang et al. 1995, Wang et al. 1997, Sun et al. 2007). In post-infarct models these changes may vary with animal model and time post-MI, being more increased in the early weeks post-MI (Leenen et al. 1999, Silvestre et al. 1999, Van Kats et al. 1999). In a rat model of MI (induced by left anterior descending coronary artery ligation), cardiac and plasma Ang II levels were markedly increased at 3 (Oyamada et al. 2010) and 6 hours after surgery. Plasma Ang II remained significantly increased at 1, 4, and 8 weeks post-MI, whereas cardiac Ang II levels were normalized by 4 weeks (Leenen et al. 1999). In another study, increases by 7-9 fold were reported in the infracted area myocardium and 3-4 fold in contralateral normal zone myocardium at 4 weeks post-MI (Tan et al. 2004). Interesting to be noted in the later study, renal AT_1R binding was significantly decreased (10-20%) in the renal medulla of rats with large (greater than 30%) infarcts and showed minor decrease in the cortex (Tan et al. 2004).

Several neurohormonal alterations including but not limited to Ang II, norepinephrine, and endothelin (McAlpine et al. 1988, Packer 1992, Yousef et al. 2000) provide an initial adaptive role but can contribute adversely to ventricular dilatation and development of HF: the so-called neurohormonal hypothesis (Packer 1992). Acute MI results in reduction

of the regional ventricular function and a complex series of compensatory responses termed "ventricular remodeling" often follows depending on the extent of ischemic injury and necrosis (Packer 1992, Yousef et al. 2000, Pfeffer et al. 2003, Yusuf et al. 2003). Studies of explanted LV myocardium of patients with end-stage HF displayed down-regulation of AT_1Rs and reduced AT_1 mRNA (Regitz-Zagrosek et al. 1995, Wharton et al. 1998). The reduction in AT_1R levels is related to increased Ang II stimulation, similar to the effects of excess catecholamines and beta-adrenergic receptor (β-AR) down-regulation in HF (Asano et al. 1997, Schultz et al. 2002). This AT_1R downregulation is likely to be favorable in patients with heart failure to blunt the response of the failing heart to enhanced production of Ang II. However it is argued in other studies that this may represent end–stage events. Circulating Ang II exerts systemic effects through vasoconstriction and aldosterone release leading to Na^+ and fluid retention subsequently increase heart afterload (Packer 1992, Yousef et al. 2000). HF represents the final common pathway for most forms of heart disease.

Accordingly, RAS blockade improve hemodynamics and attenuate LV remodeling post-MI, reducing early and late morbidity and mortality in multiple clinical trials (The CONSENSUS Trial Study Group 1987, Pfeffer et al. 1992, Dzau et al. 2001, Yusuf et al. 2003).

1.4.2. AT_1R in Hypertension

The fundamental role played by RAS through AT_1R in the pathogenesis of hypertension and target organ damage has been firmly established in animal models and human studies (Gavras et al. 1971, Brunner et al. 1972, Ito et al. 1995, Brenner et al. 2001). RAS is the master regulator of blood pressure and fluid homeostasis through actions of AT_1Rs both

inside and outside the kidney. Accordingly, RAS blockers are the most widely prescribed treatment for hypertension (Laight 2009). Homozygous mice for null mutations in the genes encoding angiotensinogen, renin, ACE, or $AT_{1A}R$ have marked reductions in blood pressure, indicating that these genes constitute a major pathway mediating the effects of the RAS in the control of blood (Ito et al. 1995, Kim et al. 1995, Esther et al. 1996, Krege et al. 1997). In elegant serial studies by Crowley et al (Crowley et al. 2005, Crowley et al. 2006, Crowley and Coffman 2008, Crowley et al. 2011), the contribution of AT_1R in the kidney vs. other tissues (vascular system, brain, adrenals) to hypertension was explored using kidney cross-transplantation method between mice lacking the dominant murine $AT_{1A}R$ and genetically matched wild-type. It was demonstrated that kidney and systemic AT_1Rs make equivalent contributions to normal blood pressure homeostasis, whereas in a hypertensive setting (through chronic Ang II infusion), the activation of AT_1R in the kidney only mediates the chronic hypertensive effects of Ang II possibly through promoting renal sodium reabsorption. Thereby a reliable non-invasive means for measuring AT_1R expression in the kidney will provide novel opportunities for optimizing treatments for hypertension and its complications.

1.5. AT_1R in Diabetes

Complications arising from diabetes have been associated with changes in AT_1R expression levels. Myocardial AT_1R mRNA upregulation was reported in diabetic rats 14 days after streptozotocin treatment (Sechi et al. 1994, Tzakos et al. 2004), and this was translated to increased LV AT_1R density at 4 and 12 weeks, and at 12 weeks in the liver and the adrenals. In addition, elevated levels of Ang II and subsequent over-stimulation of the AT_1R may also contribute to the pathophysiology of impaired glucose tolerance

and hyperglycemia, glomerulosclerosis (Kim and Iwao 2000) and renal failure (Dzau and Re 1994), thus development of diabetic nephropathy. On the other hand, AT_1R expression was reported to be reduced in the kidney at 12 weeks (Brown et al. 1997). Clinical evidence suggests that diabetic nephropathy and glomerulonephritis is associated with lower kidney AT_1R mRNA in patients (Wagner et al. 1999). Recently, landmark clinical trials investigating ACE inhibitors (ACEIs) and AT_1R blockers (ARBs) have demonstrated renal protection in patients with diabetes (Viberti et al. 1994, Brenner et al. 2001, Lewis et al. 2001). In fact, widespread use of RAS blockade as first-line treatment for albuminuria and associated hypertension in Type 1 and Type 2 diabetes mellitus has incorporated this approach into international guidelines (Kintscher et al. 2008). The ONTARGET study (Teo et al. 2004) and the HOPE trial (Yusuf et al. 2000) provided definite results demonstrating that blocking the AT_1R and activating PPARγ agonist with telmisartan is as good as ACE-inhibition with the "gold standard" ramipril in management of diabetic patients and prevention of cardiovascular complications. This evidence implicates the RAS and the AT_1R in the development and pathology of diabetes.

1.6. Chronic Kidney Diseases (CKD)

Chronic kidney disease (CKD) is a life-threatening condition characterized by progressive and irreversible loss of renal function. The clinical definition of CKD is the presence of kidney damage or reduced kidney function for more than 3 months and requires either a measured or estimated glomerular filtration rate (eGFR) of less than 60 mL/min per 1.73 m^2, or the presence of abnormalities in urine sediment, renal imaging or biopsy results (National Kidney 2002). Table 2.1 displays the classification of stages of

chronic kidney disease from the Kidney Disease: Improving Global Outcomes (KDIGO). As the disease progresses, the kidneys lose the ability to properly clear the blood from waste products leading to the need for renal replacement therapy in order to prevent azotemia, systemic organ failure and death. Given the complexity and still poor outcome of CKD, it was recommended by the Canadian Society of Nephrology in the guidelines for optimal management of CKD to provide shared care of these patients by general practitioners and specialists, including internists, endocrinologists, cardiologists and nephrologists (Levin et al. 2008).

CKD is recognized as an independent risk factor for cardiovascular-related morbidities (including hypertension, LV hypertrophies, both systolic and diastolic dysfunctions, autonomic neuropathy and arrhythmia) and all cause mortality (Sarnak et al. 2003, Go et al. 2004, Levey et al. 2007). Furthermore, the leading cause of death in chronic renal failure is known to be due to cardiovascular diseases mainly heart failure or ischemic heart disease (Kennedy et al. 2008, Sviglerova et al. 2010). The inter-relationships and bidirectional natures of heart and kidney diseases represent the pathophysiological basis for a clinical entity that is called cardiorenal syndrome (Shiba and Shimokawa 2011).

Table 1.2: Stages of CKD according to the Kidney Disease: Improving Global Outcomes KDIGO (National Kidney 2002)

Stage	Description	GFR (ml/min/1.73m^2)
1	Kidney damage with normal or increased GFR	> 90
2	Kidney damage with mild decrease in GFR	60-89
3	Moderate decrease in GFR	30-59
4	Severe decrease in GFR	15-29
5	Kidney failure (ESRD)	<15 (or dialysis)

1.6.1. Epidemiology and Prevalence

CKD is becoming a major public health problem as the incidence of the disease is increasing annually at a rate of 8%, and consumes up to 2% of the global health expenditure (Levin et al. 2008). It is estimated to affect 12.5% of Canadian adults (about 3 million) during the period 2007-2009 (Arora et al. 2013). In the United States, the 1999–2004 National Health and Nutrition Examination Survey reported a prevalence of 5.0% for stage 1 and 2 disease and 8.1% for stage 3 and 4 disease (Coresh et al. 2007, Levey and Coresh 2012). Moreover it is estimated that over 10% of adult population in developed countries suffer some degree of CKD (de Zeeuw et al. 2005). It is intriguing to note that according to the survey by Arora et al in 2013, the estimated prevalence of diabetes, hypertension and hypertriglyceridemia were more prevalent among Canadian adults with CKD than among those without it. These findings highlight the need for early intervention and secondary prevention of CKD (Arora et al. 2013).

1.6.2. Etiology and Pathophysiology

Diabetes and hypertension represent the two leading causes of CKD. Other common causes include glomerulonephritis, renal vascular disease, ureteral obstruction, autoimmune (glomerular and interstitial), and genetic alterations diseases. However, as the disease progresses, a common renal phenotype develops regardless of the etiology (Lopez-Novoa et al. 2010). The pathophysiological events involved in the progression of many nephropathies are similar regardless of their etiology, whether it is due to glomerular insult such as hypertensive nephropathy or tubular as in subtotal nephrectomy and ureteric obstruction. The persistence of the initial insult eventually activates common inflammatory pathways (TGF-β, NF-κB and JNK pathways), cytokine imbalance,

which activates other cell types and contributes to fibrosis, mesangial and vascular contraction leading to reduced GFR, tubular degeneration, extracellular matrix deposition and scarring (Lopez-Novoa et al. 2010). Hemodynamic and cellular factors play pivotal roles in the pathophysiology of CKD. Inappropriate activation of RAS and glomerular hyperfiltration synergistically contribute to glomerular epithelial cells damage and hypertrophy (if hypertension is present). This leads to proteinuria that provokes more interstitial tissue inflammation and fibrosis that aggravates the renal damage (Brewster and Perazella 2004). The induced pressure and volume overloads, and CKD associated non-hemodynamic factors results in damage and dysfunction of the cardiac tissue and vasculature (Figure 1.3).

Several models have been developed in animals to help understanding the pathophysiological mechanism involved in their onset and progression. In this sense, animal models have emerged as vital tools for understanding the mechanisms implicated in the pathogenic process, and also for assessment of novel therapeutic interventions at the preclinical level.

1.6.3. Subtotal Nephrectomy Animal Model of CKD

Significant renal mass reduction is associated with a chain of events that culminates in hypertension, inflammation and sympathetic overactivation, progressive proteinuria, glomerulosclerosis and CKD (Parmar 2002, Koomans et al. 2004, Kerr 2006, Vaziri et al. 2007, Garrido et al. 2009). As a consequence of renal mass reduction, the number of functional nephrons is dramatically reduced and becomes replaced with fibrosis and scarring (Garber et al. 2003, Prieto et al. 2005). Consequently the remnant nephrons increase their filtration rate in order to maintain the excretory function. However, over

time the compensatory mechanisms become maladaptive and contribute to the deterioration of the remnant kidney function i.e. development of CKD. Experimentally, the 5/6 nephrectomy (Nx) rodent model is used to study CKD (Strauch and Gretz 1988) which is achieved by either surgical resection, ligation of branches of the renal artery, or a combination of both procedures (Blankestijn 2004, Koomans et al. 2004, Garrido et al. 2009). The severity of renal damage is time dependent as well as on other determinants that include the extent of renal mass reduction, genetic background, sex and age of animals. An important limitation of this model to be considered is that the abrupt and extensive loss of renal mass does not occur in human diseases, where a more gradual loss of nephrons is observed (Lopez-Novoa et al. 2010).

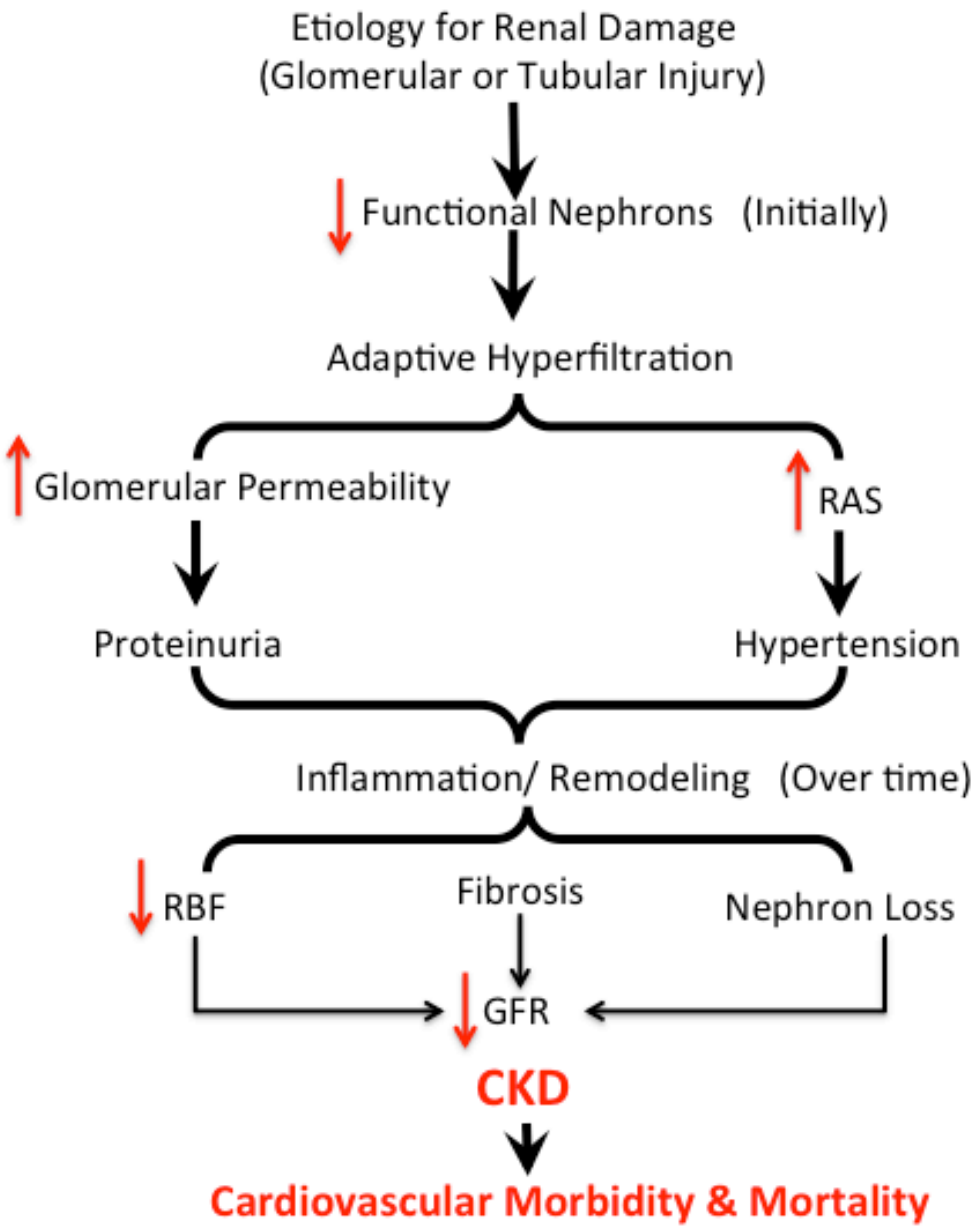

Figure 1.3: Regardless of the etiology causing renal mass reduction, the number of nephrons decreases during the progression of CKD. The remaining nephrons increase their filtration rate in order to maintain the excretory renal function. Initially there is adaptive hyperfiltration in the remaining glomeruli to compensate for the lost ones, which causes proteinuria, and activates the RAS that consequently elevates the blood pressure. However, over time inflammation and remodeling occurs due to detrimental adaptation by the kidney. This leads to decrease in renal blood flow; fibrosis and the remaining nephrons eventually lose their function. Progressive decline in GFR results in renal dysfunction and cardiovascular complications occur. RAS: renin angiotensin system; RBF: renal blood flow; GFR: glomerular filtration rate; CKD: chronic kidney disease.

1.6.4. Role of AT_1R in CKD

The critical importance of kidney AT_1Rs has been demonstrated on AT_{1A} knockout animals, which were protected from development of hypertension in response to Ang II or unilateral renal arterial constriction (Cervenka et al. 2008, Crowley et al. 2011). In a very prestigious series of experiments done by the same group, using the AT_{1A} knockout mice and kidney cross-transplantation; Crowley et al proved that in Ang II dependent hypertension, the elevated blood pressure and the consequent development of cardiac hypertrophy are caused primarily by the activation of renal AT_1R (Crowley et al. 2006, Crowley and Coffman 2008). By contrast, other research groups suggested that AT_1R plays a role in hypertrophy because of the increase in cardiac AT_1R expression and the beneficial effect of AT_1R blockade (Le Corvoisier et al. 2010, Sukumaran et al. 2010).

Previous studies examining the intrarenal RAS (mainly AT_1R expression) in CKD models have yielded conflicting results that may reflect differences in methodology and/or time points of measurements. Joly et al reported a decrease (30-40%) in AT_1R mRNA levels in cortex and outer medulla at 4 weeks post-surgery (Joly et al. 2005). Whereas no change was found in AT_1R protein expression at the same time-point in a study by Dilauro et al (Dilauro et al. 2010). Another study reported that at 8 weeks post-surgery, there was an increase (>70%) in AT_1R by Western blot (Vaziri et al. 2007).

1.7. Antihypertensive Therapy

In patients with CKD, hypertension is treated to slow progression of kidney disease and to reduce cardiovascular risk. On the basis of evidence from both prospective cohort studies and randomized clinical trials, blood pressure should be targeted to < 130/80 mmHg.

As per knowledge acquired in the last few decades from numerous landmark clinical trials, RAS inhibition is considered as first line therapy for the majority of patients with CKD either due to diabetic or non-diabetic etiology (Maschio et al. 1996, Brenner et al. 2001, Lewis et al. 2001, Brewster and Perazella 2004). However, multiple agents are frequently required to reduce the blood pressure and proteinuria for better renal and cardiovascular outcomes (Kereiakes et al. 2010, Ito et al. 2012, Kereiakes et al. 2012). For instance, thiazide diuretics are effective in combination with RAS inhibitors and can be considered as additive therapy for control of hypertension. Other antihypertensive agents include beta-blockers or long acting calcium channel blockers (CCBs) are also commonly prescribed (Levin et al. 2008).

1.7.1. RAS Inhibition

RAS blockade by ACEIs and ARBs reduce morbidity and mortality in hypertension, atherosclerosis, HF, stroke, diabetes and CKD (Yusuf et al. 2000, Maggioni et al. 2002, McMurray et al. 2003, Hanif et al. 2010). ACEIs (e.g. enalapril, ramipril, lisinopril and fosinopril) act directly by reducing Ang II synthesis, whereas ARBs (e.g. losartan, valsartan, candesartan, and telmisartan) prevent binding of Ang II to AT_1R. Both classes of drugs are clinically approved, have good pharmacological profiles and are equally effective. However other indirect mechanisms of action for ACEIs need to be highlighted: i) by inhibiting Ang II, they also prevent activation of AT_4R which has been implicated in the induction of expression of the fibrogenic and thrombotic factor, plasminogen activator inhibitor (PAI)-1 (Fogo 1999); ii) they inhibit the degradation of the vasodilatory peptide, bradykinin that has cardioprotective effect (Yang et al. 1970, Tanaka et al. 2004); and iii) they have indirect favorable pleiotropic effects as reducing

cardiac cytokine expression, oxidative stress, tissue injury and by improving cardiac hemodynamics (Ikeda et al. 1995, Kapadia et al. 1997).

Finally, it can be speculated that the combination of ACEIs and ARBs would theoretically offer more beneficial effect but it has been difficult to determine if the observed favorable effects on proteinuria are due to dual RAS blockade or just better blood pressure control (Opie and Sack 2001, Ranade and Somberg 2002, Makino et al. 2003, Levin et al. 2008). As a matter of fact, a number of trials and meta-analyses have demonstrated that combination ACEI and ARB therapies have a greater antiproteinuric effect than either agent alone (Catapano et al. 2008, Kunz et al. 2008, Susantitaphong et al. 2013). By contrast, lack of proven benefit like reduction of cardiovascular disease risk or death and even potential harms were demonstrated in various large trials (e.g. ONTARGET, ALTITUDE, VA NEPHRON-D). In addition, combination therapy increased the incidence of serious side effects as hyperkalemia and hypotension and significantly increased the risk of ESRD (Susantitaphong et al. 2013).

Other RAS blockers include aldosterone antagonists (e.g. Spironolactone) and direct renin inhibitors (e.g. aliskiren) might have a potential usage for the therapeutic management of CKD (Azizi et al. 2006, Perico et al. 2008) although to date, the impact of this approach has not been investigated and it presents an issue that needs to be addressed (Levin et al. 2008). Hence the intrarenal molecular effects of different treatments can be translated directly to clinical setting through PET imaging of AT_1R and consequently can help optimize and individualize therapy.

1.7.2. Calcium Channel Blockers (CCBs)

Although there is compelling rational for the use of RAS inhibitors as ACEI specifically

in kidney disease due to its class specific blood pressure independent renoprotection, other antihypertensives given alone such as CCBs can be equally effective in attenuating hypertension induced renal damage progression, when administered during non-proteinuric stages of disease (Black et al. 1998, Brown et al. 2000, Hansson et al. 2000, Officers et al. 2002, Wright et al. 2002). The efficiency of CCBs has been revealed in several clinical trials including the ALLHAT, VALUE, INVEST studies, the CONVINCE trial and NORdic DILtiazem (NORDIL) study (reviewed in (Nathan et al. 2005, Segura et al. 2005, Bidani and Griffin 2006).

CCBs are a family of compounds that inhibit L-type and T-type voltage dependent calcium channels. They are divided into 2 main classes: dihydropyridine (e.g. nifedipine, amlodipine and nicardipine) or non-dihydropyridine (verapamil and diltiazem) which vary in their mode of action. Non-dihydropyridines have negative inotropic effect in addition to the main vasodilation action, whereas dihydropyridines are selective for the vasculature. However, non-dihydropyridines are substantially more effective and are preferred in overtly proteinuric kidney disease and renal dysfunction (Nathan et al. 2005, Lopez-Novoa et al. 2010). The mechanisms underlying this varied effect on proteinuria may be due to the preferential afferent arteriolar dilatation induced by dihydropyridines CCBs, which allows more of the systemic blood pressure to be transmitted to the glomerulus enhancing proteinuria and progression of nephropathy (Bakris et al. 2004). Other factors that play a role in this varied effect are: the differential abilities of the non-dihydropyridine and dihydropyridine CCBs to alter renal autoregulation and the permeability of the glomerulus (Agodoa et al. 2001, Bakris et al. 2004, Kunz et al. 2008). Based on a systematic review by Bakris et al, combination of either classes of CCBs with

ACEIs or ARBs in hypertensive patients with nephropathy associated with proteinuria, induce similar reductions in blood pressure, however the mean change in proteinuria was minus 39% and plus 2% for non-dihydropyridines and dihydropyridines, respectively (Bakris et al. 2004).

1.8. Positron Emission Tomography (PET)

PET is a non-invasive nuclear imaging modality used to measure both molecular and cellular functions *in vivo* serially in the same subject reducing intersubject variability. It is a technology that allows dynamic visualization of the distribution of a radiolabeled biological or pharmacological ligand, substrate or analogue with high spatial (5-10 mm) and temporal resolution (5-10 s) (Wahl 2002). The basic principle/ advantage behind PET radioligands involves the substitution of C, N, O or OH atoms/groups in biological compounds with a radioactive isotope, such as C-11, N-13, O-15 and F-18 thereby, maintaining the chemical, biological and pharmacodynamics of the parent compound. PET isotopes are 'unstable' containing a higher number of protons than neutrons (Finn and Schlyer 2002). Upon its administration to the subject, the isotope undergoes β-decay, releasing a positron (e+) which travels for a short distance in the target tissue and meets an electron (e-) and the annihilation of both particles occur generating two gamma photons (γ) of 511 keV moving in opposite direction at approximately 180^{o} from each other. These photons are then detected coincidentally by scintillator crystals paired to photomultiplier tubes positioned in a cylindrical arrangement in the PET camera (Figure 1.4). Computerized iterative and non-iterative reconstruction algorithms generate a map of the activity distribution within the field of view (FOV) over time, producing a dynamic image and time-activity curve (TAC) for various regions of interest (ROI) in the subject

(Koeppe 2002, Thompson 2002).

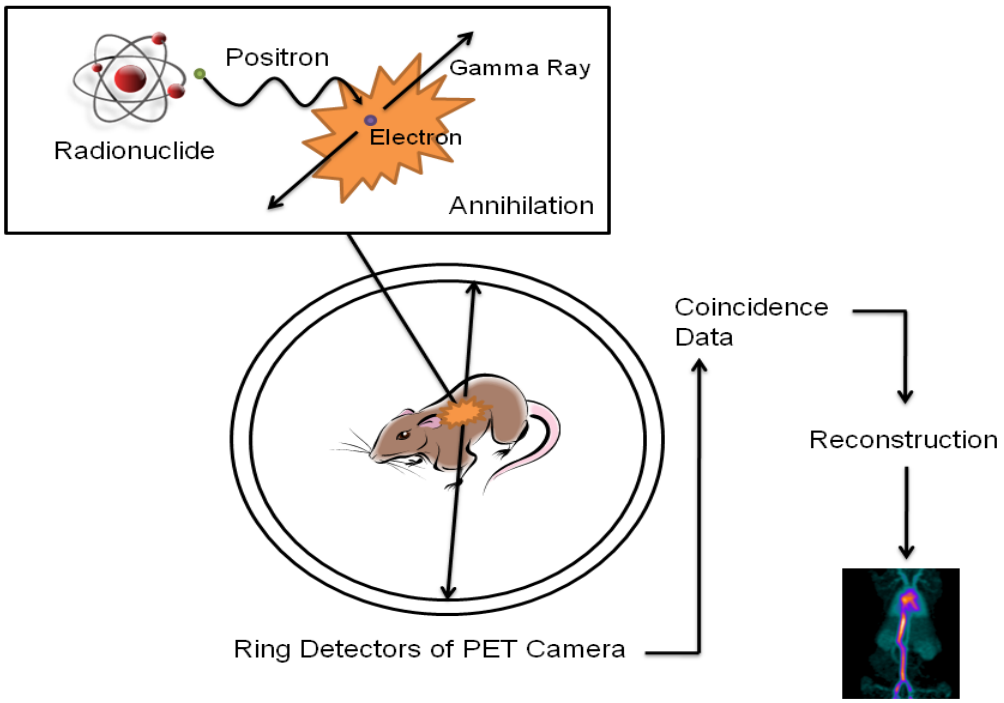

Figure 1.4: Representation of a PET scanning and radioactive positron decay. The basic principles behind PET involve the detection of a radioactive atom, such as carbon-11 and fluro-18 using a specialized scintillation crystal detection system in the PET camera. Upon decay of the radionuclide, a positron (e+) is emitted which meets an electron (e-) and the annihilation of both particles occur and release two gamma photons (γ) moving in opposite direction at approximately 180^{o} from each other. Scintillation crystals in detector rings detect the 511 keV gamma rays to produce a three dimensional PET image.

1.8.1. Small Animal PET

The development of small animal imaging technology has facilitated the application of clinical PET radiotracers for research studies in rodents allowing for accurate assessment of pathogenesis and pharmacological agent efficacy. The human cameras were developed to have increased image resolution and sensitivity by utilizing smaller crystals with a smaller detector ring diameter, and longer axial coverage. This alteration was needed to have the ability to image small animal ROI. The use of small animal PET in experimental work allows: i) full tracer kinetic evaluation providing dynamic measurement of radiotracer uptake and clearance as opposed to only one time-point for *ex vivo* dissection, and ii) possibility of repeated PET imaging using each animal as its own control, before and at various stages of a treatment. Small animal PET is a valuable tool in the investigation of the critical role of AT_1R in various cardiovascular diseases.

1.8.2. Blood flow PET Imaging

Various tracers that include rubidium-82, O-15 water or N-13 ammonia have been used widely in clinic for assessment of blood flow with imaging. Ideally, the blood flow tracer should be inert however it is not a necessary requirement. Dynamic PET with ammonia has demonstrated excellent imaging quality for absolute quantification of myocardial blood flow (MBF) despite the fact that it is rapidly metabolized. [^{13}N]-ammonia is a cyclotron product that has a physical half-life of 9.96 min. After injection, [^{13}N]-ammonia is rapidly extracted from the circulation, and is metabolically trapped in the cell as glutamine (Alpert et al. 2002). For the former fact, consideration for flow dependent changes and/ or metabolic correction may be needed to quantify blood with [^{13}N]-ammonia.

Renal blood flow (RBF) assessment with PET is feasible in research and humans; it represents a quantitative, low-risk, and minimally invasive intervention. Several reports have described methods measurement of RBF with PET. Chen et al has validated [^{13}]N-ammonia as a flow tracer for measurement of local RBF in dogs, results were compared with simultaneously acquired microsphere blood flow measurement (a gold standard for RBF quantification) (Chen et al. 1992). The same group has extended the same technique with PET [^{13}]N-ammonia in swine (Killion et al. 1993) and healthy human subjects (Nitzsche et al. 1993) confirming the accuracy and reproducibility of RBF estimates. Additionally, the values obtained with [^{13}]N-ammonia correlated well with O-15 water and rubidium-82 measurements of RBF documented in other research studies (Alpert et al. 2002).

1.8.3. RAS targets for PET Imaging

A potential determinant for the marked interindividual variability in response to RAS blockade may be the presence of local RAS, which is largely independent of its systemic component and not accessible to routine lab testing. In view of the aforementioned, the identification and characterization of local RAS system with molecular imaging probes is highly desirable. It is anticipated that such an investigative approach would provide more precise cellular and molecular information to monitor the response to therapy. Presently, AT_1R and ACE were the only RAS components to be targeted by successfully developed radioligands. AT_1R radioligands are discussed in details in the following sections. ACE radioligands included ^{11}C-zofenoprilat, ^{125}I-iodotyrosyl-lisinopril, ^{18}F-fluorobenzoyl-lisinopril, ^{99m}Tc-(CO)3D(C8)-lisinopril and ^{18}F-fluorocaptopril (reviewed in (Schindler and Dilsizian 2012).

1.8.4. AT_1R PET Radioligands

Previous characterization studies and initial testing of AT_1R radioligands have been performed. [^{11}C]MK-996 was the first AT_1R PET radioligand reported in the literature by Mathew et al. (Mathews et al. 1995). However due to difficulty of tracer synthesis, further reports were not published and [^{11}C]L-159,884 was synthesized by the same group (Hamill et al. 1996). [^{11}C]L-159,884 displayed *ex vivo* specific binding for AT_1R over AT_2,R , α and β- adrenergic receptors in the kidney, heart and lung of CD-1 mice (Kim et al. 1996). *In vivo* PET imaging was performed in Beagle dogs and baboons with the same tracer and confirmed its specific binding for renal AT_1R (Kim et al. 1996, Szabo et al. 1998). This was followed by the development of a new tracer, [^{11}C]KR31173 that showed higher specificity and less metabolism compared to [^{11}C]L-159,884 (Mathews 2003, Mathews et al. 2004). First PET imaging with [^{11}C]KR31173 was done in mice, dogs and baboons to determine the *in vivo* binding characteristics. In all three species, renal and adrenal tissues had the highest tracer uptake (Zober et al. 2006). From these experiments, it was determined that [^{11}C]KR31173 would be most appropriate to investigate AT_1R changes in animal disease models and future human PET studies (this topic will further be discussed in the following section 1.7.3.3.). See Figure 1.5 for the chemical structures of the PET tracers developed by the John Hopkins group.

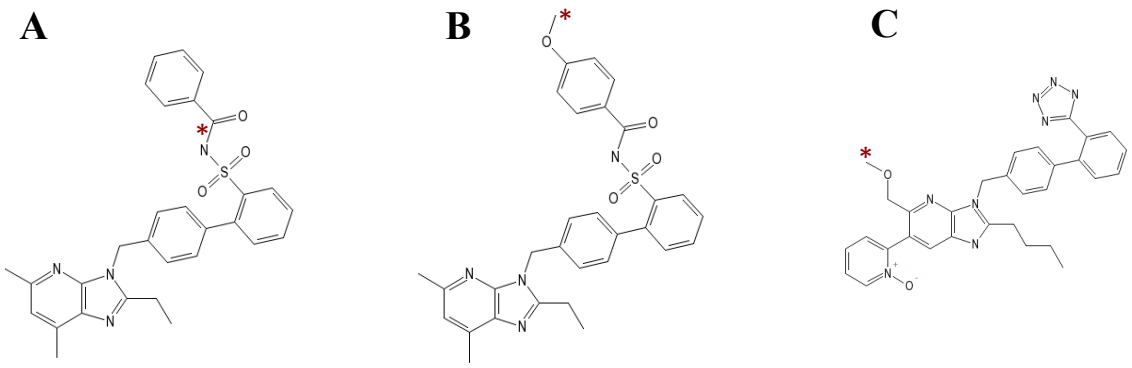

Figure 1.5: Chemical structures of the Johns Hopkins radiotracers. (A) [^{11}C]MK-996, (B) [^{11}C]L-159,884 and (C) [^{11}C]KR31173. C-11 radioactive atom position indicated by asterisk.

Likewise, our group at the University of Ottawa Heart Institute (Ottawa, Canada) has developed AT_1R PET radiotracers that are analogs of the clinically used ARBs (Figure 1.6). To increase the likelihood of success, we have chosen several compounds with different pharmacokinetics to explore. Peptide SAR studies identified the Tyr^4, His^6 and Phe^8 amino acids as important for Ang II binding and activation of AT_1R. It is suggested that the arrangement of these amino acids resembles that of the tetrazole-biphenyl ring conformation in most of the ARBs (Tzakos et al. 2004) (Figure 1.6).

Thus, [^{11}C]methyl-candesartan and its desethyl derivative [^{11}C]TH4 were synthesized as two potential AT_1R radioligands and evaluated by *ex vivo* experiments. They displayed high retention in the kidney and specificity and selectivity for AT_1R over the AT_2R, Mas, β-adrenergic and α_2-adrenergic receptors (Hadizad et al. 2009). Because of the reduced selectivity of [^{11}C]TH4, additional characterization experiments and initial *in vivo* PET modeling was performed with [^{11}C]methyl-candesartan only (Lortie et al. 2013). Afterwards, [^{11}C]methyl-losartan was synthesized by O-[^{11}C]methylation of the insurmountable AT_1R antagonist, losartan in an attempt to increase tracer retention for renal AT_1R. Previous SAR studies revealed that the imidazole 5-position can be altered and that O-methyl-losartan displays similar binding affinity to losartan for AT_1Rs (IC_{50}=32nM and IC_{50}=19nM respectively) (Carini et al. 1991). [^{11}C]Methyl-losartan was produced reliably in good yield, high radiochemical purity (>99%), and in a reasonable synthesis time (Hadizad et al. 2011).

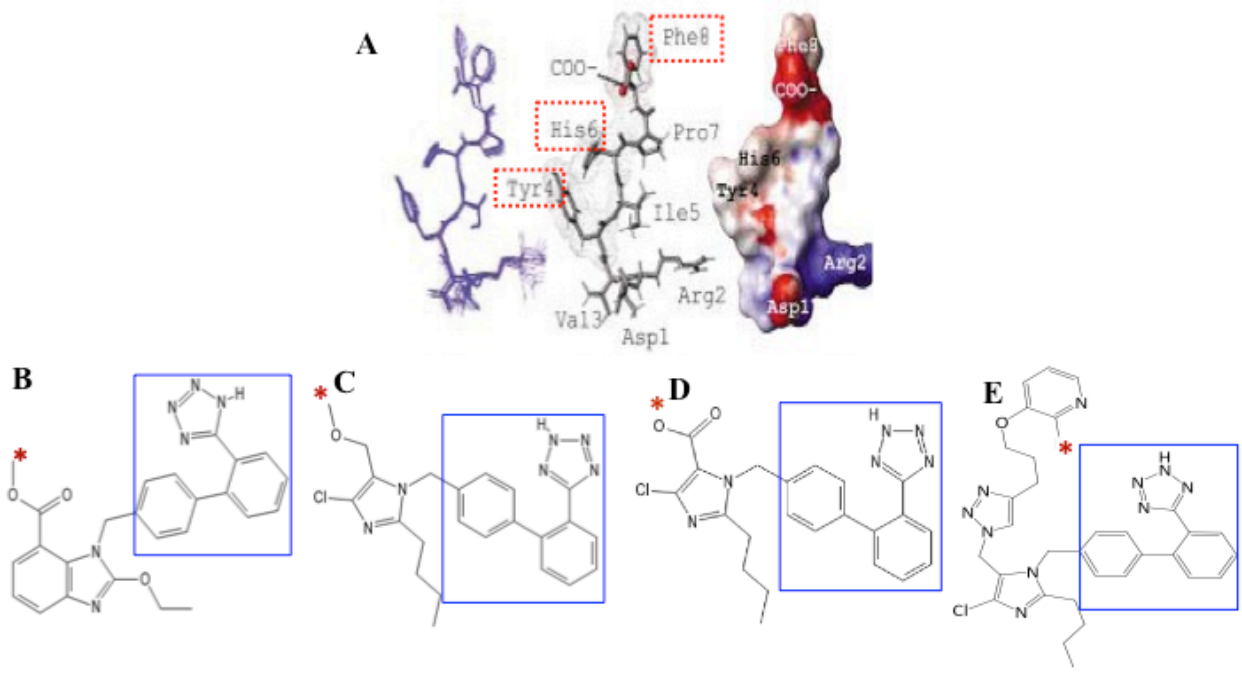

Figure 1.6: The University of Ottawa Heart Institute developed AT_1R PET radiotracers as analogs of the clinically used ARBs. Peptide SAR studies identified the Tyr^4, His^6 and Phe^8 amino acids as important for Ang II binding and activation of AT_1R. The arrangement of these amino acids resembles that of the tetrazole-biphenyl ring conformation (blue boxes) in most of the ARBs. Chemical structure of A) Angiotensin II peptide (with 3D conformation), B) [^{11}C]Methyl-Candesartan, C) [^{11}C]Methyl-Losartan, D) [^{11}C]Methyl-EXP3174 and E) [^{18}F]FPyKYNE-Losartan. C-11 and F-18 radioactive atom position is indicated by red asterisk.

1.8.4.1. [^{11}C]Methyl-EXP3174

In attempt to improve the affinity and metabolism profile of the developed AT_1R radioligands, [^{11}C]methyl-EXP3174 was also synthesized by our radiochemistry group. A similar approach to the production of [^{11}C]methyl-losartan (Hadizad et al. 2011) was explored for the synthesis of [^{11}C]methyl-EXP3174 (Figure 1.6). EXP3174, a major metabolite of losartan, that binds with higher affinity (IC_{50} of EXP3174 3.7nM and losartan 19 nM) as a reversible competitive antagonist to the AT_1R, and is 10-40 times more potent than the parent compound (Timmermans et al. 1991, Okazaki et al. 1998). Based on previous SAR studies and blood pressure measurements in rats, esterification of EXP3174 with [^{11}C]methyl group is expected to maintain a similar binding profile for AT_1Rs (Almansa et al. 1997, Okazaki et al. 1998). As it is derived from a metabolite, it is expected that [^{11}C]methyl-EXP3174 will have a favorable labeled metabolite profile than losartan.

1.8.4.2. [^{18}F]FPyKYNE-Losartan

Previous AT_1R PET tracers have been labeled with C-11, however F-18 offers some key advantages: namely, a longer half-life (109.6 vs 20.4 min) (Gad 2008), allowing for multiple patient scans from a single formulation and shipment to other sites without radiochemistry or cyclotron capabilities, and a shorter RMS (Root Mean Squared) positron range (0.23 vs 0.39 mm in soft tissue) (Tai and Laforest 2005), enabling higher resolution images. The 2-[^{18}F]fluoro-3-pent-4-yn-1-yloxypyridine ([^{18}F]FPyKYNE) analog was produced via click chemistry linking [^{18}F]FPyKYNE to azide-modified tetrazole-protected losartan followed by trifluoroacetic acid (TFA) deprotection (Arksey et al. 2014). Based on reported SAR studies by Carini et al, large prosthetic groups can

be introduced at the imidazole 5-position with minimal effects on both the binding properties and antagonistic efficacy compared to the parent compound (Carini et al. 1991, Hadizad et al. 2011). [^{18}F]FPyKYNE-Losartan is produced reliably in 5-10% yield and in a reasonable synthesis time with > 97.5% purity and specific activities up to 4,000 mCi/μmol (Arksey et al. 2014). Preliminary small animal imaging with PET in rats displayed high uptake in the kidneys with good contrast to surrounding tissue (Arksey et al. 2014). These findings supported our use of this tracer for renal AT_1R quantification with imaging in animal disease models.

1.8.4.3. AT_1R Imaging in Animal Disease Models

AT_1R radioligands were previously used to study animal disease models with PET. In a mouse model of MI, single photon emission tomography (SPECT) was used to image AT_1R *in vivo* at 3 weeks post permanent coronary artery ligation. Tc-99m labeled losartan was injected to the heart and a significantly higher uptake was observed in the infarcted hearts compared to controls. This increase was nearly 2.4-fold higher in the infarcted region of the heart compared to remote region (Verjans et al. 2008). To our knowledge, no other reports using this tracer or SPECT to measure AT_1R changes have been published.

AT_1Rs were investigated in a porcine model of renovascular hypertension with [^{11}C] KR31173 and PET (Xia et al. 2008). Animals were subjected to renal artery stenosis of the right kidney with subsequent development of renovascular hypertension. They were then scanned to investigate changes in renal AT_1R levels. PET exhibited a lower activity in stenotic kidneys due to reduced blood flow as measured by [^{15}O]H_20 compared to contralateral control kidneys. While [^{11}C]KR31173 uptake was decreased because of

reduced blood flow to the stenotic kidney, binding was increased by 40% in renal cortex. This *in vivo* result was corroborated with *in vitro* AT_1R binding assessed by [^{125}I]-[Sar^{1}Ile^8]Ang II autoradiography (Xia et al. 2008).

Another small animal *in vivo* PET study was performed using the same tracer [^{11}C]KR31173 (at high specific activity levels, ~7000 Ci/mmol) in an ischemia/reperfusion (I/R) rat model at 1-3 weeks post-MI (Higuchi et al. 2010). The animals were scanned one week post-surgery and a focal 2.2 fold increased [^{11}C]KR31173 uptake was observed in the area of reduced myocardial perfusion by [^{13}]N-ammonia (infarcted area). The number of animals dedicated for PET was small (n=3) and the authors describe the study as a proof of concept for imaging cardiac AT_1R but had limitations that need to be considered in further studies (Higuchi et al. 2010).

Finally in an I/R model of MI in pigs, [^{11}C]KR31173 retention, corrected for regional perfusion, revealed AT_1R upregulation in the infarct area relative to remote myocardium, whereas both regions showed elevated retention when compared with controls (Fukushima et al. 2012). A preliminary study was performed by the same group in four healthy human subjects who were scanned with [^{11}C]KR31173 showed detectable and specific myocardial retention, albeit at a lower level than pigs and heterogenous that can be caused by spillover from the liver (Fukushima et al. 2012).

1.8.5. PET AT_1R Quantification

Physiologically, the distribution value (DV) values is the most appropriate to be adopted for reversibly binding ligands (Logan 2000). The tracer DV provides a quantifiable parameter for repeated measurements and assessment of repeatability and reliability. It has to be noted that assessments of the metabolism, plasma input function, plasma

protein binding and nonspecific binding of the PET tracer are implicit to the DV calculation (Logan 2000). Due to technical limitations in our study, none of the former corrections were applied in the DV analysis. Consequently the standardized uptake value (SUV) was also used to compare activity concentration in a tissue of interest at one particular time-point, and to enhance the validity of DV values measured. SUV is a semiquantitative analysis where an arterial input function is not indicated. However kinetic modeling will still be needed to assess even minimal changes as tracer metabolic rate (Kreissl et al. 2011), which may be altered in disease conditions and not detected with SUV analysis.

1.8.5.1. Distribution Volume (DV)

Logan graphical analysis (Logan 2000) of the time-activity data is utilized to calculate the tracer DV, which is the expected ratio of radiotracer uptake in tissue relative to concentration in plasma at equilibrium (steady-state) for reversibly binding receptor ligands. The DV value (mL/cm^3) is an index of receptor density (B_{max}) and ligand affinity ($1/K_d$) for the receptor. Physiologically, the DV can be used as an indicator of protein expression and/or receptor-ligand binding potential (B_{max}/K_d) for reversibly binding ligands, that is, higher protein expression or binding affinity will result in a higher DV value (Logan 2000).

The mathematical representation of this is as follows: Plotting $\mathbf{0\int^{T} C_{PET}(t)dt/C_{PET}(T)(min)}$ against $\mathbf{0\int^{T} C_{P}(t)dt/C_{PET}(T)(min)}$, where $C_{PET}(T)$ is the concentration of tracer in the tissue and $C_P(t)$ is the concentration of tracer in the plasma, will transform the tissue activity to a linear plot, as if the tracer was injected as a continuous infusion. The slope of this straight line during the steady-state phase

corresponds to an estimate of the DV of the tracer (Logan 2000).

1.8.5.2. Standardized Uptake Value (SUV)

The SUV is a relative quantification of activity in a single or summed frame, normalized to the injected activity and the body weight of the subject. This normalization is required in comparing subjects of different sizes with a consistent dose administered (Law 1993). SUV is calculated according to the following standard equation:

$$\text{SUV (g/ml)} = \frac{\text{activity concentration in a region of interest (Bq/ml)}}{\text{Injected activity (Bq)/weight of the animal (g)}}$$

The SUV is calculated in the same way as tracer retention measurements from *ex vivo* biodistribution gamma well counting (Kenk et al. 2010), facilitating comparison between methods.

1.9. Research Outcome and Clinical Relevance

This proposal will examine the time course of development of renal dysfunction in an animal model of CKD, in association with renal AT_1R alterations; will help to elucidate the role of the RAS signaling in this pathogenesis; and will assess the efficacy of antihypertensive therapies. Successful development and use of a new non-invasive molecular imaging probe for quantifying AT_1R with PET has never been investigated with imaging previously in CKD. Such an approach would present a unique opportunity to advance understanding of the pathophysiology of CKD. Close analogs with similar characteristics compared to the clinically used ARBs will facilitate translational work and approval from Health Canada. This research will provide the foundation for future PET

studies in patients with various nephropathies. This will provide insights for clinicians about drug responses at AT_1R level which may help optimize dose, guide therapy and monitor disease progression, identifying patients likely to respond, thereby optimizing outcome and reducing adverse effects.

1.10. Hypothesis

The *primary hypothesis* of this doctoral proposal is that hyperactive local RAS associated with renal mass reduction will lead to down regulation of kidney AT_1R and secondary suppression of systemic RAS in subtotal nephrectomy rat model of CKD. Antihypertensive therapies prescribed in CKD will decrease the elevated systolic blood pressure (SBP), normalize renal AT_1R PET measurements and prevent deterioration of renal function.

The *secondary hypotheses* are that: 1) the novel AT_1R PET tracer, [^{11}C]methyl-EXP3174 will exhibit favorable uptake kinetics compared to [^{11}C]methyl-Losartan and will bind selectively to the AT_1R in rat kidneys; 2) the dynamic changes in renal AT_1R associated with Nx rats model of CKD will be detected and quantified reliably using small animal PET with the F18-labeled FPyKYNE-losartan; 3) presence of renal dysfunction will be reflected as increased plasma creatinine and increase in SBP; 4) renal mass reduction will activate local intrarenal RAS (increase Ang II), down regulate AT_1R and will lead to secondary suppression of systemic RAS; 5) echocardiography will eventually show abnormal parameters of heart function: LV ejection fraction (LVEF), stroke volume (SV) and end diastolic volume (EDV); 6) RAS blockade treatment by ACEI, enalapril will restore impaired renal function and morphology, reduce SBP and normalize Ang II levels and AT_1R PET changes in kidney; 7) CCB, diltiazem will decrease SBP, prevent

deterioration of renal function, and normalize AT_1R PET changes; 8) both antihypertensive therapies will prevent progressive cardiac dysfunction.

1.11. Objectives

The main objective of this proposed work is to elucidate the nature/temporal role of renal AT_1R in Nx rat model of CKD, and to explore the predictive value of using non-invasive PET imaging of AT_1R to guide the use of antihypertensive therapy in preventing the progression of the disease. Specific objectives are: 1) To characterize the pharmacokinetics and time course of [^{11}C]methyl-EXP3174 using *in vivo* microPET imaging and determine the tracer binding selectivity for AT_1R over AT_2R; 2) To measure the presence of radiolabeled metabolites in kidney and plasma that can affect PET imaging quantification; 3) To use [^{18}F]FPyKYNE-losartan PET for longitudinal imaging of AT_1R at 8-10 and 18-20 weeks post 5/6 Nx surgery in sham, untreated and treated groups with enalapril or CCB initiated at 10 weeks post-surgery; 4) To serially measure plasma creatinine and SBP at 8-10 and 18-20 weeks in all groups; 5) To evaluate cardiac function (LVEF, LV mass, SV and EDV) by echocardiography at the same time points of imaging; 6) To assess RBF and MBF in Nx animal model using [^{13}N]ammonia μPET imaging; 7) To serially measure plasma and tissue (cardiac and renal) Ang II levels and correlate with other physiologic markers and imaging results; 8) To compare PET measurements with *in vitro* AT_1R binding assays and Western blot analysis of AT_1R protein expression; 9) To assess morphological changes in kidney using histopathology; 10) To confirm efficacy of treatment with enalapril (NxE) or diltiazem (NxD).

1.12. Introduction to Manuscripts

Given the importance of AT_1R in the pathogenesis of cardiovascular diseases, this project was a top research priority of our group, and received continuous funding from CIHR (since 2006) and Ontario Research Fund for Research Excellence (2009-2015). Over the last eight years, progress was made in novel tracers synthesis, tracer characterization, column-switch high-performance liquid chromatography (HPLC) metabolism, small animal PET imaging with our Inveon TM camera and image analysis, large animal imaging using GE Discovery PET/CT (64 Slice) D690 human PET Camera, assessment of the CKD rodent model, small animal echocardiography VisualSonics Vevo system, and *in vitro* assays, resulting in the submission of several peer-reviewed manuscripts.

As part of my PhD research, I have been involved with many aspects of the AT_1R PET imaging project and I have actively participated in six peer-reviewed manuscripts that will be briefly overviewed below. However, only four main manuscripts are included in my PhD thesis (3 first-author and 1 co-author).

1.12.1. Manuscript #1 (not included in the thesis)

Lortie M., DaSilva JN., Kirkpatrick S., Hadizad T., **Ismail B.,** Beanlands RS., deKemp RA. Analysis of [^{11}C]methyl-candesartan kinetics in the rat kidney for the assessment of angiotensin II type 1 receptor density *in vivo* with PET. *Nucl Med Biol.* 2013 Feb;40(2):252-61. doi: 10.1016/j.nucmedbio.2012.10.013.

The objective of this manuscript was to assess binding potential of [^{11}C]methyl-candesartan (Hadizad et al. 2009) to AT_1R in the rat kidney *in vivo* with PET. In this study, Lortie et al describes the metabolism of ^{11}C-labeled candesartan probe and the calculations of PET derived DVs of [^{11}C]methyl-candesartan in rat kidney using a two-

compartment model, Logan analysis and tissue-to-plasma activity ratio (Lortie et al. 2013). Specific binding was confirmed by blockade with unlabeled candesartan corresponding to a significant reduction in AT_1R binding and no change in Logan slope DV with the AT_2R antagonist, PD 123,319, respectively. The results of this manuscript suggest that it may be possible to detect changes in AT_1R density and/or affinity in the rat kidney *in vivo* with [^{11}C]methyl-candesartan and PET. My role in this work was providing input on the experimental animal data and drafting the column-switch HPLC metabolism section in the manuscript.

1.12.2. Manuscript #2

Ismail B., Hadizad T., Antoun R., Lortie M., Beanlands R.S., deKemp R.A., DaSilva J.N. PET imaging of renal AT_1Receptor: Comparison between [^{11}C]methyl-losartan and [^{11}C]methyl-EXP3174 in rats. *Nucl Med Biol.* 2015 Nov;42(11):850-7. doi: 10.1016/j.nucmedbio.2015.06.012. Epub 2015 Jun 30. PMID: 26300209.

Building on the last manuscript, none of the previously synthesized ^{11}C-labeled AT_1R PET tracers have demonstrated proper kinetics, and appropriate metabolism/stability to be brought to clinical setup. Therefore the goal of this work was to describe the synthesis of the [^{11}C]methyl-ester derivative of EXP3174 and to evaluate [^{11}C]methyl-losartan and [^{11}C]methyl-EXP3174 in rats to assess their potential use as PET AT_1R radiotracers. This manuscript presented the characterization and preliminary evaluation of the two C-11 labeled radiotracers as potential PET AT_1R imaging tracers in rat kidneys. The analog of the active metabolite [^{11}C]methyl-EXP3174 was synthesized using a similar approach to the production of [^{11}C]methyl-losartan that was previously published (Hadizad et al, 2011). Both radiotracers were produced in high yields, radiochemical and chemical

purities. This manuscript demonstrated *in vivo* PET images for both radiotracers that displayed strong kidney-to-blood signal contrast which was further confirmed to correspond to specific binding for AT_1R with [^{11}C]methyl-EXP3174. Additionally, [^{11}C]methyl-losartan displayed selectivity for AT_1 over AT_2 and MAS receptors in biodistribution and autoradiography studies. However [^{11}C]methyl-losartan presented labeled metabolites in the kidney with similar pharmacological binding profile to the parent tracer that may confound the PET signal, and not optimal for tracer kinetic modeling. It was concluded in this manuscript that [^{11}C]methyl-EXP3174 displayed favorable uptake kinetics and binding profile for imaging renal AT_1Rs supporting further studies to assess its full potential as a quantitative probe for AT_1R via PET.

1.12.3. Manuscript #3 (included in the thesis appendix)

Arksey N., Hadizad T., **Ismail B.**, Hachem M., Valdivia A.C., Beanlands R.S., deKemp R.A., DaSilva J.N. Synthesis and evaluation of the novel 2-[^{18}F]fluoro-3-propoxy-triazole-pyridine-substituted losartan for imaging AT_1 receptors. *Bioorg. Med. Chem.* 2014 Aug 1;22(15):3931-7. doi: 10.1016/j.bmc.2014.06.011. Epub 2014 Jun 17. PMID: 25023539.

As mentioned previously, F-18 radionuclide has multiple advantages compared to C-11: the longer half-life allows multiple injections per formulation and shipment to sites without cyclotron or radiochemistry capability, as well as higher image resolution due to lower positron energy. Thereby the aim of this manuscript was to present the synthesis of the novel F-18 labeled FPyKYNE derivative of losartan and its preliminary evaluation in rats (Arksey et al. 2014). This work describes the radiosynthesis of the first 18F-labeled AT_1R PET tracer, [^{18}F]FPyKYNE-losartan, via "click" chemistry linking [^{18}F]FPyKYNE

to azide-modified trityl losartan in an overall yield of >10% (decay-corrected), high radiochemical purity and acceptable specific activity for multiple renal scans. PET displayed high contrast kidney images and a dose-dependent reduction (47–65%) in tracer renal uptake, while no difference was observed following AT_2R blocker PD123,319 (5 mg/kg), indicating binding selectivity for renal AT_1R over AT_2R. Additionally, [^{18}F]FPyKYNE-losartan was metabolized rapidly in plasma to mostly hydrophilic labeled compounds suggesting advantageous metabolic profile. The findings of this manuscript supported the potential of this tracer for further renal AT_1R evaluation with non-invasive imaging in rats.

1.12.4. Manuscript #4 (not included in the thesis)

Hachem M., Tiberi M., **Ismail B.**, Hunter C.R., Arksey N., Hadizad T., Beanlands R.S., deKemp R.A., DaSilva J.N. Characterization of [^{18}F]FPyKYNE-losartan for Imaging AT_1 Receptors. *J Nucl Med* (In press).

Since the preliminary microPET studies with [^{18}F]FPyKYNE (presented in manuscript #3) exhibited high binding selectivity for kidney AT_1R and rapid metabolism in rats, additional work was progressed in the lab to characterize [^{18}F]FPyKYNE-losartan binding profile. The aim of this work was to further characterize this radiotracer in rats and pigs as a PET imaging agent for AT_1Rs. Rat *in vitro* studies was performed and confirmed the binding of [^{18}F]FPyKYNE-losartan to AT_1R in the kidney with a K_d of 49.4 nM and B_{max} 348 ± 112 fmol/mm^2. FPyKYNE-Losartan displayed full antagonism for Ang II pressor effect, with 4-times less potency than losartan and an ED_{50} of 25.5 mg/kg in Sprague-Dawley rats. The metabolism studies revealed that the labeled metabolites do not bind to renal AT_1Rs facilitating quantitative PET imaging.

Additionally, rat dosimetry studies indicated that the sex averaged effective dose is $3.06E^{-02}$ - $3.13E^{-02}$ mSv/MBq, which is within an acceptable range compared with other F-18 labeled tracers and within the safety limits of parameters set by the FDA. Furthermore, PET imaging in Yorkshire pigs (n=3) was done and exhibited high kidney-to-blood contrast, and slow renal clearance with an SUV of 14.1 ± 6.2 in the right kidney cortex. Test-retest studies displayed good reproducibility (Test-retest variability= 7.2 ± 0.75%). The plasma-to-blood ratio obtained from pigs was constant over time, and used to correct the arterial input function. Plasma samples exhibited the presence of only hydrophilic-labeled metabolites. Blocking studies with AT_1R antagonist, candesartan (10 mg/kg; n=3), showed 60% reduction in the renal uptake. Finally, reproducible PET images obtained in pigs combined with favorable binding profile supported the potential of [^{18}F]FPyKYNE-losartan to reliably assess AT_1R in animal disease models for future work in humans as an AT_1R PET imaging agent.

My contributions to this manuscript included: 1) provided feedback and assisted with PET and metabolism data interpretation obtained from rats and pigs; 2) technical assistance with the rat dosimetry studies; 3) performed some of the pig control and blocking studies; 4) helped in drafting the manuscript and revising references.

1.12.5. Manuscript #5

Ismail B., deKemp R.A., Hadizad T., Mackasey K., Beanlands R.S., DaSilva J.N**.** Decreased renal AT_1 receptor binding in rats after subtotal nephrectomy: PET study with [^{18}F] FPyKYNE-losartan. *EJNMMI Res* (Submitted).

The fifth manuscript explored the capability of using [^{18}F]FPyKYNE-losartan PET to study *in vivo* renal AT_1R changes in rat model of CKD. In this work, the 5/6 Nx is

evaluated as a model of CKD in rats. At 8-10 weeks post-surgery, Nx rats developed hypertension, elevated plasma creatinine levels, and increased MBF compared to controls. Cardiac function evaluated by echocardiography showed the development of LV hypertrophy induced by subtotal 5/6 Nx. MicroPET [^{18}F]FPyKYNE-losartan scans of the Nx group showed distorted shape (hypertrophy) of the remnant left kidney and displayed significant decrease in the kidney tissue-to-blood ratio (29%), SUV (24%) and DV as determined by Logan analysis (22%) compared to the sham group. These robust *in vivo* findings were confirmed by *in vitro* ^{125}I-[Sar^1, Ile^8]Ang II autoradiography studies. The results presented in this manuscript are the first *in vivo* evidence for a reduction of renal AT_1R cortical expression in a rat model of early stage of CKD. This outcome adds value to the feasibility of use of [^{18}F]FPyKYNE-losartan PET for determination of receptor abnormalities with progression of the disease and monitoring of therapy without the need to sacrifice the animal.

1.12.6. Manuscript #6

Ismail B., deKemp R.A., Croteau E., Hadizad T., Burns K., Beanlands R.S., DaSilva J.N. Treatment with enalapril and not diltiazem normalizes renal AT_1 receptor expression in rats with chronic kidney disease. *Hypertension.* (To be submitted in coming weeks, after approval of MS #5).

This manuscript is an extension of manuscript #5 and investigates the value of using non-invasive PET AT_1R imaging to provide insights into response to commonly prescribed drugs: ACEI and CCB at AT_1R level that may help to guide therapy or aid identifying patients likely to respond, thereby personalizing medicine and improving health outcome. At 18-20 weeks, the Nx rat model of CKD exhibited renal impairment, proteinuria,

sustained hypertension and cardiac hypertrophy that was associated with augmented activity of intrarenal RAS and probably led to downregulation of AT_1Rs in the hypertrophied remnant kidney as evidenced by *in vivo* PET imaging and confirmed by *in vitro* autoradiography. Delayed administration of ACEI, enalapril attenuated renal impairment, hypertension and prevented progression of cardiac hypertrophy as expected. This was successfully accomplished through reduction of systemic and kidney Ang II and consequent normalization of renal AT_1R. On the other hand, the use of non-dihydropyridine CCB, diltiazem was equally effective only as antihypertensive but it did not normalize AT_1R renal expression and induced aggressive increases in Ang II levels in plasma, kidney and heart that appeared to exacerbate renal and cardiac dysfunction. In this manuscript, we provide strong *in vivo* evidence that agrees with previous data stating that anti-RAS therapy provides class-specific renoprotection that is independent of and additional to that achieved by reduction of blood pressure alone at least in experimental animal models of CKD.

CHAPTER 2: MANUSCRIPT #1

Ismail, B [a,b], T. Hadizad [a], R. Antoun [a], M. Lortie [a], R. A. deKemp[a], R. S. Beanlands [a,b], and Jean N. DaSilva [a,b,c,*](2015). **"Evaluation of [(^{11})C]methyl-losartan and [(^{11})C]methyl-EXP3174 for PET imaging of renal AT_1receptor in rats." Nucl Med Biol 42(11): 850-857.**

[a] *National Cardiac PET Centre, Division of Cardiology (Department of Medicine) University of Ottawa Heart Institute, 40 Ruskin St., Ottawa, ON, Canada K1Y 4W7*

[b] *Department of Cellular and Molecular Medicine, Faculty of Medicine, University of Ottawa, 451 Smyth Road, Ottawa, ON, Canada K1H 8M5*

[c] *Department of Radiology, Radio-Oncology and Nuclear Medicine, University of Montreal; University of Montreal Hospital Research Centre (CRCHUM), Montréal, Québec, Canada H2X 0A9*

Shortened title: ^{11}C-losartan derivatives for renal AT_1R imaging

*Corresponding Author: Jean N. DaSilva, Ph.D.

Department of Radiology, Radio-Oncology and Nuclear Medicine, University of Montreal; University of Montreal Hospital Research Centre (CRCHUM), *900 Rue Saint-Denis,* Montréal, Québec, H2X 0A9 Canada

Tel: (514) 890-8000 (x30653)
E-Mail: jean.dasilva@umontreal.ca

Keywords: kidney imaging; active metabolite of losartan; carbon-11 radiolabelling

Contributions of Authors

Synthesis of the radiotracers was done by Dr.Tayebeh Hadizad or under her supervision. The work with [^{11}C]methyl-losartan described (biodistribution, autoradiography, HPLC and PET) in this manuscript was part of a candidate's Masters, Rawad Antoun MSc thesis. However, [^{11}C]methyl-losartan obtained results had to be re-analyzed by myself to be inserted in the manuscript. All [^{11}C]methyl-EXP3174 experiments were performed by myself as well the conducting of data analysis and original drafting of the manuscript. Dr. Mireille Lortie was a physicist of the Cardiac PET group and has advised on the appropriate methods for analysis of the obtained PET imaging data and physicist Dr. Robert deKemp facilitated the quantification and interpretation of the data. Dr. Rob Beanlands provided clinical perspective on the obtained imaging data. All work done was under the supervision and guidance of Dr. Jean DaSilva.

ABSTRACT

Introduction: The Angiotensin II Type 1 receptor (AT_1R) is responsible for the main effects of the renin-angiotensin system (RAS), and its expression pattern is altered in several diseases. The [^{11}C]methylated derivatives of the clinically used AT_1R blocker (ARB) losartan and its active metabolite EXP3174, that binds with higher affinity to AT_1R, were evaluated as potential PET imaging tracers in rat kidneys.

Methods: [^{11}C]Methyl-losartan and [^{11}C]methyl-EXP3174 were synthesized by [^{11}C]methylation of the tetrazole-protected analogs using [^{11}C]methyl iodide. Tissue uptake and binding selectivity of [^{11}C]methyl-losartan was assessed by ex-vivo biodistribution and in-vitro autoradiography. Radiolabeled metabolites in rat plasma and kidneys were analyzed by column-switch HPLC. Both tracers were evaluated with small animal PET imaging. Due to better pharmacokinetics, [^{11}C]methyl-EXP3174 was further investigated via PET by co-injection with AT_1R antagonist candesartan or the AT_2R antagonist PD123,319.

Results: Binding selectivity to renal AT_1 over AT_2 and Mas receptors was demonstrated for [^{11}C]methyl-losartan. Plasma metabolite analysis at 10 min revealed stability of [^{11}C]methyl-losartan and [^{11}C]methyl-EXP3174 with the presence of unchanged tracer at 70.8±9.9% and 81.4 ± 6.0%, of total radioactivity, respectively. Contrary to [^{11}C]methyl-losartan, co-injection of candesartan with [^{11}C]methyl-EXP3174 reduced the proportion of unchanged tracer (but not metabolites), indicating that these metabolites do not bind to AT_1R in rat kidneys. MicroPET images for both radiotracers displayed high kidney-to-background contrast. Candesartan significantly reduced [^{11}C]methyl-EXP3174 uptake in the kidney, whereas no difference was observed following PD123,319 indicating binding

selectivity for AT_1R.

Conclusions: [^{11}C]Methyl-EXP3174 displayed favorable uptake kinetics and binding profile compared to [^{11}C]methyl-losartan for imaging renal AT_1Rs supporting further studies to assess its full potential as a quantitative probe for AT_1R via PET.

1. Introduction

Classically, systemic renin angiotensin system (RAS) was seen as the main regulator of blood volume, electrolyte balance and blood pressure. Nonetheless, tissue specific local RAS components have been found to equally contribute to the normal blood pressure homeostasis (Crowley et al. 2005, Crowley and Coffman 2008, Crowley and Coffman 2012). Most of the known physiological and pathological effects of angiotensin II (Ang II) are mediated by the G-protein coupled angiotensin II type 1 receptor (AT_1R), which is expressed in the adrenals, kidney, vascular tissues, brain, heart and gut (Timmermans et al. 1993, Allen et al. 2000, de Gasparo et al. 2000). The relationship between the RAS and disease is the mechanistic basis behind many drugs that block AT_1R (ARB) or inhibit Angiotensin Converting Enzyme (ACEI). Quantification of the RAS components in tissues, particularly AT_1R, currently requires tissue samples and is thus an invasive technique. A non-invasive imaging modality provides the opportunity to expand the current knowledge of the RAS as a whole and within selected tissues with a minimal impact on the subjects. Such application could also enable directing therapy selection and evaluating therapy response.

Previous AT_1R radioligands have been used to study animal disease models. Tc-99m labeled losartan with single photon emission tomography (SPECT) imaging displayed 2.4-fold increase retention in infarcted myocardial regions compared to remote areas at 3 weeks after coronary artery occlusion in mice (Verjans et al. 2008). The AT_1R radioligand [^{11}C]KR31173 demonstrated AT_1R changes in a porcine disease model of renovascular hypertension (Xia et al. 2008), and in ischemia/reperfusion rat (Higuchi et al. 2010) and pig models (Fukushima et al. 2012). We have previously synthesized AT_1R

radiotracers that are derived from the clinically used ARBs to facilitate their translational work to humans. Both [^{11}C]methyl-candesartan and its desethyl derivative [^{11}C]TH4 were evaluated by *ex vivo* biodistribution studies to assess renal AT_1R in rats (Hadizad et al. 2009). Because of the reduced selectivity of [^{11}C]TH4, additional characterization experiments and initial *in vivo* positron emission tomography (PET) modeling was performed with [^{11}C]methyl-candesartan only (Lortie et al. 2013). However to date, no ^{11}C-labeled AT_1R PET tracers have demonstrated proper kinetics, and appropriate metabolism/stability to bring them to clinical setup.

In attempt to increase tracer retention for renal AT_1R, [^{11}C]methyl-losartan was recently synthesized by O-[^{11}C]methylation of the clinically used ARB, losartan (Hadizad et al. 2011). Losartan is biotransformed by the liver cytochrome P450 system mainly to the active carboxylic acid derivative, EXP3174 that is considered to be responsible for most of its pharmacological effects (Christ 1995, Israili 2000, Diez 2006). EXP3174 is 10-40 times more potent and binds with higher affinity (IC_{50} of EXP3174 3.7 nM, losartan 19 nM) as a reversible competitive antagonist to AT_1R (Timmermans et al. 1991, Okazaki et al. 1998). We hypothesized that the [^{11}C]methyl-losartan will be more lipophilic than the parent compound exhibiting increased tissue uptake, and will be metabolized to radioactive moieties or unlabeled derivatives that would not confound the signal obtained with PET. Our second hypothesis was that the novel tracer [^{11}C]methyl-EXP3174, as a derivative of the active metabolite EXP3174, will have a favorable metabolism and binding profile compared to [^{11}C]methyl-losartan thus facilitating quantification of AT_1 receptor binding.

2. Materials and methods

2.1. Animals

Male Sprague-Dawley rats (200-400g; Charles River Laboratories, Montreal, Canada), were housed in pairs on a 12h:12h light:dark cycle and fed standard rat chow and water *ad libitum*. All studies were approved by the University of Ottawa Animal Care Committee and were carried out in accordance with the Canadian Council on Animal Care Guidelines.

2.2. Chemistry and Radiochemistry

[^{11}C]Methyl-losartan (Figure 2.1) was produced reliably by O-[^{11}C]methylation followed by acid removal of the trityl protecting group as described previously (Hadizad et al. 2011).

Methyl-EXP3174 was prepared by deprotection of tetrazole-protected methyl-EXP3174 (0.019 g, 0.027 mmol) using HCl (1N, 1.0 mL) at 60^{o}C following a similar approach as reported previously (Hadizad et al. 2011) (Hadizad et al. 2009). The pure product was characterized by ^{1}H-NMR and HRMS. The [^{11}C]methyl-ester derivative of EXP3174 was synthesized following the same route in 3 steps (Scheme 2.1): 1) tetrazole group of EXP3174 (0.100 g, 0.23 mmol, purchased from Toronto Research Chemicals Inc.) was protected by trityl chloride (0.100 g, 0.23 mmol) in the presence of triethylamine (0.04 g, 0.4 mmol) at 0-4^{o}C. The product was purified by extraction followed by flash column chromatography to provide 0.146 g (94%) as white powder and characterized by ^{1}H-NMR and HRMS. 2) About 15 min before end of beam, the solution of tetrazole-protected EXP3174 (0.5 g, 0.73×10^{-3} mmol) and kryptofix (0.3 mg, 0.79×10^{-3} mmol) in DMF (0.2 mL) was added onto K_2CO_3 (2 mg, 14.5×10^{-3} mmol). The mixture was vortexed well and purged with argon. [^{11}C]MeI (produced from [^{11}C]methane and I_2) was

distilled through P_2O_5 trap to the reaction vial. Once maximum activity was trapped, the reaction vial was sealed and heated at 80 ^oC for 3 min to give tetrazole-protected [^{11}C]methyl-EXP3174. 3) To remove the protecting group, the reaction vial was cooled to approximately -24 ^oC and 1N HCl (0.2 mL) was added followed by heating at 80 ^oC for 2 min. The reaction mixture was cooled down to -40 ^oC and quenched with high-performance liquid chromatography (HPLC) buffer (0.3 mL). [^{11}C]Me-EXP3174 was purified by semi-preparative HPLC (Luna C_{18}, 10µ, 250×10 mm, acetonitrile/0.1M ammonium formate, 40/60, 7 mL/min,Rt: 8.2 min) and reformulated in a saline/sterile water/8.4% sodium bicarbonate (5/4.4/0.6 v/v/v) mixture. The identity of product was confirmed by analytical HPLC (Luna C_{18}, 10µ, 250×4.6 mm, acetonitrile/0.1M ammonium formate, 40/60, 2 mL/min, Rt: 5.1 min) and compared to standard.

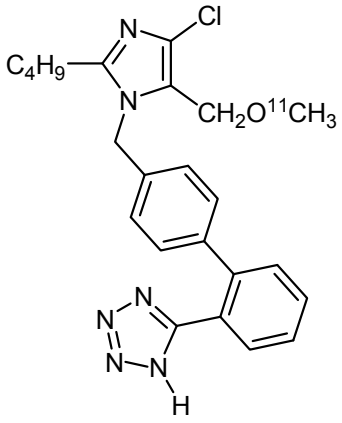

Figure 2.1: Chemical structure of [^{11}C]methyl-losartan. [^{11}C]Methyl-losartan is the *O*-methylated derivative at position-5 of the imidazole group.

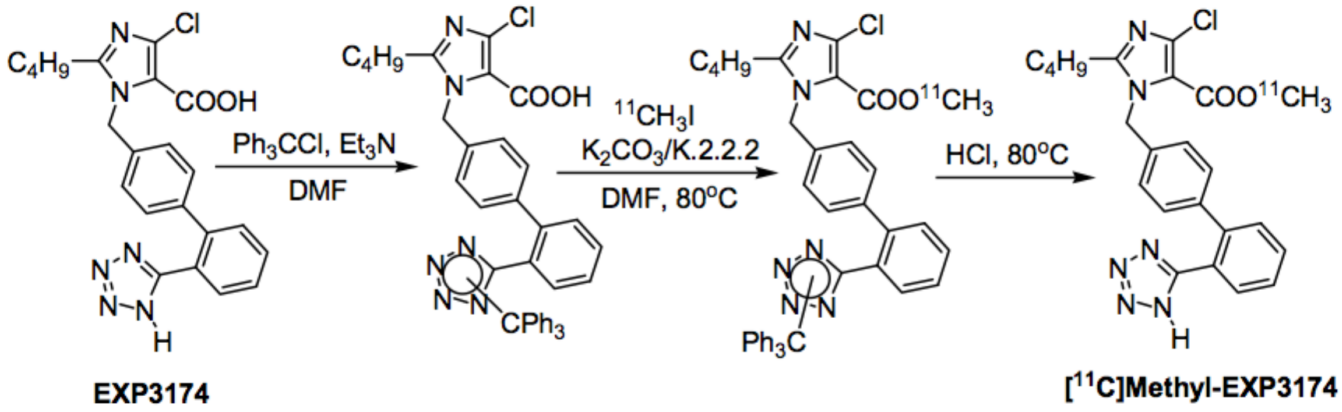

Scheme 2.1: The radiosynthesis of [^{11}C]methyl-EXP3174 in 3 steps.

2.3. [^{11}C]Methyl-Losartan Biodistribution Studies

Ex vivo competition studies were performed to evaluate tissue uptake and binding selectivity of [^{11}C]methyl-losartan for AT_1 over AT_2 and Mas receptors, using methods adapted from previous work (Kenk et al. 2007, Thackeray et al. 2007, Hadizad et al. 2009). Briefly, conscious animals were placed in rat restrainers and injected via the lateral tail vein with 11.1-59.2 MBq tracer activity. Control animals received tracer alone, whereas other groups received intravenous high pharmacological doses of selective antagonists for AT_1R (losartan 20 mg/kg, co-injected, n=4; or candesartan 5 mg/kg, co-injected, n=4), AT_2R (PD-123,319 5 mg/kg, 5 min prior, n=8), or Mas receptor (A-779 100 μg/kg, 5 min prior, n=12) (O'Donnell 1993, Bayorh et al. 2002, Naruse et al. 2002, Sun et al. 2007, Hadizad et al. 2009). Rats were sacrificed by decapitation at 10 min post-injection, corresponding to the time of maximal kidney-to-blood contrast. Trunk blood was collected in heparinized tubes and the following tissues of interest were quickly dissected out into pre-weighed gamma counter tubes: right atrium, left atrium, right ventricle, left ventricle, septum, aorta, kidney cortex, kidney outer medulla, kidney inner medulla, adrenal gland, hypothalamus, cerebellum, brain stem, rest of brain, lung sample, liver sample and skeletal muscle sample (quadriceps). All tubes were then counted (decay corrected) for radioactivity in a gamma counter (Packard, Cobra II) along with injected tracer solution as standard and then weighed. Decay corrected counts were calculated as a percent of the injected dose per gram of tissue (%ID/g), and expressed as a ratio to blood.

2.4. [^{11}C]Methyl-Losartan **Autoradiography Studies**

In vitro autoradiography was performed to validate *ex vivo* biodistribution findings using the method published previously (Kenk et al. 2007). Naïve rats were decapitated and

dissected kidneys were quickly immersed in OCT Compound (Tissue-Tek), frozen on dry ice and stored at -80°C. Kidneys were sectioned in the axial axis into 20 μm-thick slices at -18°C with a cryostat (Leica CM3050 S). Tissue sections were thaw-mounted on glass slides (VWR) and stored at -80°C. On the day of the experiment, slides were pre-washed in incubation buffer (150 mM NaCl, 10 mM sodium phosphate dibasic, 5 mM EDTA, pH 7.4) for 15 min then incubated with 5nM [^{11}C]methyl-losartan for 45 min at room temperature in the presence of 10 μM concentration of losartan, candesartan, PD-123,319 or A-799. After incubation, slides were washed twice (2 min at 4°C) in incubation buffer, once (2 min at 4°C) in deionized water and gently air dried. Sections were then exposed to phosphor imaging plates (Kodak Screen-K, Biorad) for 2 hours in complete darkness. Standards with known concentrations of [^{11}C]methyl-losartan were blotted on thin layer chromatography (TLC) plates (silica, Whatman) and exposed alongside slides to ensure that detected radioactivity was within the linear range of detection and quantification of the phosphor imaging system. Phosphor plates were then read at a 50 μm resolution (BioRad Molecular Imager FX) and analyzed using Quantity One Software (BioRad, Philadelphia). Quantification was done by drawing a same size rectangular shaped region within the kidney cortex and total radioactivity counts were recorded for that area. Each data point was then expressed as fold of the mean control value in the same experiment (n=30 control, n=30 losartan, n=35 candesartan, n=20 PD-123,319, n=21 A-779 kidney sections).

2.5. Plasma and Kidney Radiolabeled Metabolite Analysis

2.5.1. General

Conscious animals were restrained in rat holders and injected via the lateral tail vein with 259-629 MBq [^{11}C]methyl-losartan (controls) and sacrificed at 10 min post-injection (n=2). Additional group of rats were co-injected with 5 mg/kg candesartan (n=3), and were sacrificed at 10 min later. [^{11}C]Methyl-EXP3174 controls (259-629 MBq) were sacrificed at 10 min post-injection (n=4), while a second group of rats (n=3-4) was co-injected with 5 mg/kg of candesartan before sacrificing 10 min later.

2.5.2. Sample Preparation

Trunk blood and the kidneys were collected and placed on ice until processing. Blood was centrifuged at 4000 rpm for 5 min to obtain plasma. Dissected tissues were processed for HPLC analyses as previously described (Thackeray et al. 2007, Kenk et al. 2008). Briefly, kidney samples were homogenized in 80:20 ethanol/water (v/v) using a polytron homogenizer then centrifuged at 22,000 rpm (82,000g) for 15 min. Supernatant was extracted by rotary evaporation followed by reconstitution in 1:99 MeCN/water (v/v) and microfiltration at 0.22 μm (Cathivex- GS syringe filters) before injection onto the HPLC system. Urea was added to a final concentration of 1.0 and 0.4 g/ml to plasma and kidney homogenate samples respectively to disrupt plasma protein binding.

2.5.3. HPLC Procedure

A modification of the column-switch HPLC method was employed (Kenk et al. 2008). Briefly, samples dissolved in solvent A (1:99 acetonitrile/water) are eluted at 1.5 ml/min onto a capture column (in-line refillable guard column, 2x20 mm) hand packed with Oasis HLB polymeric reverse phase sorbent (Waters Corp., Milford, MA) and fitted with 2.5 μm frits (Altech, 2-mm filter elements). Eluted macromolecules are detected by a UV absorbance detector at 280 nm and coincidence radiation detection. Once the UV signal

returned to baseline, flow is switched such that Solvent B (35/65 acetonitrile/0.1 M ammonium formate) back-flushed the retained compounds off the capture column and over the analytical column (Luna C18 10 µm 100 A 250 x 4.60 mm, Phenomenex) at 1.5 ml/min passing by the detectors. Signals are integrated using the PeakSimple Six-port Chromatography data system and were analysed using PeakSimple 3.77 software, and subsequently corrected for noise and radioactive decay. Retention times were calculated from the time of switch and activity data is expressed as the percent of the total radioactivity signal. Samples of plasma and kidney directly spiked with authentic tracer prior to processing were processed as described above by HPLC for each experiment as standards.

2.6. Small Animal PET Imaging

2.6.1. General

[^{11}C]Methyl-losartan (18.5-81.4 MBq, 0.2-28 µg cold mass) microPET scans were acquired for preliminary *in vivo* evaluation of the tracer for imaging AT_1R in kidneys (n=4 scans). [^{11}C]Methyl-EXP 3174 (18.5-55.5MBq, 0.05-11.7 µg cold mass) was administered for control animals (n=7) and were scanned twice within 7 days to test repeatability of measurements. To assess binding selectivity, additional groups of rats received [^{11}C]methyl-EXP either co-injected intravenously with 5 mg/kg candesartan (ARB) or with AT_2R antagonist, PD123,319 (5 mg/kg dose) 5 minutes prior to tracer injection (n=3 per group).

2.6.2. Image Acquisition

Animals underwent 60-minute dynamic PET scans using the Inveon DPET (Siemens Preclinical Imaging, Knoxville, TN) small animal PET camera. Anaesthetized rats (2-

2.5% isoflurane) were scanned in a supine position on a heated scanner bed and physiological parameters were monitored for the duration of the scan. Following the initiation of the scan protocol, rats were injected immediately through the tail vein with the tracer formulation. A 10-min ^{57}Co transmission scan was obtained for scatter and attenuation correction. Dynamic PET images (12x10 sec, 3x60 sec, 11x300 sec frames) were reconstructed using vendor-provided 3-dimensional ordered subset expectation maximization maximum a posteriori algorithm OSEM3D/MAP (β=1, OSEM3D iterations = 2, MAP iterations = 18) with all corrections enabled.

2.6.3. Image Analysis

All images were analyzed with Inveon® Research Workplace software version 1.4 (Siemens Preclinical Imaging, Knoxville, TN). Regions of interest (ROI) were defined on reconstructed images in the left atrial cavity region and left kidney cortex to obtain time activity curves following the procedure recently published (Lortie et al. 2013). The kidney ROIs were created at frame 16 (5-10 min post-injection where the highest tissue to background contrast was observed) from 3-D ellipsoid shapes, excluding portions in close proximity to the liver to minimize spillover, and applying a threshold at 50% of the maximal value within the remaining shape. A 3-D sphere was drawn within the left atrium cavity at an early frame (10-40 sec) to sample the blood input function. The shape of this left atrium ROI was determined by thresholding at 80% of the maximal value. The tissue-to-blood activity ratio at 50-60 min post-injection was calculated for each [^{11}C]methyl-EXP3174 scan. Additionally distribution volume (DV) values were measured using Logan graphical analysis (Logan et al. 1990). DV (mL/cm^3) is the

expected ratio of radiotracer in tissue relative to plasma at equilibrium for reversibly binding receptor ligands.

2.8. Statistical Analysis

Results are presented as mean ± standard deviation. Statistical analysis was performed using one-way analysis of variance (ANOVA) and a Bonferroni-adjusted post-hoc analysis was used when comparing more than two groups. Otherwise a two-tailed t-test was used to compare between two groups. In all statistical tests applied, P values<0.05 were considered significant.

3. Results

3.1. Chemistry and Radiochemistry of [^{11}C]Methyl-EXP3174

The unlabeled standard (methyl-EXP3174) was produced as a white solid in 48.2% yield. ^{1}H NMR ($CDCl_3$, 500 MHz) δ_H 13.40-11.80 (broad singlet, 1H), 8.06 (d, 1H, J=7.4 Hz), 7.59 (t, 1H, J=7.1 Hz), 7.54 (t, 1H, J=7.3 Hz), 7.40 (d, 1H, J=7.4 Hz), 7.15 (d, 2H, J=7.6), 6.95 (d, 2H, J=7.6 Hz), 5.51 (s, 2H), 3.79 (s, 3H), 2.54 (t, 2H, J=7.7 Hz), 1.63 (quint, 2H, J=7.6 Hz), 1.30 (sext, 2H, J=7.5 Hz), 0.86 (t, 3H, J=7.3 Hz). HRMS calculated for $C_{23}H_{23}O_2N_6Cl$: 450.1571, measured: 450.1578.

[^{11}C]methyl-EXP3174 was produced in 50-70% radiochemical yield (decay-corrected, based on [^{11}C]MeI), high radiochemical purity (>99%), specific activities of 31.45 – 92.5 GBq/μmol at EOS and a synthesis time of 35 min (including QC).

3.2. [^{11}C]Methyl-Losartan Biodistribution

Highest activity concentration at 10 min post injection was obtained in the liver, kidney cortex and outer medulla; 44.6, 8.7 and 3.2 tissue-to-blood ratios, respectively (Figure 2.2). Blocking of AT_1 receptors with losartan reduced uptake significantly ($p<0.05$) in the

liver, kidney cortex and outer medulla (75 to 85%). Similar reduction ($p<0.05$) with candesartan blocking was determined in the kidney cortex and outer medulla, but no change in the liver (Figure 2.2; liver data not shown).

Blocking of the AT_2 receptor and Mas receptor produced no change in tracer uptake in any tissue (Figure 2.2). There were significant increases in tracer retention following losartan blockade in all brain regions studied ($p<0.05$). However, it is important to note that despite the statistical significance of these increases, these results may not be physiologically relevant due to the fact that the ratio-to-blood in brain regions is very small, indicating lower activity concentration in the tissue relative to blood.

3.3. [^{11}C]Methyl-Losartan Autoradiography

Similar changes in tracer retention were observed in the kidney cortex with autoradiography in comparison to biodistribution. Blocking with losartan and candesartan reduced significantly tracer uptake by 59.0% and 24.3% ($p<0.05$), respectively. No blockade was obtained with PD-123,319 or A-779 drug incubations (Figure 2.3A&B), confirming that [^{11}C]methyl-losartan binds selectively to AT_1R over AT_2 and Mas receptors.

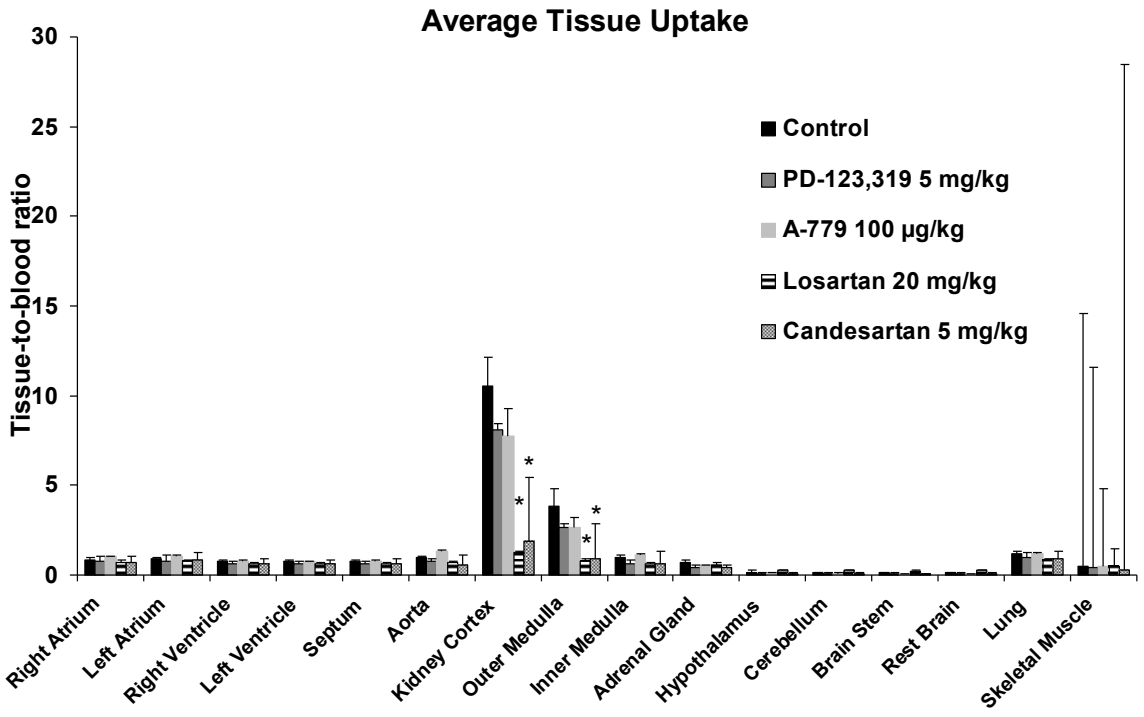

Figure 2.2: [^{11}C]Methyl-losartan (11.1-59.2 MBq) relative tissue uptake assessed by *ex-vivo* biodistribution in controls (n=10), animals co-injected with 20 mg/kg losartan (n=4), or 5 mg/kg candesartan (n=4) and after pre-injection with 5mg/kg PD 123,319 (n=8) or 20 µg/kg A-779 (n=12). Results are expressed as %ID/g ratio to blood ± SD. *$p<0.05$ vs control; one way ANOVA and Bonferroni post-hoc.

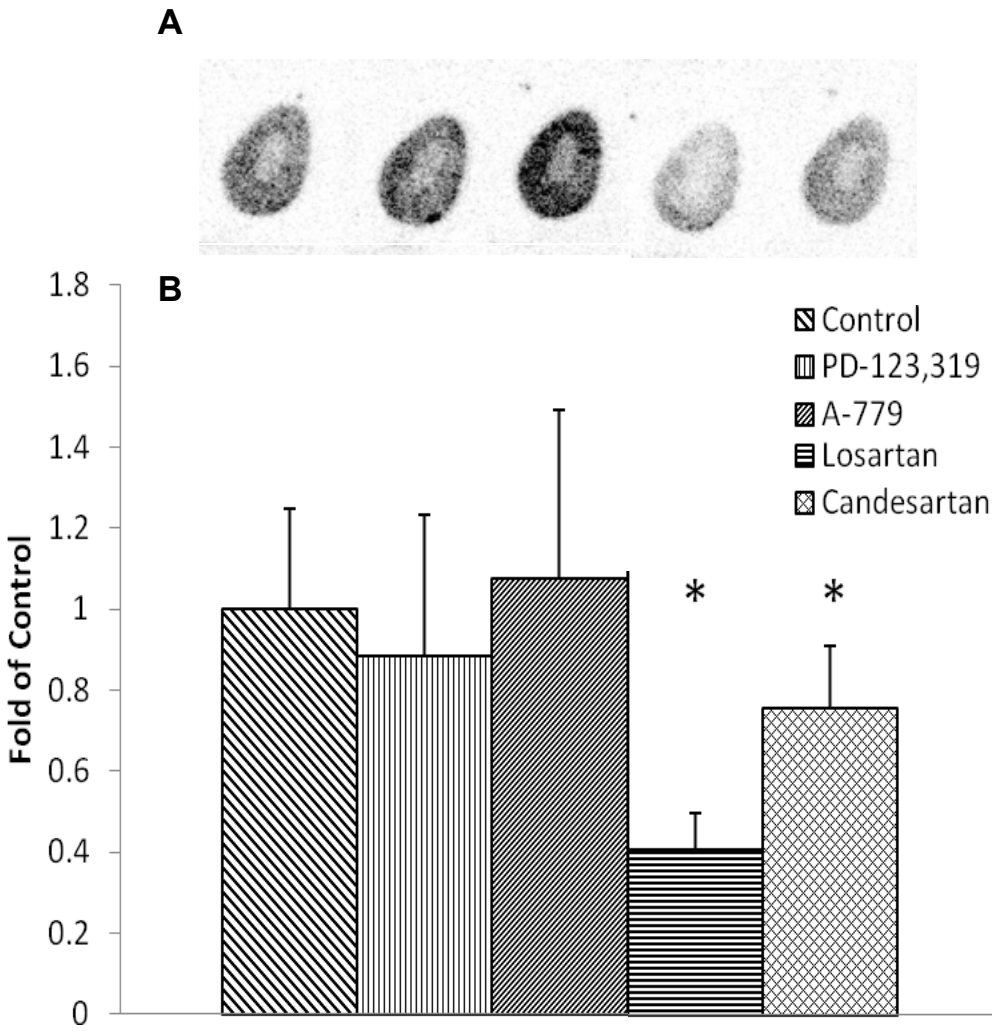

Figure 2.3: (A) Representative autoradiography images for [^{11}C]methyl-losartan (5 nM) binding in rat kidneys of (a) Control, (b) PD-123,319 5mg/kg, (c) A-779 20 µg/kg, (d) Losartan 20 mg/kg and (e) Candesartan 5 mg/kg; (B) Bar chart showing tissue binding in treated groups as compared to control group injected with radiotracer only (n=30 control, n=20 PD-123,319, n=21 A-779, n=30 losartan, n=35 candesartan kidney sections). Data is expressed a fold of control ± SD. *$p<0.05$ vs control; one way ANOVA and Bonferroni post-hoc.

3.4. Radiolabeled Metabolites Analysis

3.4.1. Standards

HPLC analysis of plasma and kidney samples with authentic tracers detected only one peak corresponding to unchanged tracer with consistent retention time (Rt; corresponding to peak 4,) after reversing the flow (post-switch). [^{11}C]methyl-losartan Rt was approximately 7 min, and [^{11}C]methyl-EXP3174 6.5 min (post-switch). No other peaks were detected and therefore it can be concluded that the processing did not affect or degrade the radiotracer.

3.4.2. [^{11}C]Methyl-Losartan

Control plasma [^{11}C]methyl-losartan samples at 10 min exhibited the presence of one hydrophilic labeled metabolite that was eluted from the capture column (Peak 1, Rt= 1 min post-switch) and one hydrophobic labeled metabolite (Peak 2, Rt= 3 min post-switch) (Table 2.1). In control kidney, [^{11}C]methyl-losartan (peak 4, Rt= 7 min post-switch) represented less than 40% of the overall signal at 10 min, with the remaining peaks corresponding to labeled metabolites (Table 2.1).

Co-administration of candesartan did not affect any of the peak proportions when compared to samples of control animals at 10 min, both in the plasma and kidney (Table 2.1).

3.4.3. [^{11}C]Methyl-EXP3174

Following administration of [^{11}C]methyl-EXP3174 to control animals, four peaks were identified in rat plasma at 10 min post-injection. Peak 1 for unretained hydrophilic metabolite (Rt = 1.4 min post-switch), peaks 2 and 3 (Rt= 3.2 and 4.3 min post-switch) correspond to hydrophobic metabolites 1 and 2, respectively, and accounting for

approximately 20% of the total radioactive signal (Table 2.2). Peak 4 eluted at 6.5 min for the unchanged radiotracer as identified in standard experiments. In contrast, only 2 labeled products were detected in kidney tissue homogenates at 10 min post-injection. Peak 2 corresponded to hydrophobic metabolite 1 that accounted for more than 65% of total radioactivity signal and peak 4 representing the unchanged tracer (Table 2.2).

Compared to control animals, plasma samples from rats co-injected with candesartan (5mg/kg) displayed an increase in percentage of peak 1 and 2, disappearance of peak 3 (hydrophobic metabolite 2) and a reduction in peak 4 corresponding to unchanged tracer (Table 2.2). Co-administration of candesartan drastically decreased peak 4 in the kidney indicating a blockade of [^{11}C]methyl-EXP3174 retention, while the proportion of metabolite 1 was unaffected (Table 2.2). The unretained hydrophilic metabolite (peak 1) detected in the kidney blocking studies was not present in control samples.

Table 2.1: [^{11}C]Methyl-losartan (259-629 MBq) metabolite analysis in plasma and kidneys at 10 min following radiotracer administration in control rats, and co-injected 5 mg/kg candesartan.

	Peak 1 (Hydrophilic metabolite)	Peak 2 (Hydrophobic metabolite 1)	Peak 3 (Hydrophobic metabolite 2)	Peak 4 (Unchanged tracer)
		Plasma		
Control at 10min	28.5% ± 9.3%	0.7%±0.8%	0.0%±0.0%	70.8%±9.9%
Blocked Candesartan at 10min	23.0% ± 13.9%	0.3%±0.4%	0.1%±0.2%	76.6%±13.6%
		Kidney		
Control at 10min	42.2% ± 13.2%	23.0%±2.5%	0.0%±0.0%	34.7%±13.9%
Blocked Candesartan at 10min	37.9% ± 11.1%	14.6%±2.0%	0.0%±0.0%	47.6%±13.2%

N=3-4 per study.

*$p<0.05$ vs control at 10 min and 45 min; Two tailed student t-test.

Table 2.2: [^{11}C]Methyl-EXP3174 (259-629 MBq) metabolite analysis in plasma and kidney at 10 min in control rats following radiotracer administration and in rats co-injected with 5 mg/kg candesartan.

	Peak 1 (Hydrophilic Metabolite)	Peak 2 (Hydrophobic metabolite 1)	Peak 3 (Hydrophobic metabolite 2)	Peak 4 (Unchanged tracer)
		Plasma		
Control at 10min	11.2%±6.5%	4.6%±1.95%	2.8%±1.51%	81.0%±6.02
Blocked Candesartan at 10min	26.0 %±6.1%	9.2%±1.23%	0.0%±0.0%*	64.8%±4.94
		Kidney		
Control at 10min	0.0%±0.0%	69.1%±17.2%	0.0%±0.0%	31.1%±17.22
Blocked Candesartan at 10min	22.9±5.1%*	69.0%±1.5%	0.0%±0.0%	8.1%±4.89

N=4-5 per study.
*$p<0.05$ vs control; Two tailed student t-test

3.5. Small Animal PET Imaging

3.5.1. [^{11}C]Methyl-Losartan

Preliminary microPET scans performed with [^{11}C]methyl-losartan displayed highest uptake in the liver and kidneys. Initial increase in blood activity is observed following injection then decreased back to baseline at 15 to 20 min post-injection. The highest retention observed in the liver was sustained until the end of scan. Rapid accumulation and slow washout was also observed in the kidneys. Signal distribution is representative of kidney cortex and outer medulla. Good signal contrast between kidneys and whole blood was found between 5 and 30 min post injection (Figure 2.4A). Logan DV values obtained from [^{11}C]methyl-losartan control scans were 1.63 ± 0.23 ml/cm^3.

3.5.2. [^{11}C]Methyl-EXP3174

Control [^{11}C]methyl-EXP3174 PET images exhibited a similar pattern to [^{11}C]methyl-losartan, however stronger tissue-to-blood signal contrast was obtained in the kidney. In the early dynamic frames (0-120s) the vasculature, heart cavities, lungs, liver and kidneys were visualized, whereas only the kidneys and liver were visible in later frames (>15 min). Kidney time-activity curves of the control scans peaked at approximately 2 min and fell to baseline at 35 min post-injection (Figure 2.4B). The average tissue-to-blood ratio at 50 to 60 min post-injection was 4.0±1.5. There was no difference between tissue-to-blood ratios obtained for the first (4.1±1.5) and second (4.0±1.5) scans performed on the control rats. Rats co-injected with candesartan exhibited faster washout from the kidney compared to controls (Figure 2.4C), with a significant tissue-to-blood ratio reduction to 0.96±0.10 (-76%, $p<0.001$). In rats treated with PD-123,319, no decline in kidney activity and no change in tissue-to-blood ratio (4.1±0.9) was observed over time (Figure 2.4D).

Using Logan analysis, kidney DV values obtained for test and retest scans were not different. Administration of candesartan induced a significant 60% reduction ($p<0.002$) compared to controls, whereas no change was observed in PD-123,319 treated rats (Table 2.3).

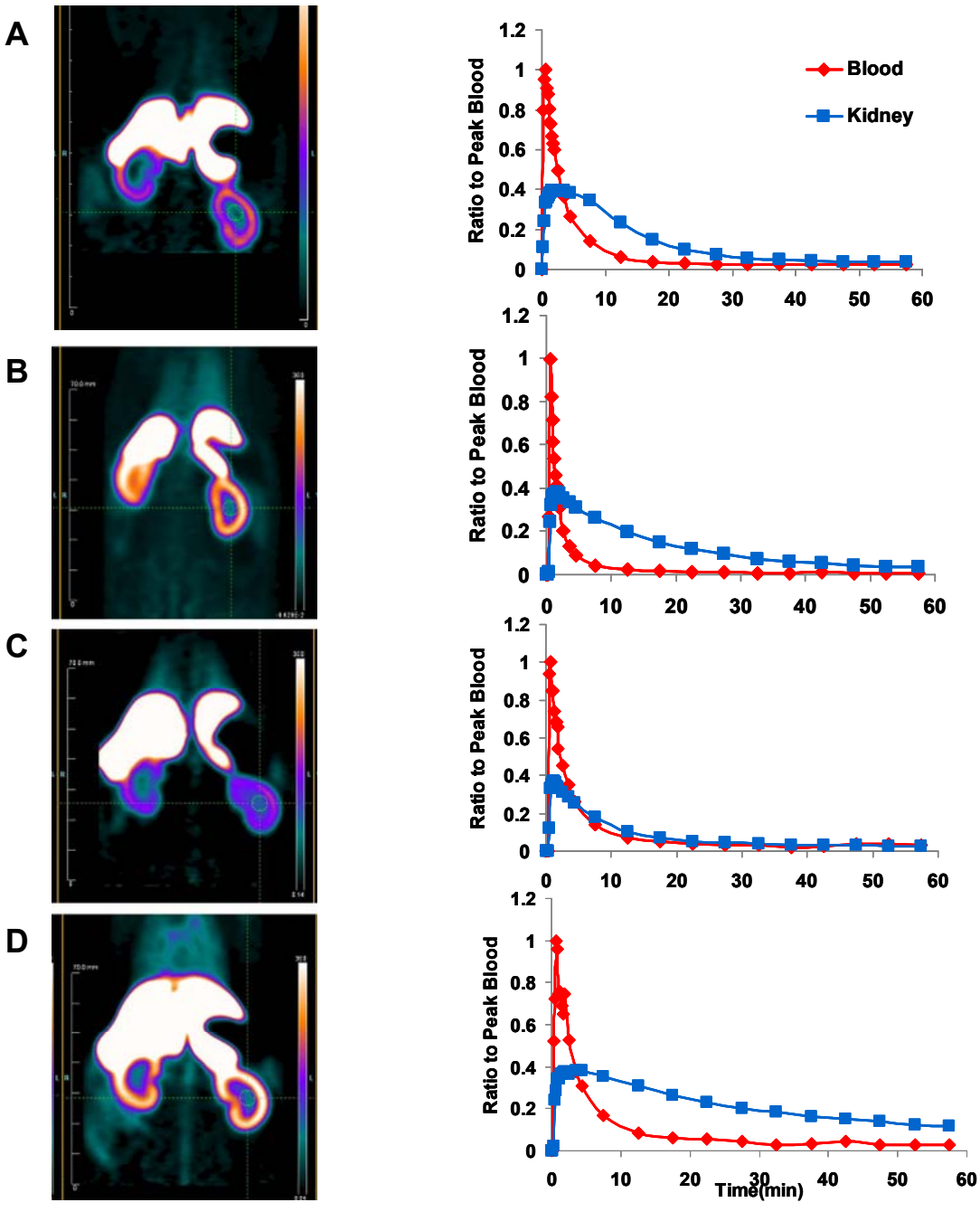

Figure 2.4: Representative coronal view microPET images (at 5-10 min) displaying liver and kidneys and time-activity curves in rats following injection of (A) [^{11}C]methyl-losartan (18.5-81.4 MBq) and (B) [^{11}C]methyl-EXP3174 (18.5-55.5 MBq) in control animals; (C) [^{11}C]methyl-EXP3174 with co-injection of candesartan (5mg/kg) and (D) with pre-injection of PD 123,319 (5mg/kg). Data is presented as ratio-to-peak blood activity.

Table 2.3: Logan distribution volume (DV) values of [^{11}C]methyl-EXP3174 (18.5-55.5 MBq) in kidney of control animals, with co-injection of candesartan (5mg/kg) and with pre-injection of PD 123,319 (5mg/kg). Data is presented as average±standard deviation.

	Control Test scan	**Control Retest scan**	**Candesartan scan**	**PD-123,319 scan**
DV (ml/cm^3)	2.53±0.63	2.54±0.69	1.03±0.07*	2.45±0.16

N=3-4 per study.
* $p<0.05$ vs control; Two tailed student t-test.

4. Discussion:

A similar approach to the production of [^{11}C]methyl-losartan (Hadizad et al. 2011) was used for the synthesis of [^{11}C]methyl-EXP3174. The ^{1}H-NMR spectrum demonstrated disappearance of the trityl peaks in aromatic region and appearance of a broad singlet at 13.40-11.80 ppm corresponding to a proton of the tetrazole group. The singlet peak at 3.79 ppm was indicative of the incorporation of the methyl group in the molecule. From our previous work with [^{11}C]methyl-candesartan (Lortie et al. 2013) and confirmed here for both tracers with microPET (see Figure 2.4), we have selected 10 min for biodistribution studies with [^{11}C]methyl-losartan due to optimal tissue-to-blood contrast in the kidneys at that time-point. The adrenal gland exhibited no retention *ex vivo,* and an explanation for this would be that the majority of AT_1R in the adrenal gland are located in the zona glomerulosa (Allen et al. 1990) which represents approximately 5 to 10 % of the adrenal mass. In the biodistribution experiments, the entire adrenal gland is excised, counted and weighed as a whole, and consequently uptake that occurs in the minute zona glomerulosa would be diminished and insignificant relative to the entire organ. *Ex vivo* competition studies demonstrated that [^{11}C]methyl-losartan binds specifically to the AT_1R as evident by the significant reductions (70-90%) in the %ID/g ratio-to-blood in the kidney cortex and outer medulla with losartan and candesartan co-injections. In the liver, losartan but not candesartan was able to block retention of [^{11}C]methyl-losartan at 10 min post-injection which is likely due to the similarity in structures. This strongly suggests that the effect is not due to AT_1R binding, but to displacement from saturable non-specific binding sites and common metabolic pathways. Competition with saturating doses of PD-123,319 (AT_2R antagonist) and A-779 (Mas receptor antagonist) displayed

similar reductions of [^{11}C]methyl-losartan retention that were not significant in any of the tissues evaluated, including non AT_1R-rich tissues such as aorta, lung and skeletal muscle. Furthermore, *in vitro* autoradiography studies confirmed binding selectivity for AT_1R over the AT_2 and Mas receptors obtained with biodistribution, which signifies that the findings are indicative of direct exposure of the tracer to the receptors thereby bypassing any pharmacokinetic or pharmacodynamic effects expected to occur in *in vivo* studies.

HPLC analysis of labeled receptor ligands and their metabolites in plasma and tissue is an important step in the evaluation of the kinetics of these ligands for PET quantification. Metabolite analyses of [^{11}C]methyl-losartan revealed stability of the tracer in plasma, and absence of hydrophobic metabolites would indicate that it is either synthesized in the kidney, or elsewhere (i.e. in the liver) and transported to the kidney via the blood. However, this latter option would require that the metabolite be present in very low concentrations at any given point in the plasma and that it accumulates in the kidney over time. There were no differences in the relative proportions of labeled metabolites and [^{11}C]methyl-losartan following co-injection of candesartan in kidney samples. This result would suggest that these metabolites share common structure or metabolic pathways with the parent compound; however no further attempts were made to identify their binding characteristics. Losartan is metabolized by cytochromes P450 system in liver (Israili 2000) and given the similarity in structures between losartan and methyl-losartan, it is possible that they would have similar metabolic profiles. As anticipated, metabolite analyses of [^{11}C]methyl-EXP3174 at 10 min post-injection revealed favorable characteristics with the presence of 1 hydrophilic labeled metabolite that accounted for

less than 6% of the total radioactive signal in the plasma. Interestingly, the high proportion of the labeled metabolite observed in the kidney accounting for 52-86% of radioactivity at the 10 min post-injection was not expected. EXP3174 is one of seven different metabolites for losartan with different relative abundance between humans and rats (Stearns et al. 1992, Stearns et al. 1995). Rats primarily transform losartan into EXP3174 by hepatic cytochrome CYP 2C9 oxidation reaction (Stearns et al. 1992). No studies were found in the literature on elimination of EXP3174. The increase in the proportion of the hydrophilic labeled metabolites (peak 1) in the kidney after AT_1 blockade is intriguing. However, the reduction of the proportion of [^{11}C]methyl-EXP3174 in kidney tissue compared to the labeled metabolites following co-injection with candesartan indicates specific binding of the tracer and non-specific binding for the labeled metabolites. Nonetheless, identification and determination of the metabolite's structure are beyond the scope of this study. Moreover, it is likely that the metabolic profile could change in large animals as dogs and pigs hence they present a preferable transition and successful link translating basic PET imaging techniques and data analysis to applications in humans (Klocke et al. 2007). Additionally, they express one type of AT_1Rs similar to humans, in contrast to rodents in which two subtypes of the receptor exist (Zober et al. 2006).

The presence of labeled metabolites that bind specifically to AT_1 receptors in ROI's will confound the PET signal, and complicate modeling calculations since the specific signal in ROI will be derived from more than one labeled molecules with different pharmacokinetics. Given the fact that HPLC [^{11}C]methyl-losartan studies displayed metabolites that have similar binding profile to the parent tracer, only control PET scans

were acquired to assess i*n vivo* uptake and no further studies were done with this tracer. However, since the labeled metabolites from [^{11}C]methyl-EXP3174 do not bind specifically to AT_1R, the portion of the signal corresponding to AT_1R specific binding obtained with this tracer will only come from the parent compound (as opposed to [^{11}C]methyl-losartan), rendering PET quantification of AT_1R levels possible especially in AT_1R-rich organs such as the kidneys. [^{11}C] Methyl-losartan small animal PET images displayed high tissue uptake in the liver, kidney cortex and outer medulla which correlates with the known physiological distribution of AT_1R in the renal cortex and outer medulla (Allen et al. 2000). The stronger tissue to blood signal intensity observed with EXP3174 was anticipated due to its higher binding affinity for AT_1R. Although AT_1R are known to be expressed in the liver (Murphy et al. 1991, Yu et al.), it is possible that the activity accumulation is due to metabolism of both tracers by the hepatobiliary system as it occurs with most ARB drugs (Israili 2000). The inability to detect specific binding in the adrenal glands with PET despite the fact that they are known to express higher AT_1R density compared to renal cortex (Chang and Lotti 1991) may be attributed to several factors: i) the partial volume effect and the relative small size of this tissue compared to kidneys, liver and bowel on PET images; ii) it should be noted that rodents express two isoforms of AT_1R: AT_{1a} and AT_{1b} (Gasc et al. 1994, Griendling et al. 1996). AT_{1a} is the closest functional analogue to the human AT_1R and predominates in most organs including kidney, whereas AT_{1b} exists mainly in the adrenal gland and some regions of the brain (Burson et al. 1994); which may suggest that our tracers are specific only to $AT_{1a}R$. It is well known that central nervous system areas involved in cardiovascular regulation, including the hypothalamus and brainstem, exhibit a predominance of AT_1Rs

(Tsutsumi and Saveedra 1991, Lenkei et al. 1995, Lenkei et al. 1997). So we speculated that increasing the lipophilicity of losartan (i.e. replacing the hydroxyl group by a methoxyl group in [^{11}C]methyl-losartan), would facilitate crossing the blood brain barrier and binding centrally to the AT_1 receptor but this was not observed with the tracers.

Following co-injection with candesartan, [^{11}C]methyl-EXP3174 renal DV and tissue-to-blood ratio were reduced by almost 60% and 80% respectively. The reduction of DV (Table 2.3) and tissue-to-blood ratios (Section 3.5.2) to the blood levels around 1 indicates no renal retention and confirms absence of binding specificity of the tracer. Whereas no change was obtained following PD-123,319 treatment, demonstrating its selectivity for AT_1R over AT_2R *in vivo*. The tracer DV (mL/cm^3) is an index of receptor density (B_{max}) and ligand affinity ($1/K_d$) for the receptor. The effects of plasma protein binding and nonspecific binding are implicit to the DV calculation, however no corrections were made in this study to account for metabolites or other factors. Physiologically, the DV can be used as an indicator of protein expression and/or receptor-ligand binding potential (B_{max}/K_d) for reversibly binding ligands, that is, higher protein expression or binding affinity will result in a higher DV value.

In conclusion, the appropriate regional distribution, pharmacology and selectivity of [^{11}C]methyl-losartan and [^{11}C]methyl-EXP3174 support their potential use for non-invasive renal AT_1R PET imaging. The presence of labeled metabolites with similar pharmacological binding profile to the parent tracer observed in kidney with [^{11}C]methyl-losartan may confound the PET signal, and complicate kinetic modeling. In comparison, [^{11}C]methyl-EXP3174 displayed favorable uptake kinetics and binding profile for

imaging renal AT_1Rs supporting further studies to assess its full potential as a quantitative probe for AT_1R via PET.

Acknowledgement

The authors acknowledge the contributions of the University of Ottawa Heart Institute Cardiac PET Centre Radiochemistry staff (Jeff Collins and Keegan Flowers) for radiochemical synthesis; Myra Kordos and Christine Archer for small animal PET imaging; Dr. Stephanie Thorn and Dr. James Thackeray for assistance with the metabolite analysis studies; and also thank Ottawa Heart Institute Animal Care and Veterinary Staff for general assistance with the experiments. This work was supported in part by, the Ontario Preclinical Imaging Consortium (OPIC) grant# RE03-51 (Ontario Research Foundation) and the Canadian Institutes of Health Research (MOP-80203 & MOP-287694) and by the Molecular Function and Imaging Heart and Stroke Foundation of Ontario Program Grant (#PRG6242).

BI was a doctoral student co-supervised by JDS and RSB and supported by the PhD scholarship from the University of Ottawa's Faculty of Medicine Endowed Funds for Cardiac Graduate Research and the UOHI Foundation. RSB is a Career Investigator supported by the Heart and Stroke Foundation of Ontario (HFSO), the University of Ottawa Heart Institute (UOHI) Vered Chair in Cardiology and Tier 1 University of Ottawa Chair in Cardiovascular Research.

CHAPTER 3: MANUSCRIPT #2

Decreased renal AT_1 receptor binding in rats after subtotal nephrectomy: PET study with [^{18}F] FPyKYNE-losartan

EJNMMI Research (Submitted, April 20, 2016)

Basma Ismail [1,2], Robert A. deKemp [1], Tayebeh Hadizad [1], Kumiko Mackasey [1], Rob S. Beanlands [1,2], Jean N. DaSilva [1,2,3]

[1] *National Cardiac PET Centre, University of Ottawa Heart Institute, 40 Ruskin St., Ottawa, ON, Canada K1Y 4W7*

[2] *Department of Cellular and Molecular Medicine, University of Ottawa, 451 Smyth Road, Ottawa, ON, Canada K1H 8M5*

[3] *Department of Radiology, Radio-Oncology and Nuclear Medicine, University of Montreal; University of Montreal Hospital Research Centre (CRCHUM), Montréal, Québec, Canada H2X 0A9*

*Corresponding Author: Jean N. DaSilva, Ph.D.

Department of Radiology, Radio-Oncology and Nuclear Medicine, University of Montreal; University of Montreal Hospital Research Centre (CRCHUM), *900 Rue Saint-Denis,* Montréal, Québec, H2X 0A9 Canada

Tel: (514) 890-8000 (x30653)
E-Mail: jean.dasilva@umontreal.ca
First Author: Basma Ismail, PhD student.

Word Counts: 5894

Shortened Title: Reduced renal AT_1R post-nephrectomy with PET

Contributions of Authors

Performance of the nephrectomy surgeries, PET imaging, autoradiography, blood pressure measurement, echocardiography, blood and urine biochemical assays (except Ang II RIA) were conducted by myself under supervision of Dr. Jean DaSilva. Interpretation and analysis of all data was carried out by myself as well as drafting of the manuscript with the assistance and final editing by Dr. Jean DaSilva. Some of the blood flow data was obtained from the MSc thesis of Kumiko Mackasey. The physicist Dr. Robert deKemp facilitated the application of kinetic modeling and quantification and assisted with editing of the manuscript. Synthesis of the radiotracer was conducted by Dr. Tayebeh Hadizad. Dr Rob Beanlands participated with the clinical implications and perspective on the PET imaging data. The whole work was performed under guidance and supervision of Dr. Jean DaSilva

ABSTRACT

Background: Significant renal mass reduction induced by 5/6 subtotal nephrectomy (Nx) is associated with a chain of events that culminates in hypertension and chronic kidney disease (CKD). Numerous studies have provided evidence for the role of angiotensin (Ang) II type 1 receptor (AT_1R) in the promotion and progression of the disease; however, conflicting results were reported on intrarenal AT_1R levels in CKD models. **Methods:** Male Sprague Dawley rats (n=26) underwent Nx or sham operations. Animals were scanned at 8-10 weeks post-surgery with PET using the novel AT_1R radioligand [^{18}F]FPyKYNE-losartan. Radioligand binding was quantified by kidney-to-blood ratio (KBR), standard uptake value (SUV) and distribution volume (DV). After sacrifice, plasma and kidney Ang II levels were measured. Western blot and ^{125}I-[Sar^1, Ile^8]Ang II autoradiography were performed to assess AT_1R expression. **Results:** At 8-10 weeks post-surgery: Nx rats developed hypertension, elevated plasma creatinine levels, left ventricle hypertrophy, increased myocardial blood flow (MBF), and reduced Ang II levels compared to shams. PET measurements displayed significant decrease in KBR (29%), SUV (24%) and DV (22%) induced by Nx ($p<0.05$), and these findings were confirmed by *in vitro* assays. **Conclusion:** Reduced renal AT_1Rs in hypertensive rats measured with [^{18}F]FPyKYNE-losartan PET at 8-10 weeks following Nx support further use of this non-invasive approach in longitudinal studies to better understand the AT_1R role in CKD progression.

Keywords: Hypertension; Angiotensin II; PET imaging; F18-losartan; Chronic kidney disease

INTRODUCTION

Significant renal mass reduction induced by subtotal 5/6 nephrectomy (Nx) is a model of chronic kidney disease (CKD), which involves deterioration of renal function due to loss of substantial number of nephrons and compensatory hypertrophy in the remnant kidney. In this model, the development of hypertension, proteinuria and progressive renal fibrosis eventually leads to end-stage renal disease (Koomans et al. 2004, Piecha et al. 2008, Garrido et al. 2009). The incidence of cardiovascular events in CKD is more frequent and severe compared to the normal population (Kennedy et al. 2008, Sviglerova et al. 2010). Cardiovascular complications including heart failure or ischemic heart disease represent the leading cause of death in CKD patients (Sukumaran et al. 2010, Sviglerova et al. 2010). Amongst others, components of the renin angiotensin (Ang) system (RAS), particularly Ang II type 1 receptor (AT_1R), are known to contribute towards the detrimental effects on the hemodynamic and inflammatory events associated with the pathogenesis of the disease (Boner et al. 2002, Vaziri et al. 2007, Bader 2010). The efficacy of anti-RAS therapies, such as AT_1R blockers (ARBs) and Ang Converting Enzyme inhibitors (ACEIs), in slowing progression of renal dysfunction, treating hypertension and reducing cardiovascular complications confirms the important role of the AT_1 signaling pathway in these disorders (Yasunari et al. 2005, Balamuthusamy et al. 2008, Piecha et al. 2008). Numerous large clinical trials demonstrated the beneficial effects of RAS blockade on clinical symptoms and outcomes of patients with CKD, however marked interindividual variability were detected in response to these treatments ranging from recognizable clinical benefit to non-detectable benefits or even serious adverse effects (Brenner et al. 2001, Hirsch

2007). PET imaging of AT_1R may help to predict the response to anti-RAS therapy and personalize medicine.

Many organs contain components involved in the synthesis and actions of the RAS, which are largely independent of the RAS systemic components and not accessible to routine laboratory testing (Allen et al. 2000, Kaschina and Unger 2003). The presence of a distinct intra-renal RAS adds complexity in interpreting its role in the progression of CKD. In rodents, there are two isoforms of AT_1R identified in rodents: the $AT_{1A}R$ and $AT_{1B}R$ (Sandberg et al. 1992, Griendling et al. 1996). The $AT_{1A}R$ represents the homologous form of the human AT_1R and are widely distributed on luminal membranes throughout the nephron segments (Harrison-Bernard et al. 2002).

Using different methodologies, previous reports have presented contradictory results on the temporal role played by AT_1Rs in the progression of kidney diseases. The exact alterations in renal AT_1Rs are not entirely understood, with studies reporting decrease in cortex and medulla AT_1R mRNA levels in (30-40%); (Joly et al. 2005) no change; (Dilauro et al. 2010) or increase (>70%) (Vaziri et al. 2007) in the receptor protein expression associated with CKD rodent models.

Non-invasive *in vivo* imaging of the AT_1R will allow for identification of receptor expression abnormalities in CKD, better understanding of the contribution of AT_1R to the development of the disease, and will aid to guide medical therapies for effective management of patients. [^{18}F]FPyKYNE-losartan is a novel PET imaging agent displaying high tissue uptake in the kidney cortex and outer medulla, and binding selectivity for AT_1R over AT_2R (Arksey et al. 2014). It binds with high affinity to renal AT_1Rs (K_D of 49.4 nM), and has antagonistic efficacy with 4-fold less potency reduction

of blood pressure (ED_{50} of 25.5 mg/kg) relative to losartan. [^{18}F]FPyKYNE-Losartan PET imaging exhibited excellent reproducibility in pigs (Hachem et al. 2015). The current work aims to evaluate the capability of using [^{18}F]FPyKYNE-losartan PET to study *in vivo* renal AT_1R changes in Nx animal model of CKD.

MATERIALS AND METHODS

Animal Model

All animal experiments were conducted in accordance with the guidelines of the Canadian Council on Animal Care and with approval of the University of Ottawa Animal Care Committee. Male Sprague-Dawley rats (N=26; 200-250g; Charles River Laboratories, Montreal, Canada), were housed in pairs on a 12h:12h light:dark cycle and fed standard rat chow and water ad libitum. Rats were subjected to either sham or Nx surgery in two sittings under total anesthesia with 2% isoflurane. In the first step, the right kidney was exposed through a lateral dorsal incision, then decapsulated and excised. One week later, the left kidney was exposed in the same way and reduced to 1/3 of its original size by resecting the superior and inferior poles to induce a total of 5/6 Nx (Vaziri et al. 2007, Bader 2010). Post-operative analgesia was provided by subcutaneous administration of buprenorphine twice daily for 3 days following surgery. Sham animals underwent the same 2 surgeries one week apart to simulate Nx conditions without removing the kidneys. Animals were weighed at baseline and end of experiment. After sacrifice by decapitation, kidney, heart and left ventricle (LV) weights were obtained.

Hemodynamic and Biochemical Parameters

Systolic blood pressure was measured in conscious rats at 8-10 weeks post-surgery using indirect tail-cuff plethysmography (CODA-S2 multi-channel, Kent Scientific). Animals were placed in rat holders and trained for 3 days to the measuring conditions. On the 4th day, 6 consecutive measurements were recorded from each rat per session, and an average blood pressure was recorded.

Echocardiography was carried out under light anesthesia using the Vevo 770 system (VisualSonics) and a 23.5 MHz probe. All studies were performed and analyzed by a single operator. Parasternal long-axis views were recorded as sequential ECG-gated M-mode sweeps (EKV-mode) to generate two-dimensional cines of the left ventricle. Analysis of results was completed with the VisualSonics cardiac measurements program, LV wall mass and percent ejection fraction (%EF) were calculated.

Blood and urine measurements for creatinine and albumin were assessed at 8-10 weeks post-surgery. Blood samples were collected, centrifuged (4000 rpm, 4°C) for 10 min, then plasma was stored at -80ºC. Prior to measuring creatinine, plasma proteins were precipitated using deproteinizing sample preparation kit (Biovision). Plasma creatinine levels were determined using a creatinine assay kit (Cell Biolabs) following the manufacturer's instructions. Urine albumin (corrected to creatinine concentration in urine) was determined. Albumin in urine samples was quantified with a commercially available rat ELISA kit (Genway Biotech).

Angiotensin II Plasma and Tissue Levels

After decapitation of animals, trunk blood was collected in EDTA tubes containing a cocktail of protease inhibitors, then centrifuged at 4000 rpm for 5 min to obtain plasma.

Kidneys were rapidly collected and snap frozen on dry ice. Tissues were homogenized in an acidic ethanol [80% vol/vol 0.1N HCl] solution consisting peptidase inhibitors described before (Nakamoto et al. 1995). Plasma and tissue samples were stored at -80°C until the day of assay. Ang II analyses were performed by the Hypertension Core Laboratory at Wake Forest University Health Science Center (Allred et al. 2000). Samples were Sep-Pak extracted and measured by RIA (ALPCo, Windham, NH, USA).

***In vivo* Imaging**

Animals were anaesthetized (2% isoflurane) and kept unconscious throughout the scan using the Inveon DPET camera (Siemens Preclinical Imaging). Rats were set for imaging with the microPET scanner as described previously (Arksey et al. 2014). Images were analyzed with Inveon® Research Workplace software version 1.4 (Siemens Preclinical Imaging) unless indicated otherwise. Dynamic PET images were reconstructed using vendor-provided 3-dimensional ordered subset expectation maximization / maximum a posteriori algorithm OSEM3D/MAP (β=1, OSEM3D iterations = 2, MAP iterations = 18) with all corrections enabled. Volumes of Interest (VOIs) were defined on reconstructed images to obtain time-activity-curves (TACs) in units of Bq/cc.

[^{13}N]Ammonia Blood Flow

Heart and kidneys perfusion studies were assessed within the same week of [^{18}F]FPyKYNE-losartan PET scans. Animals were injected [^{13}N]ammonia 55-110 MBq intravenously and scanned for 30 min. Myocardial blood flow (MBF) was quantified using FlowQuant© software (Klein et al. 2010). Blood and kidney TACs were generated and flow values (ml/g/min) were produced. For calculation of renal blood flow (RBF), the initial 2 min of the dynamic PET data was used to avoid contamination by plasma

metabolites of N-13 radioactivity. The images were reconstructed into 12 x 10 s frames applying the corrections for dead-time, isotope decay, detector efficiencies, and random events. Renal TACs were derived from VOI drawn over renal cortex and arterial input function was derived from the left atrium (LA). The one-tissue-compartment kinetic model was used to calculate K_1 for RBF analysis.

[^{18}F]FPyKYNE-Losartan PET

Rats were injected with 18-81 MBq of [^{18}F]FPYKYNE-losartan (<1ml volume) via a 26 gauge catheter into the lateral tail vein. The specific activity ranged from 6.4-168.4 to GBq/μmol (172 - 4551 mCi/μmol) at time of injection. A dynamic 60 min scan was acquired as 12x10 s, 3x60 s, 11x300 s frames. The arterial input function was obtained from the average blood pool activities within the LA and LV cavity. Briefly, a sphere was drawn inside the cavity of LA or LV at an early frame (10-40 sec post-injection) and an 80% threshold was used to define the contour of the arterial blood VOI. Kidney VOIs were drawn at frame 16 or 17 (5-15 min post-injection where the highest tissue-to-background contrast was observed) by tracing a segment of the cortex at the inferolateral side of the left kidney away from liver and bowel to avoid spillover, and the final VOI was defined using a 50% threshold contour. [^{18}F]FPyKYNE-losartan retention was measured using kidney-to-blood activity ratio (KBR), standard uptake value (SUV) and was correlated with Logan derived distribution volume (DV) values. SUV allowed relative comparison between subjects by normalization to the injected activity and the body weight of the rat. Kidney KBR and SUV values were evaluated at 12.5 min post-injection, which was the time-point displaying maximal tissue-to-blood contrast.

The tracer DV provides a quantifiable parameter for repeated measurements and assessment of repeatability and reliability. Provided the tracer binds to its receptor reversibly, Logan graphical analysis (Logan et al. 1990), of the PET time-activity data can be used to calculate the DV. In essence, tracer uptake in the kidney is plotted against concentration in the plasma at equilibrium (steady-state). Plotting $\mathbf{0 \int {}^{T}C_{PET}(t)dt/C_{PET}(T)(min)}$ against $\mathbf{0 \int {}^{T}C_{P}(t)dt/C_{PET}(T)(min)}$, where $C_{PET}(T)$ is the concentration of tracer in the tissue and $C_P(t)$ is the concentration of tracer in the plasma, will transform the tissue activity to a linear plot, as if the tracer was injected as a continuous infusion. The slope of this line during the steady-state phase corresponds to an estimate of the DV (ml/cm^3).

Western Blot

A subset of animals was dedicated to determine tissue AT_1R protein expression in left kidney cortex using the Bio-Rad Western blot system following previously described methods (Yoneda et al. 2005, Oestreicher et al. 2006). Briefly, rats were sacrificed without anesthesia, kidneys were rapidly excised and flash-frozen in liquid nitrogen, powdered and stored at -80^{o}C until the time of experiment. Tissue was prepared and protein quantification was determined using the BCA protein assay. Protein samples was loaded and separated using 10% SDS polyacrylamide gel electrophoresis followed by transfer to PVDF membranes. The primary AT_1R rabbit polyclonal antibody was purchased from Alomone. The membranes were incubated with the primary antibody (1:2000 for 3 hours in 2.5% skimmed milk), washed (5 min x 6 times) and incubated with the secondary antibody (1:5000) for 1 hour then washed. Protein bands were visualized using ECL and FlourChem 9900 imaging system. GAPDH was used as a loading control, using mouse primary monoclonal antibody (1:5000) and donkey

secondary anti-mouse antibody (1:2000). Data were expressed as integrated density volume (IDV) normalized to GAPDH.

***In vitro* Autoradiography**

In vitro ^{125}I-[Sar^1, Ile^8]Ang II binding was carried out using the method published previously (Kenk et al. 2007). Briefly, rats were sacrificed 2-3 days after PET imaging studies to allow direct comparisons. Following decapitation, dissected kidneys were quickly immersed in OCT Compound (Tissue-Tek), frozen on dry ice and stored at -80^{o}C. Kidneys were sectioned in the axial axis into 20 μm-thick slices at -18^{o}C with a cryostat. Tissue sections were thaw-mounted on glass slides and stored at -80^{o}C. On the day of the experiment, slides were pre-washed in assay buffer (150 mM NaCl, 50 mM sodium phosphate dibasic, 1 mM EDTA, 0.1 mM Bacitracin, 0.1% BSA) for 15 min then incubated with 0.8 nM ^{125}I-[Sar^1, Ile^8]Ang II (Perkin Elmer)for 90 min at room temperature in the presence of AT_2R antagonist, PD 123,319 (10μM) to determine total (non-AT_2R) binding or with unlabelled Ang II for non-specific binding. Specific binding of ^{125}I-[Sar^1, Ile^8]Ang II was calculated as total (non-AT_2R) minus non-specific binding. After incubation, slides were washed 3 times (4^{o}C) sequentially in buffer, deionized water, buffer, and then dried. Sections were exposed to phosphor imaging plates (Kodak Screen-K, Biorad) for 48hours. Phosphor plates were read at a 100μm resolution (BioRad Molecular Imager FX) and analyzed using Quantity One Software (BioRad, Philadelphia). Quantification was done manually by tracing the whole kidney cortex for the radioactivity density (counts/mm^2).

Statistical Analysis

All data are presented as mean ± standard deviation. Results were compared using two-tailed t-test; $p<0.05$ was considered significant. N values for each comparison are given

in the Figures and Tables. Pearson correlation coefficient (r) was calculated to determine correlation between SUV and DV binding parameters.

RESULTS

Animals

No significant change in body weight was observed between Nx and sham-operated rats at the end of experiment (Table 3.1). By contrast, a significant increase ($p<0.05$) was observed in left kidney (30.3%), whole-heart (42.3%) and LV myocardium (33.6%) weights of Nx animals when normalized to body weight and compared to shams (Table 3.1).

Table 3.1: Organ weights normalized to body weights in sham and Nx rats at 8-10 weeks post-surgery (n=3-4 per group).

	BW (gm)	Ht/BW	LV/BW	LK/BW
Sham	643.25±63	2.52±0.077	1.47±0.083	2.09±2.236
Nx	637.67±8	3.60±0.619*	1.96±0.297*	3.68±0.512*

Data is presented as mean ± S.D. *$p<0.05$ vs sham animals; two-tailed t-test.
Nx: 5/6 nephrectomy; BW: body weight; Ht: heart; LV: left ventricle; LK: left kidney.

Hemodynamic and Biochemical Parameters

At 8-10 weeks post-surgery, Nx rats had significantly higher blood pressure values in comparison to sham-operated (Table 3.2; $p<0.002$). At baseline, measured LV mass and %EF were comparable between groups (data not shown). Compared to shams, LV %EF was not affected in Nx rats, whereas a significant increase in LV mass was detected at 8-10 weeks post-surgery (1201±215 vs 874.4±117, respectively, $p<0.002$). As a functional marker of renal dysfunction, level of creatinine in plasma was significantly elevated in Nx rats (Table 3.2; $p<0.01$). However, the amount of albumin excreted in urine (corrected for creatinine concentration) was comparable in both groups (Table 3.2). A significant reduction (-69%) in plasma Ang II levels (Table 3.2; $p<0.05$) was observed in Nx rats at 8-10 weeks post-surgery in comparison to shams. No change in kidney levels of Ang II was observed between nephrectomized and sham-operated rats (Table 3.2).

Table 3.2: Characteristics and hemodynamic data in sham and Nx rats at 8-10 weeks post-surgery (n=4-5 per group).

	SBP (mmHg)	Plasma Cr (mg/dl)	Urine Albumin:Cr (ug/mg)	Plasma Ang II (pg/ml)	Kidney Ang II (pg/mg)
Sham	145.7±18	0.67±0.3	28±1.3	36.53±17.8	16.56±10
Nx	188.4±15.6*	1.36±0.2*	33.66±4.9*	11.2±3*	10.47±1.9

Data is presented as mean ± S.D. *p<0.05 vs sham animals; two-tailed t-test.
Nx: 5/6 nephrectomy; BW: body weight; SBP: Systolic blood pressure; Cr: Creatinine; Ang II: angiotensin II.

PET studies

MBF as measured by [^{13}N]ammonia PET was significantly increased (p<0.05) in Nx rats compared to sham-operated (4.1±0.8 vs 2.7±0.7 ml/g/min, respectively, p<0.002). While no difference in RBF values was found between both groups (5.4 ±0.9 vs 5.2 ± 1.4 ml/g/min for Nx and sham rats respectively).

Representative coronal view PET images are displayed in Figure 3.1A for sham and Figure 4.1B for Nx at 8-10 weeks post-surgery showing strong liver and kidney signal intensity. Blood and kidney TACs displayed similar pattern for uptake and washout in both groups. However, kidney TACs derived from Nx rats were consistently diminished throughout the 60 min scan by qualitative analysis (Figures 3.1C&D). Compared to shams, KBR and kidney SUV obtained from Nx rats were reduced by 29.5% and 24% respectively at 12.5 min post-injection of [^{18}F]FPyKYNE-losartan (Table 3.3). In addition, DV values demonstrated a significant 22% decrease induced by Nx (Table 3.3). Logan plots obtained using frames 17-26 (5-60 min) were linear indicating achievement of equilibrium between tissue and plasma (Figure 3.2). Correlation between corresponding SUV and DV values was significant (r=0.75).

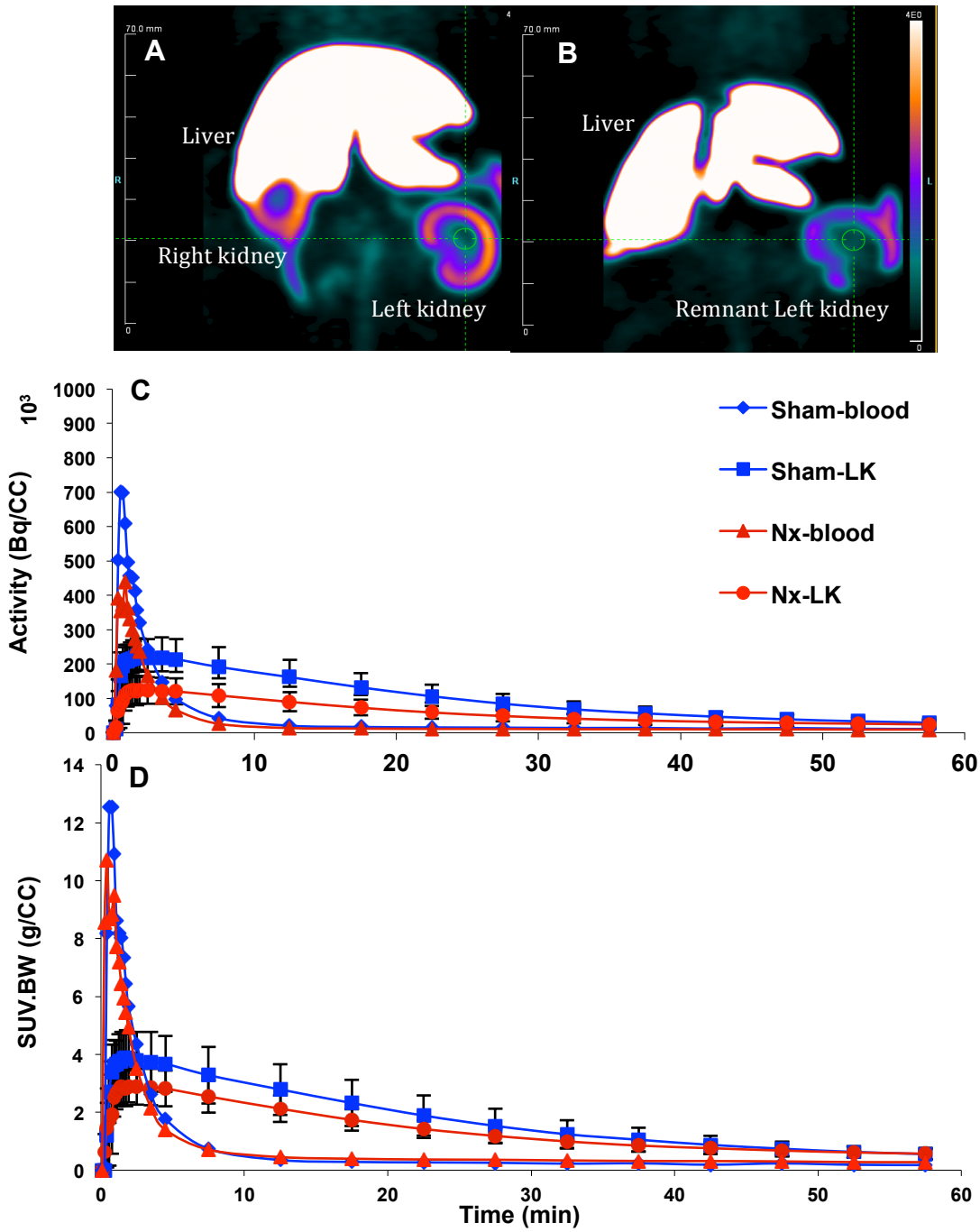

Figure 3.1 Representative [^{18}F]FPyKYNE-losartan coronal view PET images at 5–15 minutes post-injection showing liver and kidney uptake in (A) sham and (B) Nx rats scanned at 8-10 weeks post-surgery; Images are displayed using same SUV scale. Blood and kidney TACs obtained from [^{18}F]FPyKYNE-losartan 60 min scans using (C) voxel intensity in Bq/ml; and (D) SUV. Data is presented as average ± S.D. Nx: 5/6 nephrectomy

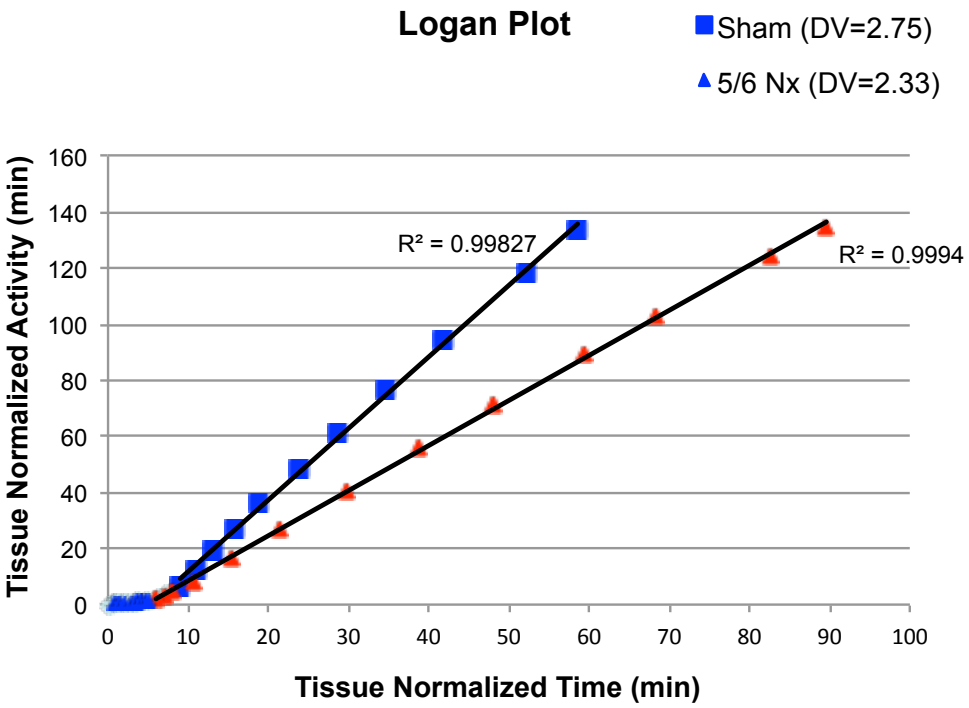

Figure 3.2 Representative [^{18}F]FPyKYNE-losartan Logan plot. The x-axis is the adjusted time and the y-axis is the adjusted activity. A straight line was fitted to each of a sham and Nx rat data. The slope of this curve represents the DV value

In vitro AT_1R expression

Analysis of left kidney cortex showed a 31% decrease in AT_1R protein expression using Western blot technique in Nx animals when compared to shams ($p<0.05$) at 8-10 weeks post-surgery (Figures 3.3A&B). While ^{125}I-[Sar^1, Ile^8]Ang II binding density displayed a significant decrease of 67% in the kidneys of Nx rats as compared to shams ($p<0.05$) (Figure 3.3C). The reduction observed *in vitro* in the AT_1R renal expression was larger than that measured *in vivo* by [^{18}F]FPyKYNE-losartan PET.

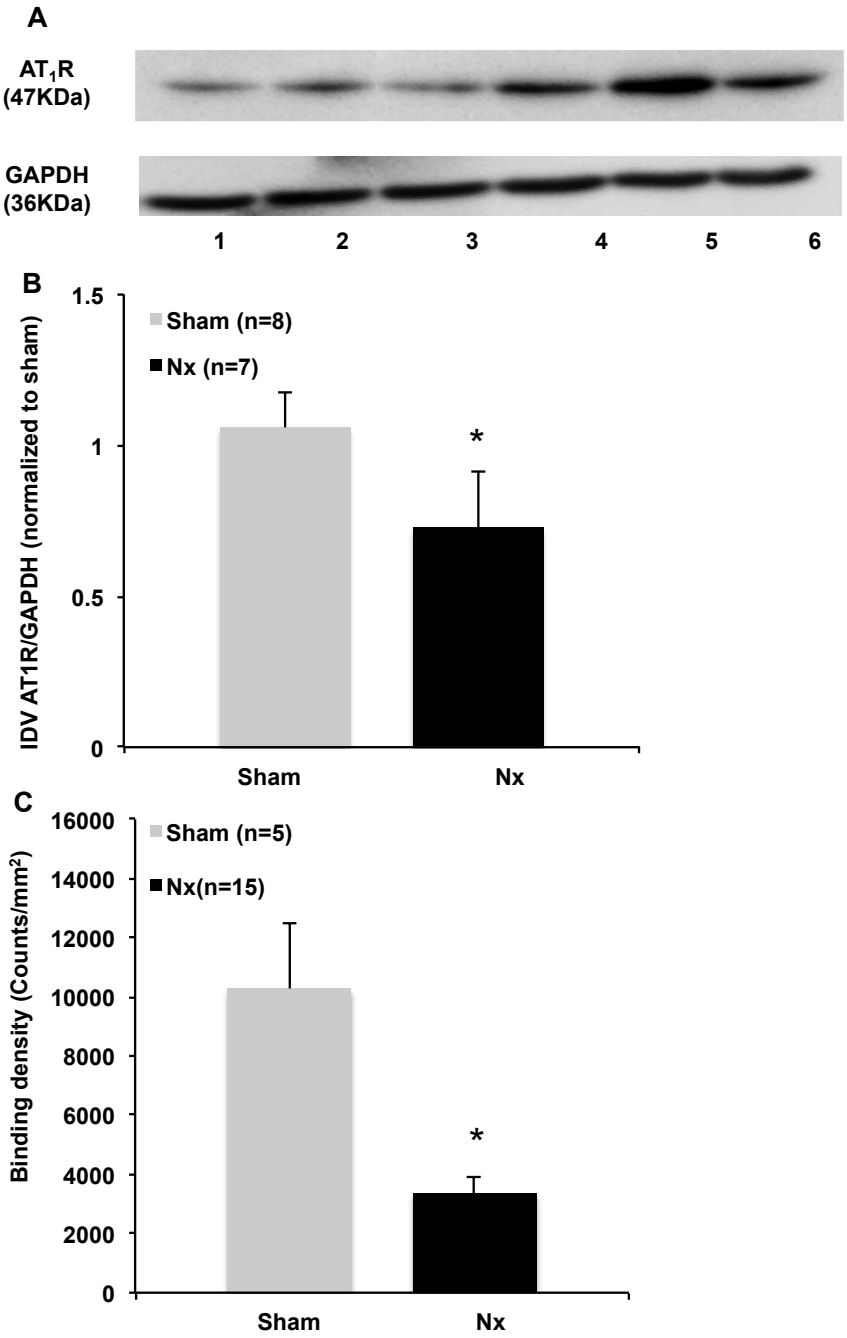

Figure 3.3 *In vitro* AT_1R expression in left kidney cortex at 8-10 weeks post Nx. Representative Western blot (Lane 1-3, 5/6 Nx, Lane 4-6, Sham) (A); Average AT_1R integrated density value (IDV) normalized to GAPDH and sham (B); ^{125}I-[Sar^1, Ile^8]Ang II binding density (C). *p<0.05 as compared to sham. N is number of kidney slices.

Table 3.3: [^{18}F]FPyKYNE-Losartan PET binding parameters in sham and Nx rats at 8-10 weeks post-surgery.

	KBR (unitless)	SUV (g/ml)	DV (ml/cm^3)
Sham	8.0±1.7	2.8±0.9	2.9±0.4
Nx	5.7±1.2*	2.1±0.5*	2.3±0.4*

Data is presented as mean ± S.D. *p<0.05 vs sham animals; two-tailed t-test.
Nx: 5/6 nephrectomy; KBR: kidney-to-blood-ratio; SUV: standardized uptake value; DV: distribution volume; Ang II: angiotensin II.

DISCUSSION

Previous PET studies have explored *in vivo* renal AT_1R alterations induced by dietary sodium changes in rats (Szabo et al. 2001) and in a porcine model of renal ischemia (Gulaldi et al. 2013), but not in the hypertensive Nx rat model of CKD. Removal of one kidney and two thirds of the other in the 5/6 Nx rat model of CKD induces a substantial reduction in the number of functioning nephrons (Koomans et al. 2004, Garrido et al. 2009). Subsequently, the remnant kidney size is excessively hypertrophied as a compensatory effect that may start initially as a true adaptive response but becomes maladaptive later in the course of the disease with deterioration of the renal function (Mackie et al. 2001, Joly et al. 2005, Piecha et al. 2008). In the current study, presence of renal dysfunction is evident by development of hypertension and increased plasma creatinine levels, whereas no overt albuminuria is observed in the Nx rats. Early albuminuria is caused mainly by mechanical damage to the glomerular cells leading to impaired selectivity of the glomerular capillary wall and excessive protein ultrafiltration (van der Meer et al. 2010), so it may be speculated that this stage of the disease was not reached yet in our experiment. No change in kidney Ang II levels was detected in this study, even though an increase in the remnant kidney was anticipated due to local intrarenal RAS activation (Mackie et al. 2001, Dilauro et al. 2010). The reduction in plasma Ang II is most likely due to secondary suppression of systemic RAS as reported previously with this model (Mackie et al. 2001, Dilauro et al. 2010).

There is a fair amount of data on the cardiac consequences secondary to renal failure established in this model (Vaziri et al. 2007, Frohlich et al. 2011). Notably, LV hypertrophy is one of the common features reported during the different stages of CKD

in animal models and patients (Amann et al. 1998, Koivuviita et al. 2009). Likewise, LV hypertrophy was observed in the Nx rats in our study. This result is probably attributed to prolonged pressure overload induced by hypertension and not necessarily due to activation of AT_1R in the heart (Kennedy et al. 2008, Sviglerova et al. 2010). It was not possible to visualize [^{18}F]FPyKYNE-losartan uptake in the heart due to the very low density of myocardial AT_1Rs compared to the kidney (Chang and Lotti 1991). Such low cardiac expression requires a very high specific activity of the injected tracer formulation (>7000 Ci/mmol) to prevent saturation of the AT_1Rs (Higuchi et al. 2010).

Cortical RBF was not statistically different in remnant kidney compared to whole left kidney of shams. Previous groups reported an increase in RBF immediately after renal mass reduction that was normalized within one-week post-surgery (Kaufman et al. 1975, Chevalier and Kaiser 1985). However normal blood flow can be explained by the presence of intact renal autoregulation in the Nx rat kidneys (Griffin et al. 2003, Vaziri et al. 2007).

The reduction in AT_1R binding obtained with PET [^{18}F]FPyKYNE-losartan in Nx rat kidneys was quantified using different parameters; DVs, SUVs and KBR values. Physiologically, the Logan derived DV values are the most appropriate indicators of protein expression and/or receptor-ligand binding potential (Bmax/Kd) for ligands that bind reversibly. However due to technical limitations, no further corrections were applied for plasma input function, plasma protein binding and nonspecific binding which are implicit to the DV calculation. Hence to enhance the validity of the measured DV values, PET findings were also represented using semiquantitative analysis (KBR and SUV), where an arterial input function is not indicated. The strong agreement

between calculated SUV and DV encourages our confidence in the accuracy of the detected results.

In fact, our imaging data agrees with prior work displaying decrease in AT_1R mRNA and protein expression, and similar renal mass reduction at different timepoints (Joly et al. 2005, Sui et al. 2010). Furthermore, Cao et al. reported that the reduction of AT_1R expression induced an imbalance in the relative proportions of AT_1 and AT_2 receptors that is consecutively implicated in progressive renal injury (Cao et al. 2002). The lower expression of AT_1R could be interpreted as a protective mechanism to avoid deleterious effects of hyperactive intrarenal RAS. On the other hand, there are studies that reported opposite effects with elevated AT_1R expression using Western blot following renal ablation (Vaziri et al. 2007, Sui et al. 2010). AT_1R is implicated in most of the detrimental effects of CKD such as inflammation, renal fibrosis and renal hypertrophy (Vaziri et al. 2007). A distinct speculation for the inconsistency in the AT_1R results can be due to the non-specificity of the commonly used AT_1R antibodies for *in vitro* assessment as demonstrated in 2 recent publications (Benicky et al. 2012, Herrera et al. 2013). This uncertainty justifies the use of autoradiography in our study in addition to Western assays in assessment of AT_1R renal expression.

However to be noted, *in vitro* autoradiography evaluates only the extent of membrane-bound receptor in non-viable tissue, whereas change in AT_1R density can be affected by internalization or turnover of the receptor. Activation of AT_1R signal transduction systems can occur within seconds through $G_{\alpha q}$ and IP_3, or within minutes to hours through MAP kinase and JAK/STAT systems (Marrero et al. 2004). Moreover, AT_1Rs are endocytosed within 10 min after activation, with ~25% recycled to plasma membrane

and the remainder degraded in lysosomes (Griendling et al. 1987). Consequently, the dynamic nature of AT_1R is a limitation for the accuracy of *in vitro* measurements and represents an added value for *in vivo* PET as an investigative tool to detect total receptor changes.

A non-invasive means for assessing renal AT_1R signaling at various stages of CKD *in vivo* would advance our understanding of the receptor abnormalities associated with progression of the disease and therapy response in patients. Measurements of a local tissue RAS components (such as AT_1Rs) in clinical or experimental CKD studies may be more predictive of the degree of renal injury compared to studies targeting the circulating RAS components. Nevertheless, it is important to note that AT_1R regulation is cell and tissue specific (Burns 2000), whereas a major drawback with PET imaging is its poor resolution (especially in rodents) to delineate specific cellular localization of [^{18}F]FPyKYNE-Losartan accumulation within the kidney.

CONCLUSION

The present study is the first to provide *in vivo* evidence for a reduction of renal AT_1R cortical expression in a rat model of CKD at 8-10 weeks post Nx. The robustness of PET findings confirmed by *in vitro* AT_1R expression suggests that [^{18}F]FPyKYNE-losartan is a promising PET tracer for longitudinal imaging renal AT_1R in multiple pathological conditions. Such an approach in clinic would present a unique opportunity to advance understanding of the pathophysiology of various diseases including myocardial infarction, hypertension, vascular and renal failure.

ACKNOWLEDGEMENT

The authors acknowledge the contributions of Dr. Etienne Croteau and Christine Archer for microPET imaging; and also thank Ottawa Heart Institute Animal Care and Veterinary Staff for general assistance with the experiments. This work was supported in part by, the Ontario Preclinical Imaging Consortium (OPIC) grant# RE03-51 (Ontario Research Foundation) and the Canadian Institutes of Health Research (MOP-80203 & MOP-287694) and by the Molecular Function and Imaging Heart and Stroke Foundation of Ontario Program Grant (#PRG6242).

BI was supported by the PhD scholarship from the University of Ottawa's Faculty of Medicine Endowed Funds for Cardiac Graduate Research and the UOHI Foundation. RSB is a Career Investigator supported by the Heart and Stroke Foundation of Ontario (HFSO), the University of Ottawa Heart Institute (UOHI) Vered Chair in Cardiology and Tier 1 University of Ottawa Chair in Cardiovascular Research.

COMPETING INTERESTS

Dr Rob deKemp receives revenue shares from FlowQuant sales.

AUTHORS' CONTRIBUTIONS

Animal surgeries, PET imaging, echocardiography, SBP measurements, creatinine and albumin assays, westerns, autoradiography and all data analysis described in this manuscript were conducted by BI, under supervision and guidance of JDS. RdK assisted with the application of kinetic modeling and quantification of PET data. TH conducted the synthesis of the novel radiotracer [^{18}F]FPyKYNE-losartan. Some of the blood flow

data was obtained from the MSc work of KM. RSB participated in the clinical implications and perspective on the AT_1R imaging data. All authors read and approved the final manuscript.

CHAPTER 4: MANUSCRIPT #3

Delayed treatment with enalapril and not diltiazem ameliorates progression of chronic kidney disease in rats: predictive value of kidney AT_1 receptor

Hypertension (to be submitted)

B. Ismail[1,2], RA. deKemp[1], E. Croteau[1], T. Hadizad[1], K.D. Burns[3], RS. Beanlands[1,2], J N. DaSilva[1,2,4]

[1] *National Cardiac PET Centre, Department of Medicine (Division of Cardiology) University of Ottawa Heart Institute, 40 Ruskin St., Ottawa, ON, Canada K1Y 4W7*

[2] *Department of Cellular and Molecular Medicine, University of Ottawa, 451 Smyth Road, Ottawa, ON, Canada K1H 8M5*

[3] *Kidney Research Centre, Ottawa Hospital Research Institute, University of Ottawa, Ontario, Canada*

[4] *Department of Radiology, Radio-Oncology and Nuclear Medicine, University of Montreal; University of Montreal Hospital Research Centre (CRCHUM), Montréal, Québec, Canada H2X 0A9*

*Corresponding Author: Jean N. DaSilva, Ph.D.

Department of Radiology, Radio-Oncology and Nuclear Medicine, University of Montreal; University of Montreal Hospital Research Centre (CRCHUM), *900 Rue Saint-Denis,* Montréal, Québec, H2X 0A9 Canada

Tel: (514) 890-8000 (x30653)

E-Mail: jean.dasilva@umontreal.ca

Shortened title: PET normalization of renal AT1 receptor with Enalapril in CKD

Word count of manuscript: 5620

Word count of abstract: 250 (max is 250)

Total number of Figures: 5

Total number of Tables: 2

Contributions of Authors

Performance of the nephrectomy surgeries, PET imaging, autoradiography, blood pressure measurement, echocardiography, blood and urine biochemical assays (except Ang II RIA) were conducted by myself under supervision and guidance of Dr. Jean DaSilva. Interpretation and analysis of all data and the manuscript was drafted by myself with the assistance and final editing by Dr. Jean DaSilva. The physicist Dr. Robert deKemp facilitated the application of kinetic modeling and quantification. Synthesis of the radiotracer was conducted by Dr. Tayebeh Hadizad. Dr Etienne Croteau performed the PET scans included in this study and data reconstruction, then contributed to the analysis of imaging results. Dr. Kevin Burns helped with his clinical expertise in the interpretation of the obtained kidney results and assisted with editing of the manuscript. Dr. Rob Beanlands provided the implications and perspective on the PET imaging data.

Abstract

ACE inhibitors are considered first line of treatment in patients with many forms of chronic kidney disease (CKD). Other antihypertensives such as calcium channel blockers achieve similar therapeutic effectiveness in attenuating hypertension-related renal damage progression. Our objective was to explore the value of positron emission tomography (PET) imaging of renal AT_1 receptor (AT_1R) to guide therapy in the 5/6 subtotal-nephrectomy (Nx) rat model of CKD. Ten weeks after Nx, Sprague-Dawley rats were administered 10mg/kg/d enalapril (NxE), 30mg/kg/d diltiazem (NxD) or left untreated (Nx) for an additional 8-10 weeks. Kidney AT_1R expression was assessed using *in vivo* [^{18}F]FPyKYNE-losartan PET and *in vitro* autoradiography. Compared to shams, Nx rats exhibited higher systolic blood pressure that was reduced by both enalapril and diltiazem. At 18-20 weeks, plasma creatinine and albuminuria were significantly increased in Nx, reduced to sham levels in NxE, but enhanced in NxD rats. Only treatment with enalapril reduced plasma and kidney angiotensin II to sham levels. Reduced PET renal AT_1R levels in Nx were normalized by enalapril but not diltiazem, and results were supported by autoradiography. Reduction of renal blood flow in Nx was restored by enalapril, while no difference was observed in myocardial blood flow amongst groups. Enhanced left ventricle mass in Nx was not reversed by enalapril but was augmented with diltiazem. Stroke volume was diminished in untreated Nx compared to shams and restored with both therapies. In summary, delayed treatment with enalapril normalized AT_1R expression and reduced progression of CKD, whereas diltiazem exacerbated renal and cardiac dysfunction.

Keywords: ACE inhibitor; Calcium channel blocker; Renal hypertension; Cardiorenal failure; [^{18}F]FPyKYNE-losartan; PET imaging

Introduction

Chronic kidney disease (CKD) is a growing health problem worldwide with increasing annual incidence at a rate of 8%, and consumes up to 2% of the global health expenditure.(Levin et al. 2008) The prevalence of hypertension is substantial in patients suffering from kidney disease,(Arora et al. 2013) and is considered a major risk factor for progression to end-stage renal disease (ESRD), and for cardiovascular complications,(Asselbergs et al. 2004, Pohl et al. 2005, Toto 2005, Appel et al. 2010) which represent the leading cause of death in CKD.(Sukumaran et al. 2010, Sviglerova et al. 2010) Accordingly, blood pressure control is a cornerstone in the management of CKD. Most recent guidelines recommend the use of renin angiotensin (Ang) system (RAS) inhibitors in the initial antihypertensive regimen due to class-specific renoprotective mechanisms independent of their blood pressure lowering effect.(Jafar et al. 2003, Griffin and Bidani 2008, Macconi 2010) Thus, RAS blockade with Ang-converting enzyme inhibitors (ACEIs) or AT_1 receptor (AT_1R) blockers (ARBs) have been shown in landmark clinical trials to dramatically attenuate the decline in renal function associated with CKD.(1997, Brenner et al. 2001, Lewis et al. 2001, Parving et al. 2001, Parving et al. 2001) Despite the widespread clinical use of RAS blockers, the exact mechanisms through which they lower blood pressure and protect the kidney from injury have not been fully elucidated. This has drawn our attention that probing of the intrarenal molecular changes associated with the development and progression of CKD can assist prediction and monitoring of therapy. We have identified AT_1R as a key molecular imaging target because of its direct involvement in the many aspects of renal pathophysiology.

Nevertheless, alternative antihypertensives given alone or in combination were shown to be successful in reaching optimal blood pressure target and in slowing progression of CKD. In this regard, calcium channel blockers (CCBs) are similarly as efficient as RAS blockers at attenuating hypertension-related renal damage progression, when administered during the non-proteinuric stages of CKD.(Black et al. 1998, Brown et al. 2000, Hansson et al. 2000, Officers et al. 2002, Wright et al. 2002) The use of dihydropyridine and nondihydropyridine CCBs has been reported to be safe and effective in management of CKD, provided that a tight control of blood pressure was achieved (reviewed in(Nathan et al. 2005, Segura et al. 2005, Bidani and Griffin 2006, Lopez-Novoa et al. 2010)).

Our group has synthesized several positron emission tomography (PET) radioligands derived from the clinically used ARBs for imaging of the AT_1R in kidney.(Hadizad et al. 2009, Hadizad et al. 2011, Lortie et al. 2013, Arksey et al. 2014, Ismail et al. 2015) Preliminary PET studies with [^{18}F]FPyKYNE-losartan radioligand exhibited high binding selectivity for kidney AT_1R over AT_2R and rapid metabolism in rats which supported the potential of this tracer for further renal AT_1R evaluation. We have successfully demonstrated an *in vivo* reduction of renal AT_1R cortical expression in rats with CKD at 8-10 weeks post 5/6 nephrectomy (Nx) using [^{18}F]FPyKYNE-losartan with PET imaging (Manuscript #2). The hypothesis of the present work was that PET imaging of renal AT_1Rs will provide mechanistic insights on the progression of the disease at the AT_1R level, and guide antihypertensive therapy in management of CKD. RAS inhibition with ACEI was selected instead of an ARB for management of CKD so as not to interfere with the binding of the losartan analog radiotracer used in PET imaging.

Materials and Methods

All animal experiments were conducted in accordance with the guidelines of the Canadian Council on Animal Care and with approval of the University of Ottawa Animal Care Committee. Male Sprague-Dawley rats (200-250 g; Charles River Laboratories, Montreal, Canada), were housed in pairs on a 12h:12h light:dark cycle and fed standard rat chow and water ad libitum. Sprague-Dawley rats were subjected to either sham or Nx surgery in two steps one week apart. Ten weeks after surgery, rats (N=34) were administered 10mg/kg/d enalapril (NxE),(Windt et al. 2006, Ghosh et al. 2009) 30 mg/kg/d diltiazem (NxD)(Podjarny et al. 1993, Podjarny et al. 2004) in drinking water or left untreated (Nx) for an additional 8-10 weeks. Animals were weighed at the beginning and end of study. Systolic blood pressure (SBP), plasma creatinine (Cr), and urine albumin: Cr were measured at 18-20 weeks post-surgery. AT_1R was evaluated using *in vivo* [^{18}F]FPyKYNE-losartan PET and *in vitro* autoradiography. Plasma and tissue Ang II, organ blood flow and heart function were also assessed. After sacrifice by decapitation, kidney, heart and left ventricle (LV) weights were obtained.

An expanded Methods section is available in the online-only Data Supplement.

Statistical Analysis

All data are presented as mean ± standard deviation. Statistical analysis was performed with one way ANOVA using Tukey test for posthoc analysis (Prism; GraphPad Software; version 6.0h); $p<0.05$ was considered significant. N values for each comparison are given in the Figures and Tables. Data are expressed either as mean and standard deviation in the Tables, or medians and interquartiles in the boxplot Figures. Pearson correlation

coefficient (r) was calculated to determine correlations between various parameters when required.

Results

Body and Organ Weights

At 8-10 weeks before the start of treatments, body weights were comparable among all groups of animals. Similarly, at 18-20 weeks post Nx, no significant differences in body weight or the percentage increase per week were observed between the groups (Figure 4.1A). No significant changes in kidney weight/body weight were observed in Nx or NxE rats, compared to shams, although there was a tendency for kidney hypertrophy in the Nx group. Kidney weight/body weight was significantly increased in diltiazem-treated rats, compared to all groups (1.7-2.7-fold, $p<0.05$; Figure 4.1B). Cardiac hypertrophy was not observed in the sham, Nx and NxE groups. However, treatment with diltiazem induced a significant increase in heart weight/body weight compared to shams (1.4-fold, $p<0.05$; Figure 4.1C).

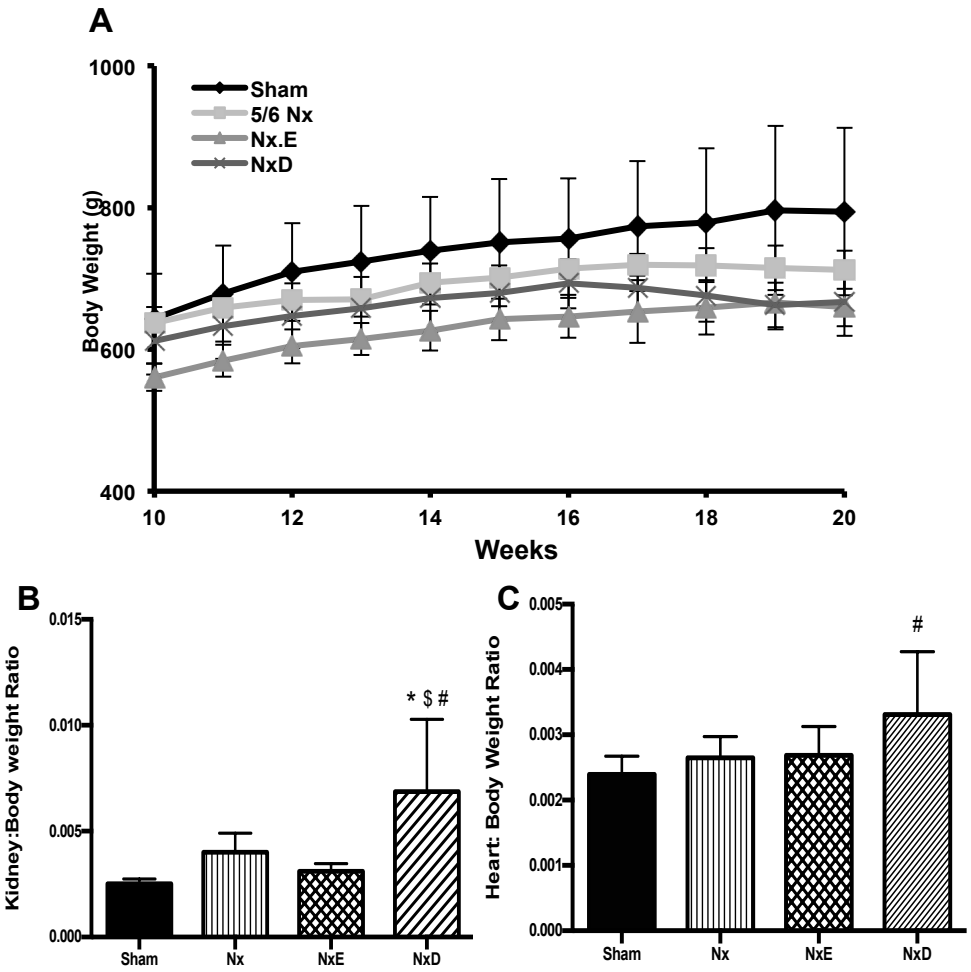

Figure 4.1: Body weight data obtained weekly over 10 weeks (A), terminal kidney weights for sham (N=8), Nx (N=8), NxE (N=6) and NxD (N=8) (B) and heart weights for sham (N=8), Nx (N=9), NxE (N=9) and NxD (N=8) (C) normalized to body weight at 18-20 weeks post-surgery. Data are presented as mean±SD. * $p<0.05$ vs sham, $^{\$}$ $p<0.05$ vs Nx, $^{\#}$ $p<0.05$ vs NxE ($p<0.05$).

Systolic Blood Pressure and Renal Function

Nx rats had significantly higher SBP at 18-20 weeks post-surgery compared to shams (1.5-fold; $p<0.001$). Both enalapril and diltiazem treatments attenuated this increase (Table 4.1).

Plasma Cr concentration was significantly higher in Nx rats at 18-20 weeks post-surgery (1.6 fold; $p<0.05$). By contrast, plasma Cr was not increased in the enalapril-treated group, compared to untreated Nx animals, while diltiazem induced a significant increase compared to all groups (1.8-3 fold; $p<0.05$) (Table 4.1). At the end of study, significant albuminuria (corrected to urine Cr concentration) developed in the untreated Nx animals, which was normalized by enalapril and exacerbated in diltiazem-treated rats (NxD: 4.8-fold increase versus sham, 1.8-fold increase versus Nx; $p<0.001$) (Table 4.1).

Table 4.1: SBP, plasma creatinine (Cr) and urinary albumin:Cr in sham, untreated Nx, NxE and NxD (at 18-20 weeks post-surgery).

Parameters	SBP (mmHg)	Plasma Cr (mg/dl)	Urine Albumin:Cr (ug/mg)
Sham	142.7±15* N=4	0.48±0.06 N=5	81.4±30.0 N=4
Nx	188.8±17.3 N=8	0.77±0.07* N=6	211.37±39.2* N=4
NxE	152±8.65$^{\$}$ N=6	0.43±0.06$^{\$}$ N=5	116.5±32.1$^{\$}$ N=4
NxD	145.8±5.78$^{\$}$ N=5	1.46±0.27*$^{\$\#}$ N=6	385.6±53.5*$^{\$\#}$ N=4

Data are presented as mean±SD.
* $p<0.05$ vs sham, $^{\$}$ $p<0.05$ vs Nx, $^{\#}$ $p<0.05$ vs NxE ($p<0.05$).

Plasma and Tissue Angiotensin II Levels

Ang II levels in plasma, kidney and LV were elevated in Nx rats compared to sham, however did not reach significance (p value = 0.15, 0.13, 0.22 respectively). Administration of enalapril did not affect Ang II levels in plasma or LV but significantly reduced levels in the kidney compared to Nx rats ($p<0.05$; Figure 4.2A, B and C). Interestingly, treatment with diltiazem induced significant elevations in plasma and kidney Ang II levels, in comparison to the sham and NxE groups at 18-20 weeks ($p<0.05$ for plasma and $p<0.001$ for kidney; Figure 4.2A and B). Moreover diltiazem caused a marked elevation of Ang II in LV compared to all other groups (3.75-fold versus sham, 5.6-fold versus Nx, and 5-fold versus NxE; Figure 4.2C).

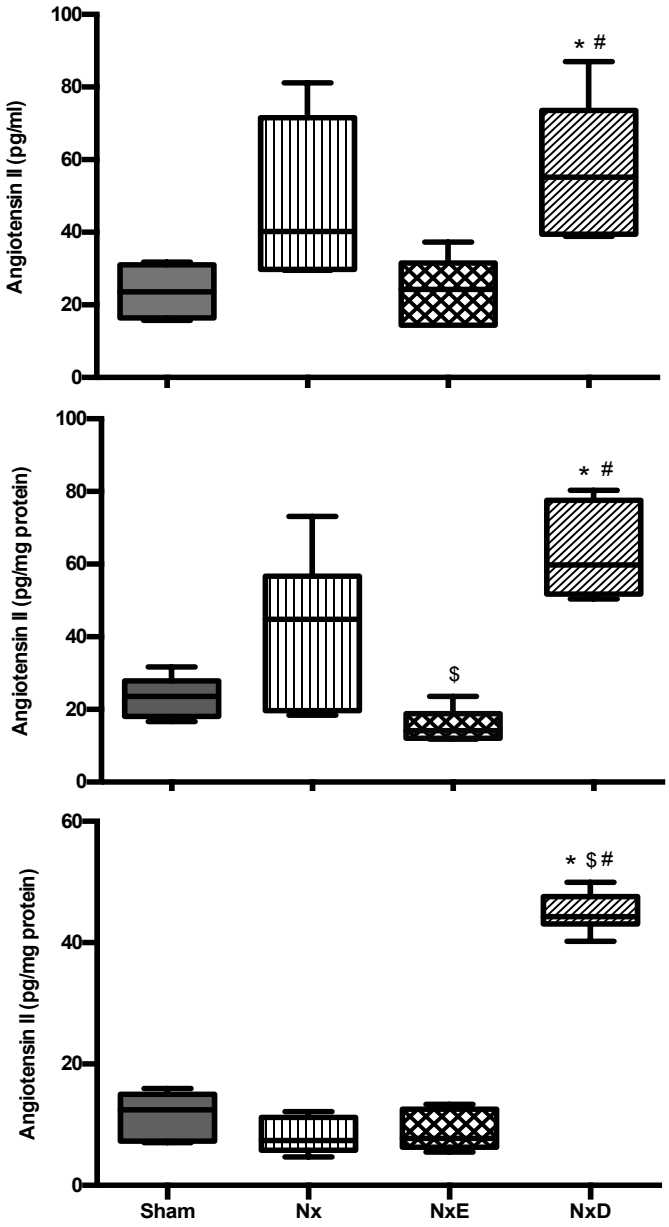

Figure 4.2: Ang II levels in plasma samples of sham (N=4), Nx (N=5), NxE (N=5) and NxD (N=6) (A), left kidney samples of sham (N=5), Nx (N=6), NxE (N=5) and NxD (N=6) (B) and left ventricle samples of sham (N=6), Nx (N=7), NxE (N=5) and NxD (N=6) (C) samples of Sham, Nx, NxE and NxD groups at 18-20 weeks post-surgery. In boxplots, horizontal lines represent median and whiskers represent minimum and maximum values. Data are presented as mean±SD. * $p<0.05$ vs sham, $^{\$}$ $p<0.05$ vs Nx, $^{\#}$ $p<0.05$ vs NxE ($p<0.05$).

AT_1R Expression

In vivo PET scans of the Nx rats revealed a distorted shape of the kidney after resection with less tracer uptake as compared to the normal kidney in shams (Figure 4A and B). While enalapril preserved the shape of the remnant left kidney and tracer retention, diltiazem-treated rats displayed further distortion of the kidney structure with minimal uptake of the tracer (Figure 4.3C and D). [^{18}F]FPyKYNE-losartan distribution volume (DV, ml/cm^3) determined by Logan analysis was quantified as an indication of AT_1R expression in the kidney of rats (Figure 4.3E). DV values were significantly lower in Nx rats compared to sham animals (-28%, $p<0.05$). Treatment with enalapril normalized these values while no change was observed in the diltiazem-treated group. [^{125}I]-[Sar^1, Ile^8]Ang II specific binding density confirmed reduction of AT_1R in the untreated Nx group at 18-20 weeks (-36%, $p<0.05$), and normalization of the receptor expression in rats receiving enalapril but not with diltiazem therapy (Figure 4.3F). These results correlated well with the *in vivo* PET findings (r=0.47, $p=0.05$).

Organ Blood Flow

Renal blood flow as assessed by [^{13}N]ammonia PET was significantly reduced in Nx rats, compared to shams ($p<0.05$), and tended to normalize with enalapril treatment, although this did not achieve statistical significance. By contrast, diltiazem caused a further significant reduction in renal blood flow, compared to untreated Nx rats (Figure 4.3G). No significant differences in myocardial blood flow occurred amongst groups (Figure 4.3H).

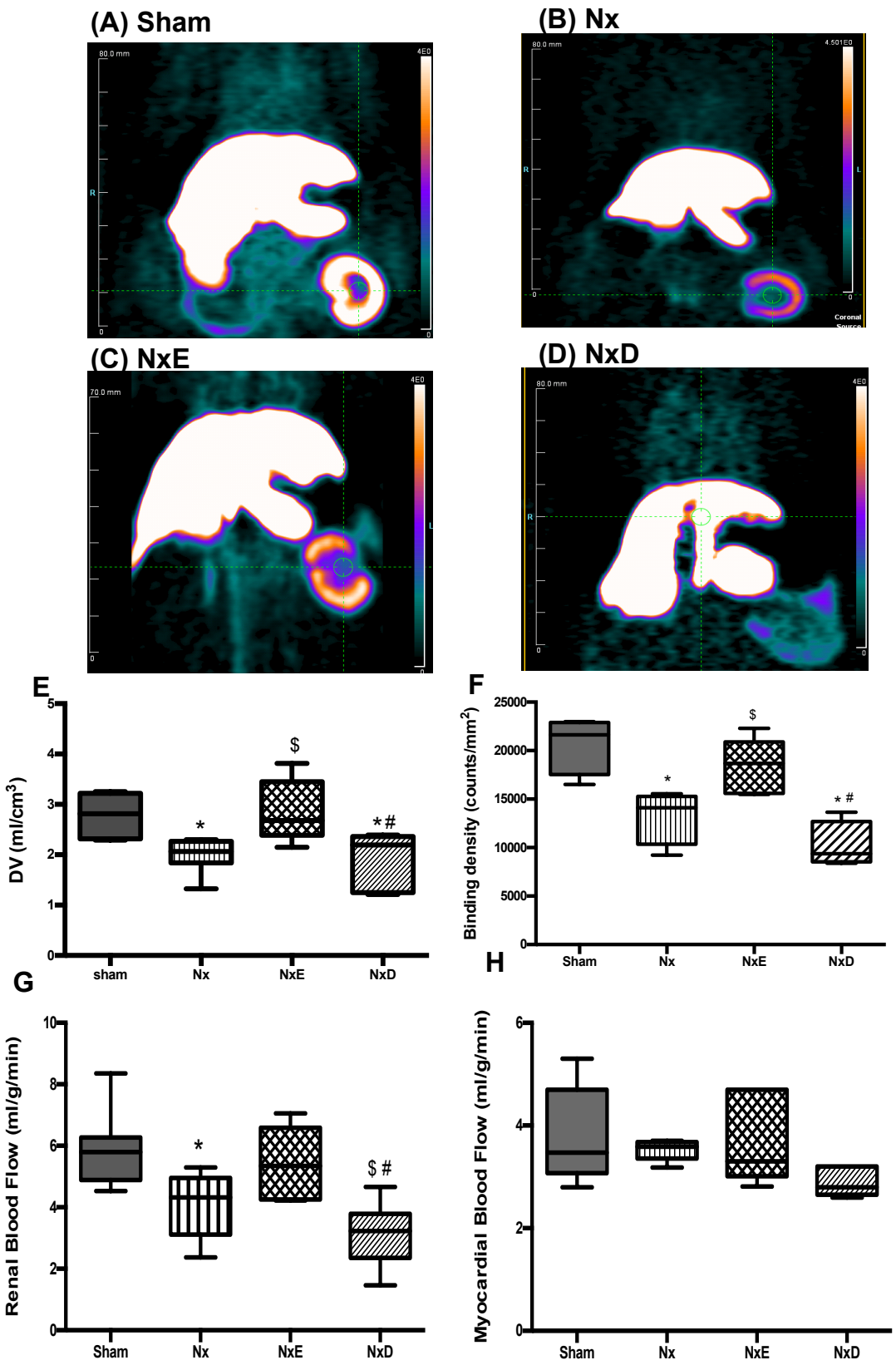
(A) Sham
(B) Nx
(C) NxE
(D) NxD
E
DV (ml/cm3)
sham
Nx
NxE
NxD
F
Binding density (counts/mm2)
Sham
Nx
NxE
NxD
G
Renal Blood Flow (ml/g/min)
Sham
Nx
NxE
NxD
H
Myocardial Blood Flow (ml/g/min)
Sham
Nx
NxE
NxD

Figure 4.3: Representative coronal view microPET scans showing liver and kidney uptake obtained at 5-10 min post-injection of [^{18}F]FPyKYNE-losartan in all groups at 18-20 weeks post-surgery; Sham (A), Nx (B), NxE (C) and NxD (D). Images are displayed using same SUV scale. Kidney distribution volume (DV, ml/cm^3) of [^{18}F]FPyKYNE-losartan obtained with PET *in vivo* in sham (N=6), Nx (N=7), NxE (N=7) and NxD (N=6) (E); and ^{125}I-[Sar^1, Ile^8]Ang II binding density (counts/mm^2) obtained with *in vitro* autoradiography in sham (N=4), Nx (N=4), NxE (N=6) and NxD (N=4) (F) at 18-20 weeks post-surgery. Renal blood flow in sham (N=7), Nx (N=7), NxE (N=5) and NxD (N=7) groups (G); and myocardial blood flow values in sham (N=5), Nx (N=6), NxE (N=5) and NxD (N=6) (H) at 18-20 weeks post-surgery. Blood flow was assessed by [^{13}N]ammonia PET imaging. In boxplots, horizontal lines represent median and whiskers represent minimum and maximum values. Data are presented as mean±SD. * $p<0.05$ vs sham, $^{\$}$ $p<0.05$ vs Nx, $^{\#}$ $p<0.05$ vs NxE ($p<0.05$).

Heart Function

Echocardiographic measures of heart functions are summarized in Table 4.2. There was no difference in LV ejection fraction (LVEF) between all groups. However, end diastolic volume (EDV) and stroke volume (SV) were significantly diminished in untreated Nx rats as compared to shams. Treatment with enalapril and diltiazem restored only SV to normal levels (Table 4.2). Echocardiographic LV mass was significantly increased in the Nx group and was not reversed in rats receiving enalapril. Dlitiazem treatment further enhanced the LV mass compared to all groups (3.5-fold versus sham, 1.7-fold versus Nx, and 1.7-fold versus NxE; $p<0.001$).

Significant Correlations

A strong inverse correlation was found between AT_1R PET kidney DV value and albuminuria (r=-0.731, $p=0.0009$) also between AT_1R PET DV kidney value and LV mass (r=-0.733, $p=0.0019$). Interestingly, a weak negative correlation was found between the AT_1R PET DV and SBP measurements (r=-0.28, $p=0.28$).

Table 4.2: Echocardiographic parameters in sham, untreated Nx, NxE and NxD groups at 18-20 weeks post-surgery.

Parameters	LV EF (%)	SV (ml)	EDV (ml)	LV mass (g)
Sham	73.3±5.3 N=6	450±89 N=6	611±91.8 N=6	450±89 N=6
Nx	63.6±7.9 N=5	285±42.3* N=5	462±74.3* N=6	923±165.3* N=6
NxE	73.3±6.5 N=9	414±89.4$^{\$}$ N=8	542±78.2 N=9	920±126.9* N=7
NxD	72.2±5.5 N=6	437±71.7$^{\$}$ N=5	577±112.3 N=6	1601±302.3*$^{\$\#}$ N=6

Data is presented as mean±SD

* $p<0.05$ vs sham, \$ $p<0.05$ vs Nx, # $p<0.05$ vs NxE ($p<0.05$). LV: left ventricle, EF: ejection fraction, EDV: end diastolic volume, SV: stroke volume.

Discussion

In this study, we used 5/6 nephrectomy rat model to investigate AT_1R alterations in CKD with PET. The major finding is the *in vivo* demonstration of renal AT_1R reduction associated with the activated RAS due to renal hypertension in Nx rats, which was normalized following administration of the ACEI enalapril. Subtotal nephrectomized rats developed hypertension, renal dysfunction and albuminuria at 18-20 weeks post-surgery. In addition to being an important prognostic factor in progressive CKD, albuminuria is considered as an independent predictor of cardiovascular morbidity and mortality.(Chronic Kidney Disease Prognosis et al. 2010, van der Velde et al. 2011) We have recently reported that induction of Nx in rats caused elevations in SBP and plasma Cr without evidence of albuminuria at 8-10 weeks post-surgery indicating intact glomerular barrier at that stage (Manuscript #2). In the current work, development of significant albuminuria was observed with sustained hypertension and renal impairment at 18-20 weeks post-surgery. Consistent with previous clinical and experimental findings,(Noda et al. 1999, Rahn 2005, Windt et al. 2006) the administration of ACEI enalapril normalized SBP, plasma Cr, and attenuated albuminuria associated with Nx.

The presence of heightened systemic and local RAS activity in CKD is well established,(Dilauro et al. 2010, Kujal et al. 2010) similarly here, an increase in the levels of plasma and kidney Ang II in the untreated Nx rats were observed although it did not reach significance. The renal blood flow was reduced displaying a similar trend to [^{18}F]FPyKYNE-losartan decreased retention in the untreated Nx rats when compared with shams. However, this reduction in blood flow is not assumed to be the cause for diminished [^{18}F]FPyKYNE-losartan uptake, since the AT_1R reduction with PET was

confirmed by [^{125}I]-[Sar^1, Ile^8]Ang II autoradiography. This assumption is further validated by the fact that using the same model of CKD, Nx rats exhibited no change in the renal blood flow associated with the PET AT_1R reduction at 8-10 weeks post-surgery (Manuscript #2). Indeed, local factors as Ang II, tumor growth factor-beta (TGF-βa)(Lopez-Novoa et al. 2010) and endothelin-1,(Bruzzi et al. 1997) or reduction of nitric oxide production(Aiello et al. 1998) among others, can be implicated in the changes in the renal hemodynamics. As expected, a reduction of systemic and renal Ang II levels was observed in the NxE treated group, confirming an inverse correlation between Ang II levels and AT_1R expression. The fact that enalapril treatment decreased Ang II in the kidney to values below the sham group is intriguing. This could be explained by the increased Ang II in the kidney due to augmentation of the remnant kidney intrinsic ability to produce Ang II through ACE-dependent pathways and/or due to uptake of Ang II from the circulation.(Kobori et al. 2007, Velez 2009, Macconi 2010)

Previous experimental studies investigating the renal RAS (mainly AT_1R expression) in various animal models of CKD have yielded conflicting results that may reflect differences in methodology and/or time points of measurements.(Joly et al. 2005, Vaziri et al. 2007, Dilauro et al. 2010) Joly et al. reported a decrease (30-40%) in AT_1R mRNA levels in cortex and outer medulla at 4 weeks post-surgery;(Joly et al. 2005) however, another study found no change in AT_1R protein expression at the same time point.(Dilauro et al. 2010) Whereas, an increase (>70%) in AT_1Rs was obtained using Western blotting at 8 weeks post-surgery by Kujal et al (2010)(Vaziri et al. 2007). A non-invasive molecular imaging probe may provide more relevant information regarding the dynamic changes in tissue AT_1R levels.

In prior work, we have shown reduced [^{18}F]FPyKYNE-losartan retention (-23%) in the hypertrophied remnant kidney of Nx rats at 8-10 weeks compared to shams (Manuscript #2). In this study, the -28% reduction obtained at 18-20 weeks with the same tracer was comparable to the early timepoint, indicating sustained reduced expression of renal AT_1Rs in the untreated Nx rat. PET imaging findings were supported by *in vitro* autoradiographic binding studies. This outcome emphasizes the benefits of using small animal PET in experimental work as it allows the usage of the same animal for longitudinal *in vivo* assessment of AT_1R in health and disease states, and monitor effect of therapy.

Cardiac hypertrophy is a typical complication of CKD in response to the persistent hypertension and activation of the systemic RAS.(Sviglerova et al. 2010, Gansevoort et al. 2013) Compared to shams, untreated Nx rats displayed significant increase in LV mass and diminished EDV with consequent decrease in SV presumably as a result of reduction of ventricular compliance due to the developed concentric hypertrophy.(Gansevoort et al. 2013). The Ang II levels were not increased in the LV, hence the cardiac hypertrophy cannot be attributed to local activation of RAS in this study. Nonetheless systemic factors like anemia or activated hormonal pathways such as the sympathetic nervous system that are known to be associated with CKD patients(Herzog et al. 2011, Shiba and Shimokawa 2011) may have contributed to the promoting of LV hypertrophy. This result may also indicate the establishment of diastolic dysfunction,(Herzog et al. 2011) however such possibility was not further analyzed with echocardiography in this work. Interestingly, treatment with enalapril had no effect on

LV levels however it prevented the progression of cardiac hypertrophy and partially improved cardiac efficiency, perhaps due to the reduced SBP and proteinuria.

The use of non-dihydropyridine CCB diltiazem was equally effective as antihypertensive therapy but failed to correct plasma Cr or albuminuria, and further increased their levels compared to untreated Nx rats. PET and autoradiographic renal AT_1R expression results were not normalized in the diltiazem group, due to persistent elevation in renal Ang II levels. Moreover diltiazem significantly increased Ang II levels in plasma and heart, although the mechanisms were not investigated. Cardiac hypertrophy was exacerbated in NxD rats compared to untreated Nx. However, SV was improved possibly due to normalization of SBP by diltiazem, despite high levels of Ang II in the heart. Consistent with previous research,(Brenner 1983, Podjarny et al. 1993, Griffin et al. 1995, Griffin et al. 2003) we demonstrated that late treatment with CCBs may further impair renal autoregulation and proteinuria in CKD.

In summary, the Nx rat model of CKD exhibited renal impairment, proteinuria, sustained hypertension and cardiac hypertrophy. This was associated with elevated Ang II levels in kidney and compensatory downregulation of renal AT_1Rs as measured *in vivo* by PET imaging and *in vitro* autoradiography. As expected, delayed administration of ACEI enalapril attenuated renal impairment, hypertension and prevented progression of cardiac hypertrophy. This was successfully accomplished through reduction of systemic and kidney Ang II levels and consequent normalization of renal AT_1R. On the other hand, use of the non-dihydropyridine CCB diltiazem was equally effective in reducing SBP but did not normalize renal AT_1R expression. Diltiazem induced increases in Ang II levels in plasma, kidney and heart, associated with exacerbation of renal and cardiac dysfunction.

Hence, PET can provide insights about drug responses at AT_1R level, which may help identifying patients likely to respond, thereby optimizing outcome and reducing adverse effects.

Perspectives

In this experimental study of CKD, strong *in vivo* evidence is provided which agrees with the postulated theory (Mackie et al. 2001, Long et al. 2004, Vaziri et al. 2007, van der Meer et al. 2010) stating that anti-RAS drug therapy provides class-specific renoprotection in addition to its blood pressure lowering effect. Additionally, our data asserts that the timing to start therapy is of crucial importance and should be strongly considered in CKD patients and therefore reinforces the need for early intervention to prevent progression of CKD and subsequently reduction of risk for cardiovascular morbidities & mortalities. This outcome adds value to the feasibility of non-invasive [^{18}F]FPyKYNE-losartan PET for determination of receptor abnormalities with progression of the disease and monitoring of therapy.

Acknowledgement

The authors would like to thank Dr. Mario Tiberi for his input on assessment of the results of the ^{125}I-[Sar^1, Ile^8]Ang II assays. We also thank the Radiochemistry staff and the Ottawa Heart Institute Animal Care and Veterinary Staff for assistance with the experiments.

Source of Funding

This work was supported in part by, the Ontario Preclinical Imaging Consortium (OPIC) grant# RE03-51 (Ontario Research Foundation) and the Canadian Institutes of Health Research (MOP-80203 & MOP-287694) and by the Molecular Function and Imaging Heart and Stroke Foundation of Ontario Program Grant (#PRG6242).

BI was a doctoral student co-supervised by JDS and RSB and supported by the PhD scholarship from the University of Ottawa's Faculty of Medicine Endowed Funds for Cardiac Graduate Research and the UOHI Foundation. RSB is a Career Investigator supported by the Heart and Stroke Foundation of Ontario (HFSO), the University of Ottawa Heart Institute (UOHI) Vered Chair in Cardiology and Tier 1 University of Ottawa Chair in Cardiovascular Research.

Disclosures

None.

1. What is New?

To our knowledge, this the first study to reveal maintained AT_1R reduction *in vivo* at late stages of animal model of CKD that was normalized by delayed treatment with ACEI enalapril. The results of this work support the use of the novel F18-labeled selective PET AT_1R probe, [^{18}F]FPyKYNE-losartan developed in our lab to better understand the AT_1R role in disease states.

2. What is Relevant?

There is ongoing debate in the hypertension community on the use of RAS-dependent versus RAS-independent antihypertensives in CKD. Non-invasive PET imaging of AT_1R could help in resolving this issue by enhancing our understanding of the role of intra-renal RAS in the disease progression and correlate it with the efficacy of therapy. Additionally, our findings reaffirm the inverse correlation between enhanced Ang II levels and reduced AT_1R expression.

3. Summary

In rats with CKD, delayed treatment with the ACEI enalapril normalized AT_1R expression and reduced progression of the disease, whereas the CCB diltiazem exacerbated renal and cardiac dysfunctions. [^{18}F]FPyKYNE-Losartan PET allows longitudinal determination of AT_1R abnormalities with progression of cardiorenal failure and monitoring of therapy.

ONLINE-ONLY DATA SUPPLEMENT

Materials and Methods

Drugs and Reagents

Enalapril and diltiazem were obtained from Apotex, Inc. (Ottawa, ON, Canada). Drugs were supplied as tablets that were powdered and dissolved in water and administered to animals in the drinking bottles and doses were calculated according to water consumption for each individual rat. [^{125}I]-Sar^{1}, Ile^{8}]Ang II was purchased from Perkin Elmer (USA). The reagent was supplied as a powder that was dissolved in distilled water, each vial contained 50μCi (1.85MBq) with a specific activity of 2200Ci (81.4TBq)/mmol. [^{18}F]FPyKYNE-Losartan was synthesized as previously described and dissolved in 0.9% saline for injection (Arksey et al. 2014). High radiochemical purity (>99%) and specific activity of 112-1630.52 mCi/umol (4.144-60.33 GBq/μmol) were obtained.

5/6 Nephrectomy Surgical Procedure

Rats were subjected to either sham or Nx surgery in two sittings under total anesthesia with 2-2.5% isoflurane by inhalation throughout the surgery. In the first step, the right kidney was exposed through a lateral dorsal incision, then decapsulated and completely removed. One week later, the left kidney was exposed in the same way and reduced to 1/3 of its original size by resecting the superior and inferior poles to induce a total of 5/6 Nx (Vaziri et al. 2007, Dilauro et al. 2010). Post-operative analgesia was administered twice daily for 3 days following surgery. Sham animals underwent the same 2 surgeries one week apart to simulate Nx conditions without removing the kidneys**.**

Systolic Blood Pressure Measurements

SBP was measured using indirect tail-cuff plethysmography (CODA-S2 multi-channel, Kent Scientific Corporation, Torrington, CT, USA) in conscious rats at 18-20 weeks post-surgery. Animals were placed in rat holders and trained for 3 days to the measuring conditions. On the 4th day, 6 consecutive measurements were recorded from each rat per session, and an average blood pressure was calculated.

Measurement of Plasma Creatinine

Plasma Cr was assessed at 18-20 weeks post Nx surgery. Blood samples were collected, centrifuged (4000 rpm, 4°C) for 10 minutes, then plasma was obtained and stored at -80ºC till assayed. Prior to measuring of Cr in samples, plasma proteins were precipitated using deproteinizing sample preparation kit (Biovision). Cr levels were determined using a Cr assay kit (Cell Biolabs, Inc. San Diego, CA, USA) following the manufacturer's instructions.

Measurement of Albumin: Creatinine Ratio in Urine

Urinary albumin excretion was determined using albumin-to-Cr ratio from spot urine collection from rats. Albumin was quantified with a commercially available rat ELISA kit (Genway Biotech, Inc. San Diego, CA, USA) and Cr was measured with Cr assay kit (Cell Biolabs, Inc. San Diego, CA, USA).

In vivo PET Imaging

MicroPET studies were performed using the Inveon DPET (Siemens Preclinical Imaging, Knoxville, TN) small animal scanner. Animals were anaesthetized and kept unconscious throughout the scan using 2% isoflurane. Rats were placed on the microPET scanner bed in supine position and body temperature was maintained at 37^{o}C. Animals were

positioned to include heart and both kidneys in the FOV. Body temperature, heart rate and respiratory rate were monitored throughout the scans. A ^{57}Co transmission scan was obtained for scatter and attenuation correction either immediately preceding or following the emission scan. Images were analyzed with Inveon® Research Workplace software version 1.4 (Siemens Preclinical Imaging, Knoxville, TN) unless indicated otherwise. Dynamic PET images were reconstructed using vendor-provided 3-dimensional ordered subset expectation maximization / maximum a posteriori algorithm OSEM3D/MAP (β=1, OSEM3D iterations = 2, MAP iterations = 18) with all corrections enabled. Volumes of Interest (VOIs) were defined on reconstructed images to obtain time-activity-curves (TACs) in units of Bq/cc.

[^{18}F]FPyKYNE-Losartan AT_1R

Rats were injected with 18-81 MBq (0.5-2.2 mCi) of [^{18}F]FPYKYNE-losartan (<1ml volume) via a 26 gauge catheter into the lateral tail vein. The specific activity ranged from 112-1630.52 mCi/umol (4.144-60.33 GBq/μmol) at time of injection. A dynamic 60 min scan was acquired as 12x10 s, 3x60 s, 11x300 s frames. The arterial input function was obtained from the average blood pool activities within the LA or the LV cavity. Briefly, a sphere was drawn inside the cavity of LA or LV at an early frame (10-40 sec post-injection) and an 80% threshold was used to define the contour of the arterial blood VOI. Kidney VOIs were drawn at frame 16 or 17 (5-15 min post-injection where the highest tissue-to-background contrast was observed) by tracing a segment of the cortex at the inferolateral side of the left kidney away from liver and bowel to avoid spillover, and the final VOI was defined using a 50% threshold contour. [^{18}F]FPyKYNE-losartan retention was measured using the Logan derived DV values. The tracer DV provides a

quantifiable parameter for repeated measurements and assessment of repeatability and reliability. Provided the tracer binds to its receptor reversibly, Logan graphical analysis (Logan et al. 1987), of the PET time-activity data can be used to calculate the DV. In essence, tracer uptake in the kidney is plotted against concentration in the plasma at equilibrium (steady-state). Plotting is the concentration of tracer in the tissue against the concentration of tracer in the plasma, will transform the tissue activity to a linear plot, as if the tracer was injected as a continuous infusion. The slope of this line during the steady-state phase corresponds to an estimate of the DV (ml/cm^3).

[^{13}N]Ammonia Blood Flow

Heart and kidneys perfusion were assessed within the same week of [^{18}F]FPyKYNE-losartan PET scans. Animals were injected [^{13}N]ammonia 55-110 MBq (1.5-3mCi) intravenously and scanned for 30 min. MBF was quantified using FlowQuant© software (Klein et al. 2010). Blood and kidney TACs were generated and flow values (ml/g/min) were produced. For calculation of RBF, the initial 2 min of the dynamic PET data was used to avoid contamination by plasma metabolites of N-13 radioactivity. The images were reconstructed into 12 x 10 s frames applying the corrections for dead-time, isotope decay, detector efficiencies, and random events. Renal TACs were derived from VOI drawn over renal cortex and derived from blood pools inside the LA and LV for average arterial input function. The one-tissue-compartment kinetic model was used to calculate K1 (ml/g/min) for RBF analysis.

In vitro Autoradiography

In-vitro ^{125}I-[Sar^1, Ile^8]Ang II binding was assessed using the method published previously (Kenk et al. 2007). Rats were sacrificed 2-3 days after PET imaging studies.

Following decapitation, dissected kidneys were quickly immersed in OCT Compound (Tissue-Tek), frozen on dry ice and stored at -80°C until subsequent autoradiography studies. Kidneys were sectioned in the axial axis into 20 μm-thick slices at -18°C with a cryostat (Leica CM3050 S). Tissue sections were thaw-mounted on glass slides (VWR) and stored at -80°C. On the day of the experiment, slides were pre-washed in assay buffer (150 mM NaCl, 50 mM sodium phosphate dibasic, 1 mM EDTA, 0.1 mM Bacitracin, 0.1% BSA) for 15 min then incubated with 0.8 nM ^{125}I-[Sar^1, Ile^8]Ang II for 90 min at room temperature in the presence of AT_2R antagonist, PD 123,319 (10μM) to determine total (non-AT_2R) binding or with unlabelled Ang II for non-specific binding. Specific binding of ^{125}I-[Sar^1, Ile^8]Ang II was calculated as total (non-AT_2R) minus non-specific binding. After incubation, slides were washed 3 times (15 min at 4°C) sequentially in assay buffer, deionized water, and again in assay buffer then gently air dried. Sections were then exposed to phosphor imaging plates (Kodak Screen-K, Biorad) for 48hours in complete darkness. Phosphor plates were then read at a 100μm resolution (BioRad Molecular Imager FX) and analyzed using Quantity One Software (BioRad, Philadelphia). Quantification was done by manually tracing the whole kidney cortex and the radioactivity density (counts/mm^2) was recorded for that area.

Measurements of Angiotensin II Plasma and Tissue Levels

After decapitation of animals, trunk blood was collected in EDTA tubes containing a cocktail of protease inhibitors including 0.44 mM 1,20 ortho-phenanthroline monohydrate (Sigma, MO, USA), 0.12 mM pepstatin (Peninsula Labs, CA, USA), and 1 mM Na p-hydroxymercuribenzoate (Sigma, MO, USA), then centrifuged at 4000 rpm for 5 min to obtain plasma. Kidneys were rapidly collected and snap frozen on dry ice.

Plasma and tissue samples were stored at -80°C until shipped for assay. Ang II analyses were performed on a user-fee basis by the Hypertension Core Laboratory at Wake Forest University Health Science Center, North Carolina, USA. Tissues were homogenized in an acidic ethanol [80% vol/vol 0.1N HCl] solution containing peptidase inhibitors described previously (Allred et al. 2000). Samples were Sep-Pak extracted extracted and measured by RIA (ALPCo, NH, USA).

Echocardiography

Echocardiography was carried out at 18-20 weeks under light anesthesia (1-2% isoflurane) using the Vevo 770 system (VisualSonics, Toronto, ON, Canada) and a 23.5 MHz probe. All echocardiography studies were performed and analyzed by a single operator. Parasternal long-axis views were recorded as sequential ECG-gated M-mode sweeps (EKV-mode) to generate two-dimensional cines of the LV. Analysis of results was completed with the VisualSonics cardiac measurements program. The LV wall mass, LVEF, EDV and SV were assessed with the standard VisualSonics cardiac measurement formulas.

CHAPTER 5: DISCUSSION

5.0. Common Discussion

The long-term goal of the proposed research was to develop a PET probe capable of detecting changes in the AT_1R binding in the kidney. Successful development of these radioligands will present a unique opportunity to advance understanding of the pathophysiology of cardiovascular diseases including hypertension and renal failure; moreover it will provide insights into response to commonly prescribed drugs at AT_1R level that may help to guide therapy or aid in identifying patients likely to respond, thereby personalizing medicine and improving health outcome.

In the first section of my work, three AT_1R radioligands derived from the clinically used ARBs, [^{11}C]methyl-losartan, [^{11}C]methyl-EXP3174 and [^{18}F]FPyKYNE-losartan were synthesized and evaluated. All tracers were produced reliably in good yield, high radiochemical (>99%) and chemical purities (>90%), and in an appropriate synthesis time considering the isotope half-life. The appropriate regional distribution, pharmacology and selectivity of [^{11}C]methyl-losartan and [^{11}C]methyl-EXP3174 supported their potential use for non-invasive renal AT_1R PET imaging. Binding selectivity to renal AT_1 over AT_2 and Mas receptors was demonstrated for [^{11}C]methyl-losartan by *ex vivo* biodistribution and *in vitro* autoradiographic studies. In the liver, losartan co-injection caused partial washout of tracer likely due to the similarity in the structure of both compounds, whereas candesartan was unable to cause blocking due to the dissimilarity in structure. This strongly suggests that the effect is not due to AT_1R binding, but to displacement from saturable non-specific binding sites and common metabolic pathways. This speculation was also observed and confirmed with PET imaging (data not shown in thesis), however, this hypothesis remains to be tested and confirmed. In autoradiography studies, it is

notable that candesartan co-injection induced small blocking effect on tracer uptake in the kidney. A much higher blocking percentage was expected given the higher affinity of candesartan to AT_1R compared to [^{11}C]methyl-losartan and losartan (IC_{50}=19 nM for losartan and IC_{50}=32 nM for methyl-losartan, K_i=0.6nM for candesartan). However this result could be due to the high error reported for these studies.

Plasma metabolite analysis at 10 min revealed stability of both tracers, however labeled metabolites of [^{11}C]methyl-losartan were present in the kidney with similar pharmacological binding profile to the parent tracer that may confound the PET signal and complicate kinetic modeling. MicroPET images for both radiotracers displayed high kidney-to-background contrast. The stronger tissue-to-blood signal intensity observed with EXP3174 was anticipated due to its higher binding affinity (IC_{50} of EXP3174 3.7 nM, losartan 19 nM) for AT_1R. Administration of candesartan significantly reduced [^{11}C]methyl-EXP3174 uptake in the kidney, whereas no difference was observed following PD123,319 indicating binding selectivity for AT_1R. Moreover, co-injection of candesartan with [^{11}C]methyl-EXP3174 reduced the proportion of un-changed tracer (but not metabolites), indicating that these metabolites do not bind to AT_1R in rat kidneys. Thus contrary to [^{11}C]methyl-losartan, the portion of the PET signal corresponding to AT_1R specific binding obtained with [^{11}C]methyl-EXP3174 will only come from the parent compound. Therefore, [^{11}C]Methyl-EXP3174 displayed a favorable binding profile compared to [^{11}C]methyl-losartan for imaging renal AT_1Rs via PET.

Afterwards, the 2-[^{18}F]fluoro-3-pent-4-yn-1-yloxypyridine ([^{18}F]FPyKYNE) analog of losartan was produced *via* click chemistry linking [^{18}F]FPyKYNE to azide-modified tetrazole-protected losartan followed by TFA deprotection. Radiosynthesis of

[^{18}F]FPyKYNE-losartan has been achieved reliably in high radiochemical and chemical purities (>99 and 90%, respectively), and specific activity permitting renal AT_1 imaging. [^{18}F]FPyKYNE-losartan displayed high kidney contrast PET images and TACs with reproducible DV values. A dose-response blockade with candesartan confirmed specific binding to renal AT_1R while no change with saturating dose of AT_2R blocker confirmed binding selectivity. *Ex vivo* HPLC metabolism studies in small and large animals revealed that the ^{18}F-labeled metabolites do not bind to renal AT_1Rs facilitating quantitative PET imaging. These findings supported further use of this tracer for renal AT_1R quantification in disease states.

The experiments in the second part of this thesis were proposed to quantify renal AT_1Rs changes in Nx rat model of CKD using [^{18}F]FPyKYNE-losartan PET. The results were correlated with *in vitro* autoradiographic assays and other physiological parameters. Radioligand binding was quantified using DV values as indirect measure for AT_1R levels with PET. KBR and SUV were determined in the early scanning process to confirm the validity of [^{18}F]FPyKYNE-losartan DV values obtained. Over the time course of the study (10-20 weeks), the Nx rats exhibited renal impairment, proteinuria, sustained hypertension and cardiac hypertrophy. These abnormalities were associated with increasing plasma and kidney levels of Ang II, and compensatory reduction of renal AT_1Rs. The robustness of the *in vivo* findings in this study were confirmed by autoradiography using ^{125}I-[Sar^1, Ile^8]Ang II assay.

Delayed administration of ACEI enalapril to the Nx rats attenuated renal impairment, hypertension and prevented progression of cardiac hypertrophy as expected. This was successfully accomplished through reduction of systemic and kidney Ang II, and

consequent normalization of renal AT_1R by PET (and autoradiography). By contrast, use of the non-dihydropyridine CCB diltiazem was equally effective in reducing SBP that was not associated with reduction of plasma creatinine or proteinuria. Diltiazem induced increases in Ang II levels in plasma, kidney and heart, associated with exacerbation of renal and cardiac dysfunction, and no change in AT_1R expression.

5.1. Development and Evaluation of Novel AT_1R PET Tracers

PET has been widely used for quantitative imaging of molecular targets in the brain and heart. However there have been relatively fewer studies in the kidney although it plays a distinct role in the body homeostasis, the actions of drugs, and development and progression of diseases. As any novel intervention, several steps are needed to establish a new PET imaging probe, which involves synthesis and evaluation of a radioligand, preclinical research and clinical investigations. Additionally, there are properties that must be considered in the development of a PET radiotracer including: reasonable synthesis time, high specific activity (activity per mass administered), binding selectivity and high affinity for the molecular target, rapid clearance, and resistance to metabolism or metabolized to products that are inert so not to complicate kinetic modeling calculations (van Waarde et al. 1995, Elsinga et al. 1998, Hutchins et al. 2008).

In the present studies, [^{11}C]methyl-losartan and [^{11}C]methyl-EXP3174 were produced at a reasonable synthesis time of <40 min, and an average specific activity allowing 2-3 renal PET scans. In order to achieve maximal specific binding (Hume and Jones 1998) and quantifiable kinetics (Hume et al. 1998, Alexoff et al. 2003, Thomas et al. 2011) without saturating the receptors, it is important that the tracer occupies a maximum of 5% of the total "amount" of receptors, explaining the necessity of very high specific activity

formulations (Jagoda et al. 2004). Therefore, it was possible to clearly visualize significant uptake by an AT_1R rich organ such as the kidney with the specific activities obtained in this project. Whereas, a higher specific activity is required/expected to quantify cardiac AT_1Rs in disease states particularly associated with upregulation of the receptor expression in the heart. Formerly in an I/R rat model, a transient AT_1R upregulation could be measured in the infarct area at 1-3 weeks post-MI using [^{11}C]KR31173 at specific activity levels >7000 Ci/mmol and PET (Higuchi et al. 2010).

Determination of the proportions of labeled metabolites vs. unchanged radiotracer is an essential requirement in establishing metabolite and decay-corrected plasma TACs used in pharmacokinetic modeling for the quantification of a radiolabeled tracer. For that reason [^{11}C]methyl-losartan was not optimal for tracer kinetic modeling due to the detection of labeled metabolites that bind specifically to AT_1R. Such metabolites will confound the PET signal, and complicate modeling calculations since the specific signal in the ROI will come from more than one labeled molecule with different pharmacokinetics. As hypothesized for [^{11}C]methyl-EXP3174, metabolism of the labeled ester derivative at the 5'-position produced cleavage of radiolabeled metabolites with little or no AT_1R binding that probably can be [^{11}C]-bicarbonate metabolite (Waydhas et al. 1978). However the presence of high proportion of labeled metabolite(s) of [^{11}C]methyl-EXP3174 present in the rat kidney were found to lack binding to AT_1Rs in the blocking studies and thus their contribution can be added to the "noise / non-specific binding" portion of the PET signal. Nonetheless, identification of the exact metabolites is beyond the scope of our work and would require synthesis of the identified metabolite, which is a full study by itself, and would not affect/change our results. Additionally it is

likely that the metabolic profile could change in large animals that represent a "preferable" transition to applications in humans.

In vivo [^{11}C]methyl-losartan and [^{11}C]methyl-EXP3174 small animal PET images were of excellent quality for deriving TACs and data analysis, and indicated that both tracers have good potential renal AT_1R imaging. The kidneys were clearly visualized even though activity in the liver was higher. As anticipated the higher binding affinity of the methyl-ester derivative of EXP3174 (Carini et al. 1991, Almansa et al. 1997, Okazaki et al. 1998) was translated to a stronger tissue-to-blood signal intensity that was further confirmed to be selective for AT_1R over AT_2R with blocking studies.

Prior AT_1R PET imaging studies were performed using C-11 labeled ligands. Our research group was the first to develop an F-18 labeled AT_1R ligand. Knowing the key advantages offered by F-18 labeled tracers over C-11, (Tai and Laforest 2005, Gad 2008) and that large prosthetic groups can be introduced at the imidazole 5-position of losartan with minimal changes of both its binding properties and antagonistic efficacy as reported previously (Carini et al. 1991, Hadizad et al. 2011), [^{18}F]FPyKYNE-losartan was synthesized by conjugation of [^{18}F]FPyKYNE with azide-modified trityl losartan via click chemistry with high chemical and radiochemical purities (Arksey et al. 2014) using an automated dual reactor module (Kolb et al. 2001). It is established that losartan manifests surmountable antagonism on the AT_1R, while candesartan is an insurmountable antagonist. Surmountable or competitive antagonists physically block the active site of the receptor, whereas insurmountable or non-competitive antagonists bind to allosteric sites and induce conformational changes to the receptor that prevent agonist binding

(Vanderheyden et al. 1999). Receptor binding of surmountable antagonists is best analyzed by the Logan plot using DV or binding potential for quantification.

The non-invasive Logan graphical analysis is a validated procedure utilized with various receptor-ligands displaying reversible binding in PET to determine the DV without blood sampling (Logan et al. 1996, Hume and Myers 2002, Alexoff et al. 2003, Ma et al. 2004, Logan et al. 2005). Therefore, Logan derived DV values was found to be an appropriate approach to quantify the uptake of [^{18}F]FPyKYNE-losartan.

Logan distribution volume is calculated as:

$$DV = \frac{K_1}{k_2} \times \left(1 + \frac{k_3}{k_4}\right) \qquad BP = \frac{B'_{\max}}{K_d} = \frac{k_3}{k_4}$$

DV is the distribution volume, K_1= uptake by tissue of interest (kidney), K_2= clearance from kidney, B_{max}= density (concentration) of free receptors (AT_1R), K_d= dissociation rate constant.

However, to accurately calculate the DV, plasma metabolite calculations should be run concurrent with each scan (Harms et al. 2011). This could be achieved by arterial blood sampling from the animals to determine a direct input function (Sharp et al. 2005) or by using an alternative blood pool image that is not affected by heart motion or spill-in from nearby high uptake in liver or bowel. Although, blood sampling provides the most accurate assessment of blood activity, it is a highly invasive method and subject to volume limitations, particularly in small animals as rats and mice. By contrast, the definition of an ROI in the LV or the thinner-walled LA may provide a superior blood pool image with reduced motion and spill-in effects. Blood data TAC used for calculation

of [^{18}F]FPyKYNE-losartan DV were obtained from an average of LV and LA measurements to decrease the possibility of errors.

Since factors like non-specific binding and serial timepoints metabolism were not accounted for in this work, tissue-to-blood ratio (KBR) and SUV were determined in the 3rd manuscript as alternative quantifications of [^{18}F]FPyKYNE-losartan uptake to be corroborated with DVs and were found to be in strong agreement.

In vivo evaluation of [^{18}F]FPyKYNE-losartan with PET scans displayed high binding selectivity for renal AT_1Rs that was reproducible in rats and pigs. High binding affinity (K_d of 49.4 nM and B_{max} 348±112 fmol/mm^2) was also displayed *in vitro* and localized well with the known AT_1R distribution. The metabolism studies revealed that the labeled metabolites do not bind to renal AT_1Rs facilitating quantitative PET imaging in small and large animals. Additionally, the *in vivo* effect of FPyKYNE-losartan on blood pressure was evaluated in rats and established a dose-dependent antagonistic effect of Ang II pressor effect albeit with 4-fold potency reduction relative to losartan. Finally the calculated sex averaged effective dose of [^{18}F]FPyKYNE-losartan was within an acceptable range compared with other F-18 labeled tracers and was verified safe for humans (Arksey et al. 2014, Hachem et al. 2015). Thereby results from our previous work justified the use of [^{18}F]FPyKYNE-losartan for reliable and accurate PET imaging of AT_1R in CKD animal model as described in my thesis.

5.2. Assessment of 5/6 Nephrectomy as a Model of CKD in Rats

Regardless of the etiology for CKD, a common renal morphology develops overtime characterized by a lower number of functioning nephrons that eventually loss the ability to cope with the extra load contributing to the deterioration of renal function (Garber et

al. 2003, Prieto et al. 2005). In this study, we have induced CKD in rats by surgical ablation of 5/6 of the total renal mass. The Nx model in rats has provided valuable insights for studying and understanding the pathogenetic mechanisms involved in the onset and progression of CKD. It represents a well-established model of progressive renal injury that is characterized by systemic hypertension, loss of renal function, proteinuria and histological changes, similar to those observed in human renal diseases (Yang et al. 1998, do et al. 2014).

Hypertension did not develop in Nx rats compared to shams at 4 weeks post-surgery (data not shown) but was evident at 8-10 weeks which agrees with previous report by Griffin and Bidani (Bidani et al. 1990). The authors in the former study stated that the surgical ablation model is accompanied by a lower renin release and delayed and gradual rise in blood pressure compared to the infarction model (Bidani et al. 1990). However in both ablation and infarction models, hypertension contributes to the development of glomerular hypertension and hypertrophy because of the compensatory afferent vasodilation in the remnant nephrons. This resulted in damage of the epithelial glomerular cells and progressive renal dysfunction (increased plasma creatinine) and proteinuria that were observed here over the course of 10-20 weeks. In addition to hemodynamic factors, the high Ang II levels contributes to the inflammation and fibrosis observed in the kidney in this model of CKD. As a proof of concept, representative histological sections were examined from all study groups at the late timepoint. Untreated Nx group was associated with mild interstitial fibrosis and glomerulosclerosis started in scattered areas of the kidney. Treatment of Nx rats with enalapril showed normal kidney structure similar to shams and almost no renal pathology was seen. By contrast, NxD rats

demonstrated significant similarity to the untreated Nx rats with more severe fibrotic changes (Figure 5.1).

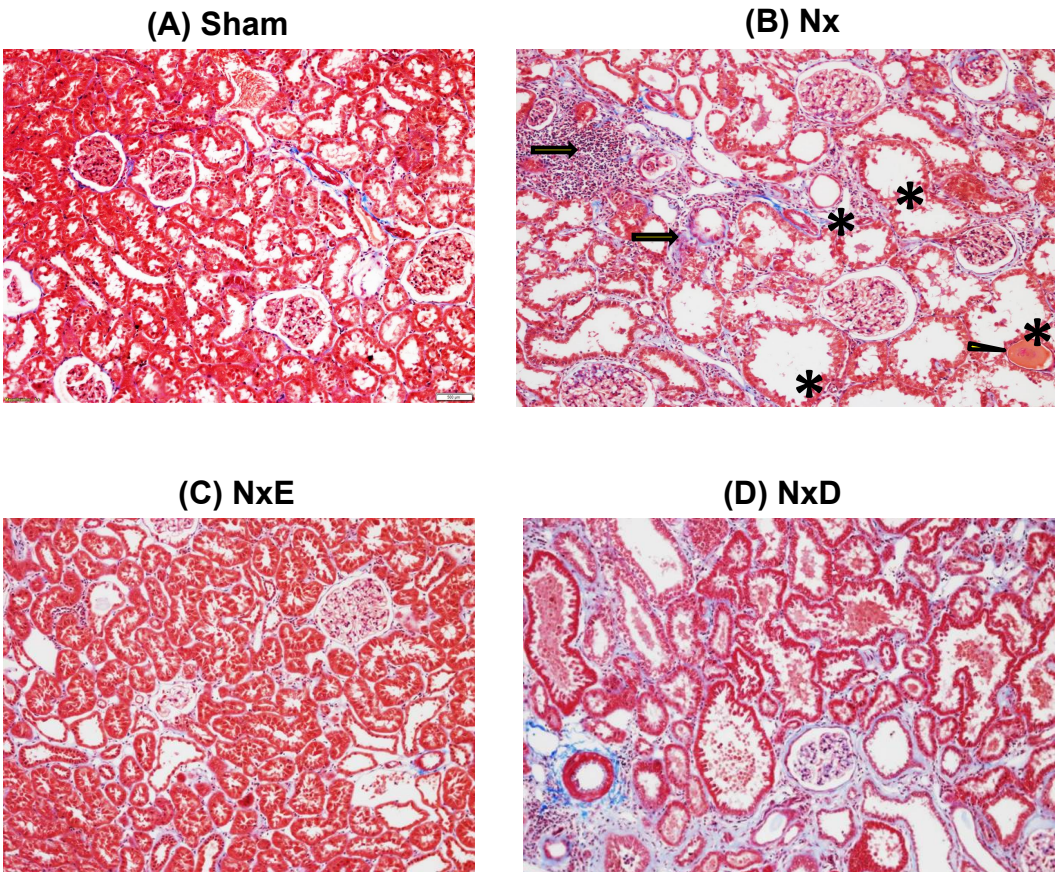

Figure 5.1: Histological sections of the kidney stained with Masson Trichrome in Sham (A), Nx (B), NxE (C) and NxD (D) groups at 18-20 weeks post-surgery. Prominent cystic dilation of the proximal and distal tubules (*). Mild interstitial fibrosis with rare monocyte infiltration (arrows) and protein casts (arrow head). Noticeable preserved glomeruli and absence of glomerulosclerosis (Original magnification x100).

There is a fair amount of clinical and experimental data on the cardiac consequences secondary to renal failure. CKD progression is accompanied by progressive LV hypertrophy and diastolic dysfunction in subtotal Nx rats (Rambausek et al. 1985), as well as in patients during the different stages of CKD (Stefanski et al. 1996). The Nx model is essentially a model of hypertension, where the pressure overload due to the increased blood pressure lead to ventricular wall thickening however results on LV dilatation may vary between studies (Shiba and Shimokawa 2011, Gansevoort et al. 2013). The changes in diastolic function occurs gradually in this model, as it is not a cardiac primary injury, however heart failure with preserved EF (HFpEF) is speculated to develop overtime (Bongartz et al. 2012). With advancing damage, systolic dysfunction may occur in the long term leading to worsening of heart failure and can become decompensated. We have observed LV hypertrophy by echocardiography as early as 8-10 weeks post-surgery in Nx rats compared to shams. Furthermore, diminished EDV with consequent decrease in SV were observed only at the 18-20 weeks timepoint that may indicate the development of diastolic dysfunction, however such possibility was not further analyzed with echocardiography in this work. The knowledge gathered from this study was beneficial in the process evaluating [^{18}F]FPyKYNE-losartan as a novel tracer for imaging AT_1R in CKD with PET.

5.3. RAS Dysfunction in CKD

Despite the presence of numerous clinical and experimental animal studies providing evidence for the fundamental role played by RAS mainly through AT_1R in the pathogenesis of renal diseases; conflicting results were reported on intrarenal AT_1R levels in CKD. An explanation for the variability in findings is probably due to the different

methodologies and/or time points used for assessments. Another explanation could be the high lability of RAS components, which makes it easily affected by handling and environmental conditions during lab testing. A distinct speculation for the inconsistency in the AT_1R results is the non-specificity of the commonly used AT_1R antibodies for *in vitro* assessment as demonstrated evidently in 2 recent publications (Benicky et al. 2012, Herrera et al. 2013) (discussed in details in the appendix section).

The current work displayed reduced renal binding of [^{18}F]FPyKYNE-losartan to AT_1Rs in kidneys of CKD rats by PET imaging. This reduction was confirmed by Western blot (in early timepoint only) and *in vitro* ^{125}I-[Sar^1, Ile^8]Ang II binding. Since AT_1R mediates most of the deleterious actions of RAS, an increase in the receptor expression was expected in Nx rats. One can postulate several theories for the reduction in AT_1R levels; first: it can be due to a true physiological response to counteract the deleterious effects of subtotal Nx (mainly at the early timepoint); second, it can be due to damage of the proximal tubular cells which express most of the AT_1R and occupy the greatest volume of the cortex where the reduction is seen (Mujais et al. 1986, Joly et al. 2005); third, it can rather be a maladaptive process by the remaining failing nephrons overtime (mainly at the late timepoint). It is noteworthy to mention that the significance of our finding remains speculative and require further investigations.

As the main effector of RAS, Ang II contributes hemodynamically to the pathogenesis of the CKD by promoting glomerular hypertension and hyperfiltration (Hostetter et al. 2001). In addition, it locally promotes pro-inflammatory pathways that cause tissue inflammation and fibrosis (Ruiz-Ortega et al. 2000, Ruiz-Ortega et al. 2000, Taal and Brenner 2000). We measured plasma Ang II as a peripheral marker for the circulating

RAS. The decrease observed at 8-10 weeks post-surgery is in accord with previous studies showing that renal ablated rats is not associated with elevation of circulating renin or Ang II levels (Anderson et al. 1986, Jackson et al. 1988, Rosenberg et al. 1991). On the other hand, kidney Ang II levels in Nx rats were comparable to shams. It is possible that an increase in Ang II level was not detected when measurements are made in homogenized kidney tissue where Ang II can be increased at some location in the kidney while decreased in other. Nonetheless, other researchers reported other several causes for unchanged Ang II levels (Jackson et al. 1988, Verhagen et al. 1999). Later in the disease, plasma and kidney Ang II levels were elevated in Nx rats compared to shams (although it did not reach significance due to the high variability in results obtained from the Nx group). The increase in renal content of Ang II could be due to higher plasma levels of Ang II and/or the enhancement of local production Ang II in the kidney (Navar and Harrison-Bernard 2000, Navar et al. 2001). We believe that this temporal increase is probably due to the heightened activity of the RAS associated with the sustained hypertension and expansion of the extracellular volume.

In this context, it can be postulated that maladaptive changes in both the circulatory and tissue RAS activity seem to be a driving force in the pathogenesis of CKD. Hence [^{18}F]FPyKYNE-losartan PET represented a valuable non-invasive investigative tool to provide more insight on the exact role played by AT_1R during disease progression, as discussed in this thesis.

5.4. Efficacy of Antihypertensives in CKD

Accumulating clinical experience from landmark clinical trials and meta-analyses in the last few decades demonstrated that RAS inhibition is considered the most effective single

therapy to attenuate progression of CKD. RAS inhibitors can be achieved with two families of compounds ACEIs and ARBs. Both classes are commonly used but ACEI treatment was chosen in this study instead of ARBs in management of CKD so as not to interfere with the binding of the losartan analog radiotracer used for PET imaging.

Despite widespread use of RAS blockers clinically, the mechanisms through which they lower blood pressure and protect the kidney from injury have not been fully elucidated. In our study, PET imaging permitted the characterization of kidney AT_1R alterations in association with different actions of the drug treatments. In my work, we were able to emphasize the contributions of renal AT_1Rs to the beneficial effects of ACEI enalapril.

ACEIs are equally effective to other antihypertensive drugs at reducing blood pressure, but their distinctive effect is more evident in the more advanced and proteinuric kidney disease (Nigbor and Lewis 2003, Rahn 2005). Enalapril was used in a dose of 10 mg/kg/d reported previously to effectively normalize blood pressure and proteinuria in Nx rats (Noda et al. 1999, Windt et al. 2006). In the presented work, enalapril completely normalized plasma creatinine, effectively lowered SBP (78%) and albuminuria (73%) compared to shams. Since a major part of kidney mass is removed in this model, a persistent deterioration of renal function is expected with any therapy. No matter how effective the drug treatment is, physical limitation on the number of nephrons would not allow return of renal function parameters to control values. Another point to consider for variability in response is the time point that the treatment started; some authors have started as early as 1 week post-surgery (Benigni et al. 1996). While other studies had addressed the efficacy of late start (≥2 weeks after disease induction) of treatment in the Nx model (Lee et al. 1993, Kolesnyk et al. 2010, Alvarez-Prats et al. 2012). Thus the

difference in results obtained from some of the previous studies and ours may be related to the study design.

Chronic administration of enalapril resulted in decreasing Ang II in the kidney whereas, plasma levels of Ang II were unexpectedly not significantly decreased. Our data are in agreement with previous reports that demonstrated distinct regulation of circulating and intrarenal Ang II levels after ACEI treatment (Navar et al. 2003). There are two possible theories to explain this observation. First, a feedback mechanism may have been activated to compensate for the inhibition of ACE mediated synthesis of Ang II either by decreasing the degradation of Ang II or by increasing alternative pathways of Ang II synthesis. Such a feedback effect has been described in both experimental animals (Funabiki et al. 2004) and in humans (Jorde et al. 2000, Petrie et al. 2001). Second, the administered dose of enalapril may not have been sufficient to suppress the conversion of Ang I to Ang II in all organs, which may have diluted the effect of ACEI on plasma Ang II levels. Nevertheless, The effect of ACEI treatment was sufficient to normalize/ upregulate AT_1R densities in the kidney by attenuating processes of Ang II-induced AT_1R downregulation.

Whether the interventions aimed at lowering BP and lowering protein excretion by way of ACE inhibition are beneficial simultaneously to both cardiovascular and renal outcome is still controversial. So far, few randomized clinical trials of renal diseases have been reported and they often exclude cardiovascular population of patients or they seldom considered cardiovascular parameters as the composite end point for analysis (Decker and Kendrick 2014). Therefore, current treatment strategies toward CKD associated cardiovascular disease have mainly been derived from experience with non-renal

dysfunction patients (Lin et al. 2015). Previous clinical studies with ACEI failed to show complete regression of LV hypertrophy in renal disease patients (Dyadyk et al. 1997, Yu et al. 2006). In line with previous published studies, enalapril could only attenuate the progression of LV hypertrophy and partially improved the cardiac function.

CCBs and all other antihypertensive agents are similarly effective to RAS blockers at attenuating hypertension-related renal damage progression, when administered during the non-proteinuric stages of CKD (Nathan et al. 2005). Both dihydropyridines and non-dihydropyridines CCBs were shown to exert beneficial effects on renal damage and renal dysfunction progression in overt disease, either alone or in combination with RAS blockers (Segura et al. 2005), provided that a tight control of blood pressure was achieved.

In my studies, non-dihydropyridines CCB diltiazem was administered at 10 weeks post-surgery to Nx rats that were hypertensive but not proteinuric. Diltiazem maintained blood pressure below normal values but did not reduce plasma creatinine levels or attenuate proteinuria and unexpectedly aggravated both measures. Furthermore, it worsened the kidney glomerulosclerotic changes and tubulointerstitial fibrosis observed in Nx rats. These results are not in line with previously available evidence from human and experimental studies demonstrating that long-term administration of nondihydropyridine CCBs, such as diltiazem, more consistently reduce proteinuria as compared to dihydropyridine CCBs, such as amlodipine and nifedipine, with similar degrees of systemic BP reduction. Our PET data exhibited reduced AT_1R kidney expression (similar to Nx rats) combined with the very high levels of plasma, kidney and heart Ang II levels compared to all other groups. Thus the deleterious effect of diltiazem on the RAS

components could provide an explanation for worsening of renal and cardiac functions however investigating the exact mechanism of action was beyond the scope of this thesis. Prior research has shown that CCBs impair renal autoregulatory responses in healthy animals or can have additive harmful effect induced by reduced renal mass (Griffin et al. 1995, Griffin et al. 1999) and completely abolish renal autoregulatory capacity in the remnant kidneys of Nx rats (Griffin et al. 1995, Griffin et al. 2004). An interpretation for this effect can be due to their potent vasodilatory effect on the afferent arteriole dependent on pressure-induced depolarization and calcium entry through voltage-gated calcium channels (Davis and Hill 1999, Griffin and Bidani 2006). Therefore the novel PET findings obtained with CCBs administration in our study reinforces previous published reviews (Epstein 2002, Segura et al. 2005) recommending that CCBs is better utilized as part of multiple drug therapy or along with RAS inhibitors for patients who need more than one drug to achieve normotension and additive renal protective effect.

5.5. Conclusions

In this research project, three AT_1R PET radioligands derived from the clinically used ARBs, [^{11}C]methyl-losartan, [^{11}C]methyl-EXP3174 and [^{18}F]FPyKYNE-losartan were developed. All tracers were produced in good yield, high radiochemical purity (>99%), and in an appropriate synthesis time that permits imaging. PET studies revealed high tissue contrast in the kidney cortex and outer medulla, which correlates well with the known physiological distribution of AT_1R (Chang and Lotti 1991). PET imaging with [^{11}C]methyl-EXP3174 and [^{18}F]FPyKYNE-losartan was reproducible and the PET signal was selective to AT_1R over AT_2R. Metabolism studies performed with [^{11}C]methyl-EXP3174 and [^{18}F]FPyKYNE-losartan revealed that their labeled metabolites do not bind

to renal AT_1Rs facilitating quantitative PET imaging. Use of F-18 radionuclide compared to C-11 has multiple advantages (mentioned previously): the longer half-life (110 mins vs 20 mins) allows multiple injections per formulation and shipment to sites without cyclotron or radiochemistry capability, as well as higher image resolution due to lower positron energy. These findings supported the use of [^{18}F]FPyKYNE-losartan for renal AT_1R quantification with imaging in animal disease models.

Serial *in vivo* small animal [^{18}F]FPyKYNE-losartan PET studies in rats demonstrated reliable and accurate quantification of the dynamic changes of renal AT_1Rs. The subtotal nephrectomy rat model of CKD exhibited renal impairment reflected as increased plasma creatinine, progressive proteinuria and sustained hypertension that was associated with hyperactive systemic RAS. In the hypertrophied remnant kidney, the activity of intrarenal RAS was probably augmented (reflected as increased Ang II levels) and led to compensatory downregulation of AT_1Rs. As such, [^{18}F]FPyKYNE-losartan imaging was successful in detecting tissue levels of AT_1R at early and late stages of the disease. Additionally, echocardiography indicated the development of cardiac hypertrophy most likely secondary to the hyperdynamic circulation and consistent with the progression of CKD in humans. Administration of ACEI enalapril at 10 weeks post-nephrectomy reduced systemic and kidney Ang II, upregulated renal AT_1R, improved kidney function, normalized blood pressure and prevented progression of cardiac hypertrophy. The use of non-dihydropyridine CCB, diltiazem was equally effective as antihypertensive but did not prevent rising of Ang II levels, and subsequently AT_1R expression was not normalized. Moreover it appeared to exacerbate renal and cardiac dysfunction. Taken together, these findings support the notion that hypertension (hyperdynamic theory) and increased local

intrarenal activity (hypertrophy theory) are two major determinants for the progression of CKD in which Ang II plays a central pathogenic role. Accordingly, one can speculate that RAS-dependent antihypertensives could halt or even promote regression of the disease through the favorable effects on both postulated theories. Furthermore, consideration should be given for the timing of the therapeutic intervention with RAS-dependent and/or RAS-independent antihypertensives. This outcome adds value to the use of [^{18}F]FPyKYNE-losartan PET for determination of receptor abnormalities with progression of the disease and monitoring of therapy.

5.6. Future Directions

This project has multiple potential clinical applicability and interest to the cardiovascular, kidney and imaging societies worldwide. Close analogs with similar characteristics compared to clinically used losartan will facilitate translational work and approval from Health Canada. Such an approach would present a unique opportunity to advance understanding of the pathophysiology of various diseases including HF, hypertension, vascular and renal failure. The advancement of [^{18}F]FPyKYNE-losartan for wide clinical applications requires the development of a kinetic model for the accurate quantification of AT_1Rs. Determination of the appropriate metabolite correction with dynamic measurements of plasma metabolites in both healthy and diseased animals is the immediate next step in the development of [^{18}F]FPyKYNE-losartan.

[^{18}F]FPyKYNE-Losartan was synthesized by click chemistry in the dual reactor module in University of Ottawa Heart Institute fed via an F-18 RD3 target and transfer line (made of polyethylene). The specific activity was expected to exceed 25,000 Ci/mmol (at end-of-synthesis), however due to failure of separation of nitroPyKYNE from FPyKYNE in

the first reaction and impossibility to purify further, the highest specific activity reached was 4000 Ci/mmol using the GE module. It is important to note that both NO2-PyKYNE-losartan and FPyKYNE-losartan are eluted at the same time in semi-prep HPLC explaining such "reduced" specific activity of the final formulation. Currently the AT_1R PET project is transferred to CRCHUM with Dr. Jean DaSilva (the principal investigator). The synthesis of [^{18}F]FPyKYNE-losartan will be accomplished with the Synthra RNplus dual reactor module (each reactor connected to HPLC system) that will allow further separation of the nitro from the FPyKYNE before the 2nd reactor. Removal of the NO2-PyKYNE will prevent production of NO2-Losartan permitting production of pure [^{18}F]FPyKYNE-losartan in higher specific activity >25,000 Ci/mmol. This will allow the possibility to visualize organs that express low levels of AT_1Rs such as the heart and brain in addition to the AT_1R-rich kidneys.

In addition to cardiovascular disease models, this research will expand to include rat models of diabetes mellitus to assess associated AT_1R alterations (if any) and investigate the effect of glycemic and RAS blockade treatment *in vivo* via PET. This work will provide the foundation for future PET studies in diabetic patients.

AT_1R PET tracers are thus expected to provide an important support for drug development in the areas of: evaluation of existing therapies, identification of potential drug candidates and validation of its effectiveness, as well as the evaluation of pharmacokinetic and pharmacodynamic parameters *in vivo*. For instance, [^{18}F]FPyKYNE-losartan can provide insights about the marked interindividual variability in response to different classes of antihypertensives demonstrated in clinical trials by yielding more precise information regarding drug responses at AT_1R tissue level which is

largely independent of its systemic component and not accessible to routine lab testing. Secondly, the information obtained from PET coupled with increasing availability of the low-cost small-animal cameras can save time and money spent on pre-clinical drug development into the clinical phases by recognizing the most promising compounds and excluding molecules with unfavorable properties (Rudin et al., 2004; Riemann et al., 2008). We plan to perform initial [^{18}F]FPyKYNE-losartan human PET studies in 2016.

CHAPTER 6: APPENDIX (MANUSCRIPT #2)

Arksey, N [a,b], T. Hadizad [a], B. Ismail [a,b], M. Hachem [a,b], A. C. Valdivia [a,b], R. S. Beanlands [a,b], Robert A. deKemp[a], Jean N. DaSilva[a,b,c*] (2014). **"Synthesis and evaluation of the novel 2-[(1)(8)F]fluoro-3-propoxy- triazole-pyridine-substituted losartan for imaging AT_1 receptors." Bioorg Med Chem 22(15): 3931-3937.**

[a] *Cardiac PET Centre, University of Ottawa Heart Institute, 40 Ruskin St., Ottawa, ON, Canada*

[b] *Department of Cellular and Molecular Medicine, University of Ottawa, Ottawa, ON, Canada*

[c] *Department of Radiology, Radio-Oncology and Nuclear Medicine,University of Montreal; University of Montreal Hospital Research Centre (CRCHUM), Montréal, Québec, Canada*

*Corresponding Author: Jean N. DaSilva, Ph.D.

Professor, Dept. of Medicine (Cardiology) and Cellular and Molecular Medicine, University of Ottawa. Director, PET Radiochemistry, Cardiac PET Centre

University of Ottawa Heart Institute, 40 Ruskin St., Ottawa, Ontario, Canada, K1Y 4W7

Tel: (613)798-5555 (x19704);

Fax: (613) 761-5406

E-Mail: JDaSilva@ottawaheart.ca

Contributions of Authors

Synthesis of [^{18}F]FPyKYNE-losartan was performed by Natasha Arksey as part of her MSc thesis with guidance of Dr.Tayebeh Hadizad, who additionally assisted in writing the chemistry section of the manuscript. PET imaging and HPLC metabolism were conducted by Natasha Arksey as well as with assistance of myself. The PET imaging studies with PD123,319, all data analysis and interpretation described in the manuscript was accomplished by myself in addition to drafting the manuscript. Maryam Hachem has contributed to the HPLC studies and Dr. Ana Valdivia helped with the chemistry. Dr Rob Beanlands participated with interpretation of data. Dr. Robert deKemp provided his input on the PET imaging data analysis. Dr. Jean DaSilva provided guide and supervision for the whole work and final editing of the manuscript.

Abstract

The 2-[^{18}F]fluoro-3-pent-4-yn-1-yloxypyridine ([^{18}F]FPyKYNE) analog of the potent non-peptide angiotensin II type 1 receptor (AT_1R) blocker losartan was produced via click chemistry linking [^{18}F]FPyKYNE to azide-modified tetrazole-protected losartan followed by TFA deprotection. Preliminary *in vivo* small animal imaging with positron emission tomography (PET) in rats displayed high uptake in the kidneys with good contrast to surrounding tissue. Rat metabolism displayed the presence of 23% unchanged tracer in plasma at 30 min. Upon co-administration with AT_1R blocker candesartan (2.5, 5 and 10 mg/kg), a dose-dependent reduction (47-65%) in tracer uptake was observed in the kidney, while no difference was observed following AT_2R blocker PD123,319 (5 mg/kg), indicating binding selectivity for AT_1R over AT_2R and potential for imaging AT_1R using PET.

Key words: fluorine-18; click chemistry; losartan; FPyKYNE; AT_1; PET

1. Introduction

The renin-angiotensin-system (RAS) is an important regulator of blood pressure and exerts its effects mainly through activation of the AT_1R and AT_2R subtypes by angiotensin II. Activation of the AT_1R induces most of the known pathophysiologic effects of angiotensin II, including vasoconstriction, sodium and water retention, hypertrophy, cell proliferation and fibrosis (Unger 2002). In addition to angiotensin-converting enzyme inhibitors, AT_1R blockers such as losartan, are well established therapies for the treatment of hypertension and cardiovascular diseases. Several diseases including renal hypertension, diabetes and myocardial infarction exhibit AT_1R dysregulation. The ability to non-invasively detect this abnormal regulation by molecular imaging modalities such as PET provides the potential to monitor disease progression and guide therapy accordingly.

Previous AT_1R PET tracers have been labeled with C-11 (Mathews et al. 2004, Hadizad et al. 2009, Hadizad et al. 2011), however F-18 offers some key advantages: namely, a longer half-life (109.6 vs 20.4 min)(Gad 2008) allowing for multiple patient scans from a single formulation and shipment to other sites without radiochemistry or cyclotron capabilities, and a shorter RMS (Root Mean Squared) positron range (0.23 vs 0.39 mm in soft tissue)(Tai and Laforest 2005) enabling higher resolution images. Structure-activity relationship studies and recent work reported that large prosthetic groups can be introduced at the imidazole 5-position with minimal changes both in binding properties and antagonistic efficacy compared to the parent compound (Carini et al. 1991, Hadizad et al. 2011).

Click chemistry (Kolb et al. 2001) is a popular method of conjugation, owing to the regiospecific nature of the reactions, mild reaction conditions, high yields and ease of purification. The mainstay of click chemistry is the copper(I)-catalyzed azide-alkyne cycloaddition (CuAAC) (Kolb and Sharpless 2003). This ligation is one of only a few truly chemoselective and regioselective reactions. The resulting linkage, a 1,4-disubstituted triazole, acts as amide bond isostere, but is more resistant to hydrolysis, oxidation and reduction in physiological conditions (Bock et al. 2007). Several ^{18}F-labeled alkynes and their subsequent use in click chemistry have been described in the literature (Marik and Sutcliffe 2006, Ramenda et al. 2009).

Herein we describe the conjugation of [^{18}F]FPyKYNE, following the procedure already published (Vaidyanathan et al. 2009), to azide-modified trityl losartan via click chemistry using an automated dual reactor module (TRACERlab FX N Pro) and provide a preliminary *in-vivo* evaluation of the novel ^{18}F-labeled losartan derivative in rats using micro-PET imaging. To the best of our knowledge, there are currently no publications describing the synthesis of an F-18 labeled AT_1R PET tracer.

2. Results and Discussion

2.1. Chemistry

The synthesis of 2-butyl-4-chloro-5-[[3-{[1-methyl-4-yl](1,2,3)triazol}propoxy]-2-fluoro-pyridine]-1-[[2´-[tetrazole-5-yl]biphenyl-4-yl]methyl]imidazol, **5a**, hereafter named FPyKYNE-losartan, is described in Scheme 3.1. It's precursor, 2-butyl-4-chloro-5-(azidomethyl)-1-[[2´-[(triphenylmethyl)tetrazole-5-yl]biphenyl-4-yl]methyl]imidazol **4,** was prepared according to the method previously reported,(Grabowski and Thompson

1995) a nucleophilic substitution reaction that converts the 5′ hydroxymethyl group in **3** to the corresponding azide moiety in 87% yield. Compound **1,** NO_2PyKYNE (2-Nitro-3-pent-4-yn-1-yloxypyridine), **2a** FPyKYNE (2-fluoro-3-pent-4-yn-1-yloxypyridine) and **2b** [^{18}F]FPyKYNE were synthesized according to the literature.(Kuhnast et al. 2008, Valdivia et al. 2012) Replacement of the nitro group on **1** by fluorine using potassium fluoride (KF) readily afforded the cold prosthetic group **2a**. Both compounds **1** and **2a** were characterized by ^{1}H and ^{13}C-NMR and high-resolution mass spectrometry (HRMS). Compound **2a** was further characterized by ^{19}F-NMR. The results proved consistent with those reported.(Kuhnast et al. 2008) Cyclocondensation of **2a** and **4** was achieved through the copper(I)-catalyzed cycloaddition reaction using an aqueous solution of copper(II) sulfate ($CuSO_4$) and sodium ascorbate as the source of Cu(I). The reaction was amenable to a range of temperatures (room temperature to 120^{o}C) and a variety of co-solvents (eg. DMSO, DMF, CH_2Cl_2, MeCN). A quick acid hydrolysis of the protected tetrazole with TFA at 80^{o}C followed by flash column chromatography purification afforded the desired product **5a**, FPyKYNE-losartan, in 44% yield. Compound **5a** was fully characterized by accurate mass measurement, ^{1}H-NMR, ^{13}C-NMR, and ^{19}F-NMR.

2.2. Radiochemistry

The first step in the production of [^{18}F]FPyKYNE-losartan, **5b** was radiofluorination of the nitro precursor **1** (Scheme 6.1). This step occurred in the first reaction vessel of the TRACERlab FX N Pro using [^{18}F]KF/K_{222}/K_2CO_3 in anhydrous DMSO at 120^{o}C for 10 min. Purified **2b** was delivered to the second reaction vessel in a 15-20% yield (decay-corrected) by passing the reaction mixture through a series of three silica cartridges with an eluent of 50:50 ether/pentane (Valdivia et al. 2012). Following evaporation of the

solvent, the labeled prosthetic group **2b** was then conjugated to the azide-modified tetrazole-protected losartan precursor **4** for 30 min at 95°C in DMSO. The reaction mixture was then cooled, treated with TFA, and heated to 80°C for 2 min prior to loading onto HPLC. The fraction containing **5b** was collected and loaded onto a preconditioned C18 cartridge (SPE) to remove the HPLC solvents. Pure **5b** was eluted with minimal EtOH and diluted in saline to provide the final product in 44-70% yield (decay-corrected from **2b**), or an overall yield of 7-14% (decay-corrected from end-of-beam (EOB)). The yield is much lower than that of the non-radioactive synthesis likely due to shorter reaction times, the amount of F-18 fluoride available for radiofluorination compared to the stoichiometric quantities used for the synthesis of the standard, and product loss in the components of the module (ie. reaction vessels, tubing, SPE cartridges).

The identity of the product was confirmed by a single peak on analytical HPLC following a co-injection of the formulated product with cold standard (Figure 6.1). The radiochemical purity was consistently greater than 98% with specific activity from 200-4200 mCi/μmol (7.4-155 GBq/μmol). The entire synthesis, including reformulation, took less than 2 h from EOB. In a representative synthesis, 40 mCi (1.48 GBq) of labeled product **5b** could be obtained from 850 mCi (31.45 GBq) of [^{18}F]fluoride.

The level of copper in the final formulations measured by inductively coupled plasma (ICP) MS was 23.3 ± 5.4 ppb, 26.3 ± 6.5 ppb in blanks, 23.6 ppb in pure saline, and 18 ppb in pure ethanol, all well below the pharmaceutically maximum acceptable exposure to residual metals on a chronic basis. These results indicate no meaningful contamination of copper in the final formulation.

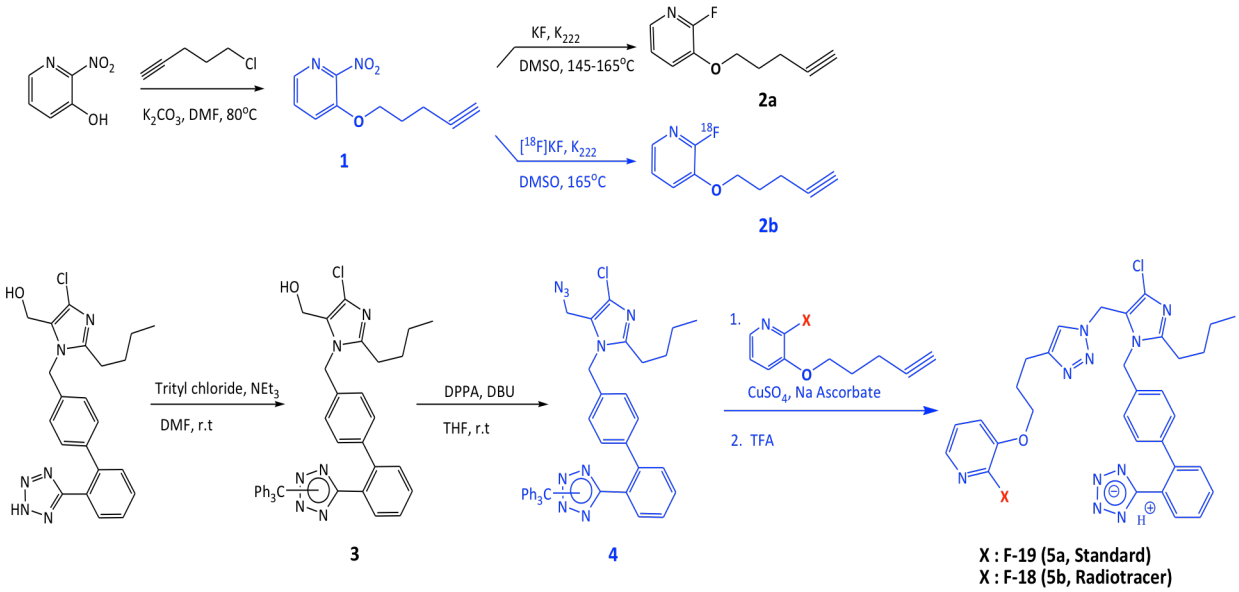

Scheme 6.1: Synthesis of [^{18}F]FPyKYNE-losartan and standard via the Cu(I)-catalyzed [2+3] cycloaddition reaction between azide-modified losartan and [^{18}F]FPyKYNE, performed in the TRACERlab FX_{F-N} automated module (GE Healthcare).

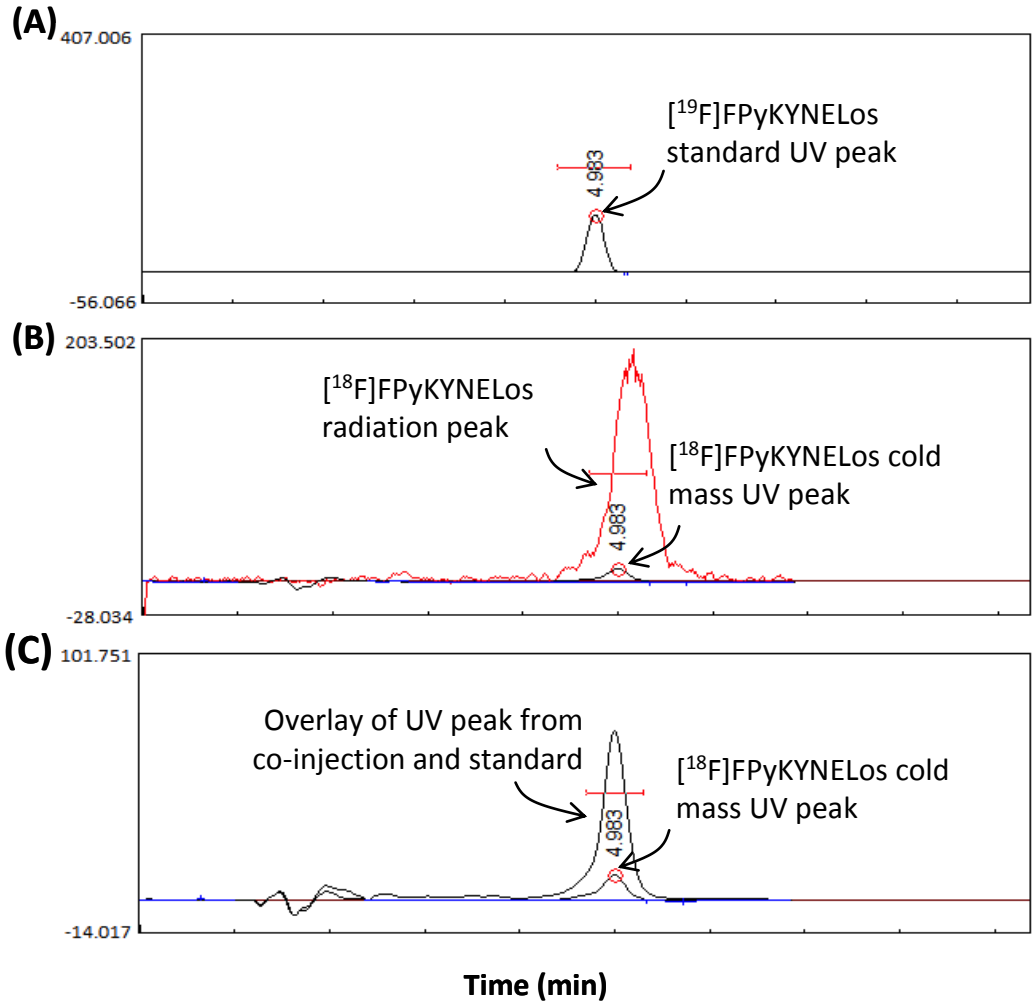

Figure 6.1: Quality control for [^{18}F]FPyKYNE-losartan formulated product by analytical HPLC. **(A)** UV chromatogram of cold standard; **(B)** radiation and UV chromatogram of product formulation; **(C)** UV chromatogram from co-injection of product and standard overlaid on UV chromatogram of product from B. UV spectra were recorded at 254 nm. Column: Phenomenex Luna C18(2) (10 µM, 250 x 4.6 mm) with 40:60 MeCN/AF (0.1 M) at 2 ml/min; PeakSimple 3.93 Analysis Software.

2.3. Biological Evaluation in Rats

Preliminary *in vivo* evaluation of the binding properties of [^{18}F]FPyKYNE-losartan was performed using micro-PET imaging. Normal untreated rats showed the greatest accumulation of activity in the liver and kidneys, respectively (Figure 6.2A). The time-activity curves (TAC) derived from the left kidney displayed a sharp increase in activity uptake in the first few minutes, following the arterial blood input functions, which then washed out slowly to background levels around 55 min (Figure 6.2B). The renal activity had a specific uptake value (SUV) of 1.52 ± 0.58 at 10 min post-injection. Using Logan graphical analysis of image-derived renal versus left atrium blood TAC, the average distribution volume (DV) of [^{18}F]FPyKYNE-losartan in the left kidney was 2.76 ± 0.68 mL/cm^3.

2.3.1. In vivo Competition Studies

In rats treated with the AT_2R antagonist PD 123,319 (IC_{50} for rat adrenal AT_2R = 34 nM) (Zhou et al. 1993), kidney TAC followed similar time course to normal rats (Figure 6.2B). No effect on tracer binding to AT_1R was observed (DV values were 2.76 ± 0.68 and 3.02±0.20 (p=0.28) for normal and PD 123,319 blocking scans respectively) confirming [^{18}F]FPyKYNE-losartan binding selectivity for AT_1R over AT_2R.

A significant 47-65% (p<0.02) dose-dependent reduction in renal uptake of the tracer was observed after administration of candesartan (IC_{50} for AT_1R = 110nM) (Kubo et al. 1993), suggesting AT_1R binding specificity. Doses of 2.5, 5.0, and 10 mg/kg reduced the SUV at 10 min to 1.25 ± 0.17, 0.99 ± 0.38 and 0.61 ± 0.15 respectively. Similarly, the DV values were reduced in a dose-dependent manner to 1.46 ± 0.30, 1.45 ± 0.21 and 0.96 ± 0.06 mL/cm^3 with doses of 2.5, 5 and 10 mg/kg respectively (Figure 6.3).

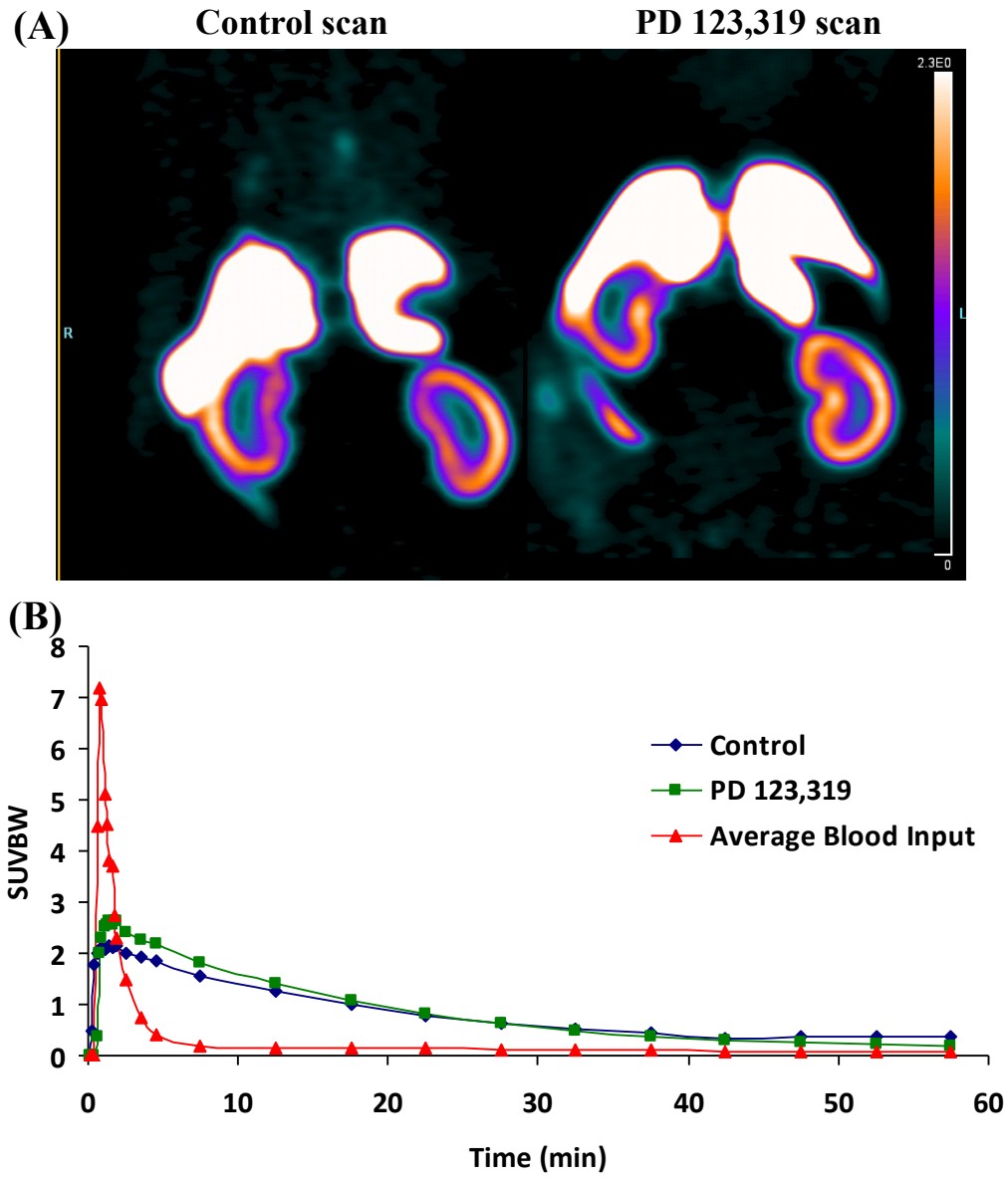

Figure 6.2: Representative microPET images (coronal view) of [^{18}F]FPyKYNE-losartan showing liver and kidney activity (specific uptake values) at 5-10 min post-injection in (A) normal animals (n=7) and AT_2R blocked animals with 5 mg/kg PD 123,319 (n=3). (B) Tracer time-activity curves for average blood input (left atrium) and kidney are presented as specific uptake values normalized to body weight (SUV_{BW}) from 0 to 60 min.

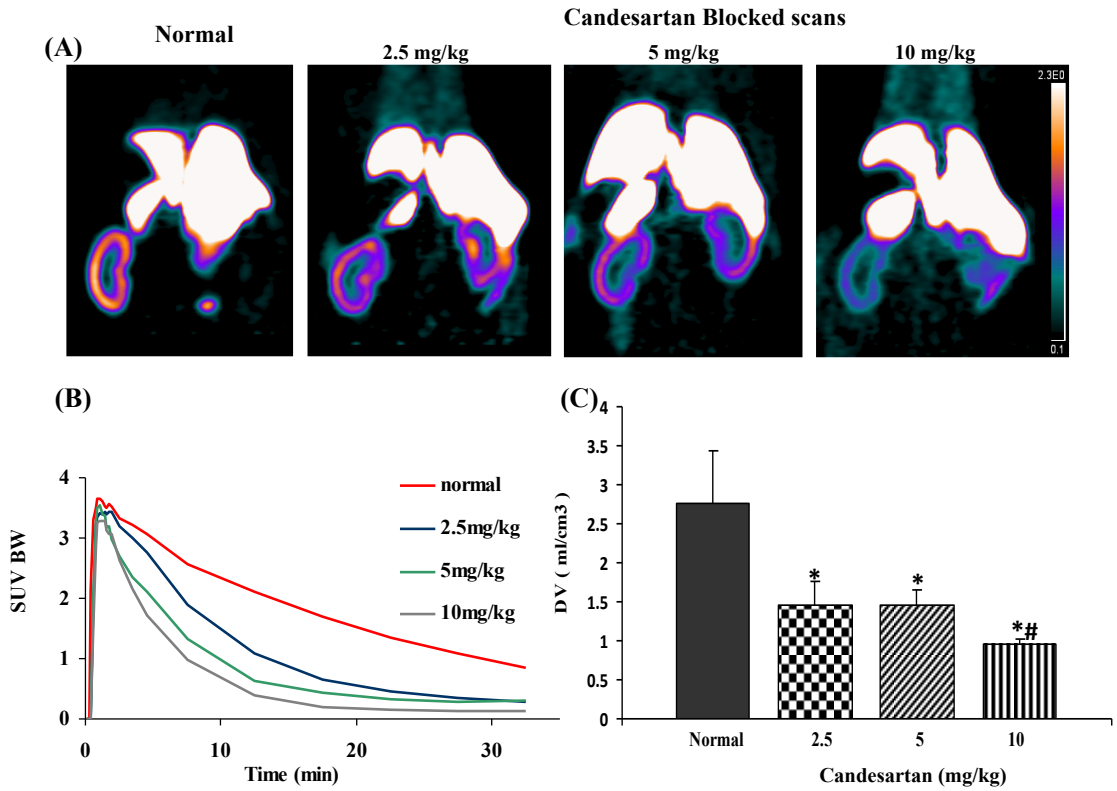

Figure 6.3: (A) MicroPET images (coronal view) of [^{18}F]FPyKYNE-losartan showing liver and kidney activity (specific uptake values) at 10-15 min post-injection. Effect of AT_1R blocking with increasing candesartan doses (2.5 mg/kg, n=3; 5 mg/kg, n=5; and 10 mg/kg, n=3) on (B) specific uptake value (SUV) time-activity curves from 0 to 60 min, and (C) distribution volume (DV) of [^{18}F]FPyKYNE-losartan determined by Logan analysis in the kidney of rats. * $p< 0.02$ compared to baseline; # $p< 0.02$ compared to previous dose.

2.3.2. Radiolabeled Metabolite Analysis of [^{18}F]FPyKYNE-Losartan in Rat Plasma

Column-switch High Performance Liquid Chromatography (HPLC) metabolite analysis of [^{18}F]FPyKYNE-losartan exhibited three distinct radioactive peaks in rat plasma, with retention times of approximately 0.5-1 min (peak 1), 6.8 min (peak 2) and 10 min (peak 3) post-switch respectively (Figure 6.4). Peak 1 corresponds to hydrophilic labeled metabolite(s) eluted from the capture column that is unlikely to bind to AT_1R. Peak 2 is a hydrophobic labeled metabolite that can potentially bind to AT_1R, and peak 3 represents unchanged tracer**.** At 30 min after injection, 78 ± 10% of total radioactivity (noise- and decay-corrected) was from peak 1, 1 ± 1% peak 2, and 23 ± 10% was unchanged [^{18}F]FPyKYNE-losartan (Figure 6.5). In control plasma samples, radioactivity present was solely representative of unchanged [^{18}F]FPyKYNE-losartan (data not shown).

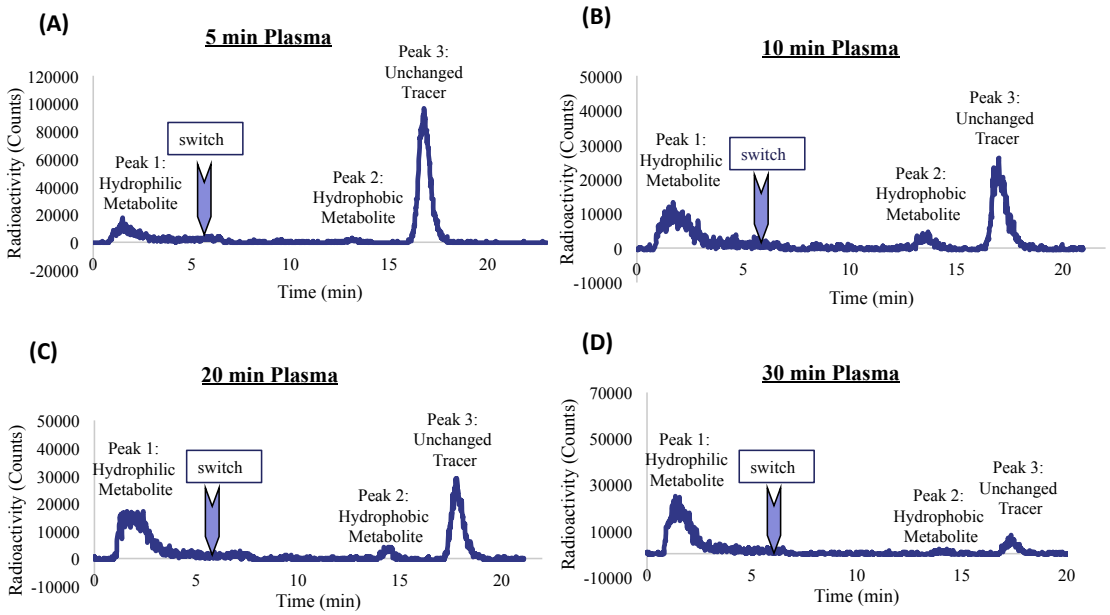

Figure 6.4: Representative HPLC chromatograms displaying presence of unchanged [^{18}F]FPyKYNE-losartan and its labeled metabolites, in rat plasma at respective time points. [^{18}F]FPyKYNE-Losartan (peak 3) is metabolized into a hydrophilic metabolite (peak 1) and a hydrophobic metabolite (peak 2). Plasma samples were analyzed at 5 min (A), 10 min (B), 20 min (C) and 30 min (D) post tracer injection.

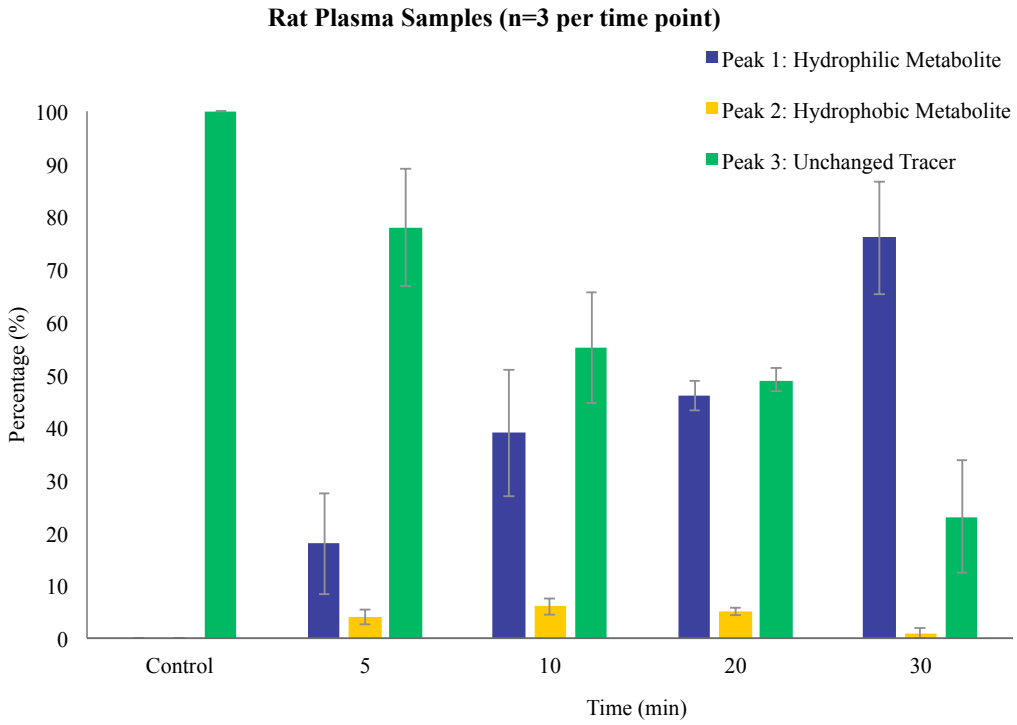

Figure 6.5: Proportions of [^{18}F]FPyKYNE-losartan and its labeled metabolites in rat plasma over time. In the control sample, 100% of radioactivity represents unchanged tracer. From 5 min to 30 min unchanged [^{18}F]FPyKYNE-losartan is rapidly metabolized and reduced from 78% to 23%, respectively.

3. Conclusions

Radiosynthesis of [^{18}F]FPyKYNE-losartan has been achieved in high radiochemical purity and acceptable specific activity for renal imaging. The production method was reliable, providing sufficient amount of tracer, with no meaningful copper contamination, for multiple PET scans. [^{18}F]FPyKYNE-losartan PET images obtained in rats displayed high tissue contrast and binding selectivity for renal AT_1R over AT_2R. [^{18}F]FPyKYNE-losartan metabolism to mostly hydrophilic labeled compounds in plasma suggests minimal interference of ^{18}F-labeled metabolites to AT_1Rs. These findings support the use of this tracer for renal AT_1R evaluation with non-invasive imaging in rats.

4. Experimental Section

4.1. Materials and Methods

Reaction solvents, including MeCN and DMSO as well as purification solvents (pentane and diethyl ether) were anhydrous (> 99%) ACS grade by Sigma-Aldrich. HPLC grade MeCN was purchased from Fisher Scientific, Trifluoroacetic acid (TFA, 99%) from Alfa Aesar and losartan potassium (98%) from LKT Laboratories, Inc (Medicorp, Montreal, QC). All other reagents, including deuterated solvents for NMR, were purchased from Sigma-Aldrich and classified as 98% purity or greater. EtOH (99.9%) and saline solution (0.9%) for reformulation were obtained from sterile capped bottles. No further manipulation or purification was made to purchased solvents and/or reagents.

Analytical TLC was performed on silica gel-coated aluminum sheets (Sigma-Aldrich). Unless specified otherwise, TLC was run with a solvent of 30:70 EtOAc/Hexanes. Preparative TLC was performed on Analtech TLC Uniplates (silica gel matrix, 1000

μM). A technical grade silica gel (Davisil® grade 633, 60 Å pore size, 200-425 mesh) purchased from Sigma-Aldrichwas used for flash column chromatography. A Phenomenex Luna C18(2) column (250 x 4.6 mm, 10 μM) was used for all analytical HPLC and a Phenomenex® Luna C18(2) column (250 x 10 mm, 10 μM) was installed in the module for HPLC purification. PeakSimple Chromatography Data System (6-port) was used in combination with a Waters 486 Tunable Absorbance Detector and Water 515 HPLC Pump and data analysed by PeakSimple (v 3.93). Sep-Pak Light Waters Accell Plus QMA cartridges and Sep-Pak Light C18 cartridges for SPE were purchased from Waters. The QMA cartridges were conditioned by passing through 7-8 mL of a 0.55M solution of potassium carbonate (7.60 g or 0.055 mol K_2CO_3 in 100 mL water), followed by water (7-8 mL) and drying under a stream of argon. The C18 cartridges were pre-conditioned by passing through 5 mL of EtOH followed by 10 mL of water. Silica cartridges were used as received. F-18 eluent was prepared by dissolving 27.5 mg (0.20 mmol) K_2CO_3 and 150 mg (0.40 mmol) Kryptofix2.2.2 (K_{222}) in a 5 mL solution of MeCN (4.75 mL) and water (250 μl). Melting points (Mp) were measured by a Fisher Scientific melting point apparatus.

NMR, HRMS, Accurate Mass Measurement and ICP MS were performed at the University of Ottawa. ^{1}H-NMR was carried out in $CDCl_3$, unless otherwise indicated either by a Bruker AVANCE 300 or 400 MHz, or a Varian Inova 500 MHz spectrometer. ^{13}C-NMR and ^{19}F-NMR spectra were obtained on a Bruker AVANCE 300 MHz spectrometer. Proton chemical shifts (δ) are reported in parts per million (ppm) relative to tetramethylsilane (TMS) internal standard. Coupling constants (*J*) are reported in Hz. HRMS were done on either a Concept HRes, EI Mass Spectrometer or a Micromass

QToF, ESI HRes Mass Spectrometer (for accurate mass measurement). ICP MS was performed on a Varian (Agilent) Vista-Pro Inductively coupled plasma emission spectrometer, equipped with a charge-coupled device (CCD) detector.

$[^{18}F]F^-$ was produced in a CTI/Siemens RDS III cyclotron by proton irradiation of $[^{18}O]H_2O$ (> 97%) via the $^{18}O(p,n)^{18}F$ nuclear reaction. The TRACERlab FX N Pro automated synthesizer, including UV detector, HPLC pump, and software, were purchased from GE Healthcare. Radioactivity was measured in a Capintec dose calibrator.

4.2. Chemistry

4.2.1. 2-Nitro-3-pent-4-yn-1-yloxypyridine (NO_2PyKYNE, 1)

Compound **1** was synthesized according to the literature.[15] A solution containing 2-nitro-3-hydroxypyridine, potassium carbonate (K_2CO_3), sodium iodide (NaI) and 5-chloropent-1-yne in DMF was stirred overnight at 80°C. The reaction mixture was cooled and diluted with EtOAc for extraction with water and brine. After drying over Na_2SO_4, the solvent was removed under reduced pressure and the residue purified by flash column chromatography on silica gel (85:15 Hexane/EtOAc) to afford **1** as a white crystalline powder. Mp 56-58 °C. HPLC [50:50 MeCN/H_2O (0.1M AF), 2mL/min]: 4.6 min. ^{1}H-NMR (300 MHz, $CDCl_3$) δ_H 8.08 (dd, J = 3.2, 2.6 Hz, 1H); 7.51-7.50 (m, 2H); 4.23 (t, J = 6.0 Hz, 2H); 2.45 (td, J = 6.8, 2.6 Hz, 2H); 2.03 (qn, J = 6.1 Hz, 2H); 1.95 (t, J = 2.6 Hz, 1H). ^{13}C-NMR (75 MHz, $CDCl_3$) δ_C 150 (C); 147.14 (C); 139.20 (CH); 128.53 (CH); 123.43 (CH); 82.68 (C); 69.43 (CH); 67.88 (CH_2); 27.58 (CH_2); 14.87 (CH_2). HRMS: calcd for $C_{10}H_{10}N_2O_3$ $[M + H]^+$, 207.0677, found 207.0323. The ^{1}H and ^{13}C-NMR as well

as HRMS data confirmed product identity and were in agreement with the reported values.

4.2.2. 2-Fluoro-3-pent-4-yn-1-yloxypyridine (FPyKYNE, 2a)

As described previously,[15] compound **2a** was synthesized by reacting NO_2PyKYNE **1** with potassium fluoride and Kryptofix2.2.2 in DMSO at 145-165^oC for 90 min. The reaction was monitored for completion by TLC. After cooling to room temperature, the reaction mixture was diluted with EtOAc and extracted with water and brine then dried over Na_2SO_4 before removing the solvent under reduced pressure. The residue was purified by flash column chromatography on silica gel (85:15 Hexanes/EtOAc) to afford **2a** as clear crystalline oil. HPLC [50:50 MeCN/H_2O (0.1M AF), 2 mL/min]: 4.6 min. ^{1}H-NMR (300 MHz, $CDCl_3$) δ_H 7.75 (dd, J = 4.8, 1.6 Hz, 1H); 7.32 (m, 1H); 7.12 (dd, J = 7.8, 4.9 Hz, 1H); 4.17 (t, J = 6.1 Hz, 2H); 2.45 (td, J = 6.9, 2.6 Hz, 2H); 2.05 (qn, J = 6.4 Hz, 2H); 2.0 (t, J = 2.6 Hz, 1H). ^{13}C-NMR (75 MHz, $CDCl_3$) δ_C 153.85 (C, $J^1_{C\text{-}F}$ = 237.3 Hz); δ: 142.23 (C, $J^2_{C\text{-}F}$ = 25.4 Hz); 137.37 (C, $J^3_{C\text{-}F}$ = 13.2 Hz); δ: 122.81 (C, $J^3_{C\text{-}F}$ = 4.4 Hz); δ: 121.66 (C, $J^4_{C\text{-}F}$ = 4.3 Hz); 82.93 (C); 69.16 (CH); 67.50 (CH_2); 27.83 (CH_2); 14.96 (CH_2). ^{19}F-NMR δ_F -84.79 (referenced with respect to TFA). HRMS: calcd for $C_{10}H_{10}FNO$ $[M + H]^+$, 180.0732, found 180.0443.

4.2.3. 2-Butyl-4-chloro-5-(hydroxymethyl)-1-[[2′-[(triphenylmethyl)tetrazole-5-yl]biphenyl-4-yl]methyl]imidazol (tetrazole-protected losartan, 3)

Compound **3** was prepared from commercially available losartan potassium as previously described[2]. Briefly, to a solution of losartan in DMF was added trityl chloride and Et_3N. The solution was stirred at room temperature overnight after which it was diluted with EtOAc, washed with water and brine, dried over Na_2SO_4 and solvent removed. The

residue was purified by flash column chromatography on silica gel to obtain a white powder. HPLC [35:65 MeCN/AF (0.1M), 2 mL/min]: 3.6 min. ^{1}H-NMR (400 MHz, DMSO-d_6) δ_H 7.79 (d, J = 6.0 Hz, 1H); 7.61 (t, J = 6.0 Hz, 1H); 7.54 (t, J = 6.0 Hz, 1H); 7.31-7.44 (m, 10H); 7.05 (d, J = 6.4 Hz, 2H); 6.90 (d, J = 6.4 Hz, 2H); 6.86 (d, J = 6.0 Hz, 6H); 5.24 (t, J = 4.0 Hz, 1H); 5.19 (s, 2H); 4.21 (d, J = 4.0Hz, 2H); 2.37 (t, J = 6.0 Hz, 2H); 1.41 (q, J = 6.0 Hz, 2H); 1.15 (sx, J = 6.0 Hz, 2H); 0.73 (t, J = 6.0 Hz, 3H). HRMS: calcd for $C_{41}H_{37}ClN_6O$ [M + Na], 687.2615, found 687.2638.

4.2.4. 2-Butyl-4-chloro-5-(azidomethyl)-1-[[2´-[(triphenylmethyl)tetrazole-5-yl]biphenyl-4-yl]methyl]imidazol (tetrazole-protected azido-losartan, 4)

To a solution of **3** (300 mg, 0.44 mmol) in THF (4 mL) were added 18-diazabicyclo[5.4.0]-7-undecene (DBU, 74 mg, 0.48 mmol) and diphenylphosphoryl azide (DPPA, 105 µl, 0.49 mmol). The reaction mixture was stirred at ambient temperature under argon for overnight (16 h) and monitored by TLC for completion. The reaction was then quenched with water (2 mL). The organic phase was separated, and the aqueous phase extracted with EtOAc. The organic phases were combined and dried over Na_2SO_4. The solvent was removed under reduced pressure and the residue purified by flash column chromatography (EtOAc/Hexanes 5:95 to 30:70) to afford **4** (275 mg, 87%) as a white crystalline powder. Mp 130-132 ^{o}C. ^{1}H-NMR (300 MHz, $CDCl_3$) δ_H 7.96 (m, 1H); 7.41-7.51 (m, 2H); 7.30-7.36 (m, 10H); 7.11 (d, J = 8.2 Hz, 2H); 6.90 (d, J = 7.7 Hz, 2H); 6.70 (d, J = 8.2 Hz, 6H); 4.98 (s, 2H); 3.94 (s, 2H); 2.51 (t, J = 7.8 Hz, 2H); 1.66 (qn, J = 7.7 Hz, 2H); 1.29 (sx, J = 7.4 Hz, 2H); 0.86 (t, J = 7.3 Hz, 3H). ^{13}C-NMR (75 MHz, $CDCl_3$) δ_C 149.42 (C); 146.80 (C); 145.20 (3×C); 141.23 (C); 130.61 (3×C); 129.64 (C); 128.40 (7×CH); 127.90 (9×CH); 127.6 (4×CH); 126.99 (3×CH); 125.31 (C);

77.24 (C); 42.14 (CH_2); 29.91 (CH_2); 29.67 (CH_2); 22.29 (CH_2); 22.23 (CH_2); 13.46 (CH_3). HRMS: calcd for $C_{41}H_{36}ClN_9$ [M + Na], 712.2680, found 712.2664.

4.2.5. 2-Butyl-4-chloro-5-[[3-{[1-methyl-4-yl](1,2,3)triazol}propoxy]-2-fluoro-pyridine]-1-[[2′-[tetrazole-5-yl]biphenyl-4-yl]methyl]imidazol (FPyKYNE-losartan, 5a)

To a stirred solution of tetrzol-protected azido-losartan **4** (50 mg, 0.072 mmol) in CH_2Cl_2 (1.5 mL) was added a solution of FPyKYNE, **2a** (14.28 mg, 0.080 mmol) in CH_2Cl_2 (400 µl) followed by aqueous solutions of copper(II) sulfate ($CuSO_4$, 50 µl, 0.06M) and sodium ascorbate (120 µl, 0.05M). The biphasic solution was stirred at ambient temperature overnight (16 h). The reaction was monitored by TLC for completion after which it was diluted with EtOAc and extracted with water (2 x 30 mL) and brine (30 mL) then dried over Na_2SO_4 before removing the solvent under reduced pressure. The residue was diluted with a solution of TFA in DMF (400 µl, 0.13 mM) and heated at 80-85^oC for 1-2 min. The product was purified by semi-prep TLC (silica on glass, EtOAc/Hexanes/MeOH 80:20:5) to obtain **5a** (20 mg, 44%) as a clear oil which was then crystallized with chloroform to yield a white solid. Mp 162-165 ^oC. ^{1}H-NMR (300 MHz, $CDCl_3$) δ_H 7.86 (dd, *J* = 7.51, 1.4 Hz, 1H); 7.65-7.68 (m, 1H); 7.52 (td, *J* = 7.47, 1.6 Hz, 1H); 7.46 (td, *J* = 7.53, 1.7 Hz, 1H); 7.24-7.36 (m, 1H); 6.98-7.07 (m,4H); 6.81 (d, *J* = 8.4 Hz, 2H); 6.39 (d, *J* = 8.3 Hz, 2H); 5.40-5.24 (m, 4H); 3.81 (t, *J* = 6.3 Hz, 2H); 2.60 (t, *J* = 7.8 Hz, 4H); 1.86 (qn, *J* = 6.7 Hz, 2H); 1.67 (qn, *J* = 7.7 Hz, 2H); 1.34 (sx, *J* = 7.5 Hz, 2H); 0.86 (t, *J* = 7.3 Hz, 3H). ^{19}F-NMR (referenced with respect to TFA) δ_F -84.88 (d, *J* = 8.78 Hz). ^{13}C-NMR (75 MHz, $CDCl_3$) δ_C 153.75 (C); 152.17 (C); 150.15 (C); 147.29 (C); 142.03 (C); 139.97 (C); 138.30 (C); 137.56 (C); 135.16 (C); 131.89 (C); 131.55 (C); 130.47 (2×CH); 130.06 (2×CH); 129.46 (CH); 128.49 (CH); 124.65 (CH);

123.15 (CH); 122.85 (CH); 121.93 (CH); 120.64 (CH); 120.24 (CH); 67.83 (CH_2); 53.62 (CH_2); 47.34 (CH_2); 42.55 (CH_2); 29.93 (CH_2); 28.33 (CH_2); 26.89 (CH_2); 22.55 (CH_2); 13.85 (CH_3). HRMS: calcd for $C_{32}H_{32}ClFN_{10}O$ [M - H], 625.2355, found 625.2357.

4.3. Radiochemistry

4.3.1. 2-Butyl-4-chloro-5-[[3-{[1-methyl-4-yl](1,2,3)triazol}propoxy]-2-[^{18}F]fluoro-pyridine]-1-[[2´-[tetrazole-5-yl]biphenyl-4-yl]methyl]imidazol ([^{18}F]FPyKYNE-losartan, 5b)

The F-18 enriched target water was delivered to the module and loaded onto a QMA cartridge whereby F-18 was then eluted with an aqueous solution of potassium carbonate and Kryptofix2.2.2 (K_{222}) into the first reaction vessel. Azeotropic drying by evaporation of acetonitrile provided active un-solvated $K^+/K_{222}/^{18}F^-$. Nucleophilic substitution of the nitro group on NO_2PyKYNE **1** with F-18 produced [^{18}F]FPyKYNE **2b** which was then transferred to a series of three silica cartridges. The labeled product was eluted into the second reaction vessel and combined with tetrazole-protected azido-losartan **4** for conjugation. The product was deprotected with acid and sent to the semi-prep HPLC for purification. The collected fraction containing the product was then diluted with water and passed through a C-18 cartridge. After washing with water it was then eluted with EtOH (minimum value 0.4 mL) and reformulated in saline (maximum 10% EtOH solution).

4.3.2. Level of Copper in the Final Formulation

The [^{18}F]FPyKYNE-losartan **5b**, was produced several times (n=11) using different amounts of copper sulfate (1.5-2.25 mg, 9.4×10^{-3}-14.1×10^{-3} mmol) and sodium ascorbate (3.25-4.9 mg, 16.4×10^{-3}-24.7×10^{-3} mmol). The level of copper in the final formulations

measured by ICP MS, was above the limit of detection (0.06 ppb), and the results were compared with blanks containing 10% ethanol in saline (prepared in different types of vials, n=3), pure ethanol (n=2) or pure saline (n=1).

4.4. Animal Studies

All experiments were performed with male Sprague Dawley rats weighing 200-660 g (Charles River Laboratories, Montreal, Canada) and were conducted in accordance with the guidelines of the Canadian Council of Animal Care (CCAC) and with approval from the Animal Care Committee (ACC) at the University of Ottawa. Rats were housed in pairs, kept on a 12 hour light-dark cycle, and followed a standard diet.

4.4.1. In vivo microPET

Dynamic PET images were acquired with a Siemens Inveon small animal dedicated micro-PET scanner (LSO scintillation crystals, 1.4 mm spatial resolution, 12.7 cm axial FOV). Rats (n=7) were anaesthetized with isoflurane (2-2.5%), weighed, and placed on the scanning bed in supine position with movement restricted by light taping. Anaesthesia was maintained throughout the scanning process by a continuous flow of isoflurane (1-2%) through a nose cone. A slow-bolus of 0.4-1.0 mCi of [^{18}F]FPyKYNE-losartan was injected via a catheter in the lateral tail vein. List-mode data were acquired for 60 min and subsequently binned into 26 frames of 12 × 10 s, 3 × 60 s, and 11 × 300 s. Dynamic data were reconstructed on a 128 × 128 pixel image matrix (0.345 mm pixel size) using OSEM3D/MAP (β = 1.0, OSEM3D iterations = 2, MAP iterations = 18) with corrections for dead-time, isotope decay, detector efficiencies, attenuation, scatter and random events. A 10 min transmission scan with two rotating Co^{57} (122 keV) point

sources was performed either prior to, or following the dynamic F-18 emission scan for attenuation correction.

In order to assess binding specificity for the AT_1R, subsets of rats (n=3-5 per group) were co-injected with AT_1R blocker candesartan (2.5 mg/kg, 5 mg/kg and 10 mg/kg). Binding specificity for AT_2R (Zober et al. 2006, Hadizad et al. 2009) was examined in another rat group (n=3) by injection of PD123,319 (5mg/kg) 5 min prior to tracer injection.

4.4.2. Image Analysis

Reconstructed dynamic images were analyzed using Siemens Inveon Research Workplace (IRW) software. TACs were generated for the arterial blood input function (derived from left atrium region of interest) and left kidney tissue uptake. [^{18}F]FPyKYNE-losartan renal activity was calculated as SUV (g/mL) at 5-10 min post-injection (frame 16). The SUV is a relative quantification of activity in a single or summed frame, normalized to the injected activity and the body weight of the rat, to allow comparison between subjects. Preliminary tracer binding was assessed by Logan graphical analysis (Logan et al. 1990). Logan analysis is a graphical method used to quantify the tracer DV, which is the expected ratio of radiotracer in tissue relative to plasma at equilibrium for reversibly binding receptor ligands. The tracer DV (mL/cm^3) is an index of receptor density (B_{max}) and ligand affinity ($1/K_d$) for the receptor. Physiologically, the DV can be used as an indicator of protein expression and/or receptor-ligand binding potential (B_{max} / K_d) for reversibly binding ligands, i.e. higher protein expression or binding affinity will result in a higher DV value.

4.4.3. Radiolabeled Metabolite Analysis in Plasma

Restrained animals were injected with 2-4 mCi (74-148 MBq) [^{18}F]FPyKYNE-losartan via the lateral tail vein and sacrificed at -5 (control), 5, 10, 20 and 30 min post-injection (n=3). Plasma samples were prepared following centrifugation (4000xg, 5 min), by mixing with 1 g urea, to break binding with macromolecules, filtered through 0.2µm syringe filters (Nylon Membrane, Acrodisc®), and injected onto the HPLC system. A modification of the HPLC column-switch method was used to quantify plasma metabolites.(Kenk et al. 2008) Briefly, the HPLC apparatus consisted of 2 pumps (Waters): one eluting solvent A (1:99 MeCN/water [v/v]) at 1.5 ml/min across the capture cartridge (Alltech Direct-Connect refillable guard column, 2 x 20 mm) packed with sorbent (HLB VAC RC, Waters Oasis) and fitted with 2.5 µm frits (Alltech, 2-mm filter elements); and the other eluting solvent B (35:65 MeCN/ 0.1M ammonium formate [v/v]) at 3 ml/min across the analytical column (Luna 10u C18 (2) 100A, 250 x 4.6 mm, 10µm; Phenomenex). Eluents of both columns were analyzed in series by two detectors: the ultraviolet (UV) absorbance detector at 254 nm (Waters 486), and coincidence radiation detector (Bioscan). Signals were integrated using the PeakSimple Six-Port Chromatography Data System (Chromatographic Specialities), and expressed as the percentage of total noise- and decay-corrected radioactivity signal. Prepared samples (2 ml) were injected onto the capture column, then after elution of proteins, macromolecules and hydrophilic metabolites (6-7min), column flow was switched delivering solvent B across the capture cartridge, eluting retained compounds onto the analytical column for analysis.

4.4.4. Statistical Analysis

All results are expressed as mean ± standard deviation (SD). Statistical analyses were performed by a two-tailed *t*-test with a P value of less than 0.05 considered statistically significant.

Acknowledgements

The authors wish to thank the radiochemistry personnel, Yanick Lee and the Department of Chemistry of University of Ottawa for the chemistry. We would also like to extend our sincerest gratitude to Dr. Stephanie Thorn and Dr. James Thackeray for the help with the PET/bio-testing portion of this project. This work was supported in part by, the Ontario Preclinical Imaging Consortium (OPIC) grant# RE03-51 (Ontario Research Foundation), the Heart and Stroke Foundation of Ontario Program Grant (PRG6242), and the Canadian Institutes of Health Research (MOP-287694).

CHAPTER 7: REFERENCES

Agodoa, L. Y., L. Appel, G. L. Bakris, G. Beck, J. Bourgoignie, J. P. Briggs, et al. (2001). "Effect of ramipril vs amlodipine on renal outcomes in hypertensive nephrosclerosis: a randomized controlled trial." JAMA **285**(21): 2719-2728.

Aiello, S., G. Remuzzi and M. Noris (1998). "Nitric oxide/endothelin balance after nephron reduction." Kidney Int Suppl **65**: S63-67.

Akishita, M., M. Horiuchi, H. Yamada, L. Zhang, G. Shirakami, K. Tamura, et al. (2000). "Inflammation influences vascular remodeling through AT2 receptor expression and signaling." Physiol Genomics **2**(1): 13-20.

Akishita, M., M. Iwai, L. Wu, L. Zhang, Y. Ouchi, V. J. Dzau, et al. (2000). "Inhibitory effect of angiotensin II type 2 receptor on coronary arterial remodeling after aortic banding in mice." Circulation **102**(14): 1684-1689.

Albiston, A. L., S. G. McDowall, D. Matsacos, P. Sim, E. Clune, T. Mustafa, et al. (2001). "Evidence that the angiotensin IV (AT(4)) receptor is the enzyme insulin-regulated aminopeptidase." J Biol Chem **276**(52): 48623-48626.

Alexoff, D. L., P. Vaska, D. Marsteller, T. Gerasimov, J. Li, J. Logan, et al. (2003). "Reproducibility of 11C-raclopride binding in the rat brain measured with the microPET R4: effects of scatter correction and tracer specific activity." J Nucl Med **44**(5): 815-822.

Allen, A., H. Yamada and F. Mendelsohn (1990). "In vitro autoradiographic localization of binding to angiotensin receptors in the rat heart." Int J Cardiol **28**: 25-33.

Allen, A. M., J. Zhuo and F. A. Mendelsohn (2000). "Localization and function of angiotensin AT1 receptors." Am J Hypertens **13**(1 Pt 2): 31S-38S.

Allred, A. J., M. C. Chappell, C. M. Ferrario and D. I. Diz (2000). "Differential actions of renal ischemic injury on the intrarenal angiotensin system." Am J Physiol Renal Physiol **279**(4): F636-645.

Almansa, C., L. A. Gomez, F. L. Cavalcanti, A. F. de Arriba, J. Garcia-Rafanell and J. Forn (1997). "Synthesis and structure-activity relationship of a new series of potent AT1 selective angiotensin II receptor antagonists: 5-(biphenyl-4-ylmethyl)pyrazoles." J Med Chem **40**(4): 547-558.

Alpert, N. M., C. A. Rabito, D. J. Correia, J. W. Babich, B. H. Littman, R. G. Tompkins, et al. (2002). "Mapping of local renal blood flow with PET and H(2)(15)O." J Nucl Med **43**(4): 470-475.

Alvarez-Prats, A., O. Hernandez-Perera, P. Diaz-Herrera, A. C. Ucero, A. Anabitarte-Prieto, A. Losada-Cabrera, et al. (2012). "Combination therapy with an angiotensin II receptor blocker and an HMG-CoA reductase inhibitor in experimental subtotal nephrectomy." Nephrol Dial Transplant **27**(7): 2720-2733.

Amann, K., I. Rychlik, G. Miltenberger-Milteny and E. Ritz (1998). "Left ventricular hypertrophy in renal failure." Kidney Int Suppl **68**: S78-85.

Anderson, S., H. G. Rennke and B. M. Brenner (1986). "Therapeutic advantage of converting enzyme inhibitors in arresting progressive renal disease associated with systemic hypertension in the rat." J Clin Invest **77**(6): 1993-2000.

Appel, L. J., J. T. Wright, Jr., T. Greene, L. Y. Agodoa, B. C. Astor, G. L. Bakris, et al. (2010). "Intensive blood-pressure control in hypertensive chronic kidney disease." N Engl J Med **363**(10): 918-929.

Arksey, N., T. Hadizad, B. Ismail, M. Hachem, A. C. Valdivia, R. S. Beanlands, et al. (2014). "Synthesis and evaluation of the novel 2-[(1)(8)F]fluoro-3-propoxy-triazole-pyridine-substituted losartan for imaging AT(1) receptors." Bioorg Med Chem **22**(15): 3931-3937.

Arora, P., P. Vasa, D. Brenner, K. Iglar, P. McFarlane, H. Morrison, et al. (2013). "Prevalence estimates of chronic kidney disease in Canada: results of a nationally representative survey." CMAJ **185**(9): E417-423.

Asano, K., D. L. Dutcher, J. D. Port, W. A. Minobe, K. D. Tremmel, R. L. Roden, et al. (1997). "Selective downregulation of the angiotensin II AT1-receptor subtype in failing human ventricular myocardium." Circulation **95**(5): 1193-1200.

Asselbergs, F. W., G. F. Diercks, H. L. Hillege, A. J. van Boven, W. M. Janssen, A. A. Voors, et al. (2004). "Effects of fosinopril and pravastatin on cardiovascular events in subjects with microalbuminuria." Circulation **110**(18): 2809-2816.

Azizi, M., R. Webb, J. Nussberger and N. K. Hollenberg (2006). "Renin inhibition with aliskiren: where are we now, and where are we going?" J Hypertens **24**(2): 243-256.

Bader, M. (2010). "Tissue renin-angiotensin-aldosterone systems: Targets for pharmacological therapy." Ann Rev Pharmacology Toxico **50**: 439-465.

Bader, M., J. Peters, O. Baltatu, D. N. Muller, F. C. Luft and D. Ganten (2001). "Tissue renin-angiotensin systems: new insights from experimental animal models in hypertension research." J Mol Med (Berl) **79**(2-3): 76-7102.

Bakris, G. L., M. R. Weir, M. Secic, B. Campbell and A. Weis-McNulty (2004). "Differential effects of calcium antagonist subclasses on markers of nephropathy progression." Kidney Int **65**(6): 1991-2002.

Balamuthusamy, S., L. Srinivasan, M. Verma, S. Adigopula, N. Jalandhara, S. Hathiwala, et al. (2008). "Renin angiotensin system blockade and cardiovascular outcomes in patients with chronic kidney disease and proteinuria: a meta-analysis." Am Heart J **155**(5): 791-805.

Balmforth, A. J., A. J. Lee, F. H. Shepherd, P. Warburton, D. Donnelly and S. G. Ball (1997). "G-protein-coupled receptors for peptide hormones: angiotensin II receptors." Biochem Soc Trans **25**(3): 1041-1046.

Bayorh, M. A., D. Eatman, M. Walton, R. R. Socci, M. Thierry-Palmer and N. Emmett (2002). "1A-779 attenuates angiotensin-(1-7) depressor response in salt-induced hypertensive rats." Peptides **23**(1): 57-64.

Benicky, J., R. Hafko, E. Sanchez-Lemus, G. Aguilera and J. M. Saavedra (2012). "Six commercially available angiotensin II AT1 receptor antibodies are non-specific." Cell Mol Neurobiol **32**(8): 1353-1365.

Benigni, A., C. Zola, D. Corna, S. Orisio, D. Facchinetti, L. Benati, et al. (1996). "Blocking both type A and B endothelin receptors in the kidney attenuates renal injury and prolongs survival in rats with remnant kidney." Am J Kidney Dis **27**(3): 416-423.

Berk, B. C. (2003). "Angiotensin type 2 receptor (AT2R): a challenging twin." Sci STKE **2003**(181): PE16.

Bidani, A. K. and K. A. Griffin (2006). "The benefits of renin-angiotensin blockade in hypertension are dependent on blood-pressure lowering." Nature clinical practice. Nephrology **2**(10): 542-543.

Bidani, A. K., K. D. Mitchell, M. M. Schwartz, L. G. Navar and E. J. Lewis (1990). "Absence of glomerular injury or nephron loss in a normotensive rat remnant kidney model." Kidney Int **38**(1): 28-38.

Black, H. R., W. J. Elliott, J. D. Neaton, G. Grandits, P. Grambsch, R. H. Grimm, Jr., et al. (1998). "Rationale and design for the Controlled ONset Verapamil INvestigation of Cardiovascular Endpoints (CONVINCE) Trial." Control Clin Trials **19**(4): 370-390.

Blankestijn, P. J. (2004). "Sympathetic hyperactivity in chronic kidney disease." Nephrol Dial Transplant **19**(6): 1354-1357.

Bock, V. D., D. Speijer, H. Hiemstra and J. H. van Maarseveen (2007). "1,2,3-Triazoles as peptide bond isosteres: synthesis and biological evaluation of cyclotetrapeptide mimics." Organic & biomolecular chemistry **5**(6): 971-975.

Boner, G., Z. Cao and M. E. Cooper (2002). "Combination antihypertensive therapy in the treatment of diabetic nephropathy." Diabetes Technol Ther **4**(3): 313-321.

Bongartz, L. G., B. Braam, C. A. Gaillard, M. J. Cramer, R. Goldschmeding, M. C. Verhaar, et al. (2012). "Target organ cross talk in cardiorenal syndrome: animal models." Am J Physiol Renal Physiol **303**(9): F1253-1263.

Booz, G. W. and K. M. Baker (1996). "Role of type 1 and type 2 angiotensin receptors in angiotensin II-induced cardiomyocyte hypertrophy." Hypertension **28**(4): 635-640.

Brenner, B., M. Cooper, D. de Zeeuw, W. Keane, W. Mitch, H. Parving, et al. (2001). "Effects of losartan on renal and cardiovascular outcomes in patients with type 2 diabetes and nephropathy." N Eng J Med **345**(12): 861-869.

Brenner, B. M. (1983). "Hemodynamically mediated glomerular injury and the progressive nature of kidney disease." Kidney Int **23**(4): 647-655.

Brewster, U. C. and M. A. Perazella (2004). "The renin-angiotensin-aldosterone system and the kidney: effects on kidney disease." Am J Med **116**(4): 263-272.

Brown, L., D. Wall and e. al (1997). "Tissue-specific changes in angiotensin II receptors in streptozotocin-diabetic rats." J Endocrinol **154**(2): 355-362.

Brown, M. J., C. R. Palmer, A. Castaigne, P. W. de Leeuw, G. Mancia, T. Rosenthal, et al. (2000). "Morbidity and mortality in patients randomised to double-blind treatment with a long-acting calcium-channel blocker or diuretic in the International Nifedipine GITS study: Intervention as a Goal in Hypertension Treatment (INSIGHT)." Lancet **356**(9227): 366-372.

Brunner, H. R., J. H. Laragh, L. Baer, M. A. Newton, F. T. Goodwin, L. R. Krakoff, et al. (1972). "Essential hypertension: renin and aldosterone, heart attack and stroke." N Engl J Med **286**(9): 441-449.

Bruzzi, I., G. Remuzzi and A. Benigni (1997). "Endothelin: a mediator of renal disease progression." J Nephrol **10**(4): 179-183.

Burns, K. (2000). "Angiotensin II and its receptors in the diabetic kidney." Am J Kidney Dis **36**(3): 449-467.

Burson, J. M., G. Aguilera, K. W. Gross and C. D. Sigmund (1994). "Differential expression of angiotensin receptor 1A and 1B in mouse." Am J Physiol **267**(2 Pt 1): E260-267.

Buxton, I. L. and L. L. Brunton (1983). "Compartments of cyclic AMP and protein kinase in mammalian cardiomyocytes." J Biol Chem **258**(17): 10233-10239.

Cao, Z., F. Bonnet, R. Candido, S. P. Nesteroff, W. C. Burns, H. Kawachi, et al. (2002). "Angiotensin type 2 receptor antagonism confers renal protection in a rat model of progressive renal injury." J Am Soc Nephrol **13**(7): 1773-1787.

Carini, D. J., J. V. Duncia, P. E. Aldrich, A. T. Chiu, A. L. Johnson, M. E. Pierce, et al. (1991). "Nonpeptide angiotensin II receptor antagonists: the discovery of a series of N-(biphenylylmethyl)imidazoles as potent, orally active antihypertensives." J Med Chem **34**(8): 2525-2547.

Catapano, F., P. Chiodini, L. De Nicola, R. Minutolo, P. Zamboli, C. Gallo, et al. (2008). "Antiproteinuric response to dual blockade of the renin-angiotensin system in primary glomerulonephritis: meta-analysis and metaregression." Am J Kidney Dis **52**(3): 475-485.

Cervenka, L., I. Vaneckova, Z. Huskova, Z. Vanourkova, M. Erbanova, M. Thumova, et al. (2008). "Pivotal role of angiotensin II receptor subtype 1A in the development of two-kidney, one-clip hypertension: study in angiotensin II receptor subtype 1A knockout mice." J Hypertens **26**(7): 1379-1389.

Chai, S. Y., R. Fernando, G. Peck, S. Y. Ye, F. A. Mendelsohn, T. A. Jenkins, et al. (2004). "The angiotensin IV/AT4 receptor." Cell Mol Life Sci **61**(21): 2728-2737.

Chang, R. S. and V. J. Lotti (1991). "Angiotensin receptor subtypes in rat, rabbit and monkey tissues: relative distribution and species dependency." Life Sci **49**(20): 1485-1490.

Chen, B. C., G. Germano, S. C. Huang, R. A. Hawkins, H. W. Hansen, M. J. Robert, et al. (1992). "A new noninvasive quantification of renal blood flow with N-13 ammonia, dynamic positron emission tomography, and a two-compartment model." J Am Soc Nephrol **3**(6): 1295-1306.

Cheng, H. F., B. N. Becker, K. D. Burns and R. C. Harris (1995). "Angiotensin II upregulates type-1 angiotensin II receptors in renal proximal tubule." J Clin Invest **95**(5): 2012-2019.

Chevalier, R. L. and D. L. Kaiser (1985). "Effects of acute uninephrectomy and age on renal blood flow autoregulation in the rat." Am J Physiol **249**(5 Pt 2): F672-679.

Christ, D. D. (1995). "Human plasma protein binding of the angiotensin II receptor antagonist losartan potassium (DuP 753/MK 954) and its pharmacologically active metabolite EXP3174." J Clin Pharmacol **35**(5): 515-520.

Chronic Kidney Disease Prognosis, C., K. Matsushita, M. van der Velde, B. C. Astor, M. Woodward, A. S. Levey, et al. (2010). "Association of estimated glomerular filtration rate and albuminuria with all-cause and cardiovascular mortality in general population cohorts: a collaborative meta-analysis." Lancet **375**(9731): 2073-2081.

Cohn, J. N. and G. Tognoni (2001). "A randomized trial of the angiotensin-receptor blocker valsartan in chronic heart failure." N Engl J Med **345**(23): 1667-1675.

Coresh, J., E. Selvin, L. A. Stevens, J. Manzi, J. W. Kusek, P. Eggers, et al. (2007). "Prevalence of chronic kidney disease in the United States." JAMA **298**(17): 2038-2047.

Corvol, P., A. Michaud, F. Soubrier and T. A. Williams (1995). "Recent advances in knowledge of the structure and function of the angiotensin I converting enzyme." J Hypertens Suppl **13**(3): 3-10.

Costerousse, O., J. Allegrini, W. Huang and F. Alhenc-Gelas (1998). "Angiotensin I-converting enzyme (kininase II) in cardiovascular and renal regulations and diseases." Biol Res **31**(3): 161-167.

Crabos, M., M. Roth, A. W. Hahn and P. Erne (1994). "Characterization of angiotensin II receptors in cultured adult rat cardiac fibroblasts. Coupling to signaling systems and gene expression." J Clin Invest **93**(6): 2372-2378.

Crackower, M. A., R. Sarao, G. Y. Oudit, C. Yagil, I. Kozieradzki, S. E. Scanga, et al. (2002). "Angiotensin-converting enzyme 2 is an essential regulator of heart function." Nature **417**(6891): 822-828.

Crowley, S. D. and T. M. Coffman (2008). "In hypertension, the kidney breaks your heart." Curr Cardiol Rep **10**(6): 470-476.

Crowley, S. D. and T. M. Coffman (2012). "Recent advances involving the renin-angiotensin system." Exp Cell Res **318**(9): 1049-1056.

Crowley, S. D., S. B. Gurley, M. J. Herrera, P. Ruiz, R. Griffiths, A. P. Kumar, et al. (2006). "Angiotensin II causes hypertension and cardiac hypertrophy through its receptors in the kidney." Proc Natl Acad Sci U S A **103**(47): 17985-17990.

Crowley, S. D., S. B. Gurley, M. I. Oliverio, A. K. Pazmino, R. Griffiths, P. J. Flannery, et al. (2005). "Distinct roles for the kidney and systemic tissues in blood pressure regulation by the renin-angiotensin system." J Clin Invest **115**(4): 1092-1099.

Crowley, S. D., J. Zhang, M. Herrera, R. Griffiths, P. Ruiz and T. M. Coffman (2011). "Role of AT(1) receptor-mediated salt retention in angiotensin II-dependent hypertension." Am J Physiol Renal Physiol **301**(5): F1124-1130.

Danser, A. H. (2010). "Cardiac angiotensin II: does it have a function?" Am J Physiol Heart Circ Physiol **299**(5): H1304-1306.

Davis, M. J. and M. A. Hill (1999). "Signaling mechanisms underlying the vascular myogenic response." Physiol Rev **79**(2): 387-423.

de Gasparo, M., K. J. Catt, T. Inagami, J. W. Wright and T. Unger (2000). "International union of pharmacology. XXIII. The angiotensin II receptors." Pharmacol Rev **52**(3): 415-472.

de Zeeuw, D., H. L. Hillege and P. E. de Jong (2005). "The kidney, a cardiovascular risk marker, and a new target for therapy." Kidney Int Suppl(98): S25-29.

Decker, E. and J. Kendrick (2014). "Research in the CKD clinic: highs and lows." Adv Chronic Kidney Dis **21**(4): 344-348.

Depierre, D., J. P. Bargetzi and M. Roth (1978). "Dipeptidyl carboxypeptidase from human seminal plasma." Biochim Biophys Acta **523**(2): 469-476.

Diez, J. (2006). "Review of the molecular pharmacology of Losartan and its possible relevance to stroke prevention in patients with hypertension." Clin Ther **28**(6): 832-848.

Dilauro, M. and K. D. Burns (2009). "Angiotensin-(1-7) and its effects in the kidney." ScientificWorldJournal **9**: 522-535.

Dilauro, M., J. Zimpelmann, S. J. Robertson, D. Genest and K. D. Burns (2010). "Effect of ACE2 and angiotensin-(1-7) in a mouse model of early chronic kidney disease." Am J Physiol Renal Physiol **298**(6): F1523-1532.

Dimitrijevic, I., M.-L. Edvinsson, Q. Chen, M. Malmsjo, P.-O. Kimblad and L. Edvinsson (2009). "Increased expression of vascular endothelin type B and angiotensin

type 1 receptors in patients with ischemic heart disease." BMC Cardiovasc Disord **9**: 40-40.

do, C. M. C., E. R. da Silva, H. D. Francescato, R. S. Costa, C. G. Silva, D. E. Casarini, et al. (2014). "Brazilian embauba (Cecropia pachystachya) extract reduces renal lesions in 5/6 nephrectomized rats." J Renin Angiotensin Aldosterone Syst **15**(4): 430-439.

Dostal, D. E. and K. M. Baker (1993). "Evidence for a role of an intracardiac renin-angiotensin system in normal and failing hearts." Trends Cardiovasc Med **3**(2): 67-74.

Drake, M. T., S. K. Shenoy and R. J. Lefkowitz (2006). "Trafficking of G protein-coupled receptors." Circ Res **99**(6): 570-582.

Dyadyk, A. I., A. E. Bagriy, I. A. Lebed, N. F. Yarovaya, E. V. Schukina and G. G. Taradin (1997). "ACE inhibitors captopril and enalapril induce regression of left ventricular hypertrophy in hypertensive patients with chronic renal failure." Nephrol Dial Transplant **12**(5): 945-951.

Dzau, V., K. Bernstein, D. Celermajer and e. al (2001). "The relevance of tissue angiotensin-converting enzyme: manifestations in mechanistic and endpoint data." Am J Cardiol **88**(9A): 1L-20L.

Dzau, V. J. and R. Re (1994). "Tissue angiotensin system in cardiovascular medicine. A paradigm shift?" Circulation **89**(1): 493-498.

Eguchi, S., K. Numaguchi, H. Iwasaki, T. Matsumoto, T. Yamakawa, H. Utsunomiya, et al. (1998). "Calcium-dependent epidermal growth factor receptor transactivation mediates the angiotensin II-induced mitogen-activated protein kinase activation in vascular smooth muscle cells." J Biol Chem **273**(15): 8890-8896.

Elsinga, P. H., A. van Waarde, T. J. Visser and W. Vaalburg (1998). "Visualization of beta-Adrenoceptors Using PET." Clin Positron Imaging **1**(2): 81-94.

Epstein, M. (2002). "Recent landmark clinical trials: how do they modify the therapeutic paradigm?" Am J Hypertens **15**(7 Pt 2): 82S-84S.

Esseltine, J. L. and S. S. Ferguson (2013). "Regulation of G protein-coupled receptor trafficking and signaling by Rab GTPases." Small GTPases **4**(2): 132-135.

Esther, C. R., Jr., T. E. Howard, E. M. Marino, J. M. Goddard, M. R. Capecchi and K. E. Bernstein (1996). "Mice lacking angiotensin-converting enzyme have low blood pressure, renal pathology, and reduced male fertility." Lab Invest **74**(5): 953-965.

Ferguson, S. S. (2001). "Evolving concepts in G protein-coupled receptor endocytosis: the role in receptor desensitization and signaling." Pharmacol Rev **53**(1): 1-24.

Ferrario, C., A. I. Abdelhamed and M. Moore (2004). "AII antagonists in hypertension, heart failure, and diabetic nephropathy: focus on losartan." Curr Med Res Opin **20**(3): 279-293.

Ferrario, C. M. (2006). "Angiotensin-converting enzyme 2 and angiotensin-(1-7): an evolving story in cardiovascular regulation." Hypertension **47**(3): 515-521.

Ferrario, C. M. and J. Varagic (2010). "The ANG-(1-7)/ACE2/mas axis in the regulation of nephron function." Am J Physiol Renal Physiol **298**(6): F1297-1305.

Finn, R. D. and D. J. Schlyer (2002). Production of Radionuclides for PET. Principles and Practice of Positron Emission Tomography. R. L. Wahl. Philadelphia, PA, Lippincott Williams & Wilkins**:** 1-15.

Fogo, A. B. (1999). "New insights into the renin-angiotensin system and hypertensive renal disease." Curr Hypertens Rep **1**(2): 187-194.

Frohlich, E. D., A. Gonzalez and J. Diez (2011). "Hypertensive left ventricular hypertrophy risk: beyond adaptive cardiomyocytic hypertrophy." J Hypertens **29**(1): 17-26.

Fukai, T., M. R. Siegfried, M. Ushio-Fukai, K. K. Griendling and D. G. Harrison (1999). "Modulation of extracellular superoxide dismutase expression by angiotensin II and hypertension." Circ Res **85**(1): 23-28.

Fukushima, K., P. E. Bravo, T. Higuchi, K. H. Schuleri, X. Lin, M. R. Abraham, et al. (2012). "Molecular hybrid positron emission tomography/computed tomography imaging of cardiac angiotensin II type 1 receptors." J Am Coll Cardiol **60**(24): 2527-2534.

Funabiki, K., K. Onishi, K. Dohi, T. Koji, K. Imanaka-Yoshida, M. Ito, et al. (2004). "Combined angiotensin receptor blocker and ACE inhibitor on myocardial fibrosis and left ventricular stiffness in dogs with heart failure." Am J Physiol Heart Circ Physiol **287**(6): H2487-2492.

Gad, S. C., Ed. (2008). Pharmaceutical Manufacturing Handbook: Production and Processes. New Jersey, Wiley.

Gansevoort, R. T., R. Correa-Rotter, B. R. Hemmelgarn, T. H. Jafar, H. J. Heerspink, J. F. Mann, et al. (2013). "Chronic kidney disease and cardiovascular risk: epidemiology, mechanisms, and prevention." Lancet **382**(9889): 339-352.

Garber, S. L., Y. Mirochnik, C. Brecklin, L. Slobodskoy, J. A. Arruda and G. Dunea (2003). "Effect of relaxin in two models of renal mass reduction." Am J Nephrol **23**(1): 8-12.

Garrido, P., F. Reis, E. Costa, E. Teixeira-Lemos, B. Parada, R. Alves, et al. (2009). "Characterization of a rat model of moderate chronic renal failure--focus on hematological, biochemical, and cardio-renal profiles." Ren Fail **31**(9): 833-842.

Gasc, J. M., S. Shanmugam, M. Sibony and P. Corvol (1994). "Tissue-specific expression of type 1 angiotensin II receptor subtypes. An in situ hybridization study." Hypertension **24**(5): 531-537.

Gavras, H., A. F. Lever, J. J. Brown, R. F. Macadam and J. I. Robertson (1971). "Acute renal failure, tubular necrosis, and myocardial infarction induced in the rabbit by intravenous angiotensin II." Lancet **2**(7714): 19-22.

Ghosh, S. S., H. D. Massey, R. Krieg, Z. A. Fazelbhoy, S. Ghosh, D. A. Sica, et al. (2009). "Curcumin ameliorates renal failure in 5/6 nephrectomized rats: role of inflammation." Am J Physiol Renal Physiol **296**(5): F1146-1157.

Gibbons, G. H., R. E. Pratt and V. J. Dzau (1992). "Vascular smooth muscle cell hypertrophy vs. hyperplasia. Autocrine transforming growth factor-beta 1 expression determines growth response to angiotensin II." J Clin Invest **90**(2): 456-461.

Go, A. S., G. M. Chertow, D. Fan, C. E. McCulloch and C. Y. Hsu (2004). "Chronic kidney disease and the risks of death, cardiovascular events, and hospitalization." N Engl J Med **351**(13): 1296-1305.

Grabowski, E. J. J. and A. S. Thompson (1995). Converting an alcohol to an azide with S.sub.N 2 inversion using a phosphoryl azide, Google Patents.

Griendling, K. K., P. Delafontaine, S. E. Rittenhouse, M. A. Gimbrone and R. W. Alexander (1987). "Correlation of receptor sequestration with sustained diacylglycerol accumulation in angiotensin II-stimulated cultured vascular smooth muscle cells." J Biol Chem **262**(30): 14555-14562.

Griendling, K. K., B. Lassegue and R. W. Alexander (1996). "Angiotensin receptors and their therapeutic implications." Annu Rev Pharmacol Toxicol **36**: 281-306.

Griffin, K. A., I. Abu-Amarah, M. Picken and A. K. Bidani (2003). "Renoprotection by ACE inhibition or aldosterone blockade is blood pressure-dependent." J Hypertens **41**(2): 201-206.

Griffin, K. A. and A. K. Bidani (2006). "Progression of renal disease: renoprotective specificity of renin-angiotensin system blockade." Clin J Am Soc Nephrol **1**(5): 1054-1065.

Griffin, K. A. and A. K. Bidani (2008). "Potential risks of calcium channel blockers in chronic kidney disease." Curr Cardiol Rep **10**(6): 448-455.

Griffin, K. A., R. Hacioglu, I. Abu-Amarah, R. Loutzenhiser, G. A. Williamson and A. K. Bidani (2004). "Effects of calcium channel blockers on "dynamic" and "steady-state step" renal autoregulation." Am J Physiol Renal Physiol **286**(6): F1136-1143.

Griffin, K. A., M. M. Picken, G. L. Bakris and A. K. Bidani (1999). "Class differences in the effects of calcium channel blockers in the rat remnant kidney model." Kidney Int **55**(5): 1849-1860.

Griffin, K. A., M. M. Picken and A. K. Bidani (1995). "Deleterious effects of calcium channel blockade on pressure transmission and glomerular injury in rat remnant kidneys." J Clin Invest **96**(2): 793-800.

Gulaldi, N. C., J. Xia, T. Feng, K. Hong, W. B. Mathews, D. Ruben, et al. (2013). "Modeling of the renal kinetics of the AT1 receptor specific PET radioligand [11C]KR31173." BioMed research international **2013**: 835859.

Gunther, S., M. A. Gimbrone and R. W. Alexander (1980). "Regulation by angiotensin II of its receptors in resistance blood vessels." Nature **287**(5779): 230-232.

Gunther, S., M. A. Gimbrone, Jr. and R. W. Alexander (1980). "Regulation by angiotensin II of its receptors in resistance blood vessels." Nature **287**(5779): 230-232.

Guo, D. F. and T. Inagami (1994). "Epidermal growth factor-enhanced human angiotensin II type 1 receptor." Hypertension **23**(6 Pt 2): 1032-1035.

Hachem, M., M. Tiberi, B. Ismail, C. R. Hunter, N. Arksey, T. Hadizad, et al. (2015). "Characterization of [18F]FPyKYNE-losartan for Imaging AT1 Receptors " J Nucl Med (In press).

Hackenthal, E., M. Paul, D. Ganten and R. Taugner (1990). "Morphology, physiology, and molecular biology of renin secretion." Physiol Rev **70**(4): 1067-1116.

Hadizad, T., J. Collins, R. E. Antoun, R. Beanlands and J. Dasilva (2011). "[11C]Methyl-losartan as a potential ligand for PET imaging angiotensin II AT1 receptors." J. Label Compd. Radiopharm **54**: 754-757.

Hadizad, T., S. A. Kirkpatrick, S. Mason, K. Burns, R. S. Beanlands and J. N. Dasilva (2009). "Novel O-[(11)C]methylated derivatives of candesartan as angiotensin

II AT(1) receptor imaging ligands: radiosynthesis and ex vivo evaluation in rats." Bioorg Med Chem **17**(23): 7971-7977.

Hall, J. E. (2003). "Historical perspective of the renin-angiotensin system." Mol Biotechnol **24**(1): 27-39.

Hamill, T. G., H. D. Burns, R. F. Dannals, W. B. Mathews, J. L. Musachio, H. T. Ravert, et al. (1996). "Development of [^{11}C]L-159,884: A Radiolabelled, Nonpeptide Angiotensin II Antagonist that is Useful for Angiotensin II, AT_1 Receptor Imaging." Appl. Radiat. Isot. **47**(2): 221-218.

Hanif, K., H. K. Bid and R. Konwar (2010). "Reinventing the ACE inhibitors: some old and new implications of ACE inhibition." Hypertens Res : official journal of the Japanese Society of Hypertension **33**(1): 11-21.

Hansson, L., T. Hedner, P. Lund-Johansen, S. E. Kjeldsen, L. H. Lindholm, J. O. Syvertsen, et al. (2000). "Randomised trial of effects of calcium antagonists compared with diuretics and beta-blockers on cardiovascular morbidity and mortality in hypertension: the Nordic Diltiazem (NORDIL) study." Lancet **356**(9227): 359-365.

Harms, H., S. de Haan, P. Knaapen, M. Huisman, R. Schuit, A. Windhorst, et al. (2011). "Tracer kinetic analysis of myocardial [11C]hydroxyephedrine studies." J Nucl Med **52**(Suppl 1): 254.

Harrison-Bernard, L. M., J. D. Imig and P. K. Carmines (2002). "Renal AT1 receptor protein expression during the early stage of diabetes mellitus." International journal of experimental diabetes research **3**(2): 97-108.

Henriksen, G., M. Herz, A. Hauser, M. Schwaiger and H. J. Wester (2004). "Synthesis and preclinical evaluation of the choline transport tracer deshydroxy-[18F]fluorocholine ([18F]dOC)." Nucl Med Biol **31**(7): 851-858.

Herrera, M., M. A. Sparks, A. R. Alfonso-Pecchio, L. M. Harrison-Bernard and T. M. Coffman (2013). "Lack of specificity of commercial antibodies leads to misidentification of angiotensin type 1 receptor protein." Hypertension **61**(1): 253-258.

Herzog, C. A., R. W. Asinger, A. K. Berger, D. M. Charytan, J. Diez, R. G. Hart, et al. (2011). "Cardiovascular disease in chronic kidney disease. A clinical update from Kidney Disease: Improving Global Outcomes (KDIGO)." Kidney Int **80**(6): 572-586.

Higuchi, S., H. Ohtsu, H. Suzuki, H. Shirai, G. D. Frank and S. Eguchi (2007). "Angiotensin II signal transduction through the AT1 receptor: novel insights into mechanisms and pathophysiology." Clin Sci (Lond) **112**(8): 417-428.

Higuchi, T., K. Fukushima, J. Xia, W. B. Mathews, R. Lautamaki, P. E. Bravo, et al. (2010). "Radionuclide imaging of angiotensin II type 1 receptor upregulation after myocardial ischemia-reperfusion injury." J Nucl Med **51**(12): 1956-1961.

Hirsch, S. (2007). "Are renin-angiotensin system inhibitors optimally prescribed?" Kidney Int **71**(5): 469.

Hostetter, T. H., M. E. Rosenberg, H. N. Ibrahim and I. Juknevicius (2001). "Aldosterone in progressive renal disease." Semin Nephrol **21**(6): 573-579.

Huang, B. S., M. Ahmad, J. Tan and F. H. H. Leenen (2009). "Chronic central versus systemic blockade of AT(1) receptors and cardiac dysfunction in rats post-myocardial infarction." Am J Physiol Heart Circ Physiol **297**(3): 968-975.

Hume, S. P., R. N. Gunn and T. Jones (1998). "Pharmacological constraints associated with positron emission tomographic scanning of small laboratory animals." Eur J Nucl Med **25**(2): 173-176.

Hume, S. P. and T. Jones (1998). "Positron emission tomography (PET) methodology for small animals and its application in radiopharmaceutical preclinical investigation [In Process Citation]." Nucl Med Biol **25**(8): 729-732.

Hume, S. P. and R. Myers (2002). "Dedicated small animal scanners: a new tool for drug development?" Curr Pharm Des **8**(16): 1497-1511.

Hunyady, L., T. Balla and K. J. Catt (1996). "The ligand binding site of the angiotensin AT1 receptor." Trends Pharmacol Sci **17**(4): 135-140.

Hunyady, L. and K. J. Catt (2006). "Pleiotropic AT1 receptor signaling pathways mediating physiological and pathogenic actions of angiotensin II." Mol Endocrinol **20**(5): 953-970.

Hutchins, G. D., M. A. Miller, V. C. Soon and T. Receveur (2008). "Small animal PET imaging." ILAR J **49**(1): 54-65.

Ibrahim, M. M. (2006). "RAS inhibition in hypertension." J Hum Hypertens **20**(2): 101-108.

Igarashi, M., A. Hirata, H. Yamaguchi, H. Tsuchiya, H. Ohnuma, M. Tominaga, et al. (2001). "Candesartan inhibits carotid intimal thickening and ameliorates insulin resistance in balloon-injured diabetic rats." Hypertension **38**(6): 1255-1259.

Ikeda, U., Y. Maeda, Y. Kawahara, M. Yokoyama and K. Shimada (1995). "Angiotensin II augments cytokine-stimulated nitric oxide synthesis in rat cardiac myocytes." Circulation **92**(9): 2683-2689.

Ismail, B., T. Hadizad, R. Antoun, M. Lortie, R. A. deKemp, R. S. Beanlands, et al. (2015). "Evaluation of [(11)C]methyl-losartan and [(11)C]methyl-EXP3174 for PET imaging of renal AT1receptor in rats." Nucl Med Biol **42**(11): 850-857.

Israili, Z. H. (2000). "Clinical pharmacokinetics of angiotensin II (AT1) receptor blockers in hypertension." J Hum Hypertens **14 Suppl 1**: S73-86.

Ito, H., M. Mifune, M. Abe, K. Oshikiri, S. Antoku, Y. Takeuchi, et al. (2012). "Hypertension resistant to antihypertensive agents commonly occurs with the progression of diabetic nephropathy in Japanese patients with type 2 diabetes mellitus: a prospective observational study." BMC nephrology **13**: 48.

Ito, M., M. I. Oliverio, P. J. Mannon, C. F. Best, N. Maeda, O. Smithies, et al. (1995). "Regulation of blood pressure by the type 1A angiotensin II receptor gene." Proc Natl Acad Sci U S A **92**(8): 3521-3525.

Itoh, H., M. Mukoyama, R. E. Pratt, G. H. Gibbons and V. J. Dzau (1993). "Multiple autocrine growth factors modulate vascular smooth muscle cell growth response to angiotensin II." J Clin Invest **91**(5): 2268-2274.

Iwai, N. and T. Inagami (1992). "Identification of two subtypes in the rat type I angiotensin II receptor." FEBS Lett **298**(2-3): 257-260.

Jackson, B., P. Hodsman and C. I. Johnston (1988). "Changes in the renin-angiotensin system, exchangeable body sodium, and plasma and atrial content of atrial natriuretic factor during evolution of chronic renal failure in the rat." Am J Hypertens **1**(3 Pt 1): 298-300.

Jafar, T. H., P. C. Stark, C. H. Schmid, M. Landa, G. Maschio, P. E. de Jong, et al. (2003). "Progression of chronic kidney disease: the role of blood pressure control, proteinuria, and angiotensin-converting enzyme inhibition: a patient-level meta-analysis." Ann Intern Med **139**(4): 244-252.

Jagoda, E. M., J. J. Vaquero, J. Seidel, M. V. Green and W. C. Eckelman (2004). "Experiment assessment of mass effects in the rat: implications for small animal PET imaging." Nucl Med Biol **31**(6): 771-779.

Joly, E., D. Nonclercq, N. Caron, J. Mertens, B. Flamion, G. Toubeau, et al. (2005). "Differential regulation of angiotensin II receptors during renal injury and compensatory hypertrophy in the rat." Clin Exp Pharmacol Physiol **32**(4): 241-248.

Jorde, U. P., P. V. Ennezat, J. Lisker, V. Suryadevara, J. Infeld, S. Cukon, et al. (2000). "Maximally recommended doses of angiotensin-converting enzyme (ACE) inhibitors do not completely prevent ACE-mediated formation of angiotensin II in chronic heart failure." Circulation **101**(8): 844-846.

Kakinuma, Y., A. Fogo, T. Inagami and I. Ichikawa (1993). "Intrarenal localization of angiotensin II type 1 receptor mRNA in the rat." Kidney Int **43**(6): 1229-1235.

Kapadia, S. R., H. Oral, J. Lee, M. Nakano, G. E. Taffet and D. L. Mann (1997). "Hemodynamic regulation of tumor necrosis factor-alpha gene and protein expression in adult feline myocardium." Circ Res **81**(2): 187-195.

Kaschina, E. and T. Unger (2003). "Angiotensin AT1/AT2 receptors: regulation, signalling and function." Blood Press **12**(2): 70-88.

Kaufman, J. M., N. J. Siegel and J. P. Hayslett (1975). "Functional and hemodynamic adaptation to progressive renal ablation." Circ Res **36**(2): 286-293.

Kenk, M., M. Greene, M. Lortie, R. A. Dekemp, R. S. Beanlands and J. N. Dasilva (2008). "Use of a column-switching high-performance liquid chromatography method to assess the presence of specific binding of (R)- and (S)-[(11)C]rolipram and their labeled metabolites to the phosphodiesterase-4 enzyme in rat plasma and tissues." Nucl Med Biol **35**(4): 515-521.

Kenk, M., M. Greene, J. Thackeray, R. A. Dekemp, M. Lortie, S. Thorn, et al. (2007). "In vivo selective binding of (R)-[(11)C]rolipram to phosphodiesterase-4 provides the basis for studying intracellular cAMP signaling in the myocardium and other peripheral tissues." Nucl Med Biol **34**(1): 71-77.

Kenk, M., J. T. Thackeray, S. L. Thorn, K. Dhami, B. J. Chow, K. J. Ascah, et al. (2010). "Alterations of pre- and postsynaptic noradrenergic signaling in a rat model of adriamycin-induced cardiotoxicity." J Nucl Cardiol **17**(2): 175-176.

Kennedy, D. J., J. Elkareh, A. Shidyak, A. P. Shapiro, S. Smaili, K. Mutgi, et al. (2008). "Partial nephrectomy as a model for uremic cardiomyopathy in the mouse." Am J Physiol Renal Physiol **294**(2): F450-454.

Kereiakes, D. J., S. G. Chrysant, J. L. Izzo, Jr., T. Littlejohn, 3rd, S. Oparil, M. Melino, et al. (2012). "Long-term efficacy and safety of triple-combination therapy with olmesartan medoxomil and amlodipine besylate and hydrochlorothiazide for hypertension." J Clin Hypertens (Greenwich) **14**(3): 149-157.

Kereiakes, D. J., J. F. Maa, A. Shojaee and R. Dubiel (2010). "Effect of an olmesartan medoxomil-based treatment algorithm on systolic blood pressure in patients

with stage 1 or 2 hypertension: a randomized, double-blind, placebo-controlled study." Am J Cardiovasc Drugs **10**(4): 239-246.

Kerr, P. G. (2006). "Renal anaemia: recent developments, innovative approaches and future directions for improved management." Nephrology (Carlton) **11**(6): 542-548.

Killion, D., E. Nitzsche, Y. Choi, H. Schelbert and J. T. Rosenthal (1993). "Positron emission tomography: a new method for determination of renal function." J Urol **150**(3): 1064-1068.

Kim, H. S., J. H. Krege, K. D. Kluckman, J. R. Hagaman, J. B. Hodgin, C. F. Best, et al. (1995). "Genetic control of blood pressure and the angiotensinogen locus." Proc Natl Acad Sci U S A **92**(7): 2735-2739.

Kim, S. and H. Iwao (2000). "Molecular and cellular mechanisms of angiotensin II-mediated cardiovascular and renal diseases." Pharmacol Rev **52**(1): 11-34.

Kim, S. E., U. Scheffel, Z. Szabo, H. D. Burns, R. E. Gibson, H. T. Ravert, et al. (1996). "In vivo labeling of angiotensin II receptors with a carbon-11-labeled selective nonpeptide antagonist." J Nucl Med **37**(2): 307-311.

Kintscher, U., A. Foryst-Ludwig and T. Unger (2008). "Inhibiting angiotensin type 1 receptors as a target for diabetes." Expert Opin Ther Targets **12**(10): 1257-1263.

Klein, R., R. S. Beanlands and R. A. deKemp (2010). "Quantification of myocardial blood flow and flow reserve: Technical aspects." J Nucl Cardiol **17**(4): 555-570.

Klocke, R., W. Tian, M. T. Kuhlmann and S. Nikol (2007). "Surgical animal models of heart failure related to coronary heart disease." Cardiovasc Res **74**(1): 29-38.

Kobori, H., M. Nangaku, L. G. Navar and A. Nishiyama (2007). "The intrarenal renin-angiotensin system: from physiology to the pathobiology of hypertension and kidney disease." Pharmacol Rev **59**(3): 251-287.

Koeppe, R. A. (2002). Data Analysis and Imaging Processing. Principles and Practice of Positron Emission Tomography. R. L. Wahl. Philadelphia, PA, Lippincott Williams & Wilkins**:** 65-99.

Koivuviita, N., R. Tertti, M. Jarvisalo, M. Pietila, J. Hannukainen, J. Sundell, et al. (2009). "Increased basal myocardial perfusion in patients with chronic kidney disease without symptomatic coronary artery disease." Nephrology, dialysis, transplantation : official publication of the European Dialysis and Transplant Association - European Renal Association **24**(9): 2773-2779.

Kolb, H. C., M. G. Finn and K. B. Sharpless (2001). "Click Chemistry: Diverse Chemical Function from a Few Good Reactions." Angew Chem Int Ed Engl **40**(11): 2004-2021.

Kolb, H. C. and K. B. Sharpless (2003). "The growing impact of click chemistry on drug discovery." Drug Discov Today **8**(24): 1128-1137.

Kolesnyk, I., D. G. Struijk, F. W. Dekker and R. T. Krediet (2010). "Effects of angiotensin-converting enzyme inhibitors and angiotensin II receptor blockers in patients with chronic kidney disease." Neth J Med **68**(1): 15-23.

Koomans, H. A., P. J. Blankestijn and J. A. Joles (2004). "Sympathetic hyperactivity in chronic renal failure: a wake-up call." J Am Soc Nephrol **15**(3): 524-537.

Krege, J. H., H. S. Kim, J. S. Moyer, J. C. Jennette, L. Peng, S. K. Hiller, et al. (1997). "Angiotensin-converting enzyme gene mutations, blood pressures, and cardiovascular homeostasis." Hypertension **29**(1 Pt 2): 150-157.

Kreissl, M. C., D. B. Stout, K. P. Wong, H. M. Wu, E. Caglayan, W. Ladno, et al. (2011). "Influence of dietary state and insulin on myocardial, skeletal muscle and brain [F]-fluorodeoxyglucose kinetics in mice." EJNMMI Res **1**: 8.

Kubo, Y., E. Reuveny, P. A. Slesinger, Y. N. Jan and L. Y. Jan (1993). "Primary structure and functional expression of a rat G-protein-coupled muscarinic potassium channel." Nature **364**(6440): 802-806.

Kuhnast, B., F. Hinnen, B. Tavitian and F. Dolle (2008). "[18F]FPyKYNE, a fluoropyridine-based alkyne reagent designed for the fluorine-18 labelling of macromolecules using click chemistry." J Label Compd Radiopharm **51**: 336-342.

Kujal, P., V. C. Chabova, Z. Vernerova, A. Walkowska, E. Kompanowska-Jezierska, J. Sadowski, et al. (2010). "Similar renoprotection after renin-angiotensin-dependent and -independent antihypertensive therapy in 5/6-nephrectomized Ren-2 transgenic rats: are there blood pressure-independent effects?" Clin Exp Pharmacol Physiol **37**(12): 1159-1169.

Kunapuli, S. P. and A. Kumar (1987). "Molecular cloning of human angiotensinogen cDNA and evidence for the presence of its mRNA in rat heart." Circ Res **60**(5): 786-790.

Kunz, R., C. Friedrich, M. Wolbers and J. F. Mann (2008). "Meta-analysis: effect of monotherapy and combination therapy with inhibitors of the renin angiotensin system on proteinuria in renal disease." Ann Intern Med **148**(1): 30-48.

Laight, D. W. (2009). "Therapeutic inhibition of the renin angiotensin aldosterone system." Expert Opin Ther Pat **19**(6): 753-759.

Lassegue, B., R. W. Alexander, G. Nickenig, M. Clark, T. J. Murphy and K. K. Griendling (1995). "Angiotensin II down-regulates the vascular smooth muscle AT1 receptor by transcriptional and post-transcriptional mechanisms: evidence for homologous and heterologous regulation." Mol Pharmacol **48**(4): 601-609.

Law, M. P. (1993). "Demonstration of the suitability of CGP 12177 for in vivo studies of beta-adrenoceptors." Br J Pharmacol **109**(4): 1101-1109.

Le Corvoisier, P., C. Adamy, L. Sambin, B. Crozatier, A. Berdeaux, J. B. Michel, et al. (2010). "The cardiac renin-angiotensin system is responsible for high-salt diet-induced left ventricular hypertrophy in mice." Eur J Heart Fail **12**(11): 1171-1178.

Lee, S. K., S. Y. Jin, D. C. Han, S. D. Hwang and H. B. Lee (1993). "Effects of delayed treatment with enalapril and/or lovastatin on the progression of glomerulosclerosis in 5/6 nephrectomized rats." Nephrol Dial Transplant **8**(12): 1338-1343.

Leenen, F. H., V. Skarda, B. Yuan and R. White (1999). "Changes in cardiac ANG II postmyocardial infarction in rats: effects of nephrectomy and ACE inhibitors." Am J Physiol **276**(1 Pt 2): H317-H325.

Lenkei, Z., P. Corvol and C. Llorens-Cortes (1995). "The angiotensin receptor subtype AT1A predominates in rat forebrain areas involved in blood pressure,

body fluid homeostasis and neuroendocrine control." Mol Brain Res **30**(1): 53-60.

Lenkei, Z., M. Palkovits, P. Corvol and C. Llorens-Cortes (1997). "Expression of angiotensin type-1 (AT1) and type-2 (AT2) receptor mRNAs in the adult rat brain: a functional neuroanatomical review." Front Neuroendocrinol **18**(4): 383-439.

Levey, A. S., R. Atkins, J. Coresh, E. P. Cohen, A. J. Collins, K. U. Eckardt, et al. (2007). "Chronic kidney disease as a global public health problem: approaches and initiatives - a position statement from Kidney Disease Improving Global Outcomes." Kidney Int **72**(3): 247-259.

Levey, A. S. and J. Coresh (2012). "Chronic kidney disease." Lancet **379**(9811): 165-180.

Levin, A., B. Hemmelgarn, B. Culleton, S. Tobe, P. McFarlane, M. Ruzicka, et al. (2008). "Guidelines for the management of chronic kidney disease." CMAJ **179**(11): 1154-1162.

Lew, R. A., T. Mustafa, S. Ye, S. G. McDowall, S. Y. Chai and A. L. Albiston (2003). "Angiotensin AT4 ligands are potent, competitive inhibitors of insulin regulated aminopeptidase (IRAP)." J Neurochem **86**(2): 344-350.

Lewis, E., L. Hunsicker and e. al (2001). "Renoprotective effect of the angiotensin-receptor antagonist irbesartan in patients with nephropathy due to type 2 diabetes." N Eng J Med **345**(12): 851-860.

Li, D. Y., Y. C. Zhang, M. I. Philips, T. Sawamura and J. L. Mehta (1999). "Upregulation of endothelial receptor for oxidized low-density lipoprotein (LOX-1) in cultured human coronary artery endothelial cells by angiotensin II type 1 receptor activation." Circ Res **84**(9): 1043-1049.

Lin, Y. P., W. C. Yu, M. E. Hsu, H. C. Tsai, C. C. Liao and C. H. Lin (2015). "Comparative proteomic analysis of rat left ventricle in a subtotal nephrectomy model." J Chin Med Assoc **78**(4): 218-228.

Llorens-Cortes, C., B. Greenberg, H. Huang and P. Corvol (1994). "Tissular expression and regulation of type 1 angiotensin II receptor subtypes by quantitative reverse transcriptase-polymerase chain reaction analysis." Hypertension **24**(5): 538-548.

Logan, J. (2000). "Graphical analysis of PET data applied to reversible and irreversible tracers." Nucl Med Biol **27**(7): 661-670.

Logan, J., Y. S. Ding, K. S. Lin, D. Pareto, J. Fowler and A. Biegon (2005). "Modeling and analysis of PET studies with norepinephrine transporter ligands: the search for a reference region." Nucl Med Biol **32**(5): 531-542.

Logan, J., J. S. Fowler, N. D. Volkow, G. J. Wang, Y. S. Ding and D. L. Alexoff (1996). "Distribution volume ratios without blood sampling from graphical analysis of PET data." J Cereb Blood Flow Metab **16**(5): 834-840.

Logan, J., J. S. Fowler, N. D. Volkow, A. P. Wolf, S. L. Dewey, D. J. Schlyer, et al. (1990). "Graphical Analysis of Reversible Radioligand Binding from Time-Activity Measurements Applied to [N-{+11}C-methyl]-(-)-Cocaine PET Studies in Human Subjects." Journal of Cerebral Blood Flow and Metabolism **10**(5): 740-747.

Logan, J., J. S. Fowler, N. D. Volkow, A. P. Wolf, S. L. Dewey, D. J. Schlyer, et al. (1990). "Graphical analysis of reversible radioligand binding from time-activity

measurements applied to [N-11C-methyl]-(-)-cocaine PET studies in human subjects." J Cereb Blood Flow Metab **10**(5): 740-747.

Logan, J., A. P. Wolf, C. Y. Shiue and J. S. Fowler (1987). "Kinetic modeling of receptor-ligand binding applied to positron emission tomographic studies with neuroleptic tracers." J Neurochem **48**(1): 73-83.

Long, D. A., K. L. Price, J. Herrera-Acosta and R. J. Johnson (2004). "How does angiotensin II cause renal injury?" Hypertension **43**(4): 722-723.

Lopez-Novoa, J. M., C. Martinez-Salgado, A. B. Rodriguez-Pena and F. J. Lopez-Hernandez (2010). "Common pathophysiological mechanisms of chronic kidney disease: therapeutic perspectives." Pharmacol Ther **128**(1): 61-81.

Lortie, M., J. N. DaSilva, S. A. Kirkpatrick, T. Hadizad, B. A. Ismail, R. S. Beanlands, et al. (2013). "Analysis of [11C]methyl-candesartan kinetics in the rat kidney for the assessment of angiotensin II type 1 receptor density in vivo with PET." Nucl Med Biol **40**(2): 252-261.

Luttrell, L. M. and D. Gesty-Palmer (2010). "Beyond desensitization: physiological relevance of arrestin-dependent signaling." Pharmacol Rev **62**(2): 305-330.

Lymperopoulos, A. and S. Negussie (2013). "betaArrestins in cardiac G protein-coupled receptor signaling and function: partners in crime or "good cop, bad cop"?" Int J Mol Sci **14**(12): 24726-24741.

Ma, B., P. S. Sherman, J. E. Moskwa, R. A. Koeppe and M. R. Kilbourn (2004). "Sensitivity of [11C]N-methylpyrrolidinyl benzilate ([11C]NMPYB) to endogenous acetylcholine: PET imaging vs tissue sampling methods." Nucl Med Biol **31**(4): 393-397.

Macconi, D. (2010). "Targeting the renin angiotensin system for remission/regression of chronic kidney disease." Histol Histopathol **25**(5): 655-668.

Mackie, F. E., D. J. Campbell and T. W. Meyer (2001). "Intrarenal angiotensin and bradykinin peptide levels in the remnant kidney model of renal insufficiency." Kidney Int **59**(4): 1458-1465.

Maggioni, A. P., I. Anand, S. Gottlieb and e. al (2002). "Effects of valsartan on morbidity and mortality in patients with heart failure not receiving angiotensin-converting enzyme inhibitors." J Am Coll Cardiol **40**(8): 1414-1421.

Makino, T., Y. Hattori, N. Matsuda, H. Onozuka, I. Sakuma and A. Kitabatake (2003). "Effects of angiotensin-converting enzyme inhibition and angiotensin II type 1 receptor blockade on beta-adrenoceptor signaling in heart failure produced by myocardial Infarction in rabbits: reversal of altered expression of beta-adrenoceptor kinase and G i alpha." J Pharmacol Exp Ther **304**(1): 370-379.

Marik, J. and J. L. Sutcliffe (2006). "Click for PET: rapid preparation of [18F]fluoropeptides using CuI catalyzed 1,3-dipolar cycloaddition." Tetrahedron Letters **47**(37): 6681–6684.

Marrero, M. B., D. Fulton, D. Stepp and D. M. Stern (2004). "Angiotensin II-induced insulin resistance and protein tyrosine phosphatases." Arterioscler Thromb Vasc Biol **24**(11): 2009-2013.

Masaki, H., T. Kurihara, A. Yamaki, N. Inomata, Y. Nozawa, Y. Mori, et al. (1998). "Cardiac-specific overexpression of angiotensin II AT2 receptor causes

attenuated response to AT1 receptor-mediated pressor and chronotropic effects." J Clin Invest **101**(3): 527-535.

Maschio, G., D. Alberti, G. Janin, F. Locatelli, J. F. Mann, M. Motolese, et al. (1996). "Effect of the angiotensin-converting-enzyme inhibitor benazepril on the progression of chronic renal insufficiency. The Angiotensin-Converting-Enzyme Inhibition in Progressive Renal Insufficiency Study Group." N Engl J Med **334**(15): 939-945.

Mathews, W. B., H. D. Burns, R. F. Dannals, H. T. Ravert and E. M. Naylor (1995). "Carbon-11 labelling of a potent, nonpeptide, AT_1-selective angiotensin-II receptor antagonist: MK-996." J Labelled Comp Radiopharm **36**(8): 729-737.

Mathews, W. B., S.E. Yoo, S.H. Lee, U. Scheffel, P.A. Rauseo, T.G. Zober, G. Gocco, K. Sandberg, H.T. Ravert, R.F. Dannals, and Z. Szabo (2003). "[^{11}C] KR31173, A Novel Radioligand for Imaging the ATI Angiotensin Receptor with PET." J Labelled Comp Radiopharm **46**(S1): 401-403.

Mathews, W. B., S. E. Yoo, S. H. Lee, U. Scheffel, P. A. Rauseo, T. G. Zober, et al. (2004). "A novel radioligand for imaging the AT1 angiotensin receptor with PET." Nucl Med Biol **31**(5): 571-574.

Matsubara, H., M. Kanasaki, S. Murasawa, Y. Tsukaguchi, Y. Nio and M. Inada (1994). "Differential gene expression and regulation of angiotensin II receptor subtypes in rat cardiac fibroblasts and cardiomyocytes in culture." J Clin Invest **93**(4): 1592-1601.

McAlpine, H., J. Morton, B. Leckie, A. Rumley, G. Gillen and D. HJ (1988). "Neuroendocrine activation after acute myocardial infarction." Br Heart J **60**: 117-124.

McMurray, J., J. Ostergren, K. Swedberg, C. Granger, P. Held, E. Michelson, et al. (2003). "Effects of candesartan in patients with chronic heart failure and reduced left-ventricular systolic function taking angiotensin-converting-enzyme inhibitors: the CHARM-Added Trial." Lancet **362**(9386): 767-771.

Mehta, P. K. and K. K. Griendling (2007). "Angiotensin II cell signaling: physiological and pathological effects in the cardiovascular system." Am J Physiol Cell Physiol **292**(1): 82-97.

Menard, S. L., E. Croteau, O. Sarrhini, R. Gelinas, P. Brassard, R. Ouellet, et al. (2010). "Abnormal in vivo myocardial energy substrate uptake in diet-induced type 2 diabetic cardiomyopathy in rats." Am J Physiol Endocrinol Metab **298**(5): E1049-1057.

Mujais, S. K., S. Kauffman and A. I. Katz (1986). "Angiotensin II binding sites in individual segments of the rat nephron." J Clin Invest **77**(1): 315-318.

Mukherjee, A., P. Kulkarni, S. M. McCann and A. Negro-Vilar (1982). "Evidence for the presence and characterization of angiotensin II receptors in rat anterior pituitary membranes." Endocrinology **110**(2): 665-667.

Murasawa, S., H. Matsubara, M. Urakami and M. Inada (1993). "Regulatory elements that mediate expression of the gene for the angiotensin II type 1a receptor for the rat." J Biol Chem **268**(36): 26996-27003.

Murphy, T. J., R. W. Alexander, K. K. Griendling, M. S. Runge and K. E. Bernstein (1991). "Isolation of a cDNA encoding the vascular type-1 angiotensin II receptor." Nature **351**(6323): 233-236.

Nakajima, M., H. G. Hutchinson, M. Fujinaga, W. Hayashida, R. Morishita, L. Zhang, et al. (1995). "The angiotensin II type 2 (AT2) receptor antagonizes the growth effects of the AT1 receptor: gain-of-function study using gene transfer." Proc Natl Acad Sci U S A **92**(23): 10663-10667.

Nakamoto, H., C. M. Ferrario, S. B. Fuller, D. L. Robaczewski, E. Winicov and R. H. Dean (1995). "Angiotensin-(1-7) and nitric oxide interaction in renovascular hypertension." Hypertension **25**(4 Pt 2): 796-802.

Naruse, M., A. Tanabe, A. Sato, S. Takagi, K. Tsuchiya, T. Imaki, et al. (2002). "Aldosterone breakthrough during angiotensin II receptor antagonist therapy in stroke-prone spontaneously hypertensive rats." Hypertension **40**(1): 28-33.

Nathan, S., C. J. Pepine and G. L. Bakris (2005). "Calcium antagonists: effects on cardio-renal risk in hypertensive patients." Hypertension **46**(4): 637-642.

National Kidney, F. (2002). "K/DOQI clinical practice guidelines for chronic kidney disease: evaluation, classification, and stratification." Am J Kidney Dis **39**(2 Suppl 1): S1-266.

Navar, L. G. and L. M. Harrison-Bernard (2000). "Intrarenal angiotensin II augmentation in angiotensin II dependent hypertension." Hypertens Res **23**(4): 291-301.

Navar, L. G., H. Kobori and M. Prieto-Carrasquero (2003). "Intrarenal angiotensin II and hypertension." Curr Hypertens Rep **5**(2): 135-143.

Navar, L. G., K. D. Mitchell, L. M. Harrison-Bernard, H. Kobori and A. Nishiyama (2001). "Intrarenal angiotensin II levels in normal and hypertensive states." J Renin Angiotensin Aldosterone Syst **2**: S176-S184.

Nickenig, G. (2002). "Central role of the AT(1)-receptor in atherosclerosis." J Hum Hypertens **16 Suppl 3**: S26-33.

Nickenig, G. and M. Bohm (1997). "Regulation of the angiotensin AT1 receptor expression by hypercholesterolemia." Eur J Med Res **2**(7): 285-289.

Nickenig, G. and T. J. Murphy (1994). "Down-regulation by growth factors of vascular smooth muscle angiotensin receptor gene expression." Mol Pharmacol **46**(4): 653-659.

Nickenig, G., K. Strehlow, A. T. Baumer, S. Baudler, S. Wassmann, H. Sauer, et al. (2000). "Negative feedback regulation of reactive oxygen species on AT1 receptor gene expression." Br J Pharmacol **131**(4): 795-803.

Nickenig, G., K. Strehlow, J. Roeling, O. Zolk, A. Knorr and M. Bohm (1998). "Salt induces vascular AT1 receptor overexpression in vitro and in vivo." Hypertension **31**(6): 1272-1277.

Nickenig, G., K. Strehlow, S. Wassmann, A. T. Baumer, K. Albory, H. Sauer, et al. (2000). "Differential effects of estrogen and progesterone on AT(1) receptor gene expression in vascular smooth muscle cells." Circulation **102**(15): 1828-1833.

Nigbor, D. A. and J. B. Lewis (2003). "Use of calcium antagonists in renal patients: therapeutic benefit or medical malpractice?" Curr Hypertens Rep **5**(5): 430-436.

Nitzsche, E. U., Y. Choi, D. Killion, C. K. Hoh, R. A. Hawkins, J. T. Rosenthal, et al. (1993). "Quantification and parametric imaging of renal cortical blood flow in vivo based on Patlak graphical analysis." Kidney Int **44**(5): 985-996.

Noda, K., Y. H. Feng, X. P. Liu, Y. Saad, A. Husain and S. S. Karnik (1996). "The active state of the AT1 angiotensin receptor is generated by angiotensin II induction." Biochemistry **35**(51): 16435-16442.

Noda, K., Y. Saad and S. S. Karnik (1995). "Interaction of Phe8 of angiotensin II with Lys199 and His256 of AT1 receptor in agonist activation." J Biol Chem **270**(48): 28511-28514.

Noda, M., T. Matsuo, R. Fukuda, M. Ohta, H. Nagano, Y. Shibouta, et al. (1999). "Effect of candesartan cilexetil (TCV-116) in rats with chronic renal failure." Kidney Int **56**(3): 898-909.

O'Donnell, J. M. (1993). "Antidepressant-like effects of rolipram and other inhibitors of cyclic adenosine monophosphate phosphodiesterase on behavior maintained by differential reinforcement of low response rate." J Pharmacol Exp Ther **264**(3): 1168-1178.

Oestreicher, E. M., C. Guo, E. W. Seely, T. Kikuchi, D. Martinez-Vasquez, L. Jonasson, et al. (2006). "Estradiol increases proteinuria and angiotensin II type 1 receptor in kidneys of rats receiving L-NAME and angiotensin II." Kidney Int **70**(10): 1759-1768.

Officers, A., A. C. R. G. T. A. Coordinators for the and T. Lipid-Lowering Treatment to Prevent Heart Attack (2002). "Major outcomes in high-risk hypertensive patients randomized to angiotensin-converting enzyme inhibitor or calcium channel blocker vs diuretic: The Antihypertensive and Lipid-Lowering Treatment to Prevent Heart Attack Trial (ALLHAT)." JAMA **288**(23): 2981-2997.

Okazaki, T., T. Watanabe, K. Kikuchi, A. Suga, M. Shibasaki, A. Fujimori, et al. (1998). "Studies on nonpeptide angiotensin II receptor antagonists. IV. Synthesis and biological evaluation of 4-acrylamide-1H-imidazole derivatives." Chem Pharm Bull (Tokyo) **46**(6): 973-981.

Opie, L. H. and M. Sack (2001). "Enhanced Angiotensin II activity in heart failure: Re-evaluation of the counter regulatory hypothesis of receptor subtypes." Circ Res **88**: 654-658.

Oppermann, M., N. J. Freedman, R. W. Alexander and R. J. Lefkowitz (1996). "Phosphorylation of the type 1A angiotensin II receptor by G protein-coupled receptor kinases and protein kinase C." J Biol Chem **271**(22): 13266-13272.

Ouali, R., M. C. Berthelon, M. Begeot and J. M. Saez (1997). "Angiotensin II receptor subtypes AT1 and AT2 are down-regulated by angiotensin II through AT1 receptor by different mechanisms." Endocrinology **138**(2): 725-733.

Oyamada, S., C. Bianchi, S. Takai, M. P. Robich, R. T. Clements, L. Chu, et al. (2010). "Impact of acute myocardial ischemia reperfusion on the tissue and blood-borne renin-angiotensin system." Basic Res Cardiol **105**(4): 513-522.

Packer, M. (1992). "The neurohormonal hypothesis: a theory to explain the mechanism of disease progression in heart failure." J Am Coll Cardiol **20**(1): 248-254.

Parmar, M. S. (2002). "Chronic renal disease." BMJ **325**(7355): 85-90.

Parving, H. H., E. Hommel, B. R. Jensen and H. P. Hansen (2001). "Long-term beneficial effect of ACE inhibition on diabetic nephropathy in normotensive type 1 diabetic patients." Kidney int **60**(1): 228-234.

Parving, H. H., H. Lehnert, J. Brochner-Mortensen, R. Gomis, S. Andersen, P. Arner, et al. (2001). "The effect of irbesartan on the development of diabetic nephropathy in patients with type 2 diabetes." N Engl J Med **345**(12): 870-878.

Paul, M., A. Poyan Mehr and R. Kreutz (2006). "Physiology of local renin-angiotensin systems." Physiol Rev **86**(3): 747-803.

Paul, M., J. Wagner and V. J. Dzau (1993). "Gene expression of the renin-angiotensin system in human tissues. Quantitative analysis by the polymerase chain reaction." J Clin Invest **91**(5): 2058-2064.

Perico, N., A. Benigni and G. Remuzzi (2008). "Present and future drug treatments for chronic kidney diseases: evolving targets in renoprotection." Nat Rev Drug Discov **7**(11): 936-953.

Persson, P. B., A. Skalweit and B. J. Thiele (2004). "Controlling the release and production of renin." Acta Physiol Scand **181**(4): 375-381.

Petrie, M. C., N. Padmanabhan, J. E. McDonald, C. Hillier, J. M. Connell and J. J. McMurray (2001). "Angiotensin converting enzyme (ACE) and non-ACE dependent angiotensin II generation in resistance arteries from patients with heart failure and coronary heart disease." J Am Coll Cardiol **37**(4): 1056-1061.

Pfeffer, M., E. Braunwald, L. Moye and e. all (1992). "Effect of ventricular dysfunction aftermyocardial infarction. Results of the survival and ventricular enlargement trial. The SAVE Investigators." N Eng J Med **327**: 669-677.

Pfeffer, M., K. Swedberg, C. Granger, P. Held, J. McMurray, E. Michelson, et al. (2003). "Effects of candesartan on mortality and morbidity in patients with chronic heart failure: the CHARM-Overall programme." Lancet **362**(9386): 759-766.

Piecha, G., N. Koleganova, M. L. Gross, A. Geldyyev, M. Adamczak and E. Ritz (2008). "Regression of glomerulosclerosis in subtotally nephrectomized rats: effects of monotherapy with losartan, spironolactone, and their combination." Am J Physiol Renal Physiol **295**(1): F137-144.

Pitt, B., P. A. Poole-Wilson, R. Segal, F. A. Martinez, K. Dickstein, A. J. Camm, et al. (2000). "Effect of losartan compared with captopril on mortality in patients with symptomatic heart failure: randomised trial--the Losartan Heart Failure Survival Study ELITE II." Lancet **355**(9215): 1582-1587.

Podjarny, E., J. L. Bernheim, A. Pomeranz, M. Rathaus, M. Pomeranz, J. Green, et al. (1993). "Effect of timing of antihypertensive therapy on glomerular injury: comparison between captopril and diltiazem." Nephrol Dial Transplant **8**(6): 501-506.

Podjarny, E., G. Hasdan, J. Bernheim, G. Rashid, J. Green, Z. Korzets, et al. (2004). "Effect of chronic tetrahydrobiopterin supplementation on blood pressure and proteinuria in 5/6 nephrectomized rats." Nephrol Dial Transplant **19**(9): 2223-2227.

Pohl, M. A., S. Blumenthal, D. J. Cordonnier, F. De Alvaro, G. Deferrari, G. Eisner, et al. (2005). "Independent and additive impact of blood pressure control and angiotensin II receptor blockade on renal outcomes in the irbesartan diabetic nephropathy trial: clinical implications and limitations." J Am Soc Nephrol **16**(10): 3027-3037.

Prieto, M., A. Rodriguez-Pena, M. Arevalo, J. V. Rivas, A. Duwel, N. Eleno, et al. (2005). "Effect of the long-term treatment with trandolapril on endoglin expression in

rats with experimental renal fibrosis induced by renal mass reduction." Kidney Blood Press Res **28**(1): 32-40.

Rahn, K. H. (2005). "The role of calcium antagonists in patients with chronic renal failure." Pediatr Nephrol **20**(9): 1208-1213.

Rambausek, M., E. Ritz, G. Mall, O. Mehls and H. Katus (1985). "Myocardial hypertrophy in rats with renal insufficiency." Kidney Int **28**(5): 775-782.

Ramenda, T., T. Kniess, J. Bergman, J. Steinbach and F. Wuest (2009). "Radiolabelling of proteins with fluorine-18 via click chemistry " Chemical communications(48): 7521-7523.

Ranade, V. and J. Somberg (2002). "Rapid determination of partition coefficients between n-octanol/water for cardiovascular therapies." Am J Ther **9**(1): 19-24.

Re, R. N. (2003). "Intracellular renin and the nature of intracrine enzymes." Hypertension **42**(2): 117-122.

Re, R. N. and J. L. Cook (2006). "The intracrine hypothesis: an update." Regul Pept **133**(1-3): 1-9.

Regitz-Zagrosek, V., N. Friedel, A. Heymann, P. Bauer, M. Neuss, A. Rolfs, et al. (1995). "Regulation, chamber localization, and subtype distribution of angiotensin II receptors in human hearts." Circulation **91**(5): 1461-1471.

Rogers, T. B., S. T. Gaa and I. S. Allen (1986). "Identification and characterization of functional angiotensin II receptors on cultured heart myocytes." J Pharmacol Exp Ther **236**(2): 438-444.

Rosenberg, M. E., R. Correa-Rotter, T. Inagami, S. M. Kren and T. H. Hostetter (1991). "Glomerular renin synthesis and storage in the remnant kidney in the rat." Kidney Int **40**(4): 677-683.

Ruiz-Ortega, M., O. Lorenzo and J. Egido (2000). "Angiotensin III increases MCP-1 and activates NF-kappaB and AP-1 in cultured mesangial and mononuclear cells." Kidney Int **57**(6): 2285-2298.

Ruiz-Ortega, M., O. Lorenzo, M. Ruperez and J. Egido (2000). "ACE inhibitors and AT(1) receptor antagonists-beyond the haemodynamic effect." Nephrol Dial Transplant **15**(5): 561-565.

Sandberg, K., H. Ji, A. Clark and e. al (1992). "Cloning and expression of a novel angiotensin II receptor subtype." J Biol Chem **267**(14): 9455-9458.

Sanders, J. D., H. K. Happe, D. B. Bylund and L. C. Murrin (2005). "Development of the norepinephrine transporter in the rat CNS." Neuroscience **130**(1): 107-117.

Santos, R. A., A. C. Simoes e Silva, C. Maric, D. M. Silva, R. P. Machado, I. de Buhr, et al. (2003). "Angiotensin-(1-7) is an endogenous ligand for the G protein-coupled receptor Mas." Proc Natl Acad Sci U S A **100**(14): 8258-8263.

Sarnak, M. J., A. S. Levey, A. C. Schoolwerth, J. Coresh, B. Culleton, L. L. Hamm, et al. (2003). "Kidney disease as a risk factor for development of cardiovascular disease: a statement from the American Heart Association Councils on Kidney in Cardiovascular Disease, High Blood Pressure Research, Clinical Cardiology, and Epidemiology and Prevention." Hypertension **42**(5): 1050-1065.

Schindler, T. H. and V. Dilsizian (2012). "Cardiac positron emission tomography/computed tomography imaging of the Renin-Angiotensin system in humans holds promise for image-guided approach to heart failure therapy." J Am Coll Cardiol **60**(24): 2535-2538.

Schmitz, U., T. Ishida, M. Ishida, J. Surapisitchat, M. I. Hasham, S. Pelech, et al. (1998). "Angiotensin II stimulates p21-activated kinase in vascular smooth muscle cells: role in activation of JNK." Circ Res **82**(12): 1272-1278.

Schultz, D., X. Su, C. C. Wei, S. P. Bishop, P. Powell, G. H. Hankes, et al. (2002). "Downregulation of ANG II receptor is associated with compensated pressure-overload hypertrophy in the young dog." Am J Physiol Heart Circ Physiol **282**(2): H749-756.

Seachrist, J. L. and S. S. Ferguson (2003). "Regulation of G protein-coupled receptor endocytosis and trafficking by Rab GTPases." Life Sci **74**(2-3): 225-235.

Sealey, J. E., R. P. White, J. H. Laragh and A. L. Rubin (1977). "Plasma prorenin and renin in anephric patients." Circ Res **41**(4 Suppl 2): 17-21.

Sechi, L. A., C. A. Griffin and M. Schambelan (1994). "The cardiac renin-angiotensin system in STZ-induced diabetes." Diabetes **43**(10): 1180-1184.

Segura, J., C. Campo and L. M. Ruilope (2005). "Influence of chronic kidney disease development and renin-angiotensin system inhibition on cardiovascular prognosis." Curr Med Chem Cardiovasc Hematol Agents **3**(1): 55-60.

Segura, J., J. A. Garcia-Donaire and L. M. Ruilope (2005). "Calcium channel blockers and renal protection: insights from the latest clinical trials." J Am Soc Nephrol **16 Suppl 1**: S64-66.

Senbonmatsu, T., S. Ichihara, E. Price, Jr., F. A. Gaffney and T. Inagami (2000). "Evidence for angiotensin II type 2 receptor-mediated cardiac myocyte enlargement during in vivo pressure overload." J Clin Invest **106**(3): R25-29.

Serneri, G. G., M. Boddi, I. Cecioni, S. Vanni, M. Coppo, M. L. Papa, et al. (2001). "Cardiac angiotensin II formation in the clinical course of heart failure and its relationship with left ventricular function." Circ Res **88**(9): 961-968.

Sharp, T. L., C. S. Dence, J. A. Engelbach, P. Herrero, R. J. Gropler and M. J. Welch (2005). "Techniques necessary for multiple tracer quantitative small-animal imaging studies." Nucl Med Biol **32**(8): 875-884.

Shiba, N. and H. Shimokawa (2011). "Chronic kidney disease and heart failure--Bidirectional close link and common therapeutic goal." J Cardiol **57**(1): 8-17.

Silvestre, J., C. Heymes, A. Oubenaissa and e. al (1999). "Activation of cardiac aldosterone production in rat myocardial infarction: effect of angiotensin II receptor blockade and role in cardiac fibrosis." Circulation **99**(20): 2694-2701.

Skorecki, K. L., B. J. Ballermann, H. G. Rennke and B. M. Brenner (1983). "Angiotensin II receptor regulation in isolated renal glomeruli." Fed Proc **42**(14): 3064-3070.

Soubrier, F., L. Wei, C. Hubert, E. Clauser, F. Alhenc-Gelas and P. Corvol (1993). "Molecular biology of the angiotensin I converting enzyme: II. Structure-function. Gene polymorphism and clinical implications." J Hypertens **11**(6): 599-604.

Stearns, R. A., P. K. Chakravarty, R. Chen and S. H. Chiu (1995). "Biotransformation of losartan to its active carboxylic acid metabolite in human liver microsomes. Role of cytochrome P4502C and 3A subfamily members." Drug Metab Dispos **23**(2): 207-215.

Stearns, R. A., R. R. Miller, G. A. Doss, P. K. Chakravarty, A. Rosegay, G. J. Gatto, et al. (1992). "The metabolism of DuP 753, a nonpeptide angiotensin II receptor

antagonist, by rat, monkey, and human liver slices." Drug Metab Dispos **20**(2): 281-287.

Stefanski, A., K. G. Schmidt, R. Waldherr and E. Ritz (1996). "Early increase in blood pressure and diastolic left ventricular malfunction in patients with glomerulonephritis." Kidney Int **50**(4): 1321-1326.

Strauch, M. and N. Gretz (1988). "Animal models to induce renal failure: a historical survey." Contributions to nephrology **60**: 1-8.

Sui, Y., H. L. Zhao, R. R. Fan, J. Guan, L. He, H. M. Lee, et al. (2010). "Renin-angiotensin system activation in renal adipogenesis." Am J Physiol Renal Physiol **298**(2): F391-400.

Sukumaran, V., K. Watanabe, P. T. Veeraveedu, R. A. Thandavarayan, N. Gurusamy, M. Ma, et al. (2010). "Telmisartan, an angiotensin-II receptor blocker ameliorates cardiac remodeling in rats with dilated cardiomyopathy." Hypertens Res **33**(7): 695-702.

Sun, C. K., L. T. Chang, J. J. Sheu, C. Y. Wang, A. A. Youssef, C. J. Wu, et al. (2007). "Losartan Preserves Integrity of Cardiac Gap Junctions and PGC-1 alpha Gene Expression and Prevents Cellular Apoptosis in Remote Area of Left Ventricular Myocardium Following Acute Myocardial Infarction." Int Heart J **48**(4): 533-546.

Susantitaphong, P., K. Sewaralthahab, E. M. Balk, S. Eiam-ong, N. E. Madias and B. L. Jaber (2013). "Efficacy and safety of combined vs. single renin-angiotensin-aldosterone system blockade in chronic kidney disease: a meta-analysis." Am J Hypertens **26**(3): 424-441.

Suzaki, Y., M. C. Prieto-Carrasquero and H. Kobori (2006). "Intratubular Renin-Angiotensin System in Hypertension." Curr Hypertens Rev **2**(2): 151-157.

Sviglerova, J., J. Kuncova, L. Nalos, Z. Tonar, D. Rajdl and M. Stengl (2010). "Cardiovascular parameters in rat model of chronic renal failure induced by subtotal nephrectomy." Physiol Res / Academia Scientiarum Bohemoslovaca **59 Suppl 1**: S81-88.

Szabo, Z., P. F. Kao, H. D. Burns, R. E. Gibson, T. G. Hamill, H. T. Ravert, et al. (1998). "Investigation of angiotensin II/AT1 receptors with carbon-11-L-159,884: a selective AT1 antagonist." J Nucl Med **39**(7): 1209-1213.

Szabo, Z., R. Speth, P. Brown, L. Kerenyi, P. Kao, W. Mathews, et al. (2001). "Use of positron emission tomography to study AT1 receptor regulation in vivo." J Am Soc Nephrol **12**: 1350-1358.

Taal, M. W. and B. M. Brenner (2000). "Renoprotective benefits of RAS inhibition: from ACEI to angiotensin II antagonists." Kidney Int **57**(5): 1803-1817.

Tai, Y. C. and R. Laforest (2005). "Instrumentation aspects of animal PET." Annu Rev Biomed Eng **7**: 255-285.

Takano, H., H. Hasegawa, T. Nagai and I. Komuro (2003). "Implication of cardiac remodeling in heart failure: mechanisms and therapeutic strategies." Internal medicine **42**(6): 465-469.

Takayanagi, R., K. Ohnaka, Y. Sakai, R. Nakao, T. Yanase, M. Haji, et al. (1992). "Molecular cloning, sequence analysis and expression of a cDNA encoding human type-1 angiotensin II receptor." Biochem Biophys Res Commun **183**(2): 910-916.

Tan, J., H. Wang and F. H. Leenen (2004). "Increases in Brain and Cardiac AT1 receptor and ACE densities after myocardial infarct in rats." Am J Physiol Heart Circ Physiol **286**: H1665-1671.

Tan, J., J. M. Wang and H. F. Leenen (2004). "Differential inhibition of brain angiotensin-converting enzyme by peripheral administration of trandolapril versus lisinopril in Wistar rats." J Cardiovasc Pharm **In press**.

Tanaka, Y., M. Nagai, T. Date, T. Okada, Y. Abe, S. Seki, et al. (2004). "Effects of bradykinin on cardiovascular remodeling in renovascular hypertensive rats." Hypertens Res **27**(11): 865-875.

Teo, K., S. Yusuf, P. Sleight, C. Anderson, F. Mookadam, B. Ramos, et al. (2004). "Rationale, design, and baseline characteristics of 2 large, simple, randomized trials evaluating telmisartan, ramipril, and their combination in high-risk patients: the Ongoing Telmisartan Alone and in Combination with Ramipril Global Endpoint Trial/Telmisartan Randomized Assessment Study in ACE Intolerant Subjects with Cardiovascular Disease (ONTARGET/TRANSCEND) trials." Am Heart J **148**(1): 52-61.

Thackeray, J. T., R. S. Beanlands and J. N. Dasilva (2007). "Presence of Specific 11C-meta-Hydroxyephedrine Retention in Heart, Lung, Pancreas, and Brown Adipose Tissue." J Nucl Med **48**(10): 1733-1740.

The CONSENSUS Trial Study Group (1987). "Effects of enalapril on mortality in severe congestive heart failure. Results of the Cooperative North Scandinavian Enalapril Survival Study (CONSENSUS)." N Engl J Med **316**(23): 1429-1435.

Thomas, A. J., J. N. DaSilva, M. Lortie, J. M. Renaud, M. Kenk, R. S. Beanlands, et al. (2011). "PET of (R)-11C-rolipram binding to phosphodiesterase-4 is reproducible and sensitive to increased norepinephrine in the rat heart." J Nucl Med **52**(2): 263-269.

Thomas, W. G., K. M. Baker, T. J. Motel and T. J. Thekkumkara (1995). "Angiotensin II receptor endocytosis involves two distinct regions of the cytoplasmic tail. A role for residues on the hydrophobic face of a putative amphipathic helix." J Biol Chem **270**(38): 22153-22159.

Thompson, C. J. (2002). Instrumentation. Principles and Practice of Positron Emission Tomography. R. L. Wahl. Philadelphia, PA, Lippincott Williams & Wilkins**:** 48-64.

Timmermans, P. B., D. J. Carini, A. T. Chiu, J. V. Duncia, W. A. Price, Jr., G. J. Wells, et al. (1991). "Angiotensin II receptor antagonists. From discovery to antihypertensive drugs." Hypertension **18**(5 Suppl): III136-142.

Timmermans, P. B., P. C. Wong and A. T. Chiu (1993). "Angiotensin II receptor and Angiotensin II receptor antagonists." Pharmacol Rev **45**: 205-251.

Timmermans, P. B., P. C. Wong, A. T. Chiu, W. F. Herblin, P. Benfield, D. J. Carini, et al. (1993). "Angiotensin II receptors and angiotensin II receptor antagonists." Pharmacol Rev **45**(2): 205-251.

Toto, R. D. (2005). "Management of hypertensive chronic kidney disease: role of calcium channel blockers." J Clin Hypertens (Greenwich) **7**(4 Suppl 1): 15-20.

Touyz, R. M., G. He, L. Y. Deng and E. L. Schiffrin (1999). "Role of extracellular signal-regulated kinases in angiotensin II-stimulated contraction of smooth muscle cells from human resistance arteries." Circulation **99**(3): 392-399.

Tsutsumi, K. and J. Saveedra (1991). "Characterization and development of angiotensin II receptor subtypes (AT1 and AT2) in rat brain." Am J Physiol **216**((1Pt 2)): 11-15.

Tsutsumi, Y., H. Matsubara, N. Ohkubo, Y. Mori, Y. Nozawa, S. Murasawa, et al. (1998). "Angiotensin II type 2 receptor is upregulated in human heart with interstitial fibrosis, and cardiac fibroblasts are the major cell type for its expression." Circ Res **83**(10): 1035-1046.

Tzakos, A. G., I. P. Gerothanassis and A. N. Troganis (2004). "On the structural basis of the hypertensive properties of angiotensin II: a solved mystery or a controversial issue?" Curr Top Med Chem **4**(4): 431-444.

Ullian, M. E., J. G. Webb, R. Chen, R. V. Paul and T. A. Morinelli (2004). "Mechanisms of vascular angiotensin II surface receptor regulation by epidermal growth factor." J Cell Physiol **200**(3): 451-457.

Unger, T. (2002). "The role of the renin-angiotensin system in the development of cardiovascular disease." Am J Cardiol **89**(2A): 3A-9A; discussion 10A.

Ushio-Fukai, M., K. K. Griendling, M. Akers, P. R. Lyons and R. W. Alexander (1998). "Temporal dispersion of activation of phospholipase C-beta1 and -gamma isoforms by angiotensin II in vascular smooth muscle cells. Role of alphaq/11, alpha12, and beta gamma G protein subunits." J Biol Chem **273**(31): 19772-19777.

Vaidyanathan, G., B. J. White and M. R. Zalutsky (2009). "Propargyl 4-[F]fluorobenzoate: A Putatively More Stable Prosthetic group for the Fluorine-18 Labeling of Biomolecules via Click Chemistry." Current Radiopharmaceuticals **2**(1): 63-74.

Valdivia, A. C., M. Estrada, T. Hadizad, D. Stewart, R. S. Beanlands and J. N. DaSilva (2012). "A fast, simple, and reproducible automated synthesis of [18F]FPyKYNE-c(RGDyK) for avb3 receptor positron emission tomography imaging." J Label Compd Radiopharm **55**(2): 57-60.

van der Meer, I. M., P. Cravedi and G. Remuzzi (2010). "The role of renin angiotensin system inhibition in kidney repair." Fibrogenesis Tissue Repair **3**: 7.

van der Velde, M., K. Matsushita, J. Coresh, B. C. Astor, M. Woodward, A. Levey, et al. (2011). "Lower estimated glomerular filtration rate and higher albuminuria are associated with all-cause and cardiovascular mortality. A collaborative meta-analysis of high-risk population cohorts." Kidney Int **79**(12): 1341-1352.

Van Kats, J., L. de Lannoy, A. Jan Danser and e. al (1997). "Angiotensin II type 1 (AT1) receptor-mediated accumulation of angiotensin II in tissues and its intracellular half-life in vivo." Hypertension **30**(1 Pt 1): 42-49.

Van Kats, J., D. Duncker, D. Haitsma and e. al (1999). "Angiotensin-converting enzyme inhibition and angiotensin II type 1 receptor blockade prevent cardiac remodeling in pigs after myocardial infarction: role of tissue angiotensin II." Circulation **99**(13): 2694-2701.

van Waarde, A., R. L. Anthonio, T. J. Visser, P. H. Elsinga, H. Posthumus, A. M. Weemaes, et al. (1995). "Quantification of an 11C-labelled beta-adrenoceptor ligand, S-(-)CGP 12177, in plasma of humans and rats." J Chromatogr B Biomed Appl **663**(2): 361-369.

Vanderheyden, P. M., F. L. Fierens, J. P. De Backer, N. Fraeyman and G. Vauquelin (1999). "Distinction between surmountable and insurmountable selective AT1 receptor antagonists by use of CHO-K1 cells expressing human angiotensin II AT1 receptors." Br J Pharmacol **126**(4): 1057-1065.

Vaziri, N. D., Y. Bai, Z. Ni, Y. Quiroz, R. Pandian and B. Rodriguez-Iturbe (2007). "Intra-renal angiotensin II/AT1 receptor, oxidative stress, inflammation, and progressive injury in renal mass reduction." J of Pharmacol Exp Ther **323**(1): 85-93.

Veerasingham, S. J. and M. K. Raizada (2003). "Brain renin-angiotensin system dysfunction in hypertension: recent advances and perspectives." Br J Pharmacol **139**(2): 191-202.

Velez, J. C. (2009). "The importance of the intrarenal renin-angiotensin system." Nat Clin Pract Nephrol **5**(2): 89-100.

Verhagen, A. M., B. Braam, P. Boer, H. J. Grone, H. A. Koomans and J. A. Joles (1999). "Losartan-sensitive renal damage caused by chronic NOS inhibition does not involve increased renal angiotensin II concentrations." Kidney Int **56**(1): 222-231.

Verjans, J. W. H., D. Lovhaug, N. Narula, A. D. Petrov, B. Indrevoll, E. Bjurgert, et al. (2008). "Noninvasive imaging of angiotensin receptors after myocardial infarction." JACC Cardiovasc Imaging **1**(3): 354-362.

Viberti, G., C. Mogensen and e. al (1994). "Effect of captopril on progression to clinical proteinuria in patients with insulin-dependent diabetes mellitus andmicroalbuminuria. European Microalbuminuria Captopril Study Group." JAMA **271**(4): 275-279.

Villarreal, F. J., N. N. Kim, G. D. Ungab, M. P. Printz and W. H. Dillmann (1993). "Identification of functional angiotensin II receptors on rat cardiac fibroblasts." Circulation **88**(6): 2849-2861.

Wagenaar, L., A. Voors, H. Buikema and W. Gilst (2002). "Angiotensin receptors in the cardiovascular system." Can J Cardiol **18**(12): 1331-1339.

Wagenaar, L. J., A. A. Voors, H. Buikema and W. H. van Gilst (2002). "Angiotensin receptors in the cardiovascular system." Can J Cardiol **18**(12): 1331-1339.

Wagner, J., F. Gehlen and e. al (1999). "Angiotensin II receptor type 1 gene expression in human glomerulonephritis and diabetes mellitus." J Am Soc Nephrol **10**(3): 545-551.

Wahl, R. L. (2002). Principles and practice of positron emission tomography. Philadelphia, Lippincott Williams and Wilkins.

Wang, D., A. Yao, H. Zhao and D. DiPette (1997). "Distinct mechanisms of modulation of angiotensin II type I receptor gene expression in heart and aorta." Hypertension **29**: 1104-1108.

Waydhas, C., K. Weigl and H. Sies (1978). "The disposition of formaldehyde and formate arising from drug N-demethylations dependent on cytochrome P-450 in hepatocytes and in perfused rat liver." Eur J Biochem **89**(1): 143-150.

Wharton, J., K. Morgan, R. A. Rutherford, J. D. Catravas, A. Chester, B. F. Whitehead, et al. (1998). "Differential distribution of angiotensin AT2 receptors in the normal and failing human heart." J Pharmacol Exp Ther **284**(1): 323-336.

Windt, W. A., A. Tahara, A. C. Kluppel, D. de Zeeuw, R. H. Henning and R. P. van Dokkum (2006). "Early, but not late therapy with a vasopressin V1a-antagonist ameliorates the development of renal damage after 5/6 nephrectomy." J Renin Angiotensin Aldosterone Syst. **7**(4): 217-224.

Wolny, A., J. P. Clozel, J. Rein, P. Mory, P. Vogt, M. Turino, et al. (1997). "Functional and biochemical analysis of angiotensin II-forming pathways in the human heart." Circ Res **80**(2): 219-227.

Wright, J. T., Jr., G. Bakris, T. Greene, L. Y. Agodoa, L. J. Appel, J. Charleston, et al. (2002). "Effect of blood pressure lowering and antihypertensive drug class on progression of hypertensive kidney disease: results from the AASK trial." JAMA **288**(19): 2421-2431.

Xia, J., E. Seckin, Y. Xiang, M. Vranesic, W. B. Mathews, K. Hong, et al. (2008). "Positron-emission tomography imaging of the angiotensin II subtype 1 receptor in swine renal artery stenosis." Hypertension **51**(2): 466-473.

Xu, J., O. A. Carretero, T.-D. Liao, H. Peng, E. G. Shesely, J. Xu, et al. (2010). "Local angiotensin II aggravates cardiac remodeling in hypertension." Am J Physiol Heart Circ Physiol **299**(5): 1328-1338.

Yang, H. Y., E. G. Erdos and Y. Levin (1970). "A dipeptidyl carboxypeptidase that converts angiotensin I and inactivates bradykinin." Biochim Biophys Acta **214**(2): 374-376.

Yang, N., L. L. Wu, D. J. Nikolic-Paterson, Y. Y. Ng, W. C. Yang, W. Mu, et al. (1998). "Local macrophage and myofibroblast proliferation in progressive renal injury in the rat remnant kidney." Nephrol Dial Transplant **13**(8): 1967-1974.

Yasunari, K., K. Maeda, M. Nakamura, T. Watanabe, J. Yoshikawa and K. Hirohashi (2005). "Left ventricular hypertrophy and angiotensin II receptor blocking agents." Curr Med Chem Cardiovasc Hematol Agents **3**(1): 61-67.

Yoneda, M., H. Sanada, J. Yatabe, S. Midorikawa, S. Hashimoto, M. Sasaki, et al. (2005). "Differential effects of angiotensin II type-1 receptor antisense oligonucleotides on renal function in spontaneously hypertensive rats." Hypertension **46**(1): 58-65.

Yousef, Z., S. Redwood and M. Marber (2000). "Postinfarction left ventricular remodelling: where are the theories and trials leading us?" Heart **83**: 76-80.

Yu, L., M. Zheng, W. Wang, G. J. Rozanski, I. H. Zucker and L. Gao (2010). "Developmental changes in AT1 and AT2 receptor-protein expression in rats." J Renin Angiotensin Aldosterone Syst **11**(4): 214-221.

Yu, W. C., Y. P. Lin, I. F. Lin, S. Y. Chuang and C. H. Chen (2006). "Effect of ramipril on left ventricular mass in normotensive hemodialysis patients." Am J Kidney Dis **47**(3): 478-484.

Yusuf , S., M. Pfeffer, K. Swedberg, C. Granger, P. Held, J. McMurray, et al. (2003). "Effects of candesartan in patients with chronic heart failure and preserved left-ventricular ejection fraction: the CHARM-Preserved Trial." Lancet **362**(9386): 777-781.

Yusuf, S., P. Sleight, J. Pogue, J. Bosch, R. Davies and G. Dagenais (2000). "Effects of an angiotensin-converting-enzyme inhibitor, ramipril, on cardiovascular events in high-risk patients. The Heart Outcomes Prevention Evaluation Study Investigators." N Engl J Med **342**(3): 145-153.

Zhang, X., D. Dostal, K. Reiss and e. al (1995). "Identification and activation of autocrine renin-angiotensin system in adult ventricular myocytes." Am J Physiol **269**(5 Pt 2): H1791-H1802.

Zhou, J., P. Ernsberger and J. G. Douglas (1993). "A novel angiotensin receptor subtype in rat mesangium. Coupling to adenylyl cyclase." Hypertension **21**(6 Pt 2): 1035-1038.

Zhuo, J. L., F. M. Ferrao, Y. Zheng and X. C. Li (2013). "New frontiers in the intrarenal Renin-Angiotensin system: a critical review of classical and new paradigms." Front Endocrinol (Lausanne) **4**: 166.

Zober, T. G., W. B. Mathews, E. Seckin, S. E. Yoo, J. Hilton, J. Xia, et al. (2006). "PET Imaging of the AT1 receptor with [11C]KR31173." Nucl Med Biol **33**(1): 5-13.